Characterisation of a Zebrafish Model of Wolfram Syndrome

George Cairns (BSc, MRes)

Thesis submitted for the degree of Doctor of Philosophy

November 2018

Institute of Genetic Medicine

Faculty of Medical Science

Abstract

Wolfram Syndrome (WS), is a neurodegenerative disorder defined historically by the combination of diabetes insipidus, diabetes mellitus, optic atrophy and sensorineural deafness (DIDMOAD). The majority of patients with WS harbour recessive mutations within the *WFS1* gene (OMIM 606201), which encodes the wolframin protein. Wolframin is implicated in a number of critical cellular pathways, in particular the ER stress response and calcium homeostasis. Mitochondrial dysfunction is suspected to play a key role in the pathology of the disease. This link is highlighted by mutations in the *CISD2* (OMIM 611507) gene, which also result in WS through a deleterious effect on mitochondrial calcium flux and disturbed ER-mitochondrial interactions. Wolframin is also suspected to have a role in the development of the brain and neuronal tissue and is associated with numerous neurological and psychiatric disorders.

The aim of this study was to characterise novel zebrafish models (*wfs1a* & *wfs1b*) of WS to further our understanding of the role of wolframin in WS, particularly in regulating mitochondrial function and neuronal development. This model could also be used to screen for therapeutic compounds.

The characterisation of this zebrafish model involved observing histological, behavioural and biochemical changes in the knockout zebrafish and determining if the model was comparable to the pathological features reported in patients with WS. We have shown that this zebrafish model of WS shares defects in the ability to cope with ER stress and importantly, it shares similar phenotypes to the human, in particular optic atrophy. Mitochondrial dysfunction was also observed in the model with changes seen in trafficking, respiration and changes in expression of Complex I of the mitochondrial electron transport chain.

This zebrafish model provides a powerful tool to observe neuronal development and mitochondrial function in a live animal model, providing new insights on the mechanisms driving neuronal degeneration in WS.

Acknowledgments

I would like to thank everybody involved in supervising this project Patrick Yu-Wai-Man, John Sayer and Angela Pyle. I would also like to thank Florence Burté and Juliane Mueller for their help and support in the lab.

My thanks, to everybody from the office and lab from the mitochondria, stem cell and single cell genomics facility that have supported me along the way. To all my family and friends that have supported me, especially to Emily, a big thank you for your help and making my time at Newcastle very enjoyable.

I also extend my thanks to Dr Mariya Moosajee and Dr Maria Toms for the time spent in UCL performing zebrafish experiments.

Contents

Table of Figures

Table of Tables

Abbreviations

ACh	Acetylcholine
AChE	Acetylcholineesterase
ADP	Adenosine diphosphate
ATP	Adenosine triphosphate
BSA	Bovine serum albumin
CaP	Caudal primary motor neurone
cDNA	Complementary DNA
CNS	Central nervous system
DIDMOAD	Diabetes Insipidus, Diabetes Mellitus, Optic Atrophy, Sensorineural Deafness
dNTP	Deoxyribonucleotide triphosphate
dpf	Days post fertilisation
ECL	Enhanced chemiluminescence
EDTA	Ethylenediaminetetraacetic acid
EGTA	Ethylene glycol-bis(β-aminoethyl ether)-N,N,N’,N’-tetraacetic acid
EM	Electron microscopy
ER	Endoplasmic reticulum
ERAD	Endoplasmic-reticulum-associated protein degradation
ERSE	ER stress response element
ETC	Electron transport chain
EZRC	European zebrafish resource centre
FAD	Flavin adenine dinucleotide
Fe-S	Iron sulphur

GFP	Green fluorescent protein
GOC	Gene order conservation
gRNA	Guide RNA
GTP	Guanosine triphosphate
hpf	Hours post fertilisation
IB	Isolation buffer
IMM	Inner mitochondrial membrane
IMS	Inter membrane space
INM	Inner nuclear membrane
IP_3R	Inositol trisphosphate receptor
LB	Lysogeny broth
LHON	Leber's hereditary optic neuropathy
MAM	Mitochondria associated membrane
MBP	Myelin basic protein
MCU	Mitochondrial Calcium Uniporter
MES	2-(N-morpholino)ethanesulfonic acid
MoP	Middle primary motor neurons
MRI	Magnetic resonance imaging
mtDNA	Mitochondrial DNA
MTPT	Mitochondrial permeability transition pore
NADH	Nicotinamide adenine dinucleotide
NE	Nuclear envelope
NMDA	N-methyl-D-aspartate

NXC	Sodium-calcium exchanger
OA	Optic Atrophy
OCR	Oxygen consumption rate
OCT	Optical coherence tomography
OKR	Optokinetic response
OMM	Outer mitochondrial membrane
ONM	Outer nuclear membrane
ORAI	Calcium release-activated calcium channel protein 1
OXPHOS	Oxidative phosphorylation
PBS	Phosphate buffered saline
PBST	Phosphate buffered saline and Tween 20
PFA	Paraformaldehyde
Pi	Inorganic phosphate
PMCA	Plasma membrane Ca^{2+} ATPase
PTU	1-phenyl 2-thiourea
PVDF	Polyvinylidene fluoride
RFP	Red fluorescent protein
RGC	Retinal ganglion cell
RNFL	Retinal nerve fiber layer
RoP	Rostal primary motor neuron
ROS	Reactive oxygen species
rpm	Revolutions per minute
RYR	Ryanodine receptor

SDS	Sodium dodecyl sulfate
SERCA	Sarco/endoplasmic reticulum Ca^{2+}-ATPase
SOCE	Store-operated calcium entry
STIM	Stromal interaction molecule
TBS	Tris-buffered saline
TBST	Tris-buffered saline and Tween 20
TCA	Tricarboxylic acid cycle
TEM	Transmission electron microscopy
tRNA	TransferRNA
TRPC	Transient receptor potential cation channels
TRPV	Transient receptor potential cation channels
TYR	Tyrosonase
UPR	Unfolded protein response
UV	Ultra violet
VDAC	Voltage-dependent anion channel
VOC	Voltage operating calcium channel
WS	Wolfram syndrome

Chapter 1: Introduction

1.1 Endoplasmic Reticulum

The endoplasmic reticulum (ER) is the largest eukaryotic organelle which forms an intracellular membrane system (Halperin *et al.*, 2014). The ER is most known for its role in protein synthesis and folding. However, it is a complex organelle critical in other cellular pathways including: protein transport, lipid and steroid synthesis, carbohydrate metabolism and calcium storage (Schwarz and Blower, 2016).

1.1.1 Structure & Function

The ER is split into two domains the nuclear envelope (NE) and the peripheral ER: which is further divided into a number of distinct domains responsible for numerous functions within the same continuous membranes (English and Voeltz, 2013; Westrate *et al.*, 2015).

The NE is made of two flat ER membrane bilayers (the inner nuclear membrane (INM) and outer nuclear membrane (ONM) is responsible for trafficking of macromolecules into the nucleus alongside its role of anchoring for both chromatin and the cytoskeleton(Hetzer *et al.*, 2005). The peripheral ER is formed from the ONM with two dominant morphologies: the peripheral ER cisternae and ER tubules. ER cisternae tend to lie closer to the NE with the ER taking a more tubule shape closer to the plasma membranes (Puhka *et al.*, 2007).

The two distinct morphologies are separated into the rough (cisternae) and smooth (tubule) ER (Figure 1.1). The rough is named so as it tends to be studded with ribosomes for protein translation leading to the hypothesis that the cisternae where responsible for protein production/modification (Westrate *et al.*, 2015). The cisternae do have a higher number of ribosomes and a larger volume (for protein folding) compared to the tubular ER supporting the hypothesis (Puhka *et al.*, 2007; West *et al.*, 2011; English and Voeltz, 2013). However, ribosomes are also found on the tubular ER, in lower concentrations, suggesting a much more complicated picture. The tubular network is better designed for lipid synthesis and has abundant membrane contact sites for ER interactions with other organelles such as the plasma membrane and mitochondria. These contact sites are integral for ER function of lipid/steroid synthesis and Calcium ion homeostasis (Phillips and Voeltz, 2016).

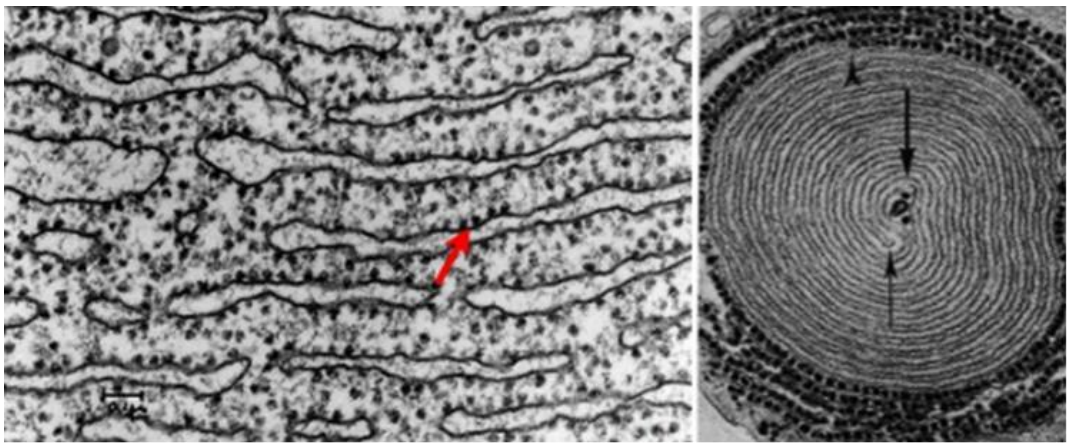

Figure 1.1 Electron Micrographs of Rough vs Smooth ER. Image adapted from (Schwarz and Blower, 2016)

1.1.2 Calcium Ion Homeostasis

Calcium ions act within the cell as an important secondary messenger that is linked to numerous cellular functions including: metabolism, gene transcription and apoptosis (Berridge *et al.*, 2003). Due to the large number of critical processes affected by Ca^{2+}, the cell needs to keep a tight control on Ca^{2+} homeostasis. This approximately 100 nM in the cytosol and under normal circumstances is tightly controlled by intracellular compartments and by Ca^{2+} ion channels found on the plasma membrane (Bollimuntha *et al.*, 2017). Other concentrations of Ca^{2+} include: 100–500 µM in the ER (Bagur and Hajnoczky, 2017), 0.1 to 1.0 mM in mitochondria (Bollimuntha *et al.*, 2017) and approximately 1mM in the extracellular milieu (Bagur and Hajnoczky, 2017).

Ca^{2+} ions enter the cell down the electrochemical gradients through plasma membrane channels that include the voltage operating calcium channel (VOC) - found in excitable cells, N-methyl-D-aspartate receptors (NMDA), transient receptor potential channels (TRPC) and store operated Ca^{2+} channels (SOCE), these channels respond to numerous stimuli to increase Ca^{2+} levels in the cell. In order to maintain control, Ca^{2+} ions are moved out of the cell using the Na^{+}/Ca^{2+} exchanger of the plasma membrane (NCX) and the plasma membrane Ca^{2+} ATPase (PMCA). The NCX, also found in the mitochondrial membrane, uses the electrochemical gradient of sodium to transport Ca^{2+} out of the cell; while PMCAs require energy in the form of ATP for transport (Berridge *et al.*, 2003; Sharma and O'Halloran, 2014;

Krebs *et al.*, 2015). Ca^{2+} is also tightly controlled by the intracellular compartments and mainly stored in the ER. Ca^{2+} is pumped into the ER by the sarco ER Ca^{2+} ATPase (SERCA) an ATP dependant reaction and is released mainly through the Inositol trisphosphate receptor (IP_3R) and the ryanodine receptor (RYR) (Berridge *et al.*, 2003; Krebs *et al.*, 2015). The other major intracellular stores are the mitochondria, where the Ca^{2+} levels are increased through the mitochondrial calcium uniporter (MCU) and reduced through the NCX. Ca^{2+} at extreme concentrations can cause the opening of the mitochondrial permeability transition pore (MTPT) which will release Ca^{2+} to the cytosol (Lemasters *et al.*, 1998).

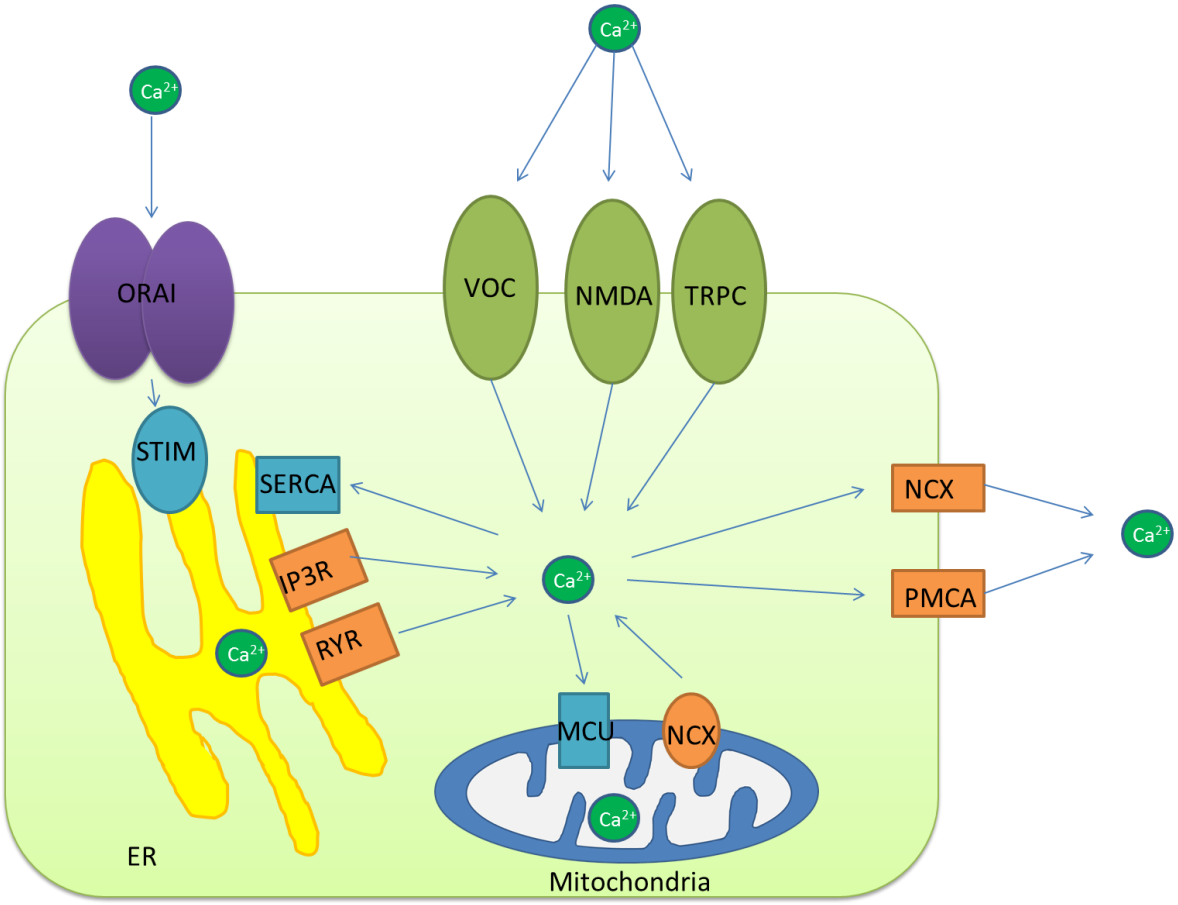

Figure 1.2 Regulation of cytoplasmic Ca2+. Schematic describing the main pathways for the regulation of cytosolic Ca2+ modified from (Krebs *et al.*, 2015)

The MCU and the NCX have higher capacities for Ca^{2+} transport making them important in the regulation of high dynamic ranges of Ca^{2+} concentrations. This makes the mitochondria an important regulator in cytosolic Ca^{2+} levels at high levels. It has been observed that the mitochondrial uptake is much higher at concentrations over 300nM of cytosolic Ca^{2+} (Collins *et al.*, 2001). The PMCA and SERCA pumps have a much higher affinity but lower capacity for Ca^{2+} making them important in the tight regulation of basal levels and coping with small

increases. The SOCE acts as the high capacity pump for refilling the endoplasmic reticulum. When low Ca^{2+} levels are detected in the ER by stromal interacting molecule (STIM) proteins: the STIM protein will interact with ORAI (a SOCE) causing Ca^{2+} to enter the ER through the plasma membrane (Roos *et al.*, 2005; Prins *et al.*, 2011) . This process is also negatively regulated by the protein SARAF in order to prevent dangerously high levels of Ca^{2+} (Palty *et al.*, 2012) . Alongside these sensors of Ca^{2+} levels are a whole host of other sensors and buffers that bind calcium in order to regulate free Ca^{2+}. One such sensor is BiP; also known as GRP78 or HSPA5, which alongside its role in buffering Ca^{2+} acts to help post translationally modify proteins, a key function of the ER.

1.1.3 Unfolded Protein Response/ER Stress Response

The ER is a key organelle in the post translational modification of proteins. Approximately one-third of all cellular proteins will be translocated to the ER lumen in which they will undergo post-translational modifications (Kaufman, 1999). Post translational modifications include formation of disulfide bonds, folding, glycosylation, proteolytic cleavages and oligomerization. The lumen of the ER is an oxidised environment that contains numerous chaperones in order to help facilitate proper folding of proteins (Kaufman, 1999). If proteins are misfolded they are targeted by the ubiquitin pathway for degradation (Claessen *et al.*, 2012). Changes in ER homeostasis can lead to the accumulation of unfolded proteins. The unfolded protein response (UPR) also known as the ER stress response is a mechanism to correct ER function or push the cell towards apoptosis if corrections cannot be made. There are three pathways that will be activated during ER stress: Inositol-requiring enzyme 1 (IRE1), Protein kinase R (PKR)-like endoplasmic reticulum kinase (PERK) and Activating transcription factor 6 ATF6, all three are regulated by BiP also known as GRP78 (Figure 1.3) (Bertolotti *et al.*, 2000; Shen *et al.*, 2002). The activation of the three pathways is caused by the dissociation of BiP from IRE1, PERK and ATF6, caused by an increase in misfolded proteins in the ER (Bertolotti *et al.*, 2000). IRE1 and PERK, when released will form oligomers in the ER membrane which activate a number of downstream signalling pathways to alleviate ER stress. ATF6 is slightly different in the fact that BiP blocks a Golgi localisation signal and when BiP dissociates ATF6 localises to the Golgi were it is cleaved and becomes active.

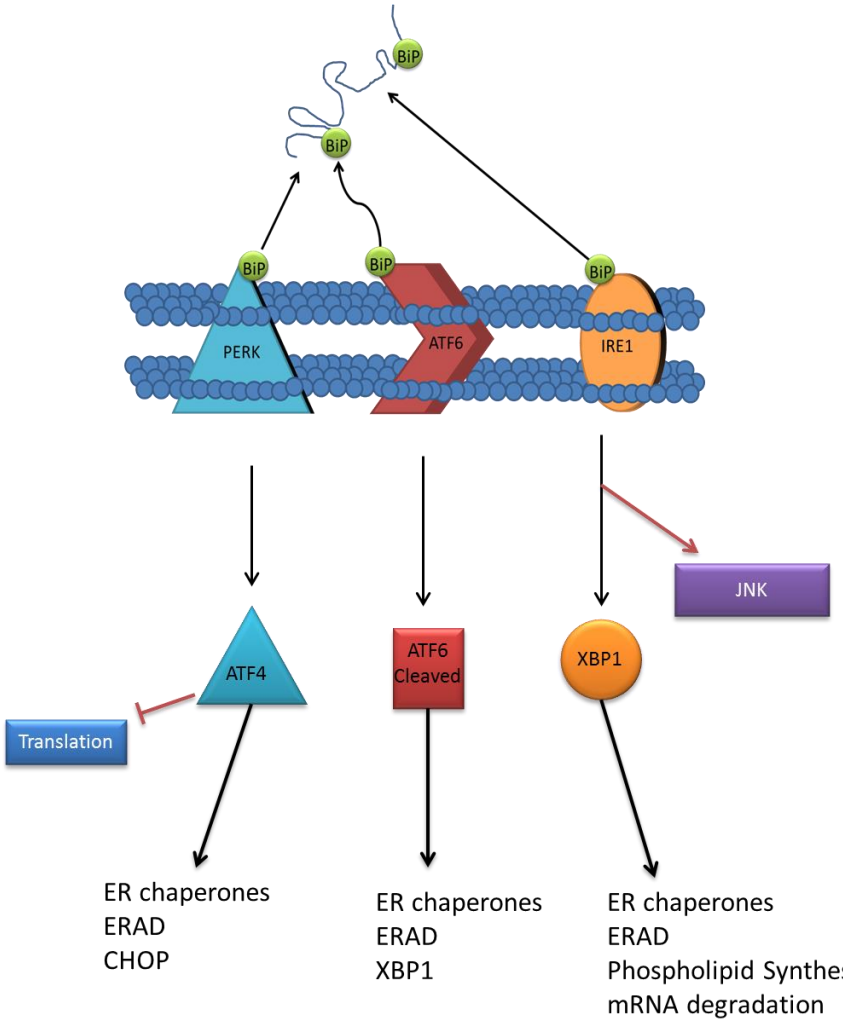

Figure 1.3 The Unfolded Protein Response. The three pathways of the UPR and the main downstream effects of each pathway.

IRE1 has two homologues IRE1α/β. After oligomerization IRE1α cleaves X-box binding protein 1 (XBP1) RNA which produces an active form of XBP (XBPu). IRE1β cleaves the 28S ribosome RNA which will lead to a reduction of translation (Iwawaki *et al.*, 2001). XBP is a transactivator which causes the upregulation of a number of genes reducing protein production and reversing ER stress (Bravo *et al.*, 2013). IRE1α also upregulates the c-Jun N-terminal kinases (JNK) which is involved in both cell survival and apoptotic pathways (Liu and Lin, 2005).

As with IRE1, when BiP dissociates with PERK it forms oligomers to produce their downstream signalling effects. PERK activation causes the phosphorylation and activation of eIF2α. This in turn activates ATF4. In combination these two factors reduce protein expression in cell undergoing ER stress (Harding *et al.*, 2000). ATF4 also upregulates CCAAT-enhancer-binding protein homologous protein (CHOP) expression, CHOP is a pro-apoptotic

factor which will eventually lead to apoptosis if homeostasis is not restored (Fawcett *et al.*, 1999). PERK activation also activates Nuclear factor (erythroid-derived 2)-like 2 transcription factor (Nrf2) which has an opposite role in cell survival (Cullinan *et al.*, 2003).

ATF6, like IRE1, has two isoforms ATF6α and ATF6β. Both are transported to the Golgi after dissociation by vesicles by the COPII protein (Schindler and Schekman, 2009). In the Golgi ATF6 is cleaved by Sphingosine-1-phosphate (S1P) and Sphingosine-2-phosphate (S2P) proteases (Shen and Prywes, 2004). Both isoforms go on to produce opposite effects. ATF6α when cleaved localises to the nucleus where it upregulates numerous proteins involved in regulating the ER stress response such as BiP (Thuerauf *et al.*, 2004). The ATF6β subunit appears to have a role in the regulation of the strength of the ATF6α response (Thuerauf *et al.*, 2004).

The ER removes unfolded proteins through two main pathways. The ER-associated protein degradation (ERAD) and autophagy. ERAD involves the retrotranslocation of misfolded proteins to the cytoplasm for ubiquitination by E3 ligase followed by degradation by the proteasome (Ruggiano *et al.*, 2014). The IRE1-JNK pathway is activated in response to ER stress and is responsible for the upregulation of autophagy (Ogata *et al.*, 2006). Autophagy is a more general degradation pathway and uses endolysosomal degradation to remove misfolded proteins, pathogens or dysfunctional organelles such as mitochondria.

1.1.4 Mitochondria Associated Membrane (MAM)

The ER and mitochondria interact at specialised locations named MAMs (Franke and Kartenbeck, 1971; Vance, 1990). These areas are where the two membranes of the two organelles are in close proximity (10–25 nm) but do not fuse (Csordas *et al.*, 2006). This domain is important for the two organelles and is involved in processes such as lipid biosynthesis, mitochondrial division, Ca^{2+} signalling and the regulation of dynamics of organelles (Rowland and Voeltz, 2012).

1.2 Mitochondria

The mitochondria are organelles that evolved by endosymbiosis of an alphaproteobacterium into a precursor eukaryotic cell. This addition of mitochondria has allowed eukaryotes to develop much more complex genomes with 200,000-fold more genes being expressed (Lane and Martin, 2010).This is due to the heavy selection pressure to remove extra DNA from prokaryotes due to the energy expenditure (Lane and Martin, 2010). The

alphaproteobacterium have been simplified with a large transfer of the mitochondrial DNA (mtDNA) across to the eukaryotic genome, it is thought that a large number of these genes have been replaced and that modern eukaryotes share few common genes with the alphaproteobacterium but most eukaryotic mitochondria contain their own genome (Huynen *et al.*, 2013; Karnkowska *et al.*, 2016). These modifications were thought to have occurred largely before eukaryotic radiation suggesting their importance in the increasing complexity of eukaryotic organisms (Huynen *et al.*, 2013). The mitochondria primary function is to produce ATP through oxidative phosphorylation (OXPHOS). The mitochondria also have a number of other roles including ROS signalling, metabolism, lipid synthesis, Ca^{2+} homeostasis, apoptosis and the production of iron sulphur clusters alongside other functions (Schmidt *et al.*, 2010).

1.2.1 Structure

As mitochondria have evolved from bacteria they maintain their separate double membrane structure with an outer (OMM) and inner membrane (IMM) separated by the inter membrane space (IMS). The outer membrane is contains many pore forming proteins which makes the OMM permeable to molecules smaller than 5kDa (Dukanovic and Rapaport, 2011). 30 different proteins were described as being localised to the OMM in yeast, predominantly involved in pore formation, protein import and mitochondrial dynamics (Schmitt *et al.*, 2006; Zahedi *et al.*, 2006). The IMM is impermeable to most of the small ions which allows for an electrochemical gradient to be produced which is utilised in OXPHOS. The IMM is folded into cristae. The IMM contains a large number of proteins responsible for the majority of important processes of the mitochondria: OXPHOS, protein import, morphology, translation, iron–sulphur cluster biogenesis, and protein degradation (Zahedi *et al.*, 2006). The IMM encircles the mitochondrial matrix where a number of important functions are carried out and the mitochondrial DNA is maintained.

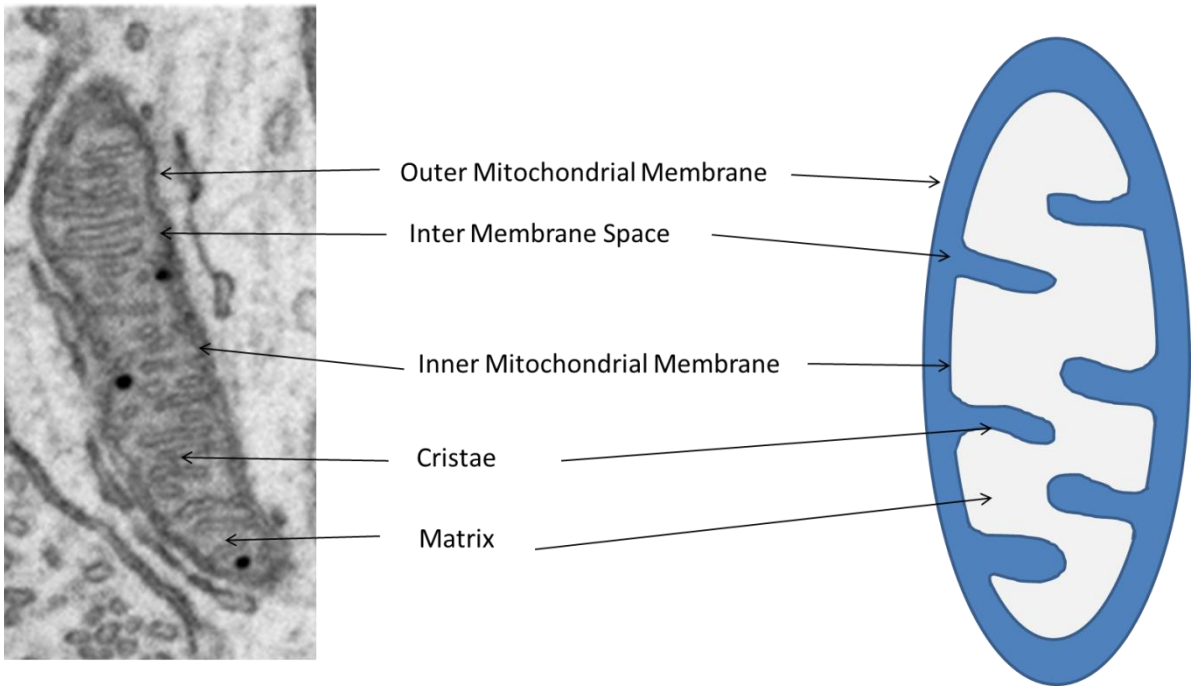

Figure 1.4 Structure of Mitochondria. Electron microscope image of a mitochondrion alongside a cartoon to better discriminate between structures. EM image taken from (Wu *et al.*, 2017)

1.2.2 mtDNA

mtDNA can vary significantly between eukaryotes with genomes found coding for 1 gene up to 100 (Karnkowska *et al.*, 2016; Lavrov and Pett, 2016). However, the number of proteins found in mitochondria are larger than the number expressed on the mtDNA (mitochondria in saccharomyces contain ~1000 proteins and mammals ~1500). The majority of mitochondrial genes are contained in the nucleus and the proteins transported to the mitochondria through protein import (Reinders *et al.*, 2006; Meisinger *et al.*, 2008).

In humans mtDNA is a circular, double-stranded DNA molecule approximately 16569 bp in length (Andrews *et al.*, 1999). The strands can be distinguished by the guanine rich heavy strand and the cytosine rich light strand. The genes are efficiently organised with no introns, one regulatory region and intergenetic sequences can overlap or separated by a few base pairs (Taanman, 1999). mtDNA codes for 37 genes: 2 genes encode the mitochondrial ribosomal subunits (a 16s and a 12s subunit); 24 genes encode tRNA molecules and the remaining 13 OXPHOS subunits (Chinnery and Hudson, 2013).

Mitochondria generally contain several copies of mtDNA (Taanman, 1999). The majority of the sequences will be identical but populations of mtDNA can be mixed referred to as heteroplasmy. A number of factors including oxidative damage and inefficient mtDNA repair

a number can contain mtDNA mutations(Chinnery and Hudson, 2013). Aging humans have increased levels of somatic mtDNA mutations suspected to be linked with respiratory chain dysfunction in ageing (Larsson, 2010). Inheritance is thought to be maternal. However, a number of cases of biparental inheritance have been discovered (Luo *et al.*, 2018).

1.2.3 Oxidative Phosphorylation

OXPHOS is the process in which mitochondria convert ADP to ATP. This process involves the five respiratory complexes (Complex I-V) as well as two electron shuttles, ubiquinone and cytochrome c. These complexes are embedded into the IMM as illustrated in Figure 1.5. Complexes I, III and IV transport H^+ ions from the matrix into the IMS and create an electrochemical gradient, this process is known as the electron transport chain (ETC). This gradient is utilised by complex V to convert ADP to ATP.

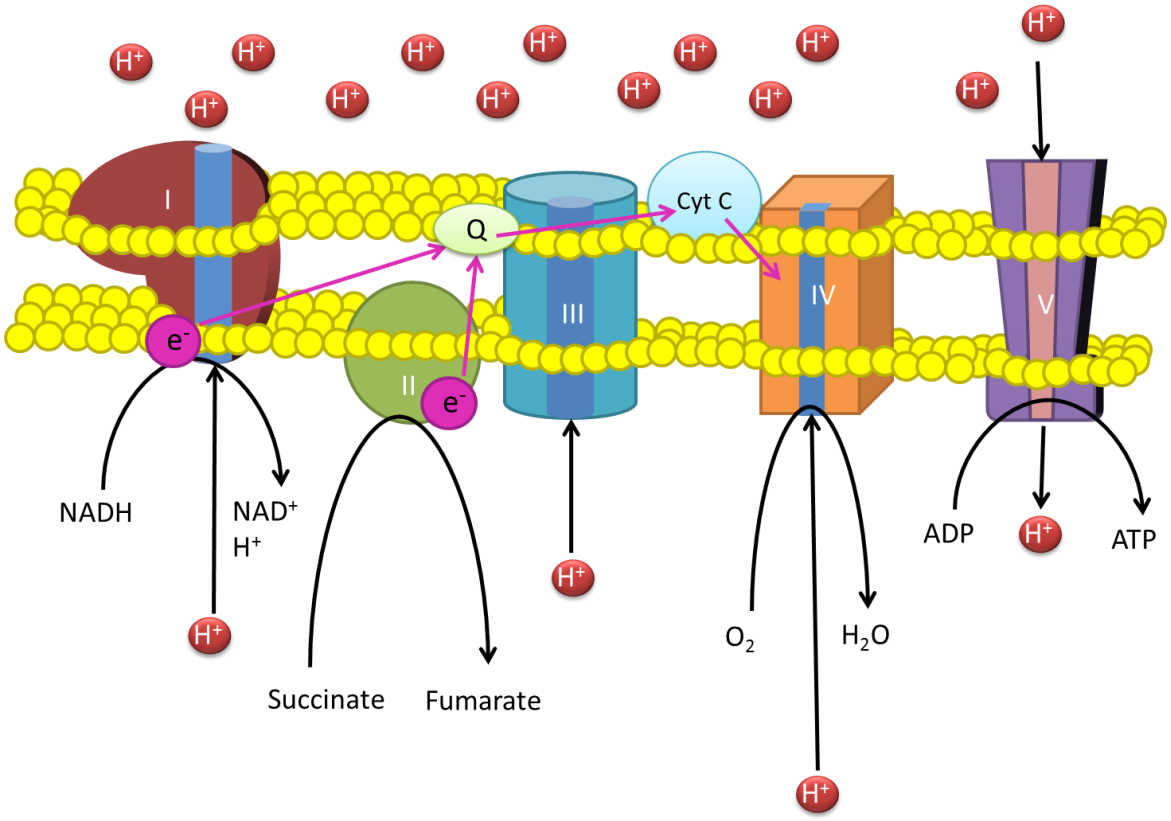

Figure 1.5 Mitochondrial OXPHOS. Schematic of electron transport and H+ ion transport through the mitochondrial OXPHS complexes.

1.2.4 Mitochondrial Complexes

The initial H^+ ion transport is powered by electron transfer from the entry points at complex I and II.

Complex I (NADH:ubiquinone oxidoreductase) contains 45 subunits 14 of these are highly conserved core subunits and 31 supernumerary subunits (Hirst, 2013; Zhu *et al.*, 2016). The core subunits form two key domains in complex I. The seven hydrophobic core subunits encoded by the mtDNA are involved in the transfer of the H^+ ions from the matrix to the IMS. The seven hydrophilic core subunits produce a redox domain for interacting with NADH (Vinothkumar *et al.*, 2014). The NADH interacts with a Flavin Mononucleotide which transfers the electrons along seven iron-sulfur clusters to be transferred to ubiquinone (Hunte *et al.*, 2010). Two H^+ ions are transferred across the membrane for every one electron. This represents around 40% of the H^+ ions moved across the membrane (Hunte *et al.*, 2010). Complex I also produces the majority of reactive oxygen species (ROS) from the ETC (Liu *et al.*, 2002; Hirst *et al.*, 2008). ROS are involved in a number of cellular signalling pathways but an over production can lead to damage of proteins and cell death so under physiological conditions these levels are tightly controlled (Zorov *et al.*, 2014). ROS can be produced at the NADH binding site but also at the ubiquinone binding site which acts as the electron shuttle between complex I and III.

Ubiquinone also known as Coenzyme Q is a fully substituted benzoquinone ring with a long polyisoprenyl tail which allows the molecule to be positioned in the midplane of the lipid bilayer with the head in the hydrophilic regions (Samori *et al.*, 1992). This allows Ubiquinone to accept electrons from complex I and II and transfer them to complex III.

Complex II (succinate dehydrogenase) is the only complex with no subunits produced from the mtDNA. The complex contains four subunits, a flavin-adenine dinucleotide (FAD); iron sulfur clusters and heme (Sun *et al.*, 2005). Complex II utilises succinate as a substrate which it converts to fumerate, this is an integral part of the tricarboxylic acid (TCA) cycle of aerobic respiration. Succinate transfers electrons to the FAD and like complex I, the electrons pass up the iron sulfur clusters and are transferred to ubiquinone. Unlike complex I this unit has no transmembrane domain to transfer H^+ ions to the IMS. ROS can also be produced by this complex at the ubiquinone binding site although under physiological conditions this effect is negligible. Complex II does also contribute to ROS production through reverse electron transfer, when high levels of succinate can be detected complex II through ubiquinone can transfer electrons back down the chain to complex I to produce ROS (Bezawork-Geleta *et al.*, 2017).

Complex III (cytochrome c reductase) contains 11 subunits (Schagger *et al.*, 1986). Three of these subunits are catalytically active, the first cytochrome b (mtDNA encoded) contains two b-type hemes and this subunit interacts with the ubiquinone. The second Rieske iron-sulfur protein contains an iron sulfur cluster that removes electrons from ubiquinone and transfers one to the third active subunit Cytocrome c_1. This transfers electrons to cytochrome c the seconded electron shuttle(Sousa *et al.*, 2018).

Cytochrome c is a 13 kDa globular and soluble protein which is predominantly found in the IMS. This shuttles the electrons from complex III to IV. Cytochrome c has other functions such as a prominent role in apoptosis when released from the mitochondria as well as less lethal roles such as platelet formation and monocyte differentiation (Ow *et al.*, 2008).

Complex IV (Cytochrome c oxidase) is the final proton pump in the ETC. It is composed of 14 different subunits three of which are encoded by mtDNA. Complex IV at its centre contains four redox-active metal cofactors, one of these factors Cu_A accepts electrons from cytochrome c which are transferred to an active site where they are converted to H_2O through an intermediary step where a hydroxide ligand is protonated to create H_2O. This reaction uses eight protons with four transferred across the IMM by complex IV and four converted to H_2O(Sousa *et al.*, 2018).

This transfer of H^+ ions creates the electrochemical proton motive force which drives ATP production by complex V. Complex V (F_1F_o ATP synthase) acts as a membrane embedded motor powered by H^+ ion movement from the IMS to the matrix (Noji *et al.*, 1997). Complex V is split into two regions F_0 which is embedded in the IMM which acts as the rotor and the F_1 region which binds the ADP (Abrahams *et al.*, 1994). The rotors movement powered by the H^+ ion movement causes conformational changes to complex V force ADP + Pi to ATP (Sousa *et al.*, 2018).

Complexes although initially thought to be independent have been observed existing as supercomplexes (Schagger and Pfeiffer, 2000). The supercomplexes found in in mammals are: complexes I_1III_2 and I_1III_2IV while complex V can exist in dimeric forms (Minauro-Sanmiguel *et al.*, 2005; Davies *et al.*, 2018). Although the function of respiratory supercomplexes is not fully understood it is suspected supercomplexes play a role in stability, ROS production and most importantly substrate channelling which creates more

efficient respiration (Vempati *et al.*, 2009; Lapuente-Brun *et al.*, 2013; Maranzana *et al.*, 2013).

1.2.5 Mitochondrial Dynamics

The mitochondria are highly dynamic organelles which undergo changes in fission and fusion and have the ability to move throughout the cell. The process of fusion increases the ATP production allows the sharing of metabolites and can prevent mitophagy (Chen *et al.*, 2005; Molina *et al.*, 2009; Gomes *et al.*, 2011). This process is mainly controlled (in mammals) by three proteins: Mfn1, Mfn2 and OPA1.

Mfn1 and Mfn2 are GTPase proteins which can be found in the OMM these tether two mitochondria together, when GTP binds it induces a conformational change and the two mitochondrial membranes are brought together and fuse (Tilokani *et al.*, 2018). OPA1 controls IMM fusion. OPA1 is cleaved into a short and long form (S and L-OPA) by alternative cleavage sites found on OPA1. Only L-OPA is required for fusion by interacting with cardiolipin on the opposing membrane bringing the two together (Ban *et al.*, 2017). While S-OPA is thought to be possibly involved in fission (Head *et al.*, 2009; Tondera *et al.*, 2009).

Mitochondrial fission is important in cell division, for dividing mitochondria between daughter cells and allowing mitochondria to undergo mitophagy - the process by which mitochondria are degraded by lysosomes (Farmer *et al.*, 2018). The ER is also involved in this process and fission occurs at points where ER tubules contacted mitochondria this reduces the mitochondrial width at this point to 150nm (Friedman *et al.*, 2011). This is possibly caused by the increase of Ca^{2+} uptake at the ER contact point (Chakrabarti *et al.*, 2018). The Drp1 protein then recruited to these constricted sites. Drp1 is a GTPase protein which is localised to the cytosol but can be recruited to mitochondria and peroxisomes when undergoing fission (Tilokani *et al.*, 2018). This constricts the mitochondria further at the cut points and is eventually cleaved by Dynamin 2 (Lee *et al.*, 2016).

In yeast mitochondria move along the actin cytoskeleton while in metazoan cells mitochondria are transported on microtubules powered by kinesin and dynein motors (Wang and Schwarz, 2009). This is to ensure mitochondria are distributed correctly throughout a cell, which can be for a number of reasons including: cell division, Ca^{2+} buffering, signalling or localised ATP production (Jayashankar and Rafelski, 2014). Mitochondria transport was initially thought to be important only for larger cells such as

neurons but recent evidence suggest knocking out important transport proteins in smaller cells has significant effects on mitochondrial morphology and cell function (Schuler *et al.*, 2017). Mitochondrial transport is control by different sets of motors depending on direction; towards the positive end of microtubules (anterograde) the kinesin-1 family controls movement. In the opposite direction (retrograde) dynein/dynactin maintain control (Yu and Pekkurnaz, 2018). These proteins bind to adaptor proteins Miro (a Rho GTPase) and Milton (TRAK1/2) which are localised to the mitochondria (Stowers *et al.*, 2002; Fransson *et al.*, 2006).

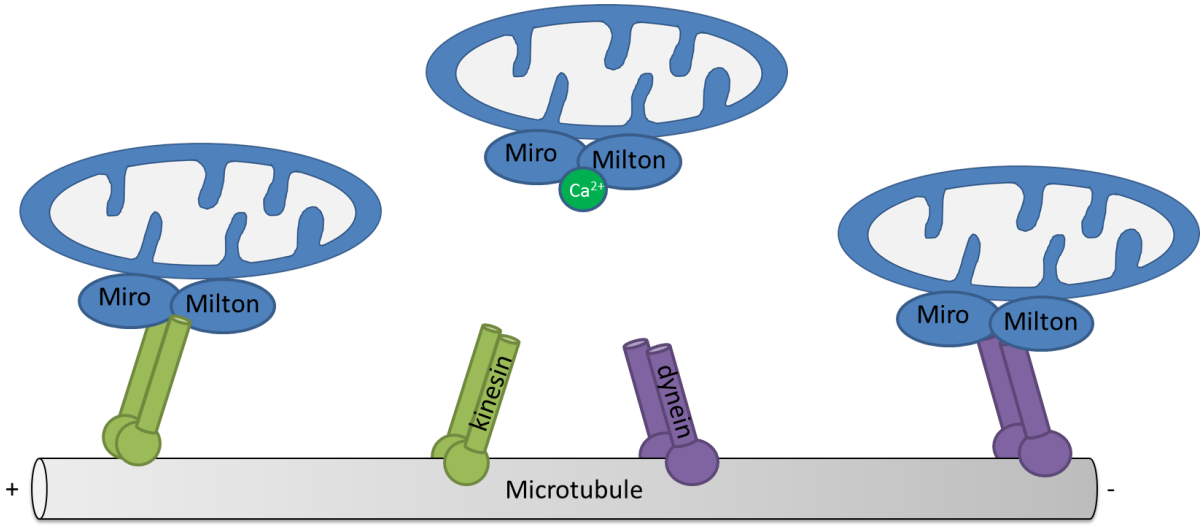

Figure 1.6 Mitochondrial Transport Along Microtubules. Mitochondria can be transported in then anterograde direction by kinesin motors and dynein motors the retrograde direction. This involves binding to the Miro Milton complex on the mitochondria which can be inhibited by Ca^{2+}.

This complex has a key role in the regulation of mitochondrial transport, as it binds the respective motors the majority of signalling pathways controlling trafficking will target this complex (Yu and Pekkurnaz, 2018). ROS can also modify motility by activating p38α which again targets the Miro Milton complex to prevent movement (Debattisti *et al.*, 2017). Metabolite availability is another factor that can control trafficking in high glucose levels Miro is glycosylated preventing any further movement ensuring the mitochondria are in the correct location for glucose utilisation (Pekkurnaz *et al.*, 2014). Cytosolic Ca^{2+} is also a regulator of this complex, it can bind to Miro modifying its shape and releasing it from motor proteins (Wang and Schwarz, 2009). This allows mitochondria to be in the correct location to act as a buffer for cytosolic Ca^{2+}

1.2.6 Calcium Flux

As described in 1.1.2 Calcium Ion Homeostasis the strict control of Ca^{2+} is necessary for cell survival and the mitochondria play an important role in this regulation. The mitochondria can buffer Ca^{2+} bound to phosphate as $Ca_3(PO_4)_2$. This is important in the control of cytosolic Ca^{2+} but a number of mitochondrial processes also depend on Ca^{2+} including steps in the TCA cycle (Pathak and Trebak, 2018). As the OMM is permeable to molecules smaller than 5kDa Ca^{2+} flows through these VDAC pores into the IMS. Ca^{2+} can enter the matrix of mitochondria through the mitochondrial calcium uniporter (MCU). This has a low affinity but high specificity for Ca^{2+} so requires a high localised Ca^{2+} concentration for entry into cell (Jiang *et al.*, 2009). This is achieved mainly through collaboration with the ER which can release Ca^{2+} localised to the mitochondria at MAMs demonstrated in Figure 1.7.

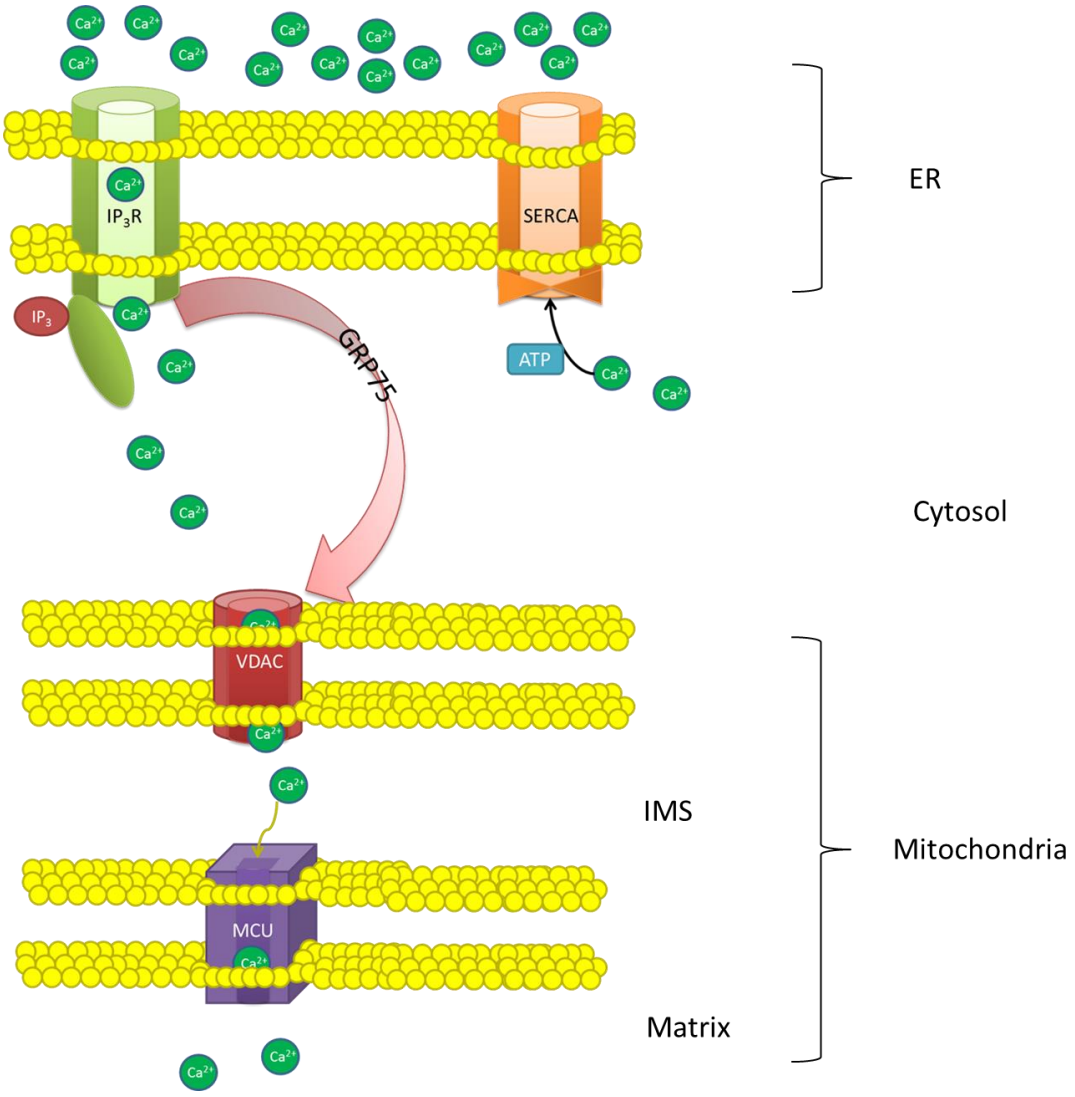

Figure 1.7 Calcium Flux from the ER to Mitochondria. Calcium flows from the ER through the IP3R to the mitochondria. A connection is made to the VDAC pore of the mitochondria by GRP75 and Ca^{2+} flows through to the matrix through the calcium specific MCU.

1.2.7 Mitochondrial Disease

As demonstrated a large number of important biological processes are affected by mitochondrial function. Due to mitochondrial importance in energy production as well as other mechanisms, dysfunction can be particularly damaging. This is especially the case in high energy tissues such as the CNS, the heart, muscles and eyes. (Chinnery and Hudson, 2013). Patients with mtDNA mutations or nuclear mutations effecting mitochondria can display a variety of phenotypes with limited treatment options.

1.3 The Retina and Optic Nerve

The retina has a number of high energy cells that may be susceptible to mitochondrial dysfunction. The retina is largely conserved through vertebrates containing similar cell types (described in Figure 1.8). Light enters the eye and interacts with the photoreceptors (the rods and cones) which transmits signals through the retina to the retinal ganglions cells (RGCs) which signal through to the brain along the optic nerve.

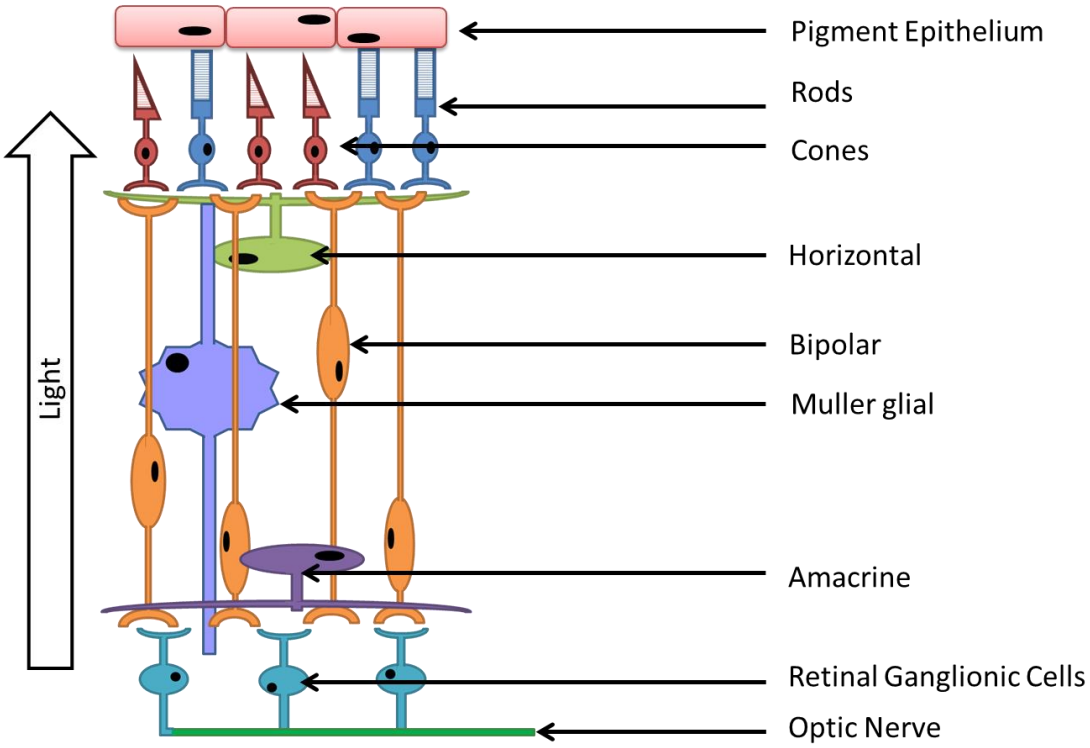

Figure 1.8 Retinal Structure. Cells found within the retinal and basic organisation.

1.3.1 Retinal Structure

The rods are the more sensitive photoreceptors that are important for low light vision as these can detect even a single photon (Sampath and Rieke, 2004). The cones are much less sensitive but have a faster signalling response, they are also more sensitive to colour so are

useful for bright colour vision (Hoon *et al.*, 2014). The cone cells can also be specific for different wavelengths of light. This can vary between species while humans have three short (λ~415–430nm (blue)), middle (λ~530–537nm (green)) or long (λ~555–565nm (red)) (Mustafi *et al.*, 2009). Zebrafish have an extra UV cone while mice only contain short and medium cones (Applebury *et al.*, 2000; Li *et al.*, 2009). Rods and cones signal to bipolar and horizontal cells by the release of glutamate. The release of this neurotransmitter is controlled by the depolarization of the cell. Photons activate rhodopsin in the photoreceptors this activates G-protein signalling which hyperpolarizes the plasma membrane reducing glutamate signalling (Mustafi *et al.*, 2009).

This signal sent is received by horizontal or bipolar cells. Horizontal cells mediate feedback inhibition to photoreceptors and are able to feedforward inhibition to bipolar cells (Diamond, 2017). Bipolar cells can exist as ON or OFF bipolar cells which react in opposite manners to glutamate. In OFF cells glutamate opens a cation channel which depolarises the cell while ON cells hyperpolarise (Mustafi *et al.*, 2009). Rod bipolar cells are always ON while cones can be either. This signals to RGCs either directly or indirectly through amacrine cells. The amacrine cells can synapse and stimulate with RGCs, other bipolar cells or form inhibitory signals with other amacrine cells (Diamond, 2017).

The RGCs will send the signal to the brain there are around 30 different types of ganglion cells with multiple functions relating to different visual cues (Sanes and Masland, 2015). The axons of the RGCs connect the eye to the brain along the optic nerve.

1.3.2 Optic Nerve Anatomy

Approximately 1 million RGC axons form the optic nerve in humans which carry visual cues from the RGCs which synapse with neurons in the lateral geniculate nucleus (Yu *et al.*, 2013). From here signals are sent to the visual cortex which processes the signals from the visual cues. These axons, in mammals, begin unmyelinated from the RGC cell bodies and become myelinated after lamina cribrosa (Yu *et al.*, 2013). Myelination of axons insulates the nerve allowing for enhanced speed of nerve impulse conduction and decreases the energy expenditure needed for electrical impulses (Hartline, 2008). Due to the high energy expenditure of these RGCs they become affected by disorders of energy production.

1.4 Wolfram Syndrome

Wolfram syndrome (WS) was first described in 1938 by Wolfram and Wagener (Wolfram DJ, 1938), who described symptoms of juvenile diabetes and optic atrophy. Since the initial discovery of WS, the symptom spectrum has expanded and now includes diabetes insipidus, diabetes mellitus, optic atrophy and sensorineural deafness (also defined as DIDMOAD). Approximately 30% of patients will present with the full DIDMOAD phenotype (66.26% when considering patients with 4 or clinical features) and as it is a progressive disease a large number of disorders can develop over a patient's life span including: ataxia, peripheral neuropathy, urinary tract dysfunction and psychiatric illnesses alongside numerous other conditions shown in Table 1.1 (de Heredia *et al.*, 2013; Urano, 2016)

Table 1.1 Symptoms Associated with Wolfram Syndrome Adapted from Urano 2016

Major Symptoms	Common Symptoms
Diabetes Mellitus	Fatigue
Optic Nerve Atrophy	Hypersomnolence
Diabetes Insipidus	Apnea
Sensorineural Deafness	Dysphagia
Ataxia	Headaches
Urinary Tract Dysfunction	Reduced sense of smell
	Reduced ability to taste
	Anxiety
	Panic attacks
	Depression
	Mood swings
	Temperature regulation dysfunction
	Dizziness
	Constipation
	Diarrhea
	Hypergonadism
	Hyponatremia

Diabetes mellitus is commonly the first symptom with 98.2% of patients developing this on average in the first 10 years of life. Then 82.14% of patients will develop optic atrophy

around 11. 48.21% develop hearing loss; 37.76% Diabetes insipidus; 19.39% Urinary tract; and 17.09% normally after the development of the first two symptoms (Barrett *et al.*, 1995; de Heredia *et al.*, 2013). The range of symptoms varies in patients but the majority will have both diabetes mellitus and optic atrophy.

An autopsy of a DIDMOAD patient revealed a loss of pancreatic β-islet cells contributing to diabetes mellitus (Hilson *et al.*, 2009). Loss of RGCs and neurons in the retina, neuronal loss in the optic nerve tract and lateral geniculate nucleus contribute to the loss of vision in patients (Hilson *et al.*, 2009). In the ear hair cells in the basal turn of both cochleae were lost as well as the organ of Corti. In the brain neuronal loss was recorded in a number of areas including the thalamus olivopontocerebellar system (Hilson *et al.*, 2009).

Neurodegeneration is a key feature of WS where patients die at a median age of 30 due to respiratory failure with brain stem atrophy (Barrett *et al.*, 1995). Changes in brain volume and myelination have been been described in patients highlighting the role of neurodegeneration in WS (Hershey *et al.*, 2012; Lugar *et al.*, 2016).

WS is a rare disease with an incidence of 1:770 000 and a carrier prevalence of 1:354, in the UK (Barrett *et al.*, 1995). The prevalence in children was found to be 1 in 500 000 and the prevalence is variable worldwide. Other estimates include 1 in 68 000 in Lebanon, 1 in 100,000 in the USA and 1 in 710,000 in Japan (Kinsley *et al.*, 1995; Medlej *et al.*, 2004; Matsunaga *et al.*, 2014)

1.4.1 Wolfram Syndrome 1

1.4.2 The WFS1 Gene

The majority of patients with WS harbour recessive mutations within the *WFS1* gene, which encodes for the Wolframin protein. Although initially suspected to be a mtDNA mutation it was observed through linkage analysis to be autosomal and that the gene is located on chromosome 4 (Inoue *et al.*, 1998; Strom *et al.*, 1998).

There is no single mutational hotspot within the *WFS1* gene although 178 different mutations have been reported they are distributed nonuniformly along the protein: a higher concentration can be found in transmembrane domains, the last the last 100 amino acids and between amino acids 94–237. However, it has been described that mutations in the last

few amino acids provided a full DIDMOAD phenotype suggesting important functional domains throughout the protein (Sam *et al.*, 2001).

Although *WFS1* mutations are generally recessive, dominant mutations have been observed and have been linked with Wolfram like syndrome where patients tend to develop visual and hearing impairment (Fukuoka *et al.*, 2007; Hogewind *et al.*, 2010; Rendtorff *et al.*, 2011; Berry *et al.*, 2013).

1.4.3 Wolframin

The Wolframin protein localises in the endoplasmic reticulum (Takeda *et al.*, 2001), in a proteomic profiling of the MAMs in mouse brains wolframin was detected suggesting it may be important in ER mitochondrial connections (Poston *et al.*, 2013). Wolframin contains 9 transmembrane domains with the c-terminus in the endoplasmic reticulum lumen and the n-terminus in the cytosol, a schematic can be seen in Figure 1.9 (Hofmann *et al.*, 2003).

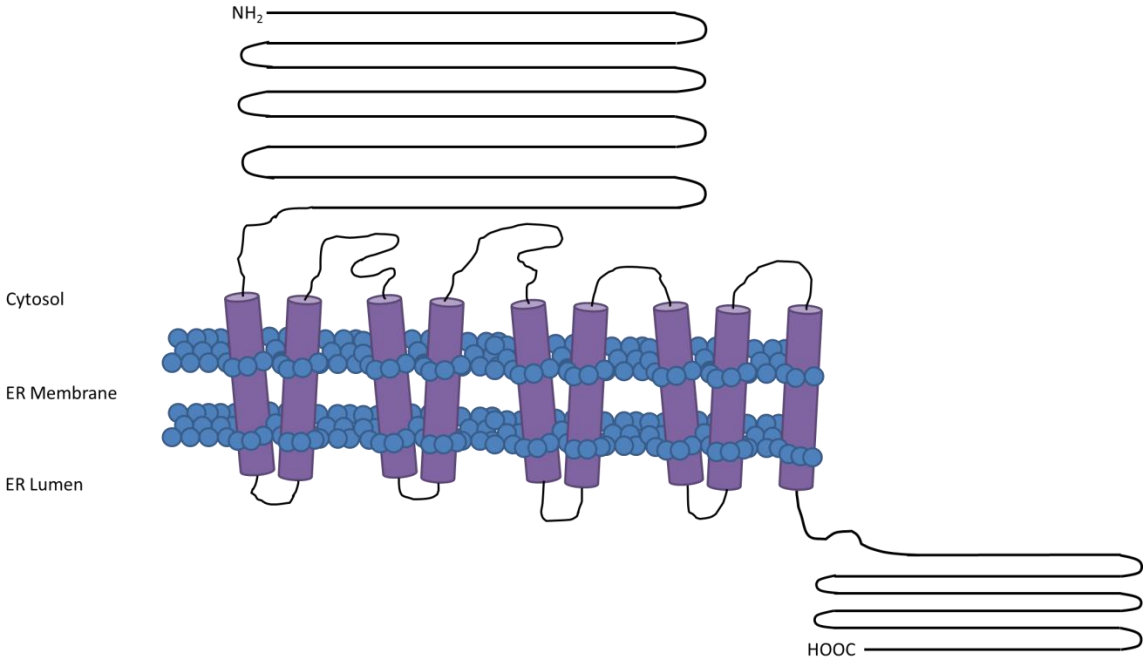

Figure 1.9 Structure and Localisation of Wolframin. Adapted from Hofmann *et al* 2003.

The protein is 890 amino acids in length corresponding to around 100 kDa; higher weight complex in the ER of around 400 kDa have been described in the membrane which are suspected to be a homo-oligomeric complex (Hofmann *et al.*, 2003). The protein is post translationally modified by N-glycosylation. This is required for protein to be stably expressed and Hofmann. *et al* suggest the glycosylation is important in the proteins stability or required for stability or proper synthesis of the protein (Hofmann *et al.*, 2003). The

human tissue atlas describes wolframin expression to be ubiquitous by RNA expression but did not show expression in all tissues when looking on a protein level (Uhlen *et al.*, 2010). This was also observed histologically were alongside expression in multiple adult tissues an almost ubiquitous expression in human foetal organs and tissues was observed (De Falco *et al.*, 2012). In the adult tissue expression appears to be variable depending on tissue types with the highest levels of expression of the protein found in the tissues responsible for some of the phenotypes of WS e.g. brain and pancreas, RGCs (Schmidt-Kastner *et al.*, 2009). The protein is thought to have multiple functions in important cellular mechanisms including regulation of the ER UPR, calcium ion homeostasis and pro-insulin modification among others.

1.5 Functions of Wolframin

1.5.1 Proinsulin Modification

Diabetes mellitus is the most common phenotype seen in WS. In patients with WS a loss of Insulin-producing β-cells is seen with no autoimmune process as seen in traditional type 1 diabetes suggesting a genetically encoded β-cell loss (Karasik *et al.*, 1989). The mechanism behind this has been suggested to be due to two main causes: apoptosis of islet cells and impaired insulin secretion. This was observed in a knockout mouse model were increased apoptosis and β-cell loss at 24 weeks with an increase in ER stress response markers BiP and CHOP has been described. However, prior to this at 12 weeks the mice had an impaired glucose-stimulated insulin secretion (Riggs *et al.*, 2005). This suggested that there may be a secretory defect alongside the apoptosis. This was confirmed by wolframin localizing to secretory granules and determines granule acidification in mouse pancreatic β-cells. Further work confirmed that wolframin had a role in stabilising Vacuolar-type H^+-ATPase V1A subunit in neuroblastoma cells leading to a failure in acidification of secretory granules (Gharanei *et al.*, 2013). It was suggested this could be having an effect on the insulin secretory granules acidification which is necessary for converting proinsulin to its active form (Hatanaka *et al.*, 2011). Increased apoptosis due to ER stress is the key factor in the development of diabetes mellitus (Riggs *et al.*, 2005; Gharanei *et al.*, 2013).

1.5.2 Unfolded Protein Response

Wolframin expression has been shown to be regulated by the upstream regulators of the UPR IRE1, PERK and ATF6β (Yamaguchi *et al.*, 2004; Odisho *et al.*, 2015). The protein

contains a highly similar sequence to the to the ER stress response element (ERSE) and its protective role in islet cells suggested the protein had a downstream regulatory role in the UPR (Kakiuchi *et al.*, 2006). It was later shown that Wolframin was negatively regulating ATF6α in islet cells through ubiquitination and proteasome-mediated degradation of the protein. This was by two mechanisms the stabilisation of the E3 ubiquitin ligase HRD1 and the trafficking of ATF6α to the proteasome (Fonseca *et al.*, 2010). This suggested that due to the lack of regulation of ATF6 was leading to chronic activation of ATF6α signalling; pushing the cells towards apoptosis through the CHOP pathway. However, it is also possible that dysregulation of Ca^{2+} ions may be one of the factors leading to apoptosis.

1.5.3 Calcium Homeostasis

It was suggested that due to mild similarities to the TRP-caspasin channel family that ion homeostasis could be a function of wolframin (Osman *et al.*, 2003). This was tested in Xenopus oocytes which showed wolframin is associated with ion channel activity in the ER membrane suggesting wolframin acted like a TRPV channel and its expression altered cytosolic calcium levels (Osman *et al.*, 2003). However, they were not able to show directly that wolframin acted as a Ca^{2+} channel and suggested it could be possible that it was regulating ER calcium channel activity. This was added to in HEK293 cells showing regulation of the filling of the ER by store-operated Ca^{2+} entry and interestingly showed that the changes seen in cytoplasmic Ca^{2+} levels were not due to changes in mitochondrial Ca^{2+} uptake (Takei *et al.*, 2006). Co-immunoprecipitation experiments in Cos-7 cell lines showed an interaction with wolframin and SERCA. It was shown that wolframin was negatively regulating SERCA expression by targeting SERCA for degradation by the proteasome in a similar manor to ATF6 (Zatyka *et al.*, 2015). It was also hypothesised that regulating SERCA expression was in order to compensate for ER calcium depletion in conditions of ER stress (Zatyka *et al.*, 2015).

It was suggested however, that SERCA may not been the key component in the regulation of cytosolic Ca^{2+}. It has been suggested that changes in ER stress leads to inositol 1,4,5-trisphosphate receptor (IP_3R) dysfunction which in turn is affecting the cytosolic Ca^{2+} levels. (Cagalinec *et al.*, 2016). It was hypothesised that the Ca^{2+} changes could be altering mitochondrial function.

1.5.4 Calpain Activation

Calpain hyperactivation has been implicated as a possible cause for neurodegeneration in WFS1 knockout mice (Lu *et al.*, 2014). Calpain is a calcium dependant protease localised to the cytosol. As an increase in cytosolic Ca^{2+} leads to the hyperactivation of Calpain in knockout mouse brains which leads to cleavage of the myelin basic protein (MBP) (Lu *et al.*, 2014). This may explain the loss of myelination in patients with WS (Lugar *et al.*, 2016).

1.5.5 Cell cycle

WFS1 is also involved in cell cycle regulation. In *WFS1* knockout β-cells BrdU incorporation was decreased suggesting a reduction in cell cycle progression and division. Alongside this p21 a cell cycle regulating protein was upregulated (Yamada *et al.*, 2006). Cell cycle disruption was also found in *WFS1* depleted neuroblastoma cells. However, p21 expression was downregulated (Gharanei *et al.*, 2013). Cell cycle regulation and p21 expression could be partially rescued by overexpressing BiP suggesting an increase in ER stress is slowing cell cycle progression (Gharanei *et al.*, 2013).

1.5.6 Evidence for Mitochondrial Dysfunction

Initially WS was considered a mitochondrial disease as it was thought the phenotypes were consistent with an ATP supply defects (Bu and Rotter, 1993; Vora and Lilleyman, 1993). The evidence was also added to by the discovery of multiple mtDNA deletions and polymorphisms (Pilz *et al.*, 1994; Barrientos *et al.*, 1996). When looked at on a larger scale at the changes in the mtDNA they found no evidence supporting a role for mtDNA in Wolfram syndrome (Barrett *et al.*, 1995; Barrett *et al.*, 2000). No abnormal mitochondrial respiratory function was detected in 5 patients muscle biopsies (Barrett *et al.*, 2000). This added with the evidence of endoplasmic reticulum localisation and a role in ER stress response made it appear as though mitochondrial dysfunction was not a primary cause of WS. This idea was disputed when the *WFS1* gene was knocked down in HEK cells and this caused the activation of genes related to mitochondrial dysfunction again bringing into question the role mitochondria play in WS (Koks *et al.*, 2013). More evidence for mitochondrial dysfunction was seen in mitochondrial trafficking in knockdown cultured rat/mouse neurons, which was argued could be caused by disturbed cytosolic Ca^{2+} homeostasis (Cagalinec *et al.*, 2016). Wolframin was observed by proteomic profiling to be found in the mitochondrial associated membrane (Poston *et al.*, 2013). This could be causing changes in the Ca^{2+} dynamics

between the two organelles and is a possible link between WS and Wolfram syndrome type 2 caused by mutations in different gene (CISD2).

1.6 Wolfram Syndrome Type 2

A second gene was identified in 16 Jordanian consanguineous families (El-Shanti *et al.*, 2000). The patients presented similar symptoms to WS with optic atrophy, diabetes mellitus and high-frequency sensorineural hearing loss. This gene *CISD2*, also known as Miner1. The encoded protein is localised to the endoplasmic reticulum but has no direct interaction with wolframin (Amr *et al*., 2007). The protein is known to have a role in Fe-S management, redox reactions, Ca^{2+} homeostasis, Calpain regulation and has a role in the regulation of ER–mitochondrial contacts (Conlan *et al.*, 2009; Lu *et al.*, 2014; Rouzier *et al.*, 2017a). A knockout mouse model of *CISD2* has been created which showed mitochondrial dysfunction and a premature aging phenotype (Chen *et al.*, 2009). These obvious mitochondrial connections with no interaction with *WFS1* may suggest similar downstream pathways are effecting in these two diseases with similar phenotypes.

1.7 Treatment

No treatment is currently available to prevent or reverse the effects of WS (Urano, 2016). Two candidates suspected to be able to improve the symptoms of WS are: sodium valproate and dantrolene. Sodium valproate is expected to increase p21 expression which is reduced in *WFS1* knockdown cells (Gharanei *et al.*, 2013). Dantrolene a target of the ryanodine receptor suppresses leakage of calcium from the ER to cytosol to prevent Calpain hyperactivation (Lu *et al.*, 2014) . As WS has multiple diverse phenotypes and possibly multiple pathways that may be responsible for symptoms, multiple drugs may have to be prescribed to counteract *WFS1* depletion. Animal models are important in discovering more about the disease as well as trialling drug treatments.

1.8 Animal Models of Wolfram Syndrome

WS has been modelled in several animal models. Mouse, rat and drosophila models have been created of *WFS1* knockouts (Ishihara *et al.*, 2004; Plaas *et al.*, 2017; Sakakibara *et al.*, 2018). The gene identity and its similarities to the human gene are described in Table 1.2

Table 1.2 Gene identity of WFS1 with orthologues of published animal models of WS. Data acquired from ensembl.

Species	Orthologue	Target % identity
Fruitfly (Drosophila melanogaster)	wfs1 (FBgn0039003)	22.86%
Mouse (Mus musculus)	Wfs1 (ENSMUSG00000039474)	86.97%
Rat (Rattus norvegicus)	Wfs1 (ENSRNOG00000005108)	86.29%

1.8.1 Mouse

The mouse model of WS was the first animal model, and multiple models have been developed. The majority of work focussed on the development of diabetes and ER stress. The original knockout mouse developed glucose intolerance while demonstrating a progressive β-cell loss (Ishihara *et al.*, 2004). An islet cell specific knockout also demonstrated glucose intolerance and insulin deficiency with a loss of beta cell mass. Expression of BiP was also increased and changes to the ER and decreased secretory granules where observed using electron microscopy (Riggs *et al.*, 2005). The *Wfs1* knockout mice however do not develop a severe diabetic phenotype as humans. The *Wfs1* KO mice have normal non-fasted blood glucose levels and is suggested they were clearing blood glucose through the urine to maintain normal glucose levels (Terasmaa *et al.*, 2011). Additional investigation into other symptoms of WS have been assessed.

The expression of *Wfs1* in the CNS has been described and expression was observed in areas associated with emotional behaviour, energy homeostasis, and hearing (Luuk *et al.*, 2008). Magnetic resonance imaging (MRI) of the brain of knockout mice demonstrated a reduction of the optic nerve and brain stem volumes (Cagalinec *et al.*, 2016). Visual function was characterised which demonstrated some visual dysfunction with changes to visual evoked potentials, but showed no substantial RGC loss or any significant changes in visual acuity (Bonnet Wersinger *et al.*, 2014). Although the mouse model shows a number of similarities with humans it appears to be a milder model of WS.

1.8.1 Rat

A knockout rat model of WS has also been described with a deletion of exon 5 in *Wfs1 (Plaas et al., 2017)*. The rat model develops diabetes mellitus with a loss of insulin secretion which leads to: glycosuria, hyperglycaemia and beta cell loss which correspond slightly better than

the mouse model to WS. Alongside this the rat develops a reduction in medullary volume suggesting neurodegeneration as seen in WS patients. The rats also develop optic nerve volume reduction as do the mice. The rats also develop cataracts, showed signs of retinal gliosis and disturbed myelin structure in the optic nerve (Plaas *et al.*, 2017). However, there are no observations made on RGCs or RNFL which are affected in patients with WS (Hoekel *et al.*, 2014).

An invertebrate to study WS (drosophila) has also been developed to look at neurological dysfunction (Sakakibara *et al.*, 2018).

1.8.3 Fly

The drosophila knockdown model of the *WFS1* orthologue was CNS specific. This was produced by creating *wfs1* RNAi expressing flies expressed under a pan-neuronal elav-GAL4 driver. Two mutant lines were also created one causing a C-terminally truncated version of the *wfs1* protein, and another showing a 60% reduction in mRNA expression. The flies demonstrated behavioural deficits, neurodegeneration and had reduced lifespans. However, in the fly ER stress was not induced and no mitochondrial dysfunction was observed which is contrary to what was reported in the culture rat and mouse neurons (Cagalinec *et al.*, 2016; Sakakibara *et al.*, 2018). It is suggested that *wfs1* in the fly is responsible for a protective role against various stressors associated with aging (Sakakibara *et al.*, 2018).

1.8.4 Zebrafish

A zebrafish morpholino model was also created during a multi gene knockdown assessment of diabetes causing genes in zebrafish. This model demonstrated a reduction in pancreatic β-islet cells (O'Hare *et al.*, 2016). As this model was not the main focus of this paper the fish was not fully characterised.

1.7 Zebrafish

Zebrafish development

The zebrafish have been studied for a number of years, though work in the 80's creating genetically modified zebrafish lead to the rise in popularity of the model(Streisinger *et al.*, 1981).

In 1995 Kimmel *et al*. described the accurate staging of the zebrafish embryonic development (Kimmel *et al.*, 1995). The first 45 minutes of development the embryo will remain at the one cell stage, from then division and development occurs rapidly with a larval zebrafish developed by 72hours post fertilisation (hpf), as demonstrated in Figure 1.10. After this point development slows and a zebrafish do not become sexually mature until approximately 3-4 months. In the wild a zebrafish would typically live for a year although in captivity the mean lifespan 42 months but can live to 66 months (Gerhard *et al.*, 2002).

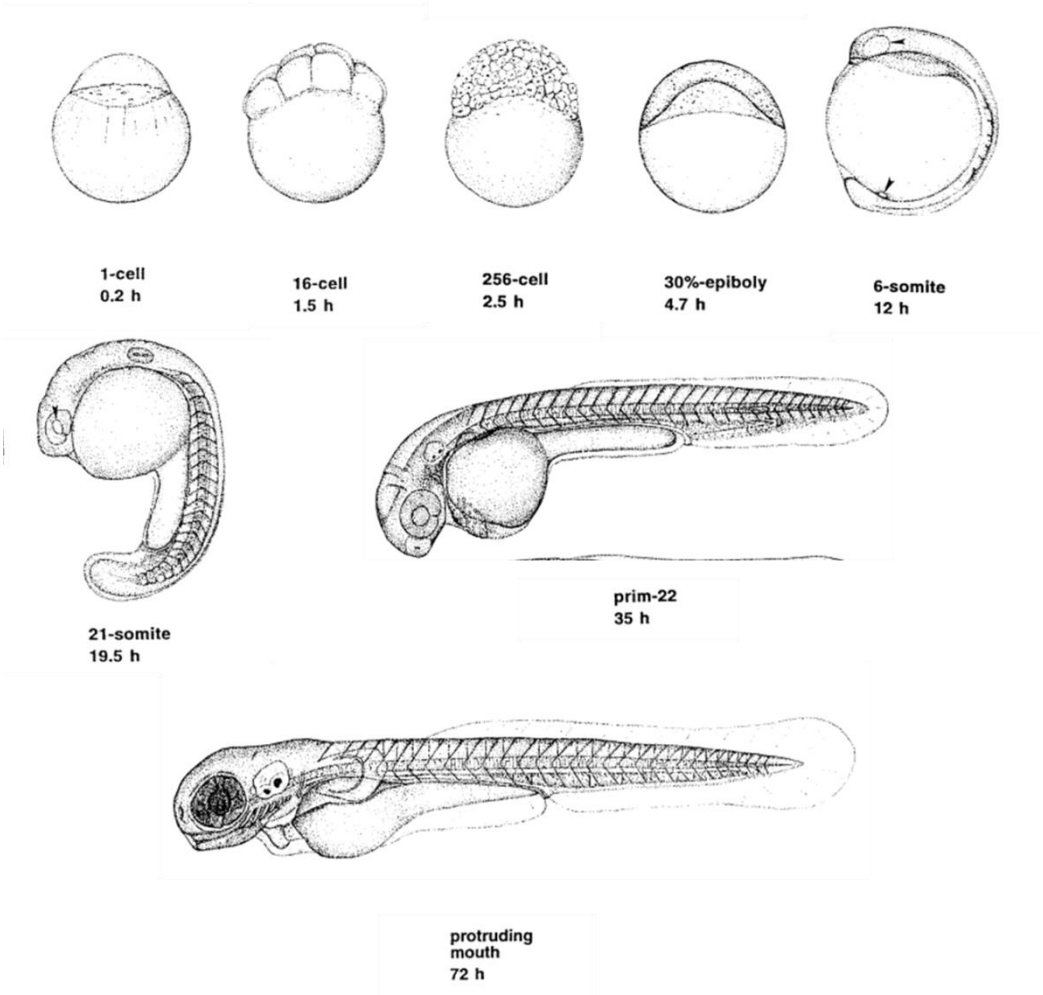

Figure 1.10 Time points of embryonic development of the zebrafish. Adapted from (Kimmel *et al.*, 1995)

Zebrafish have become a popular model for a number of reasons: they develop externally, rapidly, are transparent at early stages, the large volume of offspring from one mating and the relative ease of genetic manipulation (Bradford *et al.*, 2017).The zebrafish genome was

also fully sequenced beginning which allowed for more accurate genetic modification (Howe *et al.*, 2013).

1.7.1 Genetics

Whole genome sequencing revealed that the majority of human genes implicated in disease will have a zebrafish orthologue (82%) (Howe *et al.*, 2013). The most recent genome reference assembly GRCz11 states there are over 25,000 zebrafish genes (Zerbino *et al.*, 2018). This however includes a number of duplications as the zebrafish genome underwent duplication approximately 340 million years ago (Meyer and Schartl, 1999), which has resulted in multiple genes that may require knockout to model diseases in zebrafish.

Genetic manipulation has allowed for the modelling of a number of diseases in zebrafish either transiently by morpholino to knockdown RNA expression or by mutations to knockout genes.

1.7.2 Zebrafish as a model of retinal disease

The zebrafish has been used to develop multiple models of retinal dysfunction. Models have been developed of: glaucoma, diabetic retinopathy, retinal ciliopathies, retinitis pigmentosa alongside many other retinal diseases (Link and Collery, 2015; Richardson *et al.*, 2017). Part of the popularity of using the zebrafish model is the eye is fairly well conserved through vertebrates, reducing some of the drawbacks normally seen using a simpler animal model.

The retina of zebrafish is anatomically and functionally similar to humans and due to the rapid zebrafish development of zebrafish the eye resembles adult morphology by 72hpf (Richardson *et al.*, 2017). Although similar there are a number of differences between the two sets of eyes. The zebrafish retinal thickness is 180µm thick while the human retina measures approximately at 289µm, the zebrafish contains no macular and has tetrachromatic vision compared to humans trichromatic (Chhetri *et al.*, 2014b). Although the retinal thickness is smaller in zebrafish as the eye itself is smaller this represents a larger proportion of the eye in the zebrafish. The optic nerve also has a number of changes. The first is that the fibres of the optic nerve are fully myelinated in zebrafish while in humans myelination of fibres begins after the optic tectum. As seen in Figure 1.11 the structure of the retina contains all the same layers in humans and zebrafish.

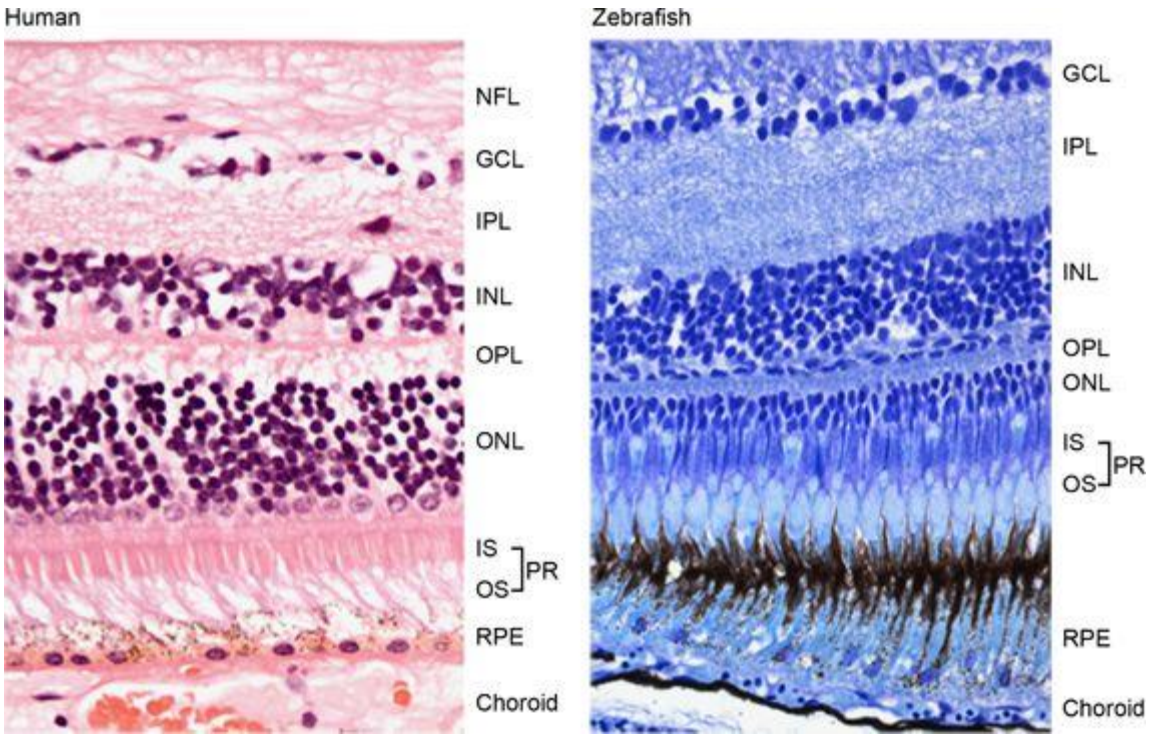

Figure 1.2 Comparison of Human and Zebrafish Retinal Sections. Figure replicated from Richardson *et al*, 2017.

This allows for both histological and functional assessments of the zebrafish eye. Zebrafish behaviour is an important marker in a number of disease models. Eye function can be tested in multiple methods: Optokinetic response, optomotor response and escape response can all be measured behaviourally and electrophysiologicaly electroretinogram can be performed (Fleisch and Neuhauss, 2006; Chrispell *et al.*, 2015). This allows for the combination of histological and functional data to provide a robust model for retinal disease.

1.7.3 Zebrafish as a model of mitochondrial disease

A number of optic neuropathies can be caused by mitochondrial dysfunction. Two examples with zebrafish models have been developed are: *OPA1* and *OPA3*. These are two nuclear encoded mitochondrial proteins, located in the IMM. The *OPA1* model was a transient knockdown using antisense morpholinos. This model demonstrated fragmented mitochondria and reduced respiratory function suggesting that *OPA1* is also involved in the fusion of mitochondria in zebrafish (Rahn *et al.*, 2013). As morpholinos are only effective in the first few days of development extensive retinal testing was not carried out but no RGC loss or ON thinning was seen in the first 48 hours.

The *OPA3* knockout was genomic which allowed the fish to be studied for a longer time period. The knockouts demonstrated optic nerve deficits at 12months, ataxia and movement

disorder (Pei *et al.*, 2010). Although normal OXPHOS function was shown under physiological conditions the fish proved more sensitive to inhibitors of OXPHOS (Pei et al., 2010).

Although no primary mtDNA mutants have been produced knockouts of DNA polymerase gamma which in involved in the proofreading during mtDNA replication leading to mtDNA mutations and depletion (Rahn *et al.*, 2015). The benefit over a mouse model of this disease is survival to 4 weeks rather than death during embryonic development in the mouse (Rahn *et al.*, 2015).

These models demonstrate a number of conserved factors of mitochondrial function in the zebrafish. This highlights a number of benefits from zebrafish models that cannot easily be replicated in other models. The transparency allows live imaging which can provide in vivo data difficult to achieve in larger animals; whole larval fish can be examined by oxygen consumption measurement to look at overall OXPHOS function external development allows for the observation of mutations that prove fatal in the early stages of development. Large numbers of offspring also make them an attractive drug screening model.

The study of WS in a zebrafish model can allow a more in depth look at mitochondrial function and also provide a model of OA for future therapeutic screening.

1.7.4 *wfs1a/b*

Two zebrafish orthologues exist and are named *wfs1a* and *wfs1b,* the two genes are compared in Table 1.3. The *wfs1a* gene located on chromosome 1 shares a 55% cDNA identity with coverage of 89% of the human cDNA. The Gene Order Conservation (GOC) score is 50 which suggest two of the surrounding 4 genes are conserved from the human. The *wfs1b* gene located on chromosome 14 has a slightly higher cDNA identity (57%) but a much higher coverage, 97% of the human cDNA is covered in the *wfs1b* gene. The GOC score is lower with only 1 of the surrounding genes being conserved.

Table 1.3 cDNA Alignment of Human and Zebrafish. Data acquired from ensembl.

Species	Gene ID	% identity (cDNA)	% coverage	GOC score
Human (Homo sapiens)	*WFS1* (ENSG00000109501)			
Zebrafish (Danio rerio)	*wfs1a* (ENSDARG00000062341)	55%	89%	50
Zebrafish (Danio rerio)	*wfs1b* (ENSDARG00000074617)	57%	97%	25

On a protein level a similar pattern emerges with similar percentage identities but a 7% higher coverage seen in *wfs1b*, demonstrated in Table 1.4.

Table 1.4 Peptide Alignment of Human and Zebrafish. Data acquired from ensembl.

Species	Peptide ID	Peptide length	% identity (Protein)	% coverage
Human (Homo sapiens)	ENSP00000226760	890 aa		
Zebrafish (Danio rerio)	*wfs1a* ENSDARP00000084458	814 aa	52%	90%
Zebrafish (Danio rerio)	*wfs1b* ENSDARP00000124957	895 aa	53%	97%

Uniprot predicts that each zebrafish proteins are located to the ER and have 8 transmembrane domains which would be one fewer than the human protein (The UniProt, 2017).

A large scale screen of in situ hybridisations has been carried out on a large number of genes in zebrafish; this study involved the expression of the *wfs1a* and *wfs1b* (Thisse, 2004). This study detected no expression until the segmentation phase of development at approximately 19hpf. This detection was said to be predominantly in the myotomes. The *wfs1b* expression was detected from the 1-cell stage detected in the whole organism, with increased expression in the notochord (Thisse, 2004). The notochord is important in the development of the nervous system and somites (Eisen, 1996).

wfs1a *wfs1b*

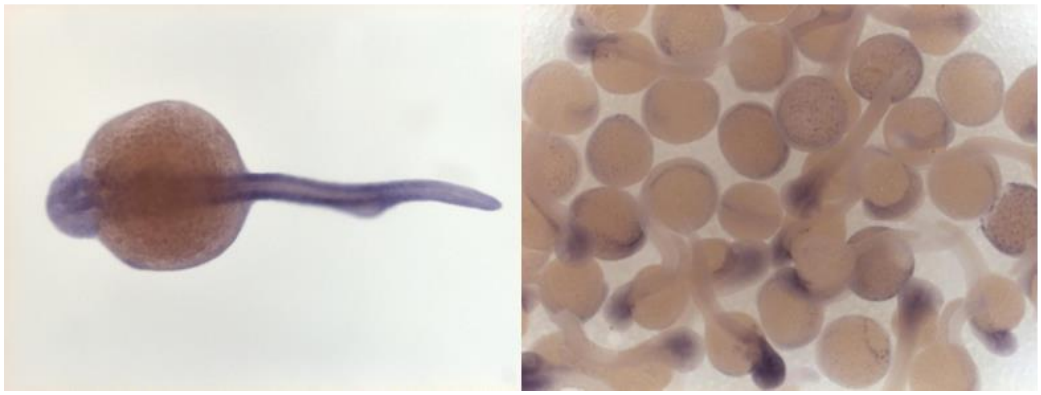

Figure 1.3 Insitu Hybridisation of *wfs1a* and *wfs1b* RNA expression. Figure adapted from Thisse, 2004.

This project involved the characterisation of two zebrafish models of Wolfram syndrome (*wfs1a* and *wfs1b*). Animal models are important in helping develop our understanding of the disease while also creating opportunities to test therapeutic compounds.

1.8 Project Aims

WS is a multisystem, complex disorder for which there are currently no treatments. A mouse model of WS has been studied for a number of years, a number of insights into the disease have been predominantly focused on the development of diabetes mellitus (Ishihara *et al.*, 2004). A rat and drosophila model of WS have recently been developed. The rat model describes diabetes, optic atrophy, hearing loss which represents a closer model to WS than in mice (Plaas *et al.*, 2017). The drosophila model was developed to model neurodegeneration but many differences in protein function were observed when compared to the mouse/human (Sakakibara *et al.*, 2018). A zebrafish model would be able to bridge the gap of using a simpler model while maintaining a closer gene identity to humans.

A zebrafish model of the disease creates unique opportunities to study WS. Using a number of whole system and live imaging techniques it is possible to determine changes during the development of WS that is not possible in other models which could provide insights into both neuronal development and mitochondrial dysfunction in an in vivo system.

The overall aim of this project was to characterise a zebrafish model of WS. A transient morpholino model and a genomic knockout model were both examined and the suitability of the two models assessed. Characterisation of the zebrafish involved observation of some of the molecular mechanisms and disease phenotypes seen in patients of WS and determining if the zebrafish knockouts accurately modelled this.

The secondary aims of this project were to observe neurodevelopment and mitochondrial function. The development of the brain and neurons in WS are impeded. Zebrafish development allows for this to be monitored in the first few days giving a unique insight into the development of this condition. Mitochondrial dysfunction has been implicated in this process and the role of further mitochondrial dysfunction in WS will be investigated within this thesis.

Chapter 2: Material and Methods

2.1 Zebrafish care

Wildtype zebrafish (*Danio rerio*) (AB) were used alongside further genetically modified fish lines described in Table 2.1.

Table 2.1 Transgenic fish lines

Lines	Function
slc24a5 (Golden)	Loss of pigment making them translucent
Islet 1 Gfp	Express GFP in the cranial motor neurons
Sa10021 (wfs1a)	Nonsense mutation in *wfs1a*
Sa16422 (wfs1b)	Nonsense mutation in *wfs1b*

Genetically modified strains sa10021 (*wfs1a*), sa16422 (*wfs1b*) were purchased from the European Zebrafish Resource Center (EZRC) as heterozygotes and crossed to create a stable line of homozygote mutants.

Zebrafish were maintained in fresh water at 28.5 °C and maintained to home office standards. Euthanasia was performed by overdose of euthanized in 4mg/ml tricaine methanesulfonate (tricane) 1:1 ratio with fresh system water.

2.2 Zebrafish breeding/embryo harvesting

The evening prior to embryo collection one male and one female zebrafish were placed into breeding tanks separated by a mesh grid with another mesh grid below to separate the fish from the eggs. This was also performed with larger tanks with multiple male and females for a higher success rate of fertilisation.

On the day of the collection the fish were combined in fresh system water to mate. The eggs were strained, rinsed and stored in E3 medium (5 mM NaCl, 0.17 mM KCl, 10 mM HEPES, 0.33 mM $MgSO_4$, 0.33 mM $CaCl_2$ 0.00002% methylene blue).

2.3 Zebrafish Heat shock

50 embryos were transferred into a 1.5ml Eppendorf with 1ml E3 medium. The Eppendorf was placed in a heat block set to 37^{o}C for 1 hour. After the hour zebrafish were either harvested or placed back in a petri dish containing E3 medium at 28.5^{o}C to develop.

2.4 Zebrafish Imaging

Imaging was carried out using bright field microscopy. Images were taken on a Leica MZ16F stereomicroscope with a Leica DFC420 C camera attachment on the Leica Application Suite V3 program. Zebrafish measurements were performed in ImageJ, a micrometer image at each magnification was used to set a scale. Measurements of length used straight lines from the head to tail. Measurements of otoliths and cerebellums were drawn round using the "freehand" tool.

2.5 Fin clip

Zebrafish were anesthetised in 1:25 (tricane:system water). The anesthetised fish were removed from water and a small amount of the tail fin removed using a scalpel. The fish were then placed in fresh system water in separate tanks to recover. Genomic DNA was extracted from fin clips using the hotshot extraction method described in Section 2.8 DNA extraction.

2.6 Microinjection

Zebrafish embryo injections were performed using glass needles made from Bo-glass capillaries with filament (Hilgenberg, Hilgenberg, Germany) using a model P-97 Flaming/Brown Micropipette Puller (Sutter Instrument Co. Novato, USA) with the settings as follows: P=500, Heat=800, Pull=150, Velocity = 100 and Time= 150.

Needles containing 2.5µl of required solution were held in a micromanipulator attached to a FemtoJet™ Microinjector (Eppendorf, Stevenage, UK) and viewed down a Leica MZ9.5 Stereomicroscope. The needle was broken at the tip and calibrated using a micrometer to obtain a 2nl droplet by changing pressure and time setting on the microinjector (80-100(kPa) 0.1-0.6 seconds).

Embryos were taken at the 1-4 cell stage and manipulated into a single file line against a glass slide in a petri dish. The embryos were turned so the cell was in line with the slide edge

and any dead or small embryos were removed. Embryos were injected through the yolk and as close as possible to the cell without puncturing.

2.6.1 Morpholino Preparation

Morpholinos were obtained from Gene Tools, LLC and arrived as 300 nmols of lyophilized powder; these were diluted to a 2mM stock in ddH2O. The morpholinos used are listed in Table 2.2.

Table 2.2 Morpholino utilised

Morpholino	Morpholino Oligonucleotide Sequence	Exon Target
wfs1a Splice Blocking	5'-TGCAGACCCTAAAGTGAAAGAATGA-3'	8
wfs1b Splice Blocking	5'-CCAATCTGCCCAACAAGACAAATGT-3'	3
wfs1b Translation Blocking	5'-ACGTGTCCATTTTTAAGCCTGAGCT-3'	2
P53	5'-GCGCCATTGCTTTGCAAGAATTG-3'	1

Prior to injection morpholino stocks were heated to 65^0C for 10 minutes to avoid precipitation, diluted to the desired concentration in Deneau solution (58 mM NaCl, 0.7 mM KCl, 0.4 mM $MgSO_4$, 0.6 mM $Ca(NO_3)^2$, and 5.0 mM HEPES [pH 7.6]) with 0.05% phenol red dye.

2.6.2 CRISPR Preparation

The CRISPR solution contained: 1µl 10x Cas9 buffer, 2µl Cas9 protein (2uM), 3000ng RNA, 1.5µl 2M KCl, 1µl 0.5% phenol red and the reaction made up to 10µl with RNase free H_2O. This was heated to 37^oC for 5 minutes prior to injection.

2.7 RNA extraction

RNA was extracted using a combined method of TRIzol (ThermoFisher, Waltham, USA) and RNeasy kit (Qiagen, Manchester, UK). Prior to RNA extraction all surface areas and equipment were cleaned with 70% ethanol then RNaseZap (ThermoFisher). ~50mg of tissue was homogenised in 500 µl TRIzol and incubated at room temperature for 5 minutes. 1:5 ratio of chloroform to TRIzol added and mixed before centrifugation at 12000g for 15

minutes. The aqueous phase is removed and added to 70% ethanol at a 1:1 ratio. This is then added to an RNeasy spin column and followed the manufacturer's instructions. Sample concentrations and purity were measured on a NanoDrop 2000 (ThermoFisher) and purified RNA was stored at -80^{o}C.

2.8 DNA extraction

Genomic DNA was extracted using the Hotshot method. Tissue was placed in an appropriate volume of 50mM NaOH (50µl single embryo/100µl fin clips/500µl tissue) in eppendorfs and heated to 95^{o}C at a speed of 1500rpm on a Labnet AccuTherm (Labnet, Edison, USA) for 15 minutes. After cooling to 4^{o}C 1/10th volume of 1 M Tris-HCl pH8 was added to neutralise the solution. The solution was centrifuged at 16000g and the supernatant stored at -20^{o}C (Meeker *et al.*, 2007).

2.9 cDNA Synthesis

cDNA synthesis was performed using the Applied Biosystems: High-Capacity cDNA Reverse Transcription Kit using the following reaction: 2µl 10x RT Buffer, 0.8µl dNTPs (100mM), 10x 2µl RT Random Primers, 1µl MultiScribe Reverse Transcriptase and 4.2µl Nuclease Free H2O. This was added to 10µl of 1000ng RNA in RNase free water and the reaction carried out on a thermocycler to the following programme.

Table 2.3 cDNA reaction thermocycler steps

Step	1	2	3	4
Temperature (^{0}C)	25	37	85	4
Time (minuted)	10	120	5	∞

2.10 PCR GoTaq® Hot Start Polymerase

The GoTaq PCR method was used on morpholino experiments.

Table 2.4 Zebrafish morpholino primers

Primer	Sequence
wfs1a_splice-F	5'-GCAAATGAAGAGGAGGGGATA-3
wfs1a_splice-R	5'-CGATGGTGAGATTGGAGATG-3'
wfs1b_splice-F	5'-CTCCTTCAGCCATGACTCCG-3'
wfs1b_splice-R	5'-CCTCTCTGTTCTCCGCTGTG-3'

10µl 5X Green Go Taq Flexi Buffer(Promega, Portsmouth, UK), 8µl $MgCl_2$ (25mM), 5µl dNTPs (10mM each, (Rovalab, Teltow, Germany)), 1µl Forward Primer (10µM), 1µl Reverse Primer (10µM), 5µl betaine (5M, Merck Darmstadt, Germany), 0.25µl GoTaq® Hot Start Polymerase (5u/µl) (Promega) and 17.75µl ddH_2O.

Table 2.5 GoTaq® Hot Start polymerase reaction thermocycler steps

Step	1	2	3	4	5	6
Temperature (^{0}C)	95	95	variable	75	75	4
Time	2 minutes	30s	30s	30s	5minutes	∞
Cycles		x30				

Mytaq polymerase (Bioline, London, UK) was used for all other PCR reactions

2.11 PCR MyTaq DNA Polymerase

5x MyTaq Reaction Buffer 5 µl, Primers 10µM each 0.5 µl MyTaq DNA Polymerase 1 µl 18µl (Bioline) water (ddH_2O) up to 25 µl.

Table 2.6 MyTaq DNA polymerase reaction thermocycler steps

Step	1	2	3	4	5	6
Temperature (^{0}C)	95	95	variab	75	75	4
Time	2 minutes	15s	15s	30s	5 minutes	∞
Cycles		x30				

2.12 Gel Electrophoresis

Depending on the size of the designed fragment, 1-2% (w/v) agarose (Bioline) gels were made in 100mls of 1x TAE buffer (EDTA · Na2 · 2H2O, Acetic Acid glacial and Tris (AppliChem, Maryland Heights, USA)). 10µl Gel red (Merck) or 5µl SafeView (NBS Biologicals, Huntingdon, UK) was added to the mix and the gel poured into a casting tray. The gel was inserted into a FHU10 submarine gel tank (ThermoFisher) covered in 1x TAE, 19µl of PCR product with loading dye(Blue/Orange Loading Dye, 6X (Promega)) was added to the wells and 5µl Bioline hyperladder IV or I and electrophoresed at 80V.

Gels were imaged using a GelDoc-IT Imaging system (UVP, Upland, USA)

2.13 Gel extraction

Gels were viewed on a GelVue UV Transilluminator (SYNGENE, Cambridge, UK) with bands of interest cut out with a scalpel and purified using a QIAquick Gel Extraction Kit to manufacturer's instructions.

2.14 qPCR

qPCRs used the BioRad: iTaq™ Universal SYBR® Green Supermix (BioRad, Hercules, USA). Reactions were set up containing: 9ul water, 2.5ul primer mix (500nM), 12.5 SYBR Green Supermix (2x) and 1µl cDNA. Correct cDNA concentrations were optimised by serial dilution of stock cDNA with appropriate primers (heat shock primers taken from: (Vacaru *et al.*, 2014)).

Reactions were run a CFX96 Touch Real Time detection system (BioRad). With a reaction as follows: 3 minute 95^{o}C, a cycle of 40x 10 seconds 95^{o}C and 1 minute 58^{o}C and a melt curve which ran from 65^{o}C to 90^{o}C at 0.5^{o}C increments. Data analysis was performed in CFX Manager software (version3.0)

Table 2.7 qPCR primers

Primer	Sequence
*xbp1*s-F	5’-TGTTGCGAGACAAGACGA-3’
*xbp1*s-R	5’-CCTGCACCTGCTGCGGACT-3’
*xbp1*t-F	5’-GAGGAGCCCACAAAGTCCTC-3’
*xbp1*t-R	5’-CGAAGTGCTTTTTCCTCTGG-3’
atf4-F	5’-TTAGCGATTGCTCCGATAGC-3’
atf4-R	5’-GCTGCGGTTTTATTCTGCTC-3’
atf6-F	5’-CTGTGGTGAAACCTCCACCT-3’
atf6-R	5’-CATGGTGACCACAGGAGATG-3’
bip-F	5’-AAGAGGCCGAAGAGAAGGAC-3’
bip-R	5’-AGCAGCAGAGCCTCGAAATA-3’
ddit3-F	5’-AAGGAAAGTGCAGGAGCTGA-3’
ddit3-R	5’-TCACGCTCTCCACAAGAAGA-3’
dnajc3-F	5’-TCCCATGGATCCTGAGAGTC-3’
dnajc3-R	5’-CTCCTGTGTGTGAGGGGTCT-3’
edem1-F	5’-ATCCAAAGAAGATCGCATGG-3’
edem1-R	5’-TCTCTCCCTGAAACGCTGAT-3’
wfs1a-qF	5’-TGTGCCCTGTGTGCTCTAC-3’
wfs1a-qR	5’-GGCAACACAAGTACGGATCA-3’
wfs1b-qF	5’-CGCCCCGAATCTAAGCTTTT-3’
wfs1b-qR	5’-GCGGAAGTGTGTGTTTGTCT-3’
wfs1b-q2F	5’-CCAAACAATACGCTGAGGGT-3’
wfs1b-q2R	5’-GCCCAGTCAATCAACACCTC-3’

Table 2.8 qPCR housekeeping primers

Primer	Sequence
s18-F	5'-AAGAAGATCAGGGCTCACCG-3'
s18-R	5'-GCGACGACCAGTTGTTTTGG-3'
b2m-F	5'-AAACGGCCACAATGAGAGCA-3'
b2m-R	5'-AGCAGATCAGGGTGTTTGGT-3'
ef1α-F	5'-CTGGAGGCCAGCTCAAACAT-3'
ef1α-F	5'-ATCAAGAAGAGTAGTACCGCTAGCATT-3'
β-actin-F	5'-CGAGCTGTCTTCCCATCCA-3'
β-actin-R	5'-TCACCAACGTAGCTGTCTTTCTG-3'

2.15 Zebrafish mtDNA Levels

A modified protocol from Bestman *et al.*, 2015 was performed to measure mtDNA in zebrafish larvae. gDNA and mtDNA was extracted from individual zebrafish at 48hpf by the hot shot method described in Section 2.8 DNA extraction. Primers were used from the described protocol (Table 2.9) and the qPCR protocol (Section 2.14) was performed. ΔCq was calculated by subtracting nd1 value from ef1α value to give a ratio of genomic to mtDNA (Bestman *et al.*, 2015).

Table 2.9 mtDNA primers

Primer	Sequence
ef1a F	5'-AAGCCGCTGAGGTAAGCGTTCAAC-3'
ef1a R	5'-TTGAGCCGAGAAACGCGTGCTG-3'
nd1 F	5'-GGGCACCCATACCCATGCCCTAT-3'
nd1 R	5'-TGCGCTACAGCTCGTAAGGC-3'

2.16 Guide RNA (gRNA) synthesis

gRNAs were designed for CRISPR cas 9 genome editing. Crisprscan (http://www.crisprscan.org/) was used to design oligos. gRNAs were picked due to high scores on the CRISPRscan predictive sgRNA-scoring algorithm (>70), that targeted the correct exons described in Table 2.10.

Table 2.10 gRNA oligos

Oligos	Sequence
wfs1b-70F:	5'-TTACCTGAGACTAGCCGAGC-3'
wfs1b-70R:	5'-TGCAAGCACAGAGAAAGAGA-3'
wfs1b-83F:	5'-GCTTGAATCTCAGCTGTCGG-3'
wfs1b-83R:	5'-ACAATCACTGACATGGGACTG-3'
wfs1b-78F:	5'-TCATGAGGGTTTTAGGGCGA-3'
wfs1b-78R:	5'-GTATTGGGCTGGAGAGAGGG-3'
Universal bottom-strand Ultramer	5'AAAAGCACCGACTCGGTGCCACTTTTTCAAGTTGATAACGGACTAGCCTTATTTTAACTTGCTATTTCTAGCTCTAAAAC-3'

The oligos for gRNA are then combined with the universal bottom-strand ultramer in the following reaction: 5x MyTaq Reaction Buffer 5 μl, Top strand oligo (100μM) 2 μl, universal bottom-strand ultramer (100μM) 2 μl, MyTaq DNA Polymerase 0.2 μl Water (ddH_2O) up to 25 μl. The reaction was placed in a thermocycler on the following programme:

Table 2.11 gRNA template reaction thermocycler steps

Temperature (°C)	Time
95	05:00
89	00:15
83	00:15
77	00:15
71	00:15
65	00:15
59	00:15
53	00:15
50	10:00
72	10:00
4	∞

The reactions were purified using a Qiagen PCR purification kit to manufacturer's instructions. The purified product was used as template DNA for a MEGAshortscript™ T7 Kit reaction with 8 reactions for each oligo mixture.

2 µl T7 10X Reaction Buffer, 2 µl T7 ATP Solution (75 mM), 2 µl T7 CTP Solution (75 mM), 2 µl T7 GTP Solution (75 mM), 2 µl T7 UTP Solution (75 mM), 8 µl Template DNA, 2 µl T7 Enzyme Mix. The reaction was incubated at 37°C overnight. 1 µl of TURBO DNase was added and incubated for a further 15 minutes.

Reactions were pooled and RNase free water added to a volume of 800 µL. This was pipetted on to a Mirvana spin column from the mirVana miRNA Isolation Kit (ThermoFisher) and washed as per manufacturer's instructions.

RNA was eluted in 30 µl RNase free water aliquoted and stored at -80^{o}C.

2.17 Sequencing

Primers used for sequencing reactions:

Table 2.12 Sequencing Primers

Primer	Sequence
*wfs1b*seq-f	5'-AGCCATACCTCTACTTTCTCCT-3'
*wfs1b*seq-R	5'-AGATGCACACTGTTACGATCA-3'
*wfs1a*seq-f	5'-ACCCCAATCAGACACACCTT-3'
*wfs1a*seq-R	5'-ATCGAGTCCAGAGTCGCAGT-3'
*wfs1a*_splice_seq-F	5'-GCGATGTAGCCAGATTTGATAAG-3'
*wfs1a*_splice_seq-R	5'-AGCTTTTATGTCCAGGGCTCT-3'
*wfs1b*_splice_seq-F	5'-GGACAATCAGCGTTTCCTCC-3'
*wfs1b*_splice_seq-R	5'-ACAGCAGTAACAGCATTCACC-3'

2.18.1 Exo I/Fast AP DNA purification

PCR reactions were purified by Exo I/Fast AP DNA purification. 5µl of PCR reaction were added to Exonuclease I (Exo I) 0.5 µl (10 U) and 1µl FastAP Thermosensitive Alkaline Phosphatase (1U). The samples were placed on a thermocycler for the following reaction (Table 2.13)

Table 2.13 Exo I/Fast AP reaction thermocycler steps

Step	1	2	3	4
Temperature (^{0}C)	25	37	85	4
Time (minutes)	10	120	5	∞

2.18.2 BigDye terminator cycle sequencing reaction

5µl of purified PCR product was added to 15µl big dye (Applied Biosystems, Foster City, USA) master mix containing 1µl big dye, 2µl 5x Big Terminator Sequencing buffer, 1µl of either the forward or reverse primer and 11µl H_20.

Table 2.14 BigDye reaction thermocycler steps

	1	2	3	4	5
Temperature (^{0}C)	96	96	50	60	4
Time	1 minute	10s	5s	4 minutes	∞
Cycles		X25			

2.18.3 Ethanol Precipitation

Prior to sequencing the big dye reaction had to be cleaned by ethanol precipitation. 2µl 3M sodium Acetate (Merck), 2µl 125mM EDTA (Merck) and 70µl 100% ethanol were added to each big dye reaction, mixed and incubated for 15 minutes at room temperature. The reactions were centrifuged at 2000g for 30 minutes then the supernatant removed, 70µl 70% ethanol added and the samples were centrifuged for 15 minutes at 1650g. The supernatant was removed and the samples left to air dry in the dark for 15 minutes.

2.18.4 Sanger Sequencing

Samples were resuspended in 10µl Hi-Di (Applied Biosystems) and sequenced using a capillary electrophoresis on a 3130XL Genetic Analyser (Applied Biosystems). The analysis was performed using SeqScape V2.6.

2.18.5 Commercial Sequencing

A proportion of sequencing was also sent to GATC and Eurofins Genomics (Germany) for sequencing. 250ng of purified PCR products and 5 µM primers were sent to per reaction for the GATC lightrun. The Eurofins PlateSeq Service was also used 150ng of unpurified PCR product and 30pmol of primer per reaction sent separately.

2.19 Western Blot

2.19.1 Protein lysates extraction

Zebrafish <48hpf were homogenised using a p200 pipette tip while older larvae and adult tissue were homogenised using a tissue ruptor. Tissue was homogenised in RIPA buffer with cOmplete™, Mini, EDTA-free Protease Inhibitor Cocktail (Roche, Basel, Switzerland) and left

to incubate on ice for 10 minutes. The samples were centrifuged at 13000g for 10 minutes at 4^0C, the protein concentration determined by Bradford assay, aliquoted and stored at -80^0C.

2.19.2 Bradford assay

Protein standards were made using BSA (bovine serum albumin) and sterile water at the following concentrations (mg/ml) 0, 0.05, 0.1, 0.2, 0.3, 0.4 and 0.5. 10 µl of standard were added to a 96 well plate in triplicate alongside protein at a 1:10 dilution to ddH_2O.

190 µl of 1 part Bradford Dye Reagent Concentrate with 4 parts ddH_2O was added to each well and incubated in the dark for 10 minutes.

Absorbance at 610nm was measured on a Magelan Tecan F50 plate scanner (Tecan, Männedorf, Switzerland)

2.19.3 Antibodies

Table 2.15 Antibodies for Western blots

Antibody	Company	Dilution	Species	Company Identifier
Anti-NDUF9A	abcam	1:1000 1:500	Mouse	ab14713
Anti-MTCO1	abcam	1:1000	Mouse	ab14705
Anti-SDHA	abcam	1:1000	Mouse	ab14715
Anti-HSPA5	abnova	1:1000	Mouse	PAB2462
Anti-VDAC	abcam	1:1000	Rabbit	ab15895

2.19.4 SDS Page Gel and Transfer

Zebrafish lysates of 50µg were made up in NuPAGE LDS Sample Buffer and NuPAGE Sample Reducing Agent (ThermoFisher). Pre cast NuPAGE 4-12% Bis-Tris Protein Gels (ThermoFisher) were loaded with the samples alongside a SeeBluePlus2 marker (ThermoFisher) in an XCell SureLock electrophoresis system (ThermoFisher). NuPAGE MES buffer was added to the upper

chamber with 500µl NuPAGE Antioxidant solution. To the lower chamber unaltered MES buffer was added and the gels run at 150V until the desired endpoint had been reached.

Transfer to PVDF membranes was by dry transfer performed using i Blot 2 PVDF mini Stacks (ThermoFisher) on an iBlot 2 system. This was performed to manufactures' instructions using the "P0" programme (20 V for 1 minute, 23 V for 4 minutes and 25 V for 2 minutes).

Membranes were incubated in 5 % (w/v) milk in Tris buffer saline (Santa Cruz, Dallas, USA) with 1 % (v/v) Tween 20 (TBST; (Bio-Rad)). These were blocked for 1 hour at room temperature with gentle agitation. Then an appropriate antibody was added in a 5% milk TBST solution and incubated at 4 degrees overnight (Section 3.12.3). The membranes were washed 3 times for 10 minutes in TBST then either anti-rabbit or anti-mouse polyclonal HRP conjugated antibody (Agilent, Santa Clara, USA) was added in 5% milk TBST at a dilution of 1:2500, for 1 hour. The membrane was washed a further 5 times in TBST prior to imaging.

2.19.5 Chemiluminescent Detection

Biorad Clarity ECL (BioRad) was used to detect the HRP signal using an Amersham Imager 600. Clarity Western Peroxide Reagent and Clarity Western Luminol/Enhancer Reagent were added to the membrane at a 1:1 ratio. Excess ECL reagent was removed and the membrane imaged on an auto setting on the Amersham Imager 600. If no signal was detected incremental settings were used for a longer exposure.

2.19.6 Coomassie

The SDS gel from the transfer was coomassie stained to determine equal protein loading of the samples. Coomassie staining solution (0.1% Coomassie Brilliant Blue G-250 Dye (ThermoFisher), Methanol (50% (v/v)) Glacial acetic acid (10% (v/v)) ddH_20 (40% (v/v))) was added to the gel for 30 minutes until the gel was stained blue. Background Coomassie stain was removed from the gel by Coomassie destain solution (Methanol (50% (v/v)) Glacial acetic acid (10% (v/v)) H20 (40% (v/v))) for 1 hour with two changes of destain solution. Gels were washed overnight in ddH_20 before imaging.

2.20 Mitochondria Isolation

Mitochondria isolation from zebrafish was modified from Jha P *et al,* 2016. Zebrafish were lysed in isolation buffer (IB) (6.846% of sucrose (w/v), 0.121% Tris (w/v), 1% 0.1 M EGTA/Tris (v/v). Adjusted to pH 7.4 with 1 M HEPES in ddH_20) with cOmplete™, Mini, EDTA-free

Protease Inhibitor Cocktail (Roche). Homogenate was centrifuged at 600g for 10 minutes (all centrifugation steps at 4^{o}C). This process was repeated; the supernatant was removed and centrifuged at 7,000g for 10 min. The pellet contained isolated mitochondria and was resuspended in IB to determine concentration by Bradford assay.

50µg aliquots of mitochondria were pelleted at 7000g the supernatant discarded and aliquots used immediately or stored at -80^{o}C.

2.21 Digitonin Solubilisation of Isolated Mitochondria

A concentration of 8 g/g digitonin to mitochondrial proteins was added to 50 µg protein, 5 µl of NativePAGE sample buffer (4×) (ThermoFisher) and made up to 20µl with ddH_20. The solution was incubated on ice for 20 minutes then centrifuged at 20000g for 10 minutes. The supernatant was taken and added to 2µl coomassie G-250 sample additive (ThermoFisher).

2.22 Native Page Gel

Samples were loaded on 3-12% NativePAGE Bis-Tris Gels with a NativeMark™ Unstained Protein Standard (ThermoFisher).The gels were electrophoresed for the first 30 minutes at 150V with dark blue cathode buffer (1X Native page running buffer 1X Dark Blue Cathode buffer (ThermoFisher) to the upper chamber of an XCell SureLock electrophoresis system and 1X Native page running buffer in the bottom. After 30 minutess the dark blue cathode buffer was replace by light blue buffer (1X Native page running buffer 0.1X Dark Blue Cathode buffer)

The remaining steps of the protocol followed the Western Blot protocol from the Page Gel and Transfer although “P0” was altered with 2 additional minutes at 25V for the transfer using the iBlot 2. The membrane had to be destained in Coomassie destain with three 10 minutes washes before blocking.

2.23. Whole Mount Staining of Zebrafish Larvae

2.23.1 Staining

Embryos were euthanised in a 1:1 dilution of tricane:system water. To preserve the tissue embryos were fixed overnight at 4^{0}C in 4% paraformaldehyde (PFA). The PFA removed and the embryos were rinsed with PBS for 5 minutes the ddH_20 for 5 minutes. The embryos were then permeabilised in acetone at -20^{0}C for 7 minutes. The acetone was removed and embryos washed in ddH_20.

Embryos were transferred to a 6 well plate and washed in 1XPBSTween20 (0.1%) (PBST). The PBST was replaced with 2ml 5% Horse serum (in PBST) to block for an hour with gentle agitation. Primary antibodies were diluted to concentrations listed in Table 2.16 in 5% Horse serum and incubated with zebrafish embryos overnight at 4^0C with gentle agitation. The embryos were washed in PBST four times for 20 minutes. Secondary antibodies were prepared in 5% horse serum and incubated with the fish for 2 hours at room temperature. The embryos were then washed twice more in PBST for 20 minutes and then washed again overnight. The embryos were then mounted on permafrost slides or confocal dishes and taken for confocal microscopy.

2.23.2 Antibodies

Table 2.16 Antibodies for whole mount staining

Antibody	Company	Concentration	Species	Company Identifier
SV2	The Developmental Studies Hybridoma Bank	1:1000	Mouse	
Alexa Fluor™ 546 Phalloidin	ThermoFisher	1:1000	Mouse	A22283
Goat anti-mouse – Alexa 488	ThermoFisher	1:1000	Goat	A-11029
Alpha-Bungarotoxin – Alexa 594	ThermoFisher	1:500	Mouse	B13423

2.23.3 Acquisition by Confocal Microscopy

Zebrafish were mounted on glass Superfrost Plus™ slides in Vectorshield fluorescent mounting medium. Glass coverslips were raised by placing electrical tape around the outside of slides and placed over the zebrafish. This was sealed with nail varnish to prevent drying. A Nikon A1R confocal (invert) was used for imaging Z-stacks were acquired using a high speed piezo Z stage.

Analysis was carried out in ImageJ.

2.24 Seahorse XF Mito Stress Test

Oxygen consumption rate of 48hpf embryos (OCR) was measured using the Seahorse XFe96 Extracellular Flux Analyzer (Agilent). 48hpf embryos were anesthetised in a 1:25 tricane E3 solution and single embryos still within the chorion added to a single well on a Seahorse XFe96 Spheroid Microplate, in 150µl E3 tricane. Modifying the seahorse stress test 3 Basal reading were recorded, Oligomycin (final conc 25µM) with 5 recording cycles, FCCP (final conc 4µM) 3 recordings and Rotenone + Antimycin A (final concentration 25µM) were all added. Calculations for parameters (Non-mitochondrial respiration, Basal respiration, Maximal respiration, Proton leak, ATP-prodiction and Spare respiratory capacity) were made from the Seahorse XF Cell Mito Stress Test Kit User Guide (Agilent).

2.25 Live Trafficking of Mitochondria in a 48hpf Zebrafish

2.25.1 Plasmid Preparation

neuroD:GFP and neuroD:mito-RFP (a gift from Tamily A. Weismann) plasmids were used (Marra *et al.*, 2015). The plasmids were transformed into JM109 *E. coli.* (Promega).

2.25.2 Transformation

Plasmids were added to 25µl of JM109 competent cells, mixed and incubated on ice for 30 minutes. The mixture was then heat shocked at 42^{o}C for 45 seconds in a water bath, then returned to ice for 2 minutes. 475µl Luria-Bertani (LB) broth was added to the mixture and incubated at 37^{o}C for 1 hour shaking at 225rpm in a C5 shaking incubator (New Brunswick, Enfield, USA). 200µl of the reaction was spread on an LB agar plate containing 100 µg/ml ampicillin, allowed to dry and incubated upside down at 37^{o}C overnight. 100 µg/ml ampicillin LB broth was then inoculated with a single colony and incubated at 37^{o}C overnight shaking to allow for plasmid replication.

2.25.3 Plasmid Purification

Plasmids were purified following the Qiagen mini prep protocol. Plasmids were eluted in 30µl elution buffer and plasmid concentration check by 2000 UV-Vis spectrophotometer (ThermoFisher) and quality and size assessed by agarose gel electrophoresis.

2.25.4 Zebrafish Preparation

Zebrafish were co injected with both neuroD:GFP (3 pg) and neuroD:mito-RFP (5 pg) plasmids at the 1 cell stage to visualise both the lateral line and the mitochondria. The fish

were allowed to develop to 48hpf in E3 medium and screened for good GFP transfection rates using a Leica MZ16F fluorescent stereomicroscope and these fish picked for confocal microscopy.

2.25.5 Acquisition by Confocal Microscopy

Zebrafish were embedded in 1% low melt agarose (Merck) on Thermo Scientific™ Nunc™ Glass Bottom Dishes (ThermoFisher) and covered with E3 medium. Images were acquired at 60x magnification using 1.40 NA oil objective and a 5 minute time lapse of both GFP and RFP at 5 second intervals.

2.25.6 Kymograph Analysis

Images were analysed in ImageJ using kymographs using the following plugin (https://www.embl.de//eamnet/html/body_kymograph.html). A segmented line was used to highlight the neuron, the channels were split and the RFP image used from this point onwards. The width of the line was altered to encompass the whole neuron (line width 9). The kymograph plugin was used to create a kymograph. Straight lines were drawn using the line tool tracking mitochondria (Figure 2.1).

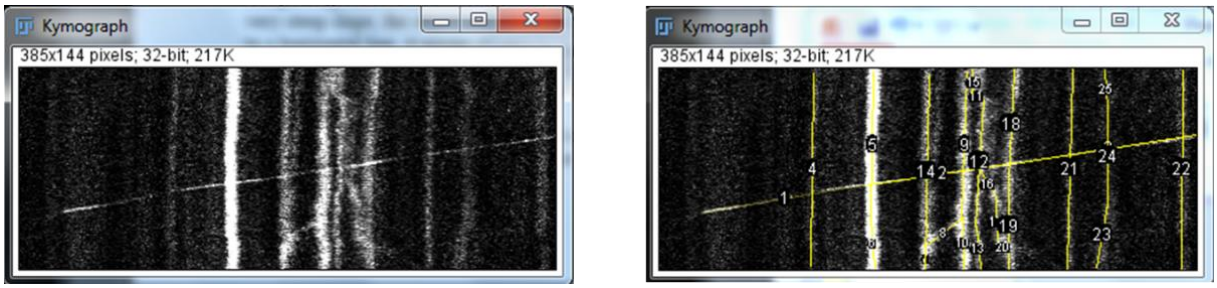

Figure 2.1 Representative Kymographs with mitochondrial movement marked with yellow lines.

The lines values were calculated using tsp050706. These values were converted from pixels to µm and from frames to seconds. Velocity, percentage movement and changes in direction can be extrapolated from these data.

2.26 OKR

The zebrafish were anesthetised and fixed between two sponges using needles to keep them in place. The sponge was fixed to the bottom of a clear plastic drum. System water was added and the fish left to relieve the effects of anaesthesia. This was placed inside a variable speed rotating drum with a black and white grating. When the fish had sufficiently recovered the grating was rotated at 8rpm for 30 seconds clockwise and 30 seconds anti-clockwise.

This was repeated at 16 rpm and the videos recorded using a Nikon camera attached to a stereomicroscope. The eye movements were counted manually.

2.27 OCT

OCT images were captured using the Bioptigen Envisu R2200 SDOIS (Bioptigen, Inc., Morrisville, USA). The zebrafish were anesthetised in a 1:20 ticane to system water ratio and placed on the imager in a grooved plasticine wedge placed and submerged 1mm underwater, or placed in a rubber hold. For SD-OCT cross-sectional B-scans 1000 A-scans per B-scan with 100 total scans. Images were created using the Diver software (Bioptigen,Inc.) (Toms *et al.*, 2017).

2.28 Histology

2.28.1 Fixation

Zebrafish were fixed in 4% paraformaldehyde (PFA). Zebrafish up to 5 days were fixed whole overnight at 4^{o}C while adult zebrafish were decapitated to allow better perfusion into the head and fixed for 1 week at 4^{o}C.

2.28.2 Decalcification

Decalcification was required on adult fish to allow for whole head sections. The PFA was removed and the head washed twice in PBS. 0.5M EDTA was added to each head and incubated at room temperature for 10 days.

2.28.3 Tissue Processing

Fish heads were removed from EDTA washed twice in ddH_2O and placed in M512 – Macrosette (Simport, Beloeil, Canada) the cassettes were then placed in a Microm STP 120 tissue processor. The program is described in Table 2.17

Table 2.17 Microm STP 120 tissue processor programme

Time	Reagent
7 hours	70% ethanol
1 hour	70% ethanol
45 minutes	90% ethanol
45 minutes	90% ethanol
45 minutes	90% ethanol
45 minutes	100% ethanol
45 minutes	100% ethanol
30 minutes	100% ethanol
30 minutes	Xylene
30 minutes	Xylene
1 hour	Paraffin
1 hour	Paraffin

2.28.4 Paraffin Wax Embedding and Sectioning

Zebrafish heads were embedded in disposable plastic moulds (Simport). These were orientated in a face down position and molten paraffin wax added to the base moulds. M512 – Macrosette were placed on top and used as a base for the paraffin blocks. Blocks were rested on ice for 5 minutes prior to sectioning. Fish heads were sectioned at 4 µm using a Leica RM 2135 microtome (Leica Biosystems). When the optic nerve was located multiple tissue sections were collected on Superfrost Plus™ slides and incubated at 37^{o}C to melt onto slides.

3.28.5 H&E Stain

Sections were deparaffinised in two changes of Histoclear (NationalDiagnostics, Atlanta, USA) for 5 minutes. Rehydration of tissues occurred through two changes of 100% ethanol, 90% ethanol 70% ethanol and then H_20 for 5 minutes each. Tissue stained in Mayers Haemalum (ThermoFisher) for 1 minute and washed in running tap water until blue. Tissue was then counterstained in 1% aqueous eosin solution (ThermoFisher) and washed to remove excess eosin. Tissue was dehydrated through the ethanol gradient and cleared in Histoclear (1 minute in each). Slides were mounted with DPX mounting medium (Merck) and glass coverslips.

2.29 Retinal Cell Counts

Images were acquired by light microscopy using an Axio Imager Z1 fluorescence microscope (Zeiss, Oberkochen, Germany) using a 20x objective. The images were analysed on ImageJ. Six 100µm^2 sections, three on each side of the optic nerve were selected spaced along the retina as displayed in Figure 2.2, RGCs were counted from these sections to give an average RGC number. Three tissue sections were examined from an area displaying the optic nerve of each zebrafish and averaged.

Figure 4.2 Representative Retinal sections and 100µm^2 section of retina.

2.30 Optic Nerve measurements

At the optic head measurements of the optic nerve were taken across from the retinal pigment epithelial cells.

2.31 Electron Microscopy

Electron microscopy was performed by the Newcastle University Electron Microscopy Research Services.

2.32 Zebrafish Twitch Response

Zebrafish were grown in E3 medium up to 24 hpf, 15 zebrafish from each condition were recorded for 1 min per dish using a Leica stereomicroscope with a Chameleon digital camera (CMLN-13s2M). The 15 fish movements were counted and averaged.

2.33 Zebrafish Touch Response Assay

Zebrafish were grown in E3 medium up to 48hpf. Fish were dechorionated at least 1 hour prior to testing. Single zebrafish were placed in fresh E3 medium on an illuminated stage and the back of the head touched using a fine pipette tip to see the response to tactile stimulation. Videos were recorded using a Canon legria hfr76 camera at 25 frames per second suspended 7cm above the zebrafish using a clamp, a ruler was recorded for scale.

Analysis was performed in ImageJ as described in O'Connor *et al.* 2018. Videos imported using the Movie FFMPEG plugin. The images were converted to 8bit and thresholding was performed to acquire a black and white image which could be converted to binary and analysed using the Trackmate plugin. Thresholding performed in Trackmate to assure only fish movements tracked. Values for distance travelled and average speed could be extracted from data (O'Connor *et al.*, 2018).

2.34 Adult Movement

Adult zebrafish were placed in pairing tank with enough water to move in horizontal directions but not vertically. The fish were allowed 3 minutes to become acclimatised to the tank and recorded for 1 minute. Videos were recorded using a Canon legria hfr76 camera at 25 frames per second suspended above the zebrafish using a clamp, a ruler was recorded for scale.

Videos were analysed the same as in the "Zebrafish Touch Response Assay".

3.35 Blood Glucose

Blood Glucose was measured using a modified protocol from Eames *et al.*, 2010 (Eames *et al.*, 2010) OneTouch Ultra blood glucose monitor and OneTouch Ultra test strips (Lifescan, Milpitas, USA). Zebrafish were separated overnight in breeding tanks to prevent feeding.

Zebrafish were euthanized in tricane then decapitated. The decapitation cut through the heart and blood could be taken from here onto the OneTouch Ultra test strips. The blood glucose in mmol/L was recorded (Eames *et al.*, 2010).

3.36 Mitochondrial Ca2+ uptake

Mitochondria were isolated but instead of resuspending in IB, they were washed then resuspended in KCl buffer (125 mM KCl, 2 mM K2HPO4, 1 mM MgCl2, 5 mM glutamate, 5 mM glutamate and 20 mM HEPES (pH 7)). Protein concentration was determined by Bradford assay and 50µg protein added to 1ml KCL buffer and centrifuged at 10600g for 10 minutes. The pellet was resuspended in 180 µl of KCL medium containing 1 µM of the cytosolic calcium probe OregonGreen 5N. This was transferred into a black 96-well plate with flat and transparent bottom measurements were taken on a Varioskan LUX platereader (ThermoFisher) every 2 seconds at excitation at 485 nm and emission at 510 nm. After 30 seconds 20 µl of KCL buffer supplemented with 200 µM $CaCl_2$ was added and fluorescence measured for a further 4 minutes 30 seconds (Prudent *et al.*, 2013).

3.37 Acetylcholine Esterase Assay

The Acetylcholine esterase assay was modified from Teixido *et al.*, 2013. Zebrafish tissue and pooled embryos were homogenized in 0.5 ml ice-cold sodium phosphate buffer (0.1 M, pH 7.4, and 0.1% v/v Triton X-100). Homogenates were centrifuged for 15 minutes at 4^{o}C at 10000g. After quantification through BCA assay 10µg of protein had 0.3mM DNTB and 0.45mM AChE added and the spectrophotometric reading at 405nm read for 10 minutes on a Varioskan LUX platereader (ThermoFisher) (Teixido *et al.*, 2013).

Chapter 3: A Morphant Model of Wolfram Syndrome

3.1 Introduction

Morpholinos were developed in 1998 by Dr James Summerton's group and have been used as a tool to transiently knockdown expression of mRNA in zebrafish since 2000 (Partridge *et al.*, 1996; Nasevicius and Ekker, 2000). Morpholinos are normally comprised of 25 bases that work by complimentary base pair binding to RNA through an RNase-H–independent mechanism (Summerton, 1999). Due to a phosphorodiamidate backbone the neutrally charged oligo has a very high affinity for RNA (Bill *et al.*, 2009). By binding to mRNA they are predominantly designed to effect translation in two ways: splice blocking and translation blocking as seen in Figure 3.1.

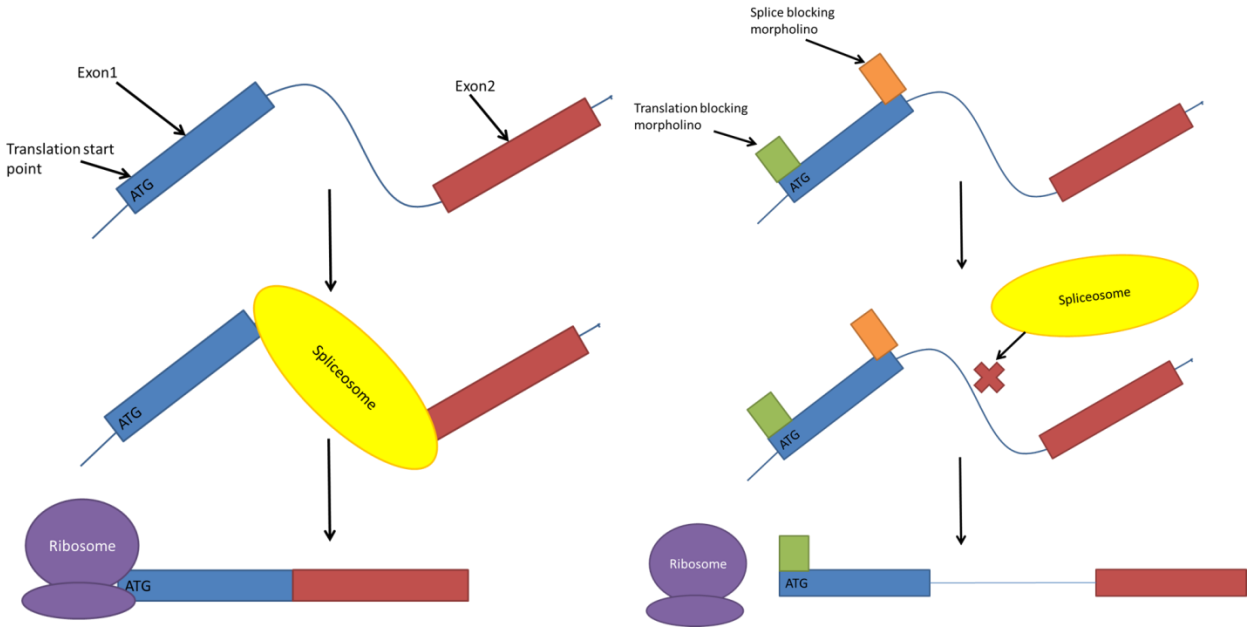

Figure 3.1 Morpholino Function. The principle of splice blocking and translation blocking morpholinos and action on RNA transcripts.

A splice blocking morpholino is designed to target splice sites and will prevent splicing machinery from functioning, leaving intronic mRNA, this defective transcript is degraded resulting in a knockdown in expression of the selected protein. Translation blocking morpholinos work by steric hindrance of the translation machinery by binding at transcription start points. This also results in lower protein expression. This highlights that a morpholino model is not a true knockout, but rather a knockdown of protein expression.

A number of issues have been known to occur when using morpholinos in zebrafish. This includes a number of off target effects that can be caused by the off target activation of p53

pathways (Robu *et al.*, 2007). In response to this discovery a number of guidelines (Eisen and Smith, 2008) were published in which a number of controls were established to ensure non-specific effects were mediated. However, even with these guidelines it was described that a number of morpholino experiments did not match up when equivalent CRISPR knockouts were made (Kok *et al.*, 2015) and morpholino knockdowns tend to be more severe in phenotype then their CRISPR counterparts. New guidelines have been produced (Stainier *et al.*, 2017) that suggest genetic knockouts should be used as a control for any morpholino experiment and if complete knockout is lethal, rescue experiments should be attempted to ensure the phenotype is corrected by co-injection with mRNA. Rossi *et al*. suggest that the more subtle effects of the CRISPR knockouts may be due to compensatory mechanisms after deleterious mutations (Rossi *et al.*, 2015). They observed that when morpholino was injected into genetic knockouts they were less sensitive than the wild-type knockdowns. This suggested that morpholino off target effects were not the main cause of differences seen but another mechanism. Alongside this they showed that knocking down *vegfaa* showed an upregulation of *vegfab* in the knockout but not the morphant. This shows that compensatory mechanisms are being upregulated in knockouts suggesting phenotypes seen in morphants may be a truer representation of protein function compared to knockouts (Morcos *et al.*, 2015).

The *WFS1* orthologues *wfs1a* and *wfs1b* were knocked down by morpholinos in zebrafish. This was performed in order to ascertain the feasibility of using genetic knockouts as a model of WS.

3.2 Characterisation of Abnormal Phenotypes

In order to create a consistent marking scheme for phenotyping, a number of specific phenotypic markers were assessed for severity. The markers were: the eye, the otoliths (ear) and the brain, these were chosen as they are similar tissues that are affected in WS in patients, the tails also showed a large number of changes so were also included in the phenotyping. Using a combination of marks an overall phenotypic score was created to assess the effectiveness of the morpholino models: 0-2 points mild, 3-5 moderate and 6+ severe. Examples of each category of phenotype can be seen in Figure 3.2.

The markers were visually assessed at 72hpf for mild/moderate/severe phenotypes. For the zebrafish tails (Figure 3.2A) slight curvature was classed as mild, while severe tails were

severely curved and much smaller in size. For eyes (Figure 3.2B), mild eyes had a size reduction while moderates started to develop structural abnormalities with severe eyes being substantially smaller or even lacked eyes. The zebrafish heads/brains (Figure 3.2C) appeared to develop oedema and substantially different cranial features at the severe end of the scale. The zebrafish ear, which is comparable to a human inner ear, contains two otoliths at 72hpf that are moved to sit on the macular in the zebrafish ear. In the morphants these appeared displaced either moving towards each other (mild) or fused or missing (severe).

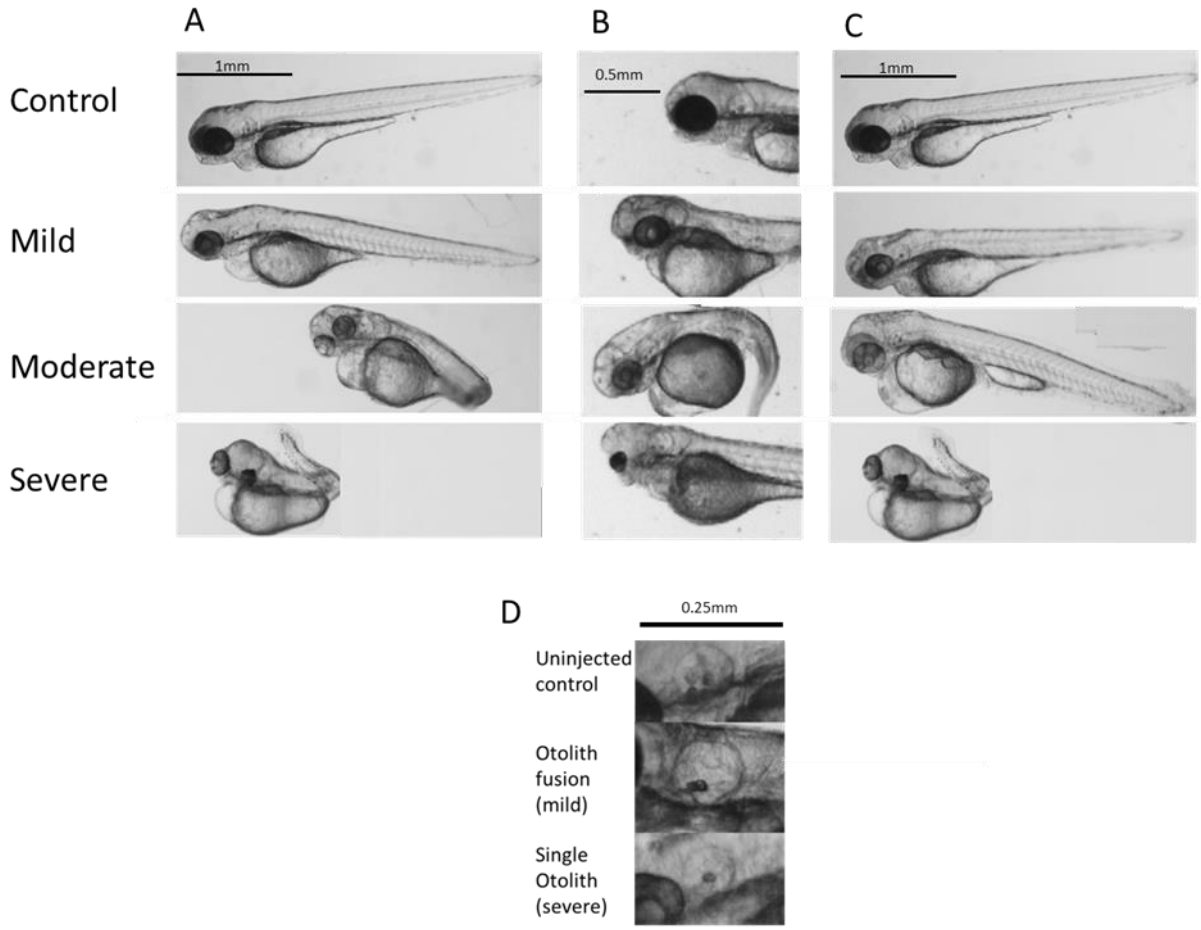

Figure 3.2 Phenotyping of *wfs1* Morpholino Zebrafish. A-Examples of tails in each category, B- Examples of eyes in each category, C- Examples of head/brain abnormalities in each category and D- Examples of Otoliths in each category. A point system was designed with: 1 point was given for a mild phenotype, 2 for moderate and 3 for severe. These were used to separate zebrafish into gross phenotypic groups 0-2 points mild, 3-5 moderate and 6+ severe.

3.3 Optimisation

Morpholino concentrations had to be optimised to find the best concentration for use in future experiments. Three morpholinos were tested a *wfs1a* and *wfs1b* splice blocking morpholino, a *wfs1b* translation blocking morpholino was also used.

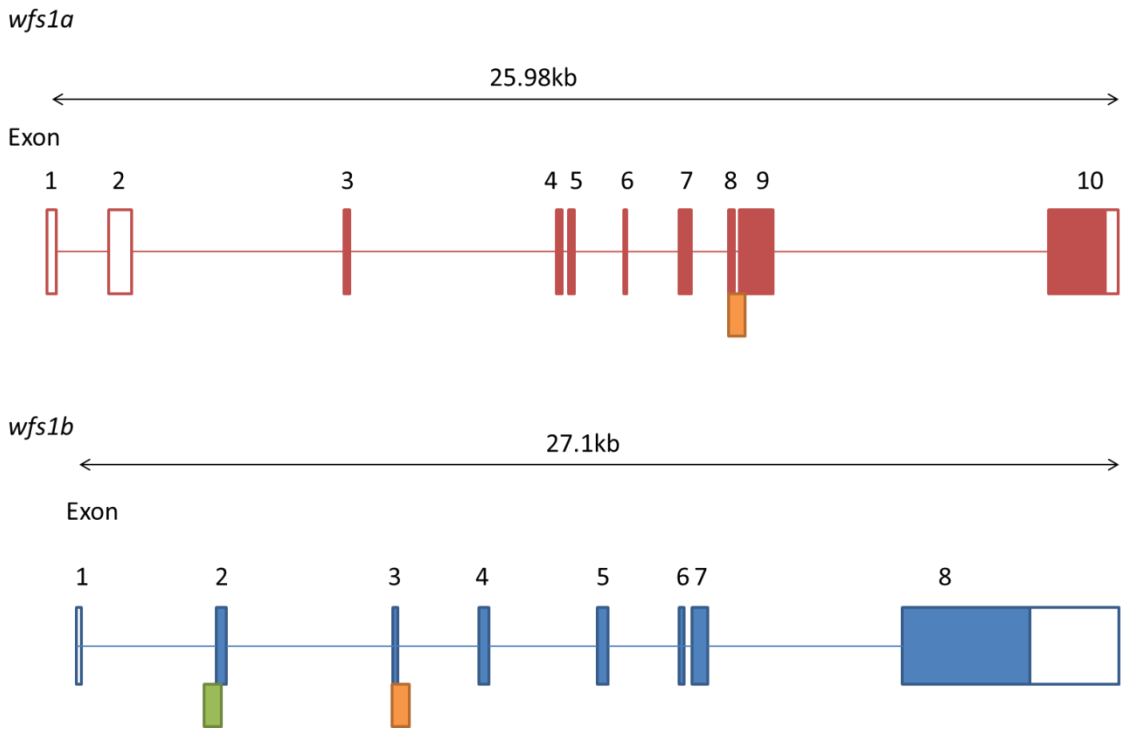

Figure 3.3 *wfs1a* and *wfs1b* gene and location of morpholinos. The orange blocks represent splice blocking morpholinos and the green translation blocking. The *wfs1a* splice blocking morpholino interrupts splicing between exon 8 and 9 and the *wfs1b* morpholino between exon 3 and 4.

For *wfs1a* three concentrations were used 0.2mM, 0.4mM and 0.8mM. Clutches of 50 zebrafish embryos were injected with 3 the three concentrations of *wfs1a* splice blocking morpholino. At 72hpf the phenotypes were scored and sorted into gross morphological phenotypes as described in Figure 3.1., dead fish were also recorded.

The *wfs1a* morpholino at low concentrations did not provide any significant differences to uninjected zebrafish. At higher concentrations (0.8mM) the morpholino appeared to be toxic resulting in a higher percentage of fish dying (40%), this was not significant although injections at this concentration were not repeated. It was decided to continue using 0.4mM of the morpholino as it had a total of 11% of fish with a phenotype (mild, moderate and severe).

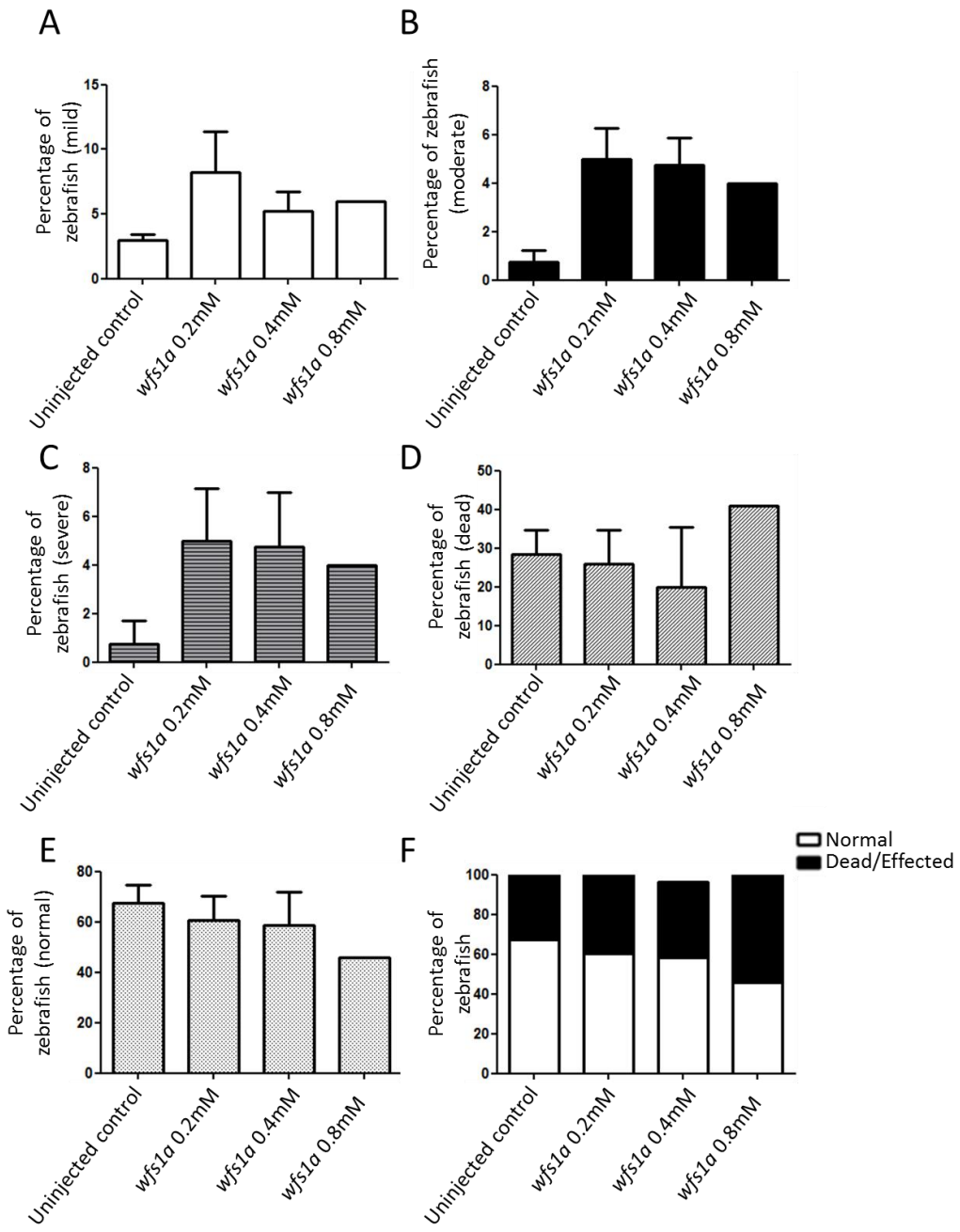

Figure 3.4 *wfs1a* Splice Blocking Morpholino Optimisation. A: Percentage of zebrafish with mild phenotypes. B: Percentage of zebrafish with moderate phenotypes C: Percentage of zebrafish with severe phenotypes. D: Percentage of zebrafish with no phenotypes. E: Percentage of fish with that were normal compared to effected/dead.

The percentage of fish in each group was calculated alongside number of deaths and plotted on a grouped column graph +SEM using Graphpad Prism (mean only for F). Uninjected control n=4, 0.2mM n=4, 0.4mM n=4, 0.8mM n=1. A-E: Two-way ANOVA was performed and no significant differences were seen when compared to the control using Bonferroni multiple comparisons: $p>0.05$.

For the *wfs1b* splice blocking morpholino (Figure 3.5) four concentrations were used: 0.2mM, 0.4mM, 0.5mM and 0.6mM. Clutches of 50 zebrafish embryos were injected with the 4 concentrations of *wfs1b* splice blocking morpholino. The phenotypes were scored and sorted into gross morphological phenotypes as described in Figure 3.2. 0.5mM and 0.6mM of morpholino resulted in a significantly higher proportion of dead zebrafish (80% $p<0.001$) while 0.2mM and 0.4mM provided significantly different numbers of mild phenotypes compared to the control (0.2mM $p>0.05$ and 0.4mM $p>0.001$). 0.4mM also had a higher proportion of severe phenotypes 4% compared to 0.1% for controls.

It was decided to continue with 0.4mM of morpholino as the optimum concentration due to the higher percentage of mild phenotypes while not increasing the death rate Figure 3.5 A and D.

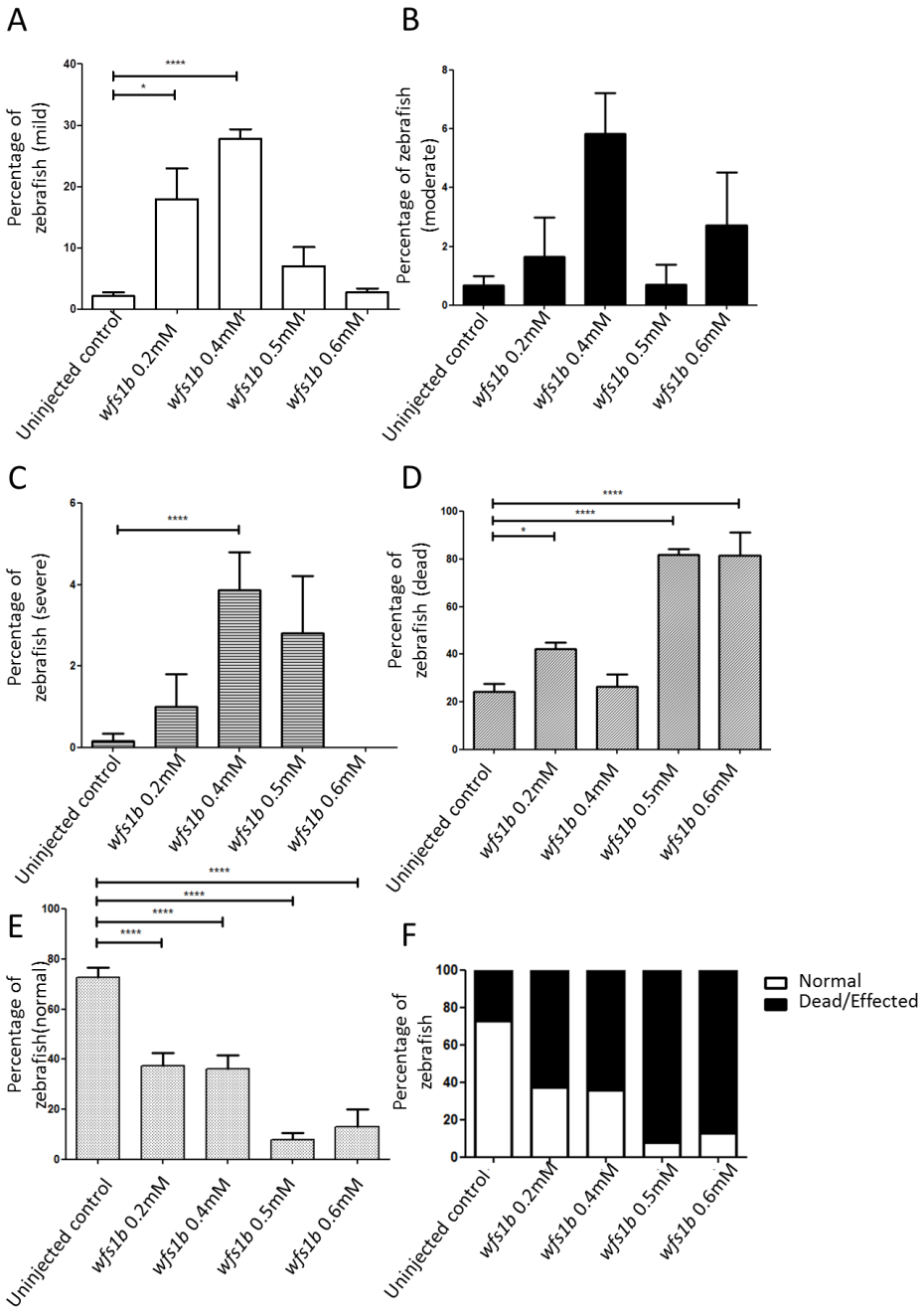

Figure 3.5 *wfs1b* Splice Blocking Morpholino Optimisation. A: Percentage of zebrafish with mild phenotypes. B: Percentage of zebrafish with moderate phenotypes C: Percentage of zebrafish with severe phenotypes. D: Percentage of zebrafish with no phenotypes. E: Percentage of fish that were normal compared to affected/dead.

The percentage of fish in each group was calculated alongside number of deaths and plotted on a grouped column graph +SEM using Graphpad Prism (mean only for F). 0.2mM n=4 0.4mM n=6 0.5mM n=3, 0.6mM n=3 uninjected control n=6. A-E: Two way ANOVA was performed and significant differences were seen when compared to the control using Bonferroni multiple comparisons and noted on the graph $p<0.05$ = *, $p<0.005$ = ***.and $p<0.001$ = ****

As a control for the *wfs1b* splice blocking morpholino a *wfs1b* translation blocking morpholino was purchased. This was injected at 6 different concentrations: 0.2mM, 0.4mM, 0.5mM, 0.6mM, 1mM and 1.4mM. The zebrafish were injected and scored using the previously categorised system.

The results had no consistently significant changes in mild, moderate and severe phenotypes. Suggesting the translation blocking morpholino was unsuccessful; this could not be confirmed by western blot as there is currently no zebrafish specific *wfs1* antibody available. Although an increased number of mild phenotypes could be seen this was not significant and did not seem to change with increasing doses, as off target effects could not be ruled out the experiments were continued with splice blocking morpholinos only.

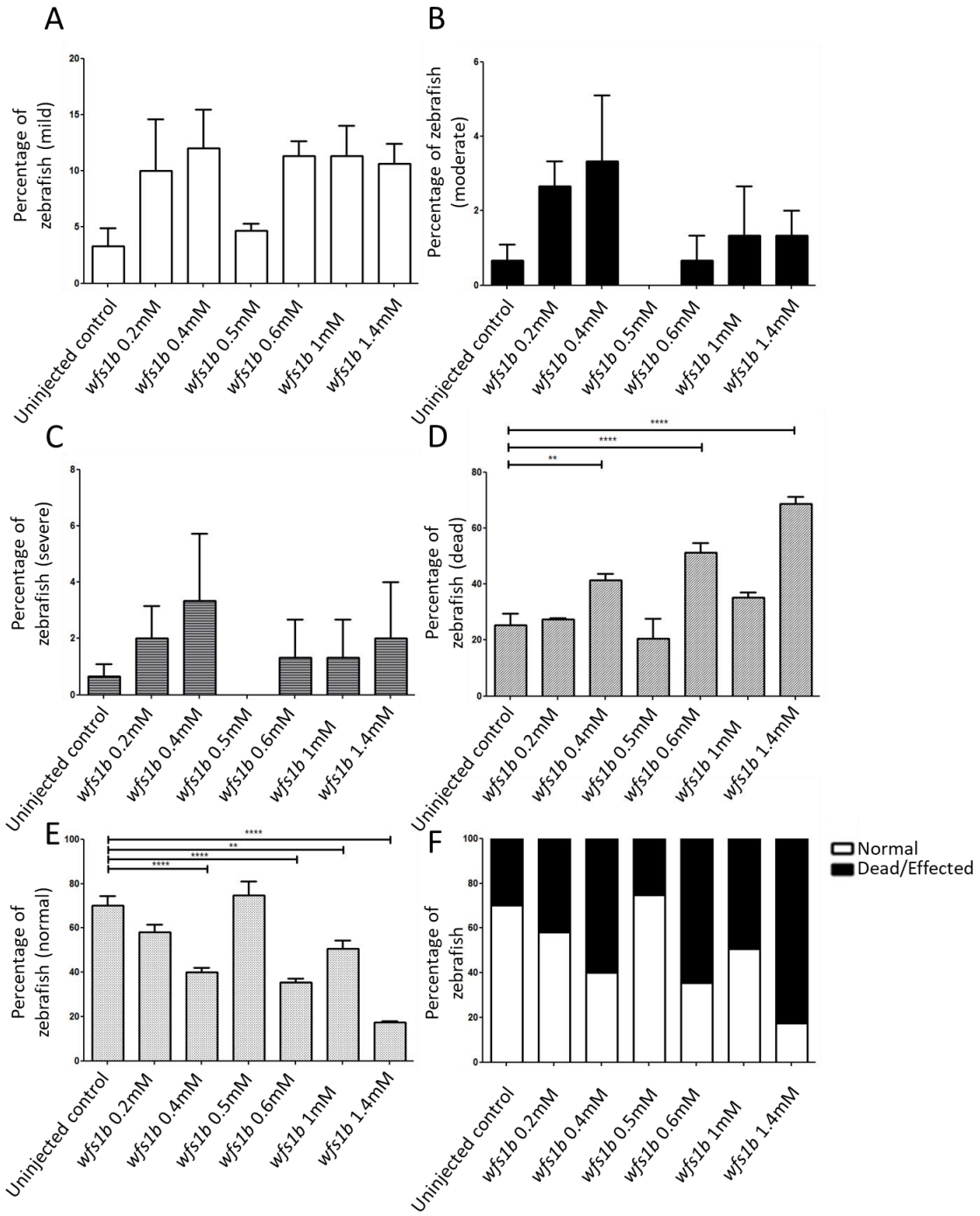

Figure 3.6 *wfs1b* Translation Blocking Morpholino Optimisation. A: Percentage of zebrafish with mild phenotypes. B: Percentage of zebrafish with moderate phenotypes C: Percentage of zebrafish with severe phenotypes. D: Percentage of zebrafish with no phenotypes. E: Percentage of fish with that were normal compared to effected/dead.

The percentage of fish in each group was calculated alongside number of deaths and plotted on a grouped column graph +SEM using Graphpad Prism (mean only for F). 0.2mM n=4 0.4mM n=6 0.5mM n=3, 0.6mM n=3 uninjected control n=6. A-E: Two way ANOVA was performed and significant differences were seen when compared to the control using Bonferroni multiple comparisons and noted on the graph $p<0.01$ = ** and $p<0.001$ = ****.

The two splice blocking morpholinos were combined at their optimum concentrations (0.4mM) in order to determine if a double knockdown morphant was viable. The zebrafish were injected and scored using the previously categorised system.

The combination of the two morpholinos only resulted in a significant increase in deaths compared to normal phenotypes in uninjected controls. In addition, a large change is observed in the reduction of mild phenotypes seen in *wfs1b* 0.4mM compared to the combined morphants (Figure 3.7A). This change suggests that the double knockdown is causing the zebrafish to die instead of these less severe phenotypes.

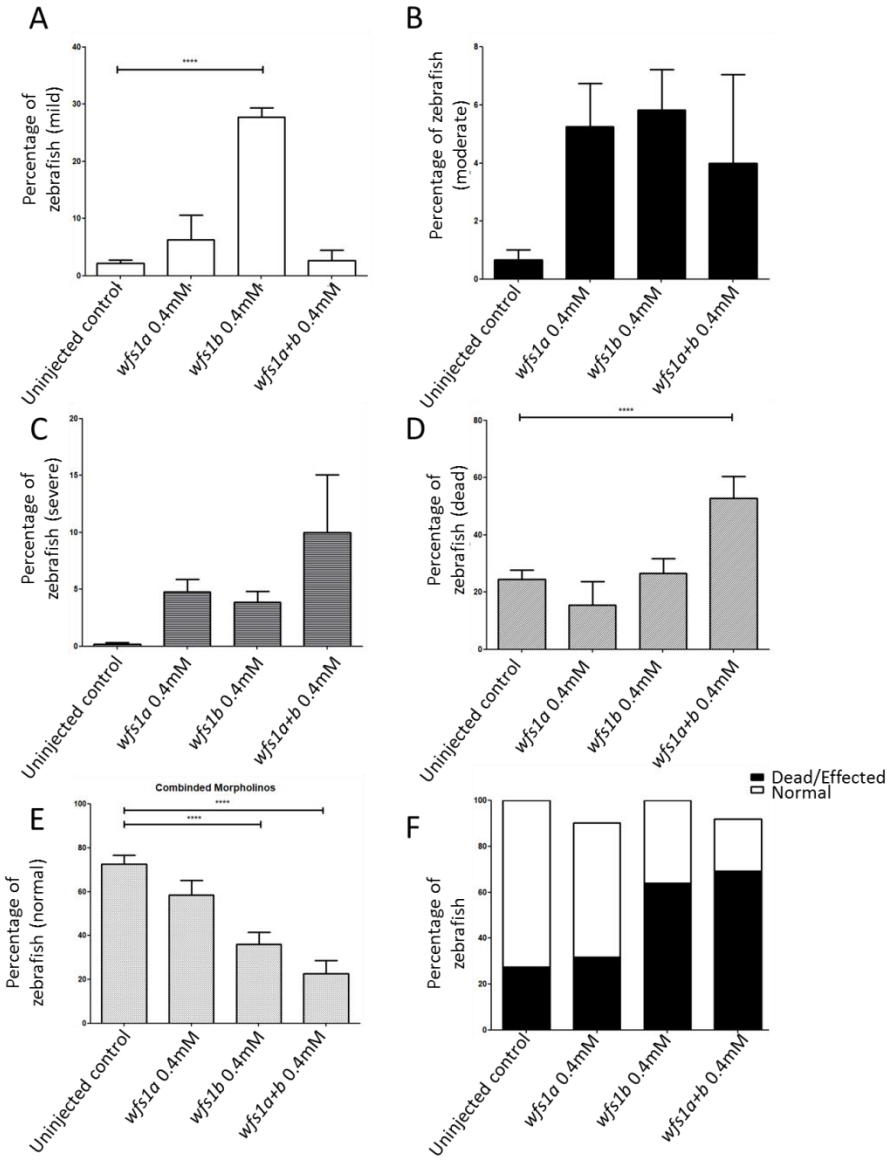

Figure 3.7 Phenotyping for combined injection of *wfs1a* and *wfs1b* morpholinos. A: Percentage of zebrafish with mild phenotypes. B: Percentage of zebrafish with moderate phenotypes C: Percentage of zebrafish with severe phenotypes. D: Percentage of zebrafish with no phenotypes. E: Percentage of fish with that were normal compared to effected/dead.

Zebrafish embryos were co-injected with 0.4mM concentrations of either *wfs1*b or *wfs1*a or *wfs1*a+*wfs1b* splice blocking morpholinos into 1-4 cell zebrafish embryos. The percentage of fish in each group was calculated alongside number of deaths and plotted on a grouped column graph +SEM using Graphpad Prism (mean only for F). Replicates of 50 embryos were taken for each concentration. *Wfs1a* 0.4mM n=4 *wfs1b* 0.4mM n=6, uninjected control n=6 and Combined 0.4mMa+b n=3. A-E: Two way ANOVA was performed and compared to the control using Bonferroni multiple comparisons. Significant differences were seen and noted on the graph, $p<0.001$ = ****.

3.4 Confirmation of Splicing Defects

To confirm that the splice blocking morpholinos were modifying the RNA transcripts RT-PCRs were performed on pooled embryos which displayed a phenotype.

For *wfs1a* knockout fish there were very obvious changes in splicing. This can be seen in Figure 3.8 where there is no trace of a normal (~350bp) sized band seen in the uninjected control. The larger molecular weight product suggests a retained intronic sequence and the fact no 350bp fragment is seen in the morphants suggested very efficient splice blocking. These bands were extracted and subjected to a second round PCR in order to get enough material for sequencing. The larger molecular weight product was sequenced to reveal intronic DNA being retained in the *wfs1a* morphants. Intron 7-8 was shown to be completely retained and partial coverage of intron 6-7 was also detected. Band shifts in the *wfs1b* splice blocking morpholino (Figure 3.9) were less clear than the *wfs1a* counterpart.

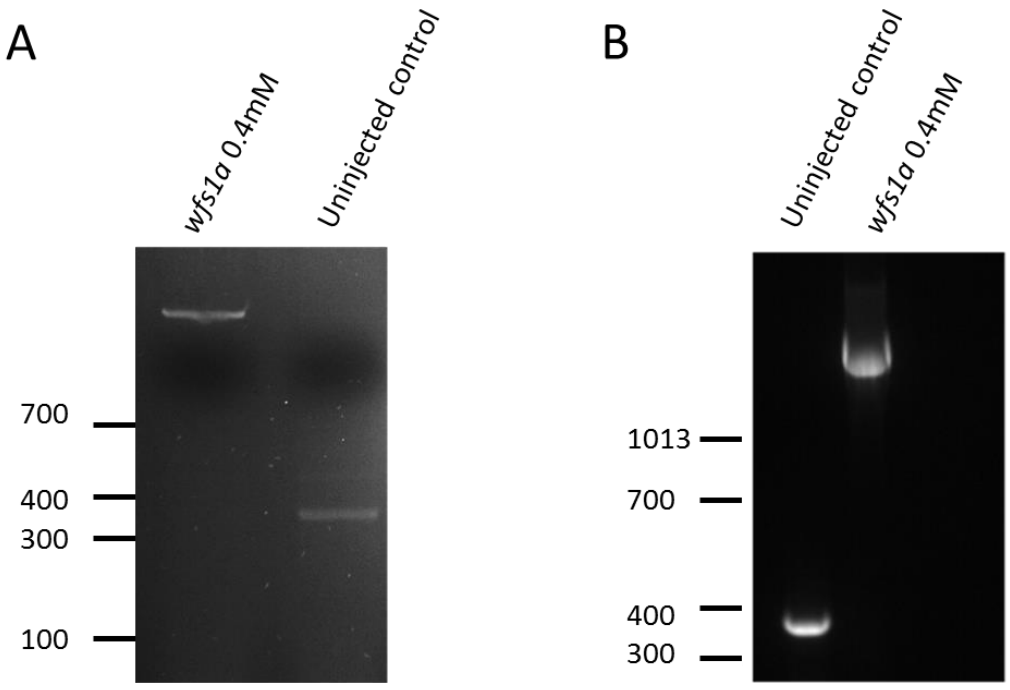

Figure 3.8 Confirmation of abnormal *wfs1a* splicing. A: PCRs were performed of cDNA from *wfs1a* splice blocking morpholino and uninjected control zebrafish. PCRs were performed using the *wfs1a*_splice primer set from Table 2.4.B: Second round PCRs of gel extracted product. The PCR products were extracted from the gel (Figure 4.5A) and subjected to a second round PCR 19µl of product was loaded (Figure 4.5B). To visualise products samples was loaded on a 1.5% agarose gel, alongside Hyperladder IV (Bioline) and electrophoresed at 80V for 2 hours. Gels were visualised using UV imaging on a GelDoc-IT Imaging system (UVP) (A)

Multiple bands could be observed and bands in both 48hpf and 72hpf that differed from the control were extracted for further analysis.

The bands extracted were: “48hpf High Band”, “48hpf expected”, “72hpf expected” and “72hpf Lower Band” noted in Figure 4.6A. The four bands with successful PCR reactions were marked with arrows in Figure 4.6A. Second round PCR reactions were extracted and sequenced the 48hpf High Band when sequenced included a 60bp intronic sequence.

At 72hpf, a lower band was observed and sequencing only detected exon 2 indicating that exon 3 might be skipped. However, a large amount of the non-spliced product can be seen suggesting this morpholino was not as effective as the *wfs1a* morpholino.

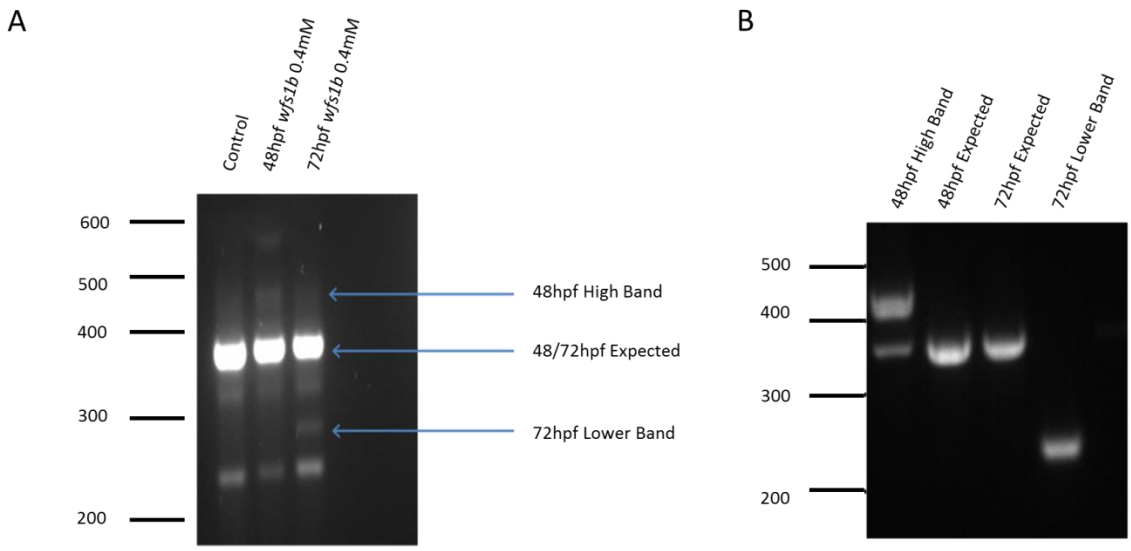

Figure 3.9 Confirmation of abnormal *wfs1b* splicing. A: PCRs were performed of RT-PCR products from *wfs1b* splice blocking morpholino and uninjected control zebrafish. PCRs were performed using the wfs1b_splice primer set from table 2.4.B: Second round PCRs of gel extracted product. The PCR products were extracted from the gel (Figure 4.5A) and subject to a second round PCR 19µl of product was loaded (Figure 4.6B). To visualise products samples was loaded on a 1.5% agarose gel alongside Hyperladder IV (Bioline) and electrophoresed at 80V for 2 hours. Gels were visualised using UV imaging on a GelDoc-IT Imaging system (UVP)

3.5 Controls

3.5.1 p53 Morpholino co-injection

Wfs1b zebrafish were co-injected with a p53 morpholino as a control for off target effects. Percentages of phenotypes accurately mirror the results of the *wfs1b* morpholino by itself. It can also be seen that the phenotypes are also similar between the two groups as seen in Figure 3.10b with eyes, heads and tails all having similar effects.

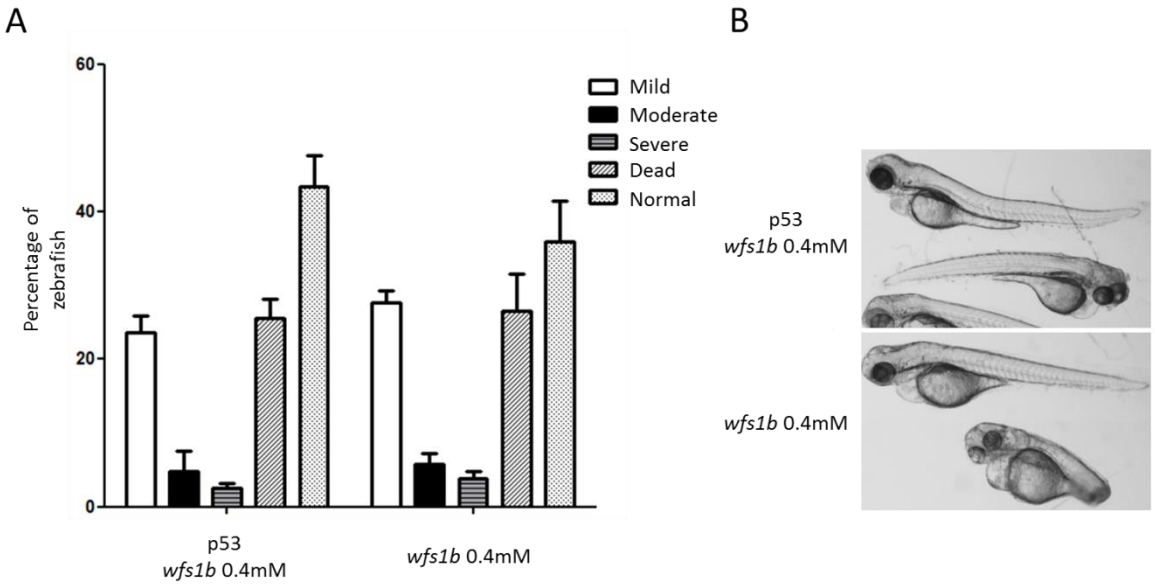

Figure 3.10 Co-injection of p53 and *wfs1b* splice blocking morpholino. A: Percentage of zebrafish with mild, moderate, severe, dead and normal phenotypes when injected with *wfs1b* splice blocking morpholino and p53 morpholino, compared to *wfs1b* splice blocking alone. B: Representative images of p53+ *wfs1b* and wfs1b splice blocking morpholino by itself. The phenotypes were sorted into gross morphological phenotypes as shown in Figure 4.2. The percentage of fish in each group was calculated alongside number of deaths and plotted on a grouped column graph +SEM using Graphpad Prism (mean only for F). Replicates of 50 embryos were taken for each concentration. p53 *wfs1b* 0.4mM n=3 *wfs1b* 0.4mM n=6. Two way ANOVA was performed and compared to the control using Bonferroni multiple comparisons. No significant differences were seen.

3.5.2 Conformation with CRISPR

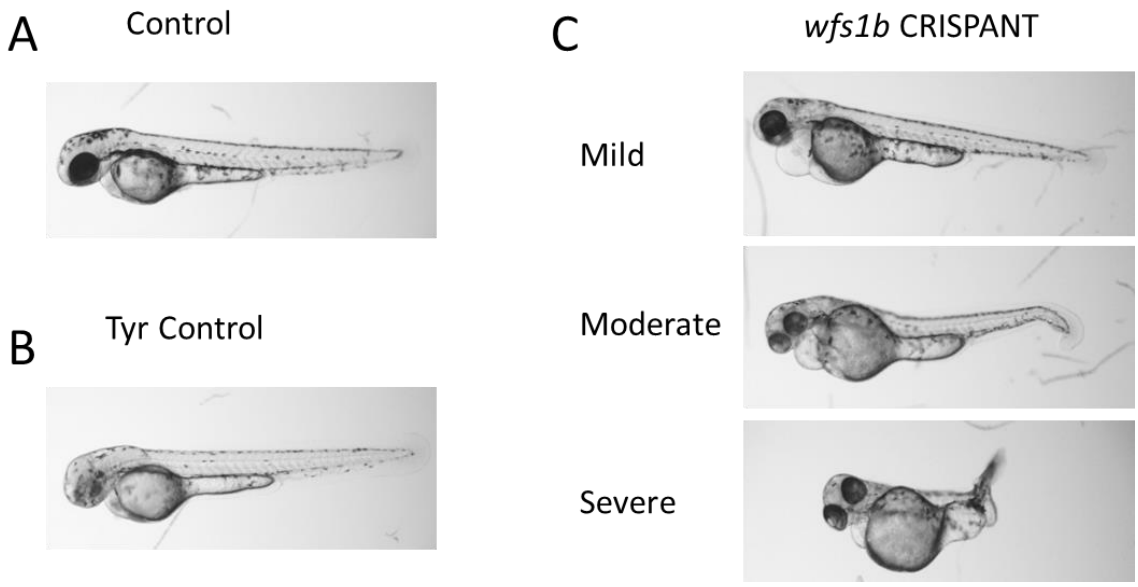

Figure 3.11 CRISPANT *wfs1b* mosaic knockout zebrafish at 48hpf. A: Control wildtype zebrafish at 48hpf. B: Tyrosinase CRISPANT with mosaic pigment knockout. C: wfs1b CRISPANTS. Zebrafish were injected with 3000ng of appropriate gRNA and Cas9 protein at the 1 cell stage. Zebrafish showing equivalent phenotypes were imaged at 48hpf.

Cas9 protein was co-injected with two *wfs1b* guide RNAs to create mosaic CRISPANT *wfs1b* knockouts. As a control a tyrosinase (Tyr) CRISPANT was also made to knockdown pigment formation (Figure 3.11B). Pigment loss can be seen in the eyes and on the top of the head. This highlights the mosaic nature of CRISPANTs with some pigment still developing. A selection of *wfs1b* mosaic knockouts are seen in Figure 3.10c which have similar brain eye and tail phenotypes to the *wfs1b* morpholino knockdowns.

3.6 Discussion

The aim of this chapter was to model WS in zebrafish using morpholinos to transiently knockdown *wfs1* expression. This was a proof of principle experiment to determine if using a transgenic model of WS could accurately model WS.

Attempts to transiently knockdown the *wfs1* gene in zebrafish had mixed results. Splice blocking morpholinos were used in both the *wfs1a* and *wfs1b* knockout models. Although both splice blocking morpholinos showed abnormal phenotypes the *wfs1b* morpholino appeared to give a higher percentage of zebrafish with adverse effects. When the two morpholinos were combined the in the majority of embryos died. This could be explained by a double knockout being lethal or toxic off target effects of being injected with too much morpholino (Robu *et al.*, 2007).

In the *wfs1a* knockdown there were very few changes in the morphology of the zebrafish with no significant differences in categories from the controls. The *wfs1b* splice blocking morpholino had more significant changes with a large number of morphant zebrafish with mild or abnormal phenotypes. The phenotypes seen appear consistent with a number of symptoms observed in the WS patient population: eye, ear and brain abnormalities (Barrett and Bundey, 1997). However, when looking at the changes of splicing from the *wfs1b* morpholino in the changes in splicing are not as clear as the *wfs1a* morpholino. One option why this may happen could be the levels of expression. If *wfs1b* is more highly expressed compared to *wfs1a* there would be more transcript to be altered resulting in a lower number of differentially spliced transcripts. It may also be that off target effects of the morpholino are the reason for seeing such phenotypes due to (Robu *et al.*, 2007; Kok *et al.*, 2015). In order to determine if this may be the case a number of controls were performed.

The first control was to use an ATG translation blocking morpholino, this morpholino acts in a different manner to the splice blocking (Bill *et al.*, 2009) so if it provided similar results would help to suggest this is not a splice morpholino specific phenotype. Although, a number of zebrafish appeared to have similar phenotypes to Figure 3.1 the translation blocking morpholino did suggest any changes with increasing doses. There is currently no zebrafish *wfs1* antibody and therefore any reduced *wfs1* protein expression could not be confirmed this way. As a result of this we decided to try a p53 knockdown in an attempt to offset the p53 mediated off target effects. The experiment replicated very similar results when co-injected with a *wfs1b* splice blocking morpholino suggesting p53 mediated off target effects may not be responsible for the changes seen in *wfs1b* knockdowns.

The final control that was used was a CRISPANT knockdown which uses mosaic F_0 generations to determine if any phenotypes can be seen. The *wfs1b* CRISPANT knockouts had a number of similar phenotypes such as small eyes and tail deformities. This combined with the p53 morpholino data suggests *wfs1b* knockouts are providing a real phenotype and not off target effects. The “Guidelines for morpholino use in zebrafish” recommend rescue experiments as one of the key controls for morpholino experiments (Stainier *et al.*, 2017). This was not completed due to problems with cloning of the *wfs1b* gene into an expression vector. However, data presented here shows the *wfs1* morpholinos confirming proof of principle and the two controls demonstrate that the effects of the morpholinos are specific. *Wfs1a* controls were not performed due to the lack of phenotypes seen in the morphants

and the total splicing seen in the PCRs suggested *wfs1a* may not be as important as *wfs1b* in the development of a zebrafish model of WS.

Although there are a number of controversies surrounding morpholinos, they still provide an inexpensive quick tool to determine, as a first step, if gene knockouts are worth pursuing. The aim was to use morpholinos to transiently knockdown the two orthologues of *WFS1* in zebrafish (*wfs1a/wfs1b*) to determine if transgenic mutant lines would be a project worth pursuing. With promising data from the *wfs1b* morpholino transgenic models were used to determine if WS could be accurately modelled in zebrafish.

3.7 Conclusions

Two transient *wfs1* knockdown models in zebrafish were developed using a morpholinos (*wfs1a* and *wfs1b*). The phenotypes seen appear consistent with a number of symptoms observed in patients with WS. Controls for the morpholinos were not consistent, leading to the use of a genetic knockout for all future experiments.

To fully confirm the morpholino models a rescue experiment would have to be carried out. This would require the co-injection of functioning mRNA with the morpholino to determine any phenotypes are non-specific. This model could then be compared to the genetic knockout to determine possible explanations for the difference in severity between the two models, which may possibly involve compensatory mechanisms not upregulated in morpholino experiments.

Chapter 4: Characterisation of Transgenic *wfs1* Mutant Zebrafish Lines

4.1 Introduction

Due to the promising data seen in the morpholino knockdown zebrafish (Chapter 3), a genomic knockout model of WS was investigated in zebrafish. Morpholinos work to transiently affect expression are only effective for the first few days of development (Eisen and Smith, 2008). As WS is mainly a degenerative disease and in order to look at zebrafish at older timepoints. Knockdowns will also have some functional transcript remaining, in order to counter these limitations found in a morpholino model a genetic knockout was used.

Zebrafish genomes can be modified in a number of methods, more recently zebrafish genomes have been modified with high specificity using CRISPR Cas-9, TALENS and Zinc finger nucleases (Doyon *et al.*, 2008; Sander *et al.*, 2011; Jao *et al.*, 2013). These methods use specifically targeted nucleases to edit the genome. However, more traditionally N-ethyl-N-nitrosourea (ENU) screens were used to create large numbers of random mutations in spermatogonia. These developed spermatozoa were used to out cross to wild type fish, and future generations in crossed to develop phenotypes and mutations worked out in reverse (Patton and Zon, 2001). More recently this has become more specific using targeting induced local lesions in genomes (TILLING), this involved sequencing F1 sperm from ENU mutated zebrafish and outcrossing for specifically targeted genes (Kettleborough *et al.*, 2013). This has resulted in a large repository of zebrafish containing mutations in specific genes which are available to purchase. This includes lines containing nonsense mutations in the orthologues of *WFS1,* the gene responsible for WS.

The zebrafish genome contains a number of duplicated genes with an average of 2.28 zebrafish genes for every human orthologue (Howe *et al.*, 2013). This was due to a genome duplication specific to the ray fin fish species approximately 340 million years ago (Meyer and Schartl, 1999; Howe *et al.*, 2013). It has been observed that these duplications have diverged in expression and when a number of gene functions were tested a quarter had diverged in function, through changes in protein domains or subcellular localisation (Kassahn *et al.*, 2009). Duplicates were also more likely to be involved in the following pathways: signalling, transcription, calcium ion transport, and metabolism; which *WFS1* is known to be involved in (Kassahn *et al.*, 2009). It is possible that a divergence in function has occurred in *wfs1*.

In order to determine if *wfs1a* or *wfs1b* may be a truer representation of the disease, their expression and role in the unfolded protein response were determined by assessing a range of WS-like phenotypes.

4.2 Confirmation of Knockout Sequences

The transgenic lines purchased from the EZRC were sent as a heterozygote outcross of F3 outcrossed mutants. The F4 generation were in crossed to create a stable line of mutants; these fish were further in crossed and outcrossed to produce further generations. Knockout zebrafish were fin clipped and sequenced to confirm they carried the mutation, for both *wfs1a* and *wfs1b* knockouts.

In *wfs1a* knockouts the mutation is in exon 9 and the 692nd amino acid where a G>A mutation causes a premature stop codon: TAG. An example of wild type and homozygote knockout sequences can be seen in Figure 4.1.

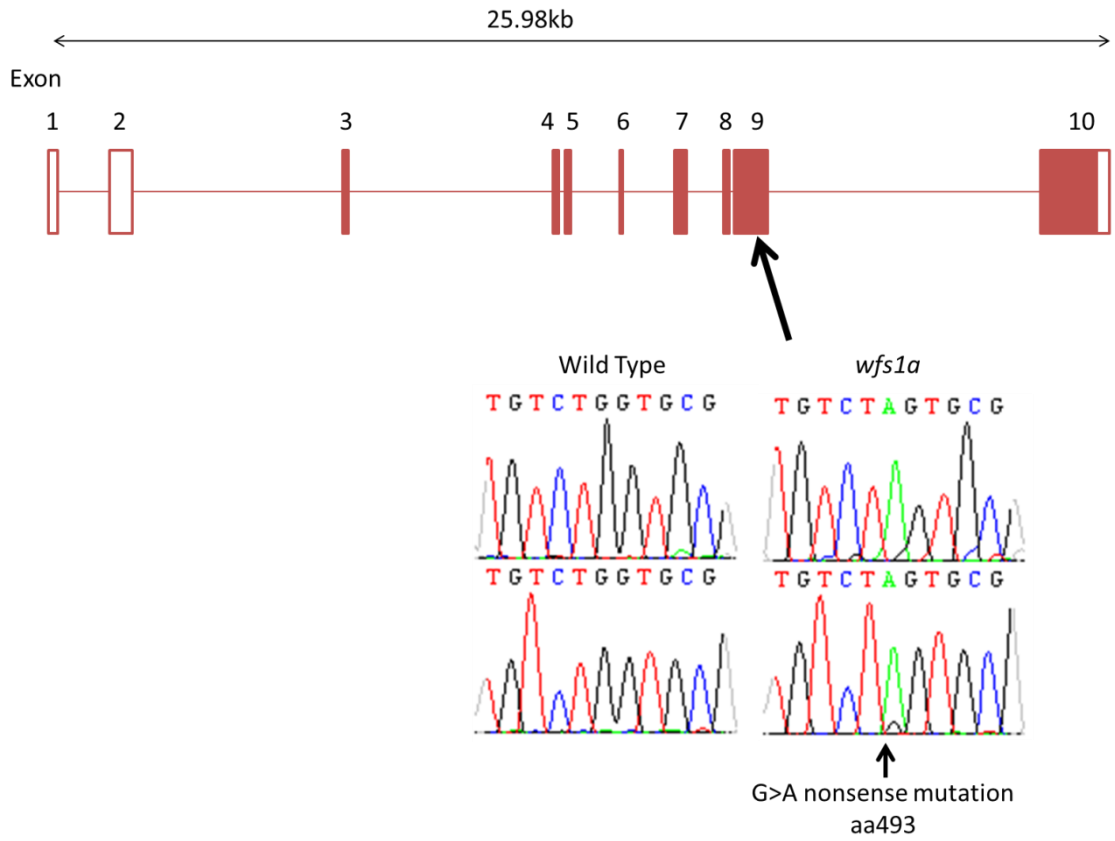

Figure 4.1. The *wfs1a* gene with *wfs1a* knockout mutation. A schematic of the *wfs1a* gene was designed showing coding (red) and non-coding exons (white), the size of the gene and location of nonsense mutation. Electropherogram of wild type and knockout mutations.

In *wfs1b* knockouts the mutation is in the final exon (exon 8) and the 493rd amino acid where a G>A mutation causes a premature stop codon: TGA. An example of wild type and homozygote knockout sequences can be seen in Figure 4.2.

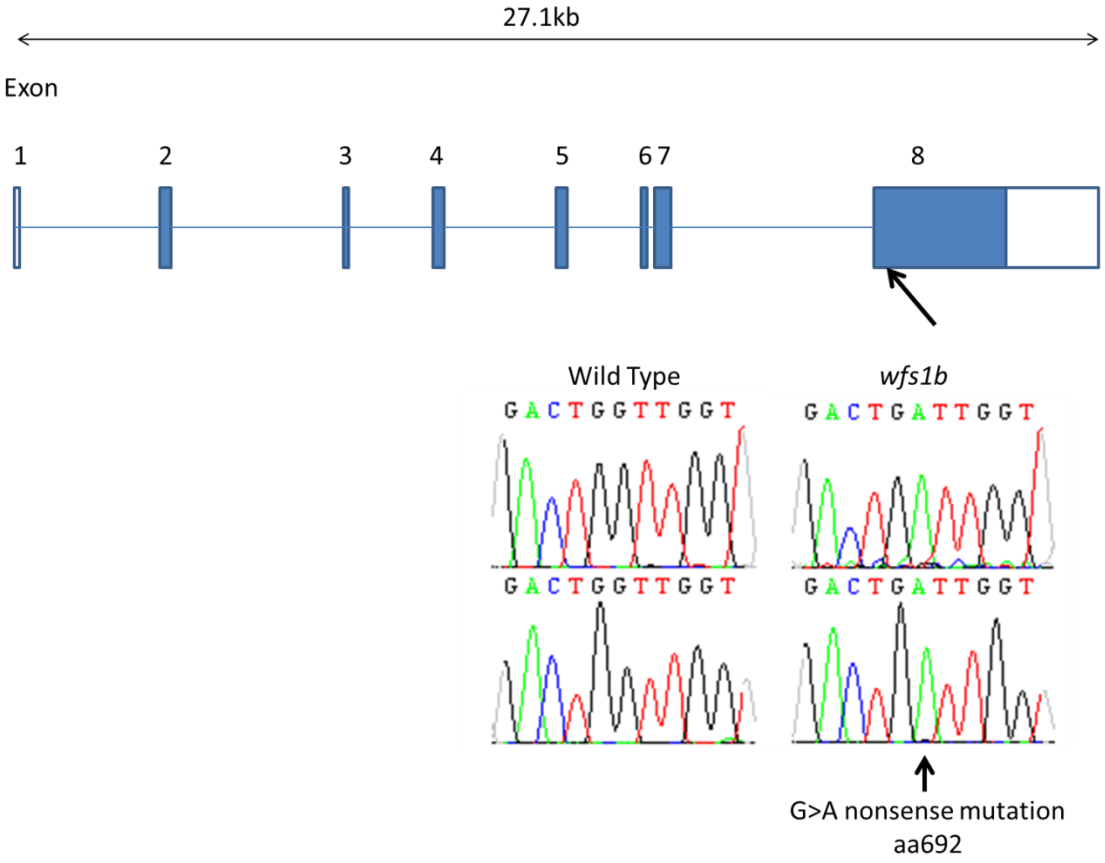

Figure 4.2 The *wfs1b* gene with *wfs1b* knockout mutation. A schematic of the *wfs1b* gene was designed showing coding (blue) and non-coding exons (white), the size of the gene and location of nonsense mutation. Electropherogram of wild type and knockout mutations.

With confirmation of the knockout sequences in zebrafish it was important to look at the expression and molecular mechanism of both *wfs1* homologues in zebrafish.

4.3 Expression of *wfs1*a/b

The expression was determined in embryos and a number of adult tissues by RT and qRT-PCR. The *wfs1b* expression in embryos appears at the 1 cell stage suggesting possible maternal expression and is constitutively expressed. *wfs1a* expression begins at a later time point and expression seems to be altered through development. In adults cDNA was analysed from the eyes, brains, spines and muscle of control zebrafish (Figure 4.3B). *wfs1a* expression appeared higher in muscle compared to the other tissues as quantified by qRT-

PCR in Figure 4.8C. This finding was confirmed to show that expression of *wfs1a* in muscles was far higher than other tissues and *wfs1b* slightly lower. This suggests a specific tissue localisation of *wfs1* homologues in *wfs1* that may explain some differences noted between the two knockout models.

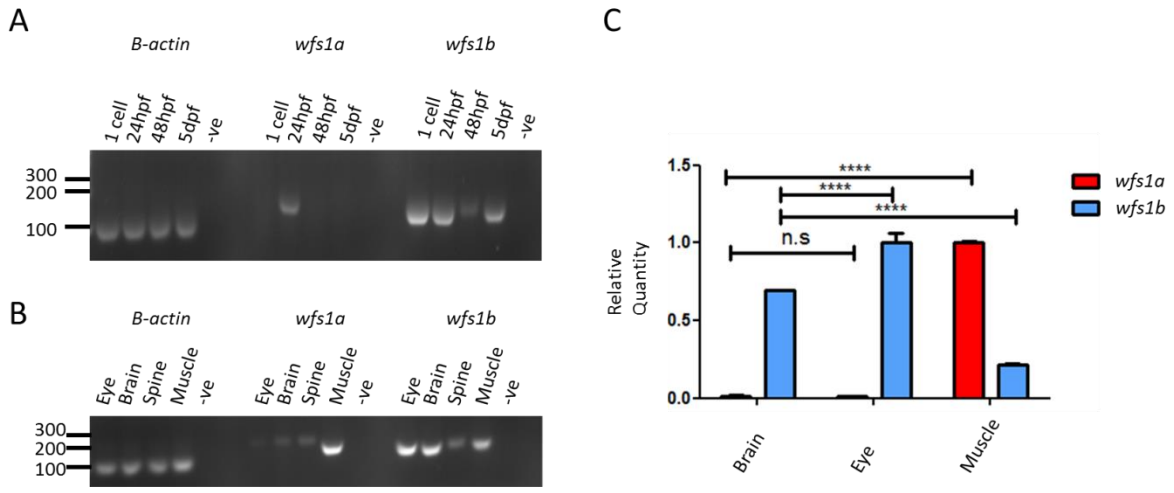

Figure 4.3 Expression of *wfs1* in embryonic and adult zebrafish. A: Embryonic expression of *wfs1*. B: Adult tissue expression of *wfs1*. Zebrafish cDNA generated from RNA isolated by TRIzol and RNeasy kit. PCR primers wfs1aq, wfs1bq1 and β-actin from Table 2.5-2.6. 1% agarose gel and run against hypperladder IV (bioline) and run at 100V for 30 minutes and visualised using UV imaging on a GelDoc-IT Imaging system (UVP). C: qPCR of *wfs1* adult tissue expression. cDNA expression quantified by analysed on Bio-Rad CFX Manager and plotted mean +SEM using Graphpad Prism performed in triplicate. Significance determined by unpaired t-test ****p<0.0001

4.4 UPR

In WS the UPR is upregulated through the lack of regulation of ATF6. If the UPR is upregulated with wolframin to regulate ATF6 the pathway is left "on" causing an increased response to ER stress. To determine if this pathway may be upregulated in the zebrafish, the UPR was increased by heat shocking the zebrafish at 37°C.

When zebrafish were heat shocked a number of the zebrafish appeared abnormal, (Figure 4.4A) the *wfs1a* and *wfs1b* knockouts had more severe phenotypes than the equivalent controls. Figure 4.4B shows the percentage of zebrafish that died within 24hours after heat shock at 6hpf. No significant differences were seen between deaths in the control and the heat shock control. As significant differences were seen between the heat shock *wfs1a* and *wfs1b* and their untreated equivalents (*wfs1a* p<0.01 and *wfs1b* p<0.001) In order to measure ER stress, the expression of BiP, the master regulator of ER stress, was quantified

by western blot. (Figure 4.4C). This showed an increase in BiP expression when heat shocked but also interestingly *wfs1a* BiP basal expression appeared higher than the control and *wfs1b*.

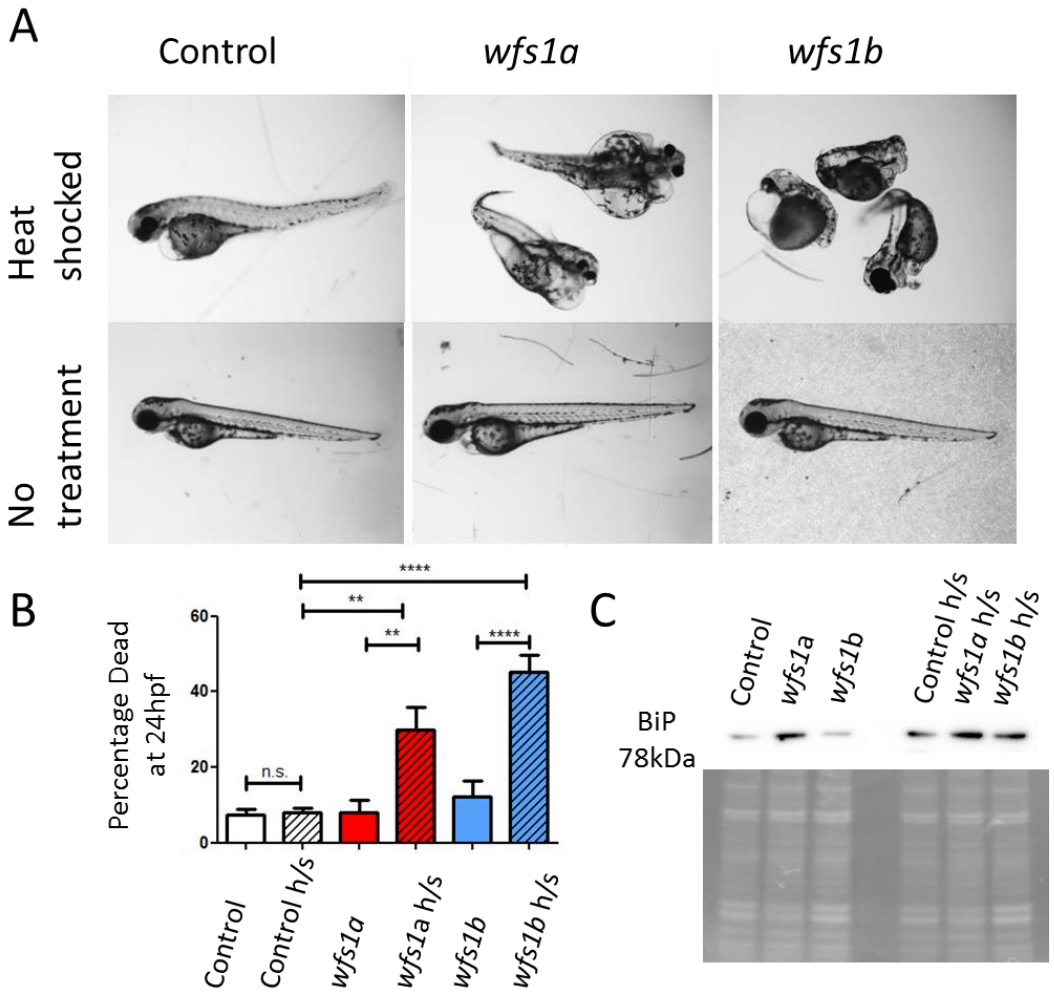

Figure 4.4 The unfolded protein response in *wfs1* knockout zebrafish. A: Representative images of abnormal zebrafish after heat shock compared to untreated. B: The Percentage of dead embryos at 24hpf heat shocked vs controls. 50 embryos treated or untreated were incubated in E3 overnight and dead determined at 24hpf. Data plotted mean +SEM using Graphpad Prism n=5. Significance determined by Two-Way ANOVA with Bonferroni multiple comparisons **p<0.01 ****p<0.0001.

4.5 Expression of key UPR transcripts

To determine if other UPR proteins were increased at basal levels four UPR markers ATF6, BiP, CHOP, and the spliced form of XBP (XBPs) expression was measured by qRT-PCR. These represent the master regulator and parts of all 3 pathways of the UPR. All four UPR markers were slightly upregulated. However, only CHOP was significantly upregulated ($p<0.01$) in the *wfs1a* knockouts.

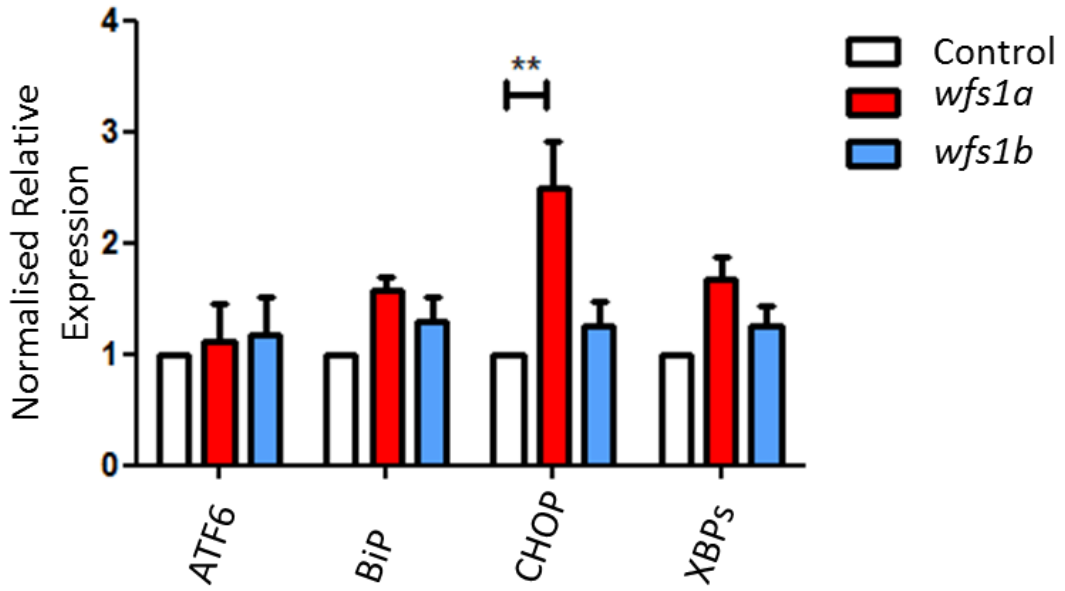

Figure 4.5 Expression of UPR markers in *wfs1* knockouts relative to control. Expression of ATF6, BiP, CHOP and XBPs normalised to *ef1α* and *β-actin* (Primers in Table 2.5-2.6). Normalised relative expression values taken from Bio-Rad CFX Manager and plotted mean +SEM using Graphpad Prism n=3. Significance determined by Two-Way ANOVA with Bonferroni multiple comparisons **p<0.01.

4.6 Developmental Delay

The transgenic knockouts did not share the obvious phenotypes observed in the morpholino model, such as the curly tails and smaller eyes. *wfs1* knockout zebrafish were imaged at time points within the first 3 days of development to determine if any gross abnormalities could be seen. Development at 30hpf in the *wfs1b* knockouts appeared to be delayed. This development seems to be much less prevalent at 50hpf with a slight change in head tail angle; this change disappeared by 80hpf, suggesting an initial delay in development which is rectified overtime.

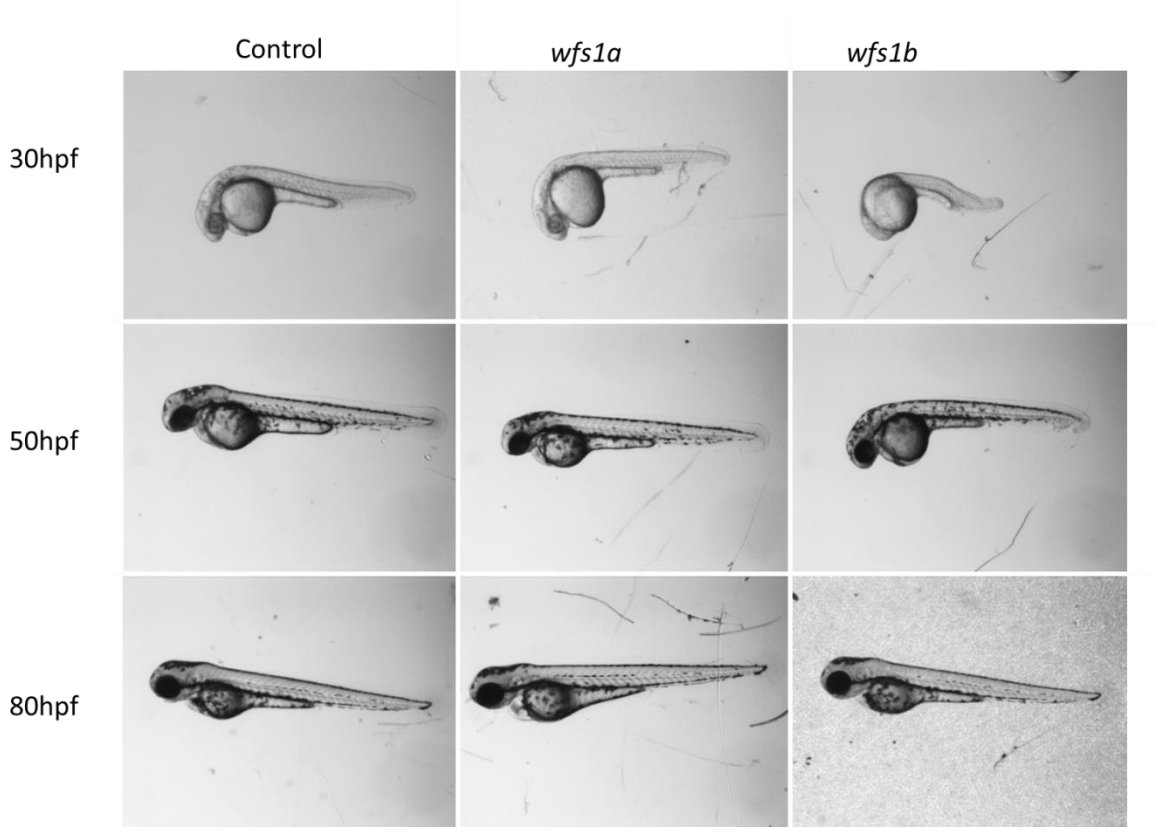

Figure 4.6 Representative images of developing embryos over the first 80 hours of life. Control and *wfs1* knockout fish imaged at 30, 50 and 80hpf on a Leica MZ16F stereomicroscope with a Leica DFC420 C camera attachment.

4.7 Size difference in *wfs1* knockouts

As the knockout zebrafish appeared slightly shorter in length (Figure 4.6), this was also quantified at each timepoint (Figure 4.7). For both knockouts the zebrafish were significantly smaller at all 3 time points. At 30hpf *wfs1a* knockouts are significantly shorter than controls and *wfs1b* knockouts are significantly shorter than both $p<0.001$. At the 50hpf time point the *wfs1b* knockouts have caught up with *wfs1a* but the significant difference remains when comparing the knockouts and controls for the remaining timepoints.

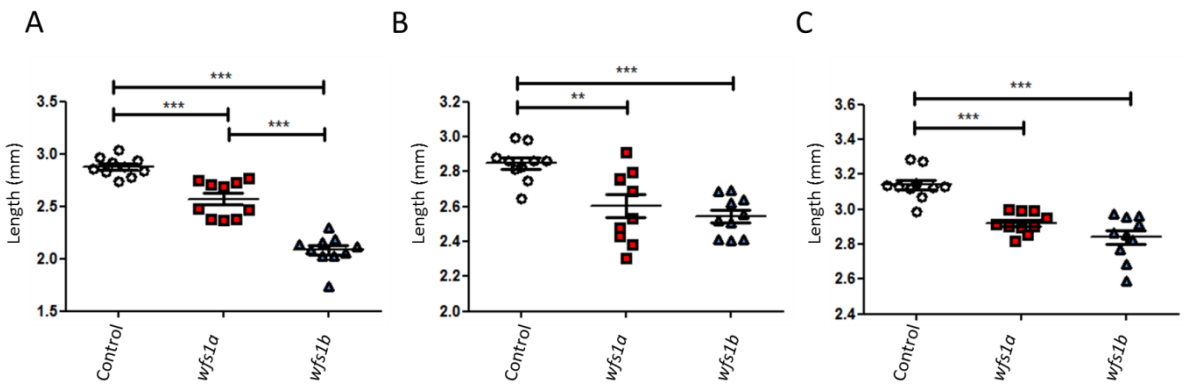

Figure 4.7 Zebrafish length during embryonic development. A: Zebrafish length at 30hpf. B: Zebrafish length at 50hpf. C: Zebrafish length at 80hpf. Images from Leica MZ16F stereomicroscope with a Leica DFC420 C camera attachment measured using ImageJ and plotted mean ±SEM using Graphpad Prism n=10. Significance determined by One-Way ANOVA with Bonferroni multiple comparisons **p<0.01, ***p<0.001.

4.8 Ears

On closer inspection at 72hpf the zebrafish otoliths in the zebrafish ear appeared to be slightly smaller with a few otoliths not developing in the *wfs1b* population (Figure 4.8A). This was quantified by measuring the size of the otoliths (Figure 4.8B). The quantification showed significantly smaller otoliths were found in both *wfs1a* and *wfs1b* knockouts. However, this was found in the minority of knockout zebrafish, when images were screened for abnormalities, 40.74% of *wfs1a* and 37.04% of *wfs1b* zebrafish ears could be easily identified as “abnormal” (Figure 4.8C).

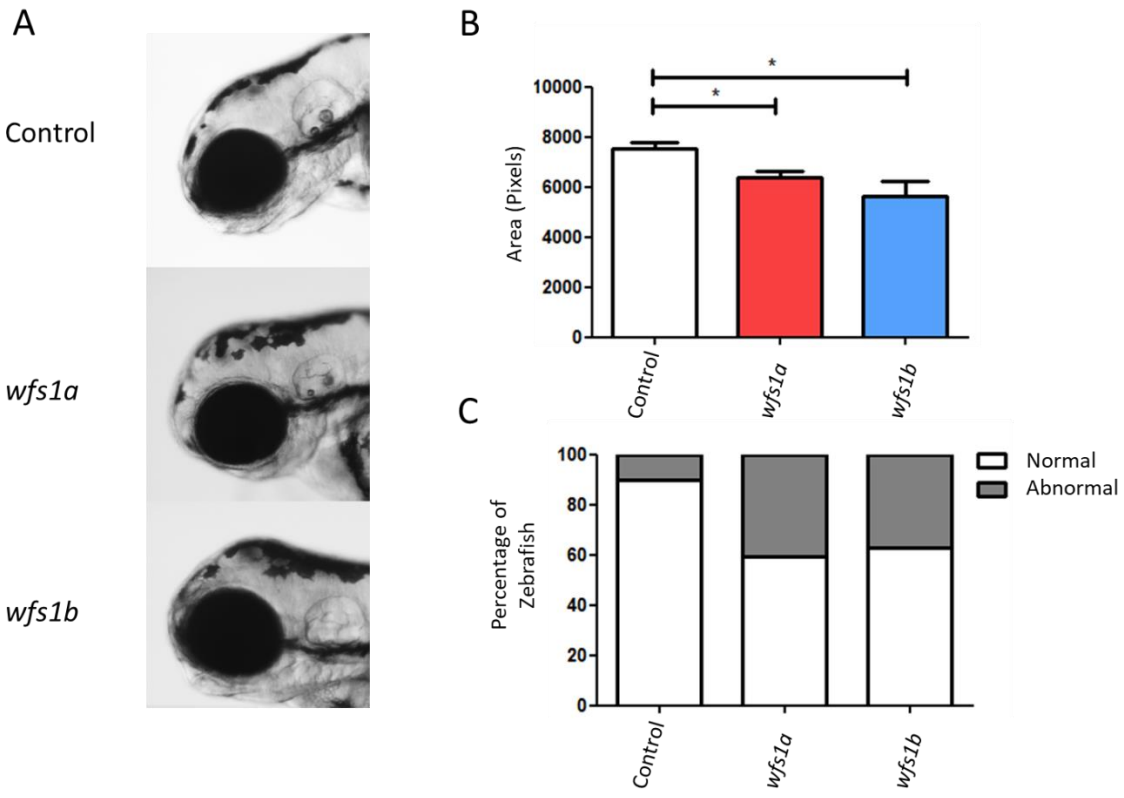

Figure 4.8 Abnormalities in *wfs1* knockout zebrafish otoliths. A: Images of abnormal otoliths in *wfs1* knockouts compared to controls at 72hpf. Images from Leica MZ16F stereomicroscope with a Leica DFC420 C camera attachment. B: Otolith Area measurements. On Imagej circles were drawn round each otolith and the area measured. Bar graph plotted mean +SEM using Graphpad Prism n=25. Significance determined by One-Way ANOVA with Bonferroni multiple comparisons *p<0.05. C: Percentage of zebrafish that had abnormal otoliths by eye. Zebrafish images were assessed by eye for normal and abnormal otoliths this was plotted on a stacked bar graph using Graphpad Prism n=25.

4.9 Weights of Adult Fish

The adult *wfs1* knockout fish had no obvious distinct phenotypes. At 4 month and 12 month endpoints, zebrafish were euthanized and weighed prior to dissection. At 4 months of age both the *wfs1a* and *wfs1b* knockouts had no significant differences from the control fish. However, at 12 months *wfs1b* zebrafish were significantly heavier than control ($p<0.001$) and *wfs1a* fish ($p<0.05$). Zebrafish weights were not controlled for population density but it was decided to observe movement in adult zebrafish to determine if activity levels were resulting in heavier zebrafish.

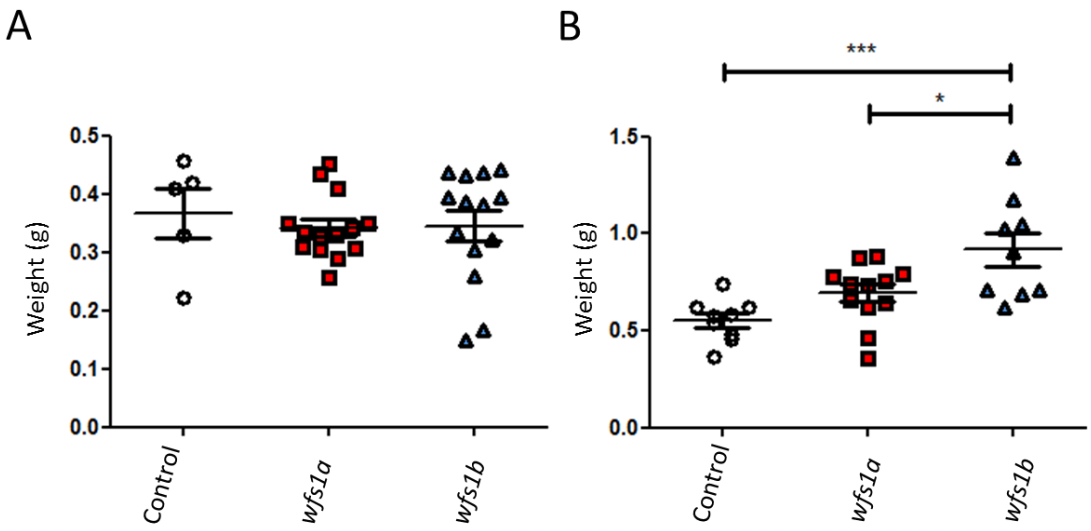

Figure 4.9 Weights of zebrafish at 4 and 12 months of age. A: Weight of zebrafish at 4 months of age. Control n=5 *wfs1a* n=14 *wfs1b* n=14. B: Weight of zebrafish at 12 months of age. Control n=9 *wfs1a* n=12 *wfs1b* n=9. Significance determined by One-Way ANOVA with Bonferroni multiple comparisons *p<0.05 ***p<0.001. Data plotted mean ±SEM using Graphpad Prism

4.10 Adult Movement

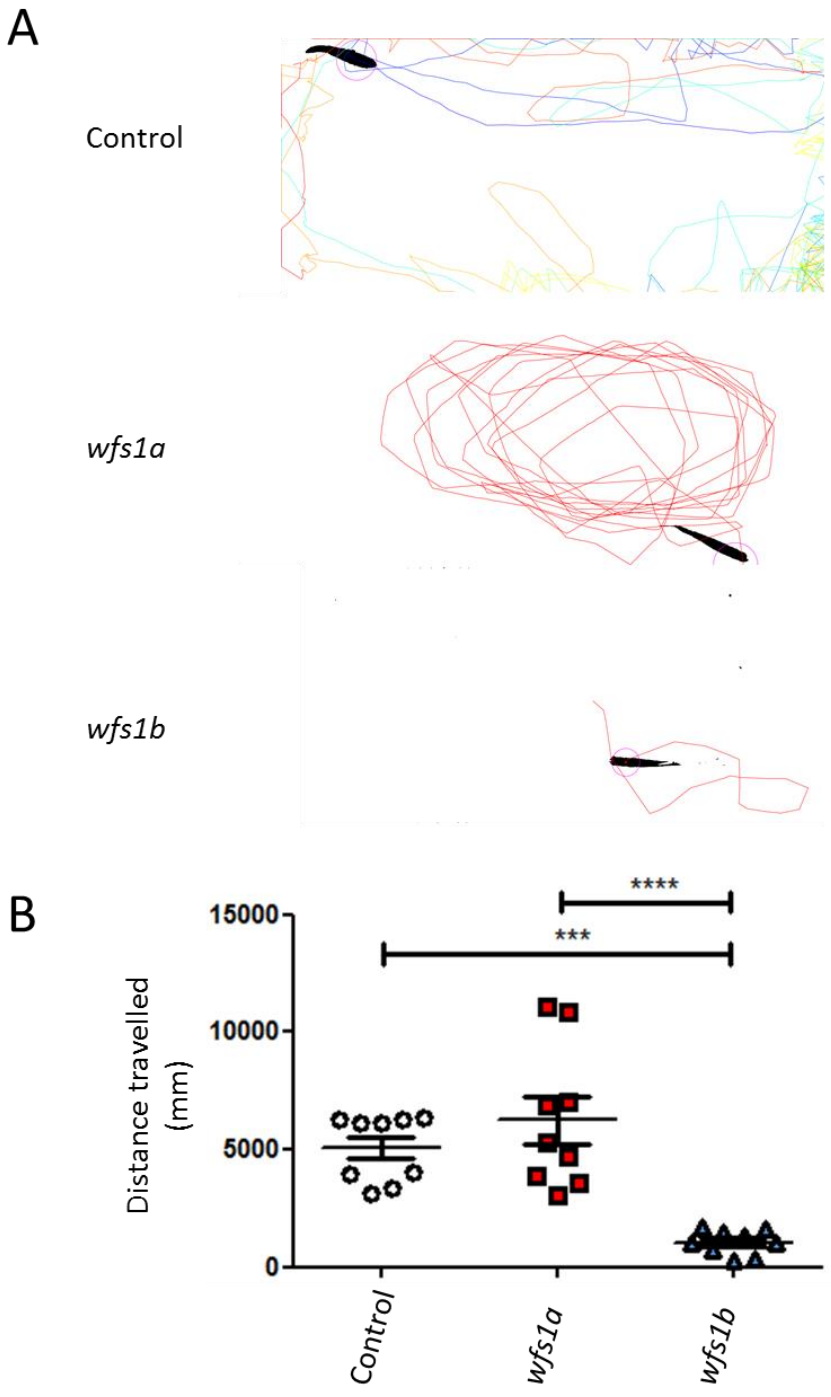

Figure 4.10 Movement tracking of adult zebrafish. A: Representative 1 minute traces of zebrafish swimming made in ImageJ using the trackmate plugin. B: Distance travelled by zebrafish. Displacement values per frame from Trackmate were added together to determine the total distance travelled. Data plotted mean ±SEM using Graphpad Prism. Significance determined by One-Way ANOVA with Bonferroni multiple comparisons ***p>0.001, ****p>0.001. Example video can be found in Supplementary evidence 1

Adult zebrafish were moved to a tank underneath a video camera and movements recorded after 3 minutes of acclimatisation for a period of 1 minute. This showed significant

reductions in movement for *wfs1b* knockouts compared to controls p<0.001 with a 4000mm change in total movement. The *wfs1b* knockouts were stationary for the majority of the time period. Freezing bouts can be considered a marker for anxiety in zebrafish, leaving the possibility that lower mobility could be due to stress rather than immobility.

4.11 Embryonic Lethality/ Fertility

An observation was made that a number of embryos were not surviving to 24hpf. Further investigation revealed the number of unfertilised embryos increased in *wfs1b* knockout zebrafish. As reduced fertility has been shown in WS, the fertility of the knockout models was assessed. In order to quantify this, 50 random embryos were collected and the number of embryos that did not survive 24 hours were recorded (Figure 4.11A). This showed a significant increase of unfertilised embryos in *wfs1b* knockouts, suggesting a fertility problem. It may be possible that this could have been due to fertilised embryos dying within the first 24 hours. To determine if this was the case, eggs were collected at 8hpf and embryos that were likely unfertilised were removed. The number of embryos dying in the first 24hpf could then be quantified. Although this was slightly increased with a difference of 5.8% between fertilised control and fertilised *wfs1,* this was not significant. The difference in the randomly selected embryos was higher at 24.34%. The difference in fertilised embryo death does not account for the full difference suggesting *wfs1b* knockouts are less fertile.

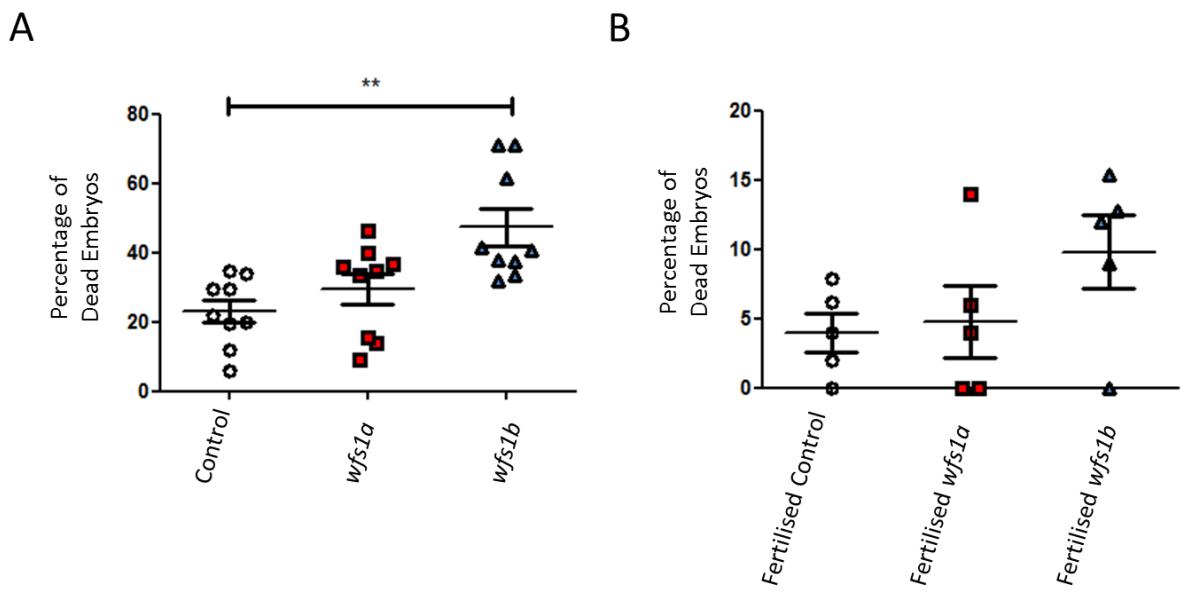

Figure 4.11 Fertility of *wfs1* knockout zebrafish. A: Percentage of randomly selected embryos at 24hpf (n=9). B: Percentage of selected fertilised embryos dead at 24hpf (n=5). 50 random or fertilised embryos were place in E3 medium, left overnight and the dead determined in the morning. Data plotted mean ±SEM using Graphpad Prism. Significance determined by One-Way ANOVA with Bonferroni multiple comparisons **p<0.01.

As the *wfs1b* knockout zebrafish reach 9 months the fertility drops further. A Significantly increased number of *wfs1b* embryos are infertile (control p<0.001 wfs1a p<0.01). *wfs1b* males and *wfs1b* females were outcrossed to control lines and the fertility of these embryos measured. The *wfs1b* males had a significantly increased number of dead embryos at 24hpf (control p<0.0001 *wfs1a* p<0.001).

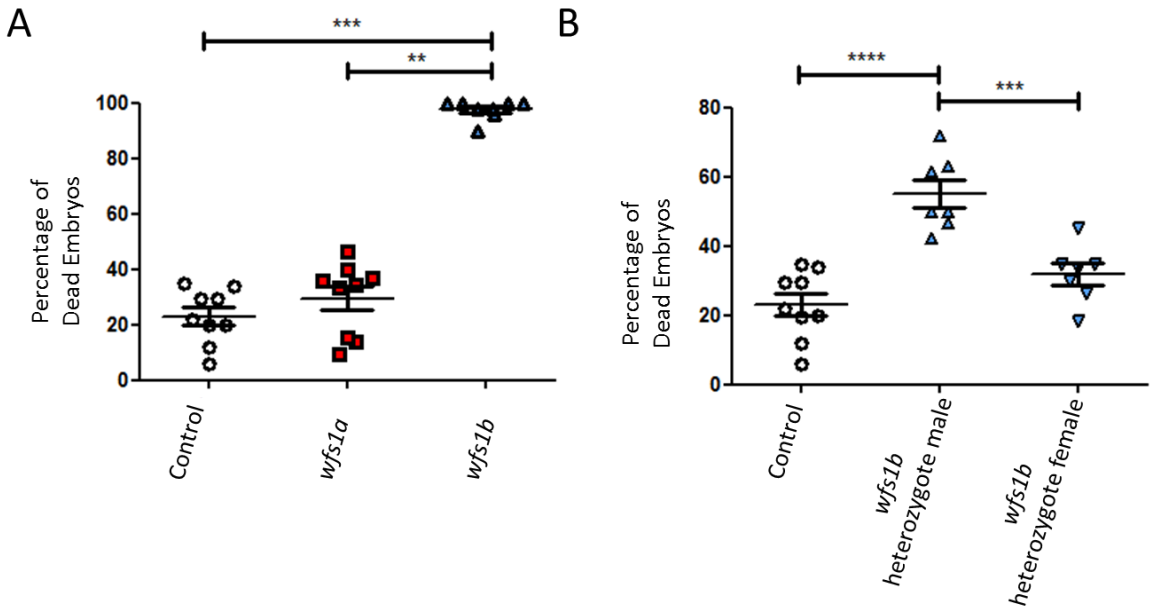

Figure 4.12 Fertility of *wfs1* knockout zebrafish. A: Percentage of randomly selected embryos at 24hpf produced by adults over 9 months (n=9). B: Percentage of randomly selected embryos at 24hpf produced by adults over 9 months with *wfs1b* knockouts outcrossed to controls (control n=9, *wfs1b* heterozygotes n=7). 50 random or fertilised embryos were place in E3 medium, left overnight and the dead determined in the morning. Data plotted mean ±SEM using Graphpad Prism. Significance determined by One-Way ANOVA with Bonferroni multiple comparisons **p<0.01, ***p<0.001 and ****p<0.0001.

A knockout model carrying both *wfs1a* and *wfs1b* mutations were bred. This would create a line of double knockout fish that could be used for future experiments. When *wfs1ab* heterozygotes were crossed one double knockout mutant survived to adulthood which was completely infertile.

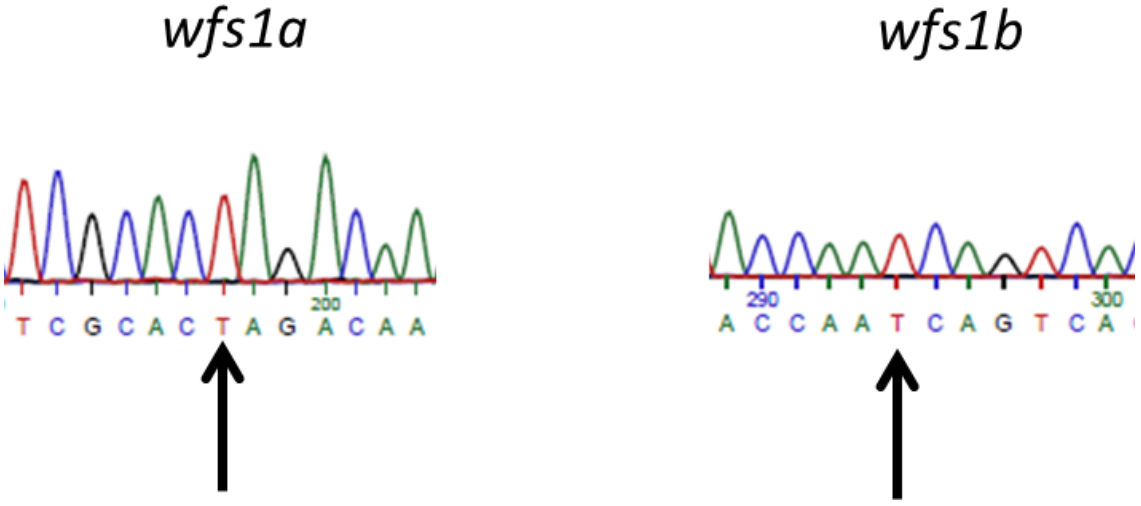

Figure 4.13 Double Knockout Mutant Sequencing. Chromatogram of reverse primer sequencing of *wfs1a* and *wfs1b* mutations. Sequencing of PCR product by Eurofins.

4.12 Blood Glucose

Blood glucose regulation is tightly controlled under normal conditions. Blood glucose of zebrafish at 10 months of age was determined from control and *wfs1b* knockout zebrafish. The blood glucose in overnight fasted zebrafish was significantly lower in *wfs1b* knockout zebrafish (p=0.0354).

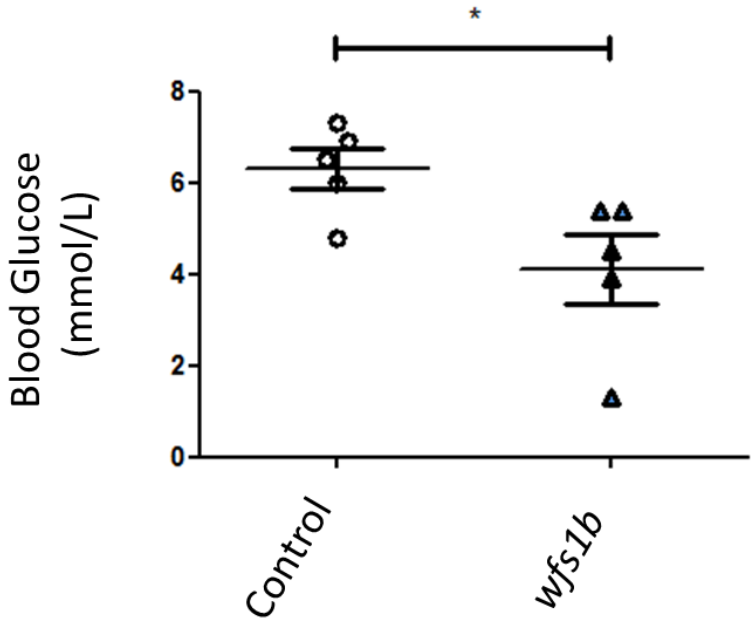

Figure 4.14 Blood Glucose Measurements. Control and *wfs1b* mutants were decapitated and the blood glucose measurements taken from heart using a Onetouch ultra glucose monitor. Data plotted mean ±SEM using Graphpad Prism. Significance determined by unpaired t-test p=0.0354.

4.8 Discussion

Mutations in the zebrafish *wfs1* genes were confirmed and a number of gross phenotypic abnormalities were assessed alongside the underlying expression and mechanism of *wfs1* in zebrafish.

Mutations in the *wfs1* genes were confirmed by Sanger sequencing and nonsense mutations were described. Expression of *wfs1a* and *wfs1b* were quantified in wild type fish to determine if any differences could be seen between the two homologues. The *wfs1a* expression was variable in the first few days of zebrafish development, with a higher expression observed in the adult muscle tissue when compared to other tissues. Although expression of wolframin is found in the muscle of humans, there are a number of other tissues more relevant to the disease phenotype such as in the brain and retina (Schmidt-Kastner *et al.*, 2009; Uhlen *et al.*, 2010; De Falco *et al.*, 2012). In these tissues *wfs1b* expression is predominant which may account for many differences seen between the two gene knockouts. *Wfs1b* was also more constantly expressed at embryonic stages and also present at the 1 cell stage suggesting there is maternally translated transcript from *wfs1b* (Pelegri, 2003). This may be why a delay in development is observed in transgenic models, which was not observed in the morpholino model. Due to the divergence in expression, determining the subcellular localisation of *wfs1a* and *wfs1b* to see if they were localised to the ER would have helped determine the roles of *wfs1* in comparison to humans. This was not possible due to the lack of specific *wfs1* zebrafish antibody. However it was possible to determine functional changes by investigating UPR and ER stress pathways in WS.

It was important to determine if *wfs1* knockout fish were exhibiting similar molecular pathways to humans with WS. This would provide evidence to determine the accuracy of the model. The UPR is an important well characterised pathway in WS (Fonseca *et al.*, 2005); to determine if the UPR was also affected in the zebrafish the fish were heat shocked to induce ER stress (Lam *et al.*, 2013). The results observed were an increased death in the *wfs1a* and *wfs1b* knockouts suggesting increased apoptosis due to an increased ER stress response. In order to demonstrate the ER stress response had been upregulated, protein expression of the master regulator of the ER stress response (BiP) was measured and showed an increased expression upon heat shock. Interestingly BiP also appeared to be upregulated in *wfs1a* knockouts in untreated fish, which could suggest an increase in the *wfs1a* UPR proteins under unstressed conditions.

In order to monitor this, a number of proteins from the UPR were assessed in the knockout models by qRT-PCR. Although all 4 genes (ATF6, BiP, CHOP, and XBPs) showed slight increases in expression only CHOP was significantly upregulated ($p<0.01$) in the wfs1a knockouts. *WFS1* regulates ATF6 at a protein level by targeting it for degradation (Fonseca *et al.*, 2010), therefore looking at the protein expression of ATF6 would be a much more appropriate method for measuring ATF6 expression in *wfs1* knockouts. However, when an ATF6 antibody was tested on zebrafish lysates no signal was detected as it was not zebrafish specific and zebrafish specific antibodies are limited.

With the zebrafish knockouts showing changes in one of the major pathways of WS, the UPR, the gross morphology of the fish was checked for any phenotypic markers of WS. The zebrafish were imaged for each of the first three days of development, this showed changes in the *wfs1b* knockouts showing a delay in development at 30hpf. This seemed to be less obvious at 50hpf with no differences observed at 80hpf. A delay in growth of neurons in *Wfs1* knockout rats has been described previously and may be a reason developmental delay is being observed (Cagalinec *et al.*, 2016). These differences were quantified by measuring the size of the fish at each time point, which showed *wfs1a*, and *wfs1b* knockouts to be significantly smaller than the controls at all time points. An additional observation at 30hpf was a much smaller *wfs1b* fish, significantly smaller than the *wfs1a* knockouts. These fish caught up to the *wfs1a* knockouts by 50hpf but stayed smaller than control zebrafish. This suggests that there was an initial developmental delay. However, at the 50hpf time point the zebrafish are no longer behind in terms of staging but are slightly smaller. As impaired cell cycle progression has been observed in *WFS1* knockout cells (Yamada *et al.*, 2006; Gharanei *et al.*, 2013), this can explain the molecular mechanism seen in the initial delay in development. As no antibody exists for the p21 protein implicated in this process for zebrafish this was not tested for.

The zebrafish ears also appeared to show a difference in *wfs1* knockouts. The zebrafish ear is comparable to other vertebrate inner ears (Whitfield, 2002). As patients in WS suffer sensorineural deafness, the inner ear is all that is needed to model sensorineural deafness in WS. A number of smaller or missing otoliths were seen in the *wfs1* knockouts which were shown to be significantly smaller than the controls. As the otoliths are formed by cilia moving Ca^{2+} together there may be a neuronal issue causing this, which may overlap with

the developmental delay. As WS is a progressive disease it was also important to determine if the adults showed any WS phenotypes.

The *wfs1* knockouts were grown to end points at 4 and 12 months; at these time points, prior to dissection, fish were weighed to determine if there was any weight difference between controls and knockouts. At 4 months no difference in size was seen, at 12 months *wfs1b* zebrafish were significantly heavier than both controls and *wfs1a* knockouts. This may have been due to non-population matched tanks resulting in a higher amount of food thus bigger fish in the *wfs1b* zebrafish. It could also be due to inactivity of the *wfs1b* fish. To test this, zebrafish movement was recorded over a one-minute period. w*fs1b* knockouts were observed moving significantly less than the controls and *wfs1a* knockouts, suggesting the possibility that *wfs1b* fish were less active and therefore larger at 12 months. It was however noted that *wfs1b* knockouts during this experiment did not move at all for large periods of time, this was not obvious when observed in their own tanks. Freezing bouts have been linked to increased anxiety (Egan *et al.*, 2009). As anxiety is observed in patients with WS (Urano, 2016) a number of zebrafish were placed in a tank together (supplementary video 2), as zebrafish are more comfortable as a group. The zebrafish showed no freezing bouts suggesting *wfs1b* zebrafish were more anxious than controls and *wfs1a* knockouts when isolated.

The fertility of adult fish also seemed to be affected in *wfs1b* knockouts, with the number of unfertilised embryos significantly increased. This is another feature seen in knockout mice and patients with WS (Noormets *et al.*, 2009; Haghighi *et al.*, 2013), confirming a number of phenotypes observed in the zebrafish match a number of patient conditions (Urano, 2016). When the older >9month adults were outcrossed with controls they were able to produce viable offspring. However, the wfs1b males had a significantly higher percentage of unfertilised offspring. This suggests that although the fertility is affected in both genders, the male infertility may be more severe. In mouse knockout models, sperm morphology and reduced number of spermatogenic cells was hypothesised to be the cause of infertility (Noormets *et al.*, 2009). However, infertility is reported in both male and female patients (Urano, 2016). It could be possible that something more general is affecting the fertility such as Ca^{2+} dynamics or mitochondrial dysfunction: two processes implicated in WS that are important in the process of fertilisation (Osman *et al.*, 2003; Zatyka *et al.*, 2015; Cagalinec *et al.*, 2016).

Although a number of patient symptoms have been replicated in the zebrafish, the majority were seen in *wfs1b* zebrafish and not *wfs1a*. This may be partially due to the expression of *wfs1a* being less prevalent in the eyes and neural tissue, which would be more histologically relevant in WS. It may also be due to differences in affected pathways. Although the UPR is the best characterised pathway in WS, proinsulin modification and Ca^{2+} flux has also been shown to be implicated, although the underlying role of Ca^{2+} is much less well understood (Osman *et al.*, 2003; Gharanei *et al.*, 2013), it is possible these roles may differ between the two knockouts.

Overnight fasted blood glucose was significantly lower in *wfs1b* knockouts. Blood glucose homeostasis is disrupted in diabetes mellitus due to the inability to synthesise insulin and correctly store glycogen (Eames *et al.*, 2010). Zebrafish had to be culled for the reading of blood glucose which resulted in low number of replicates. The knockout zebrafish had a significantly lower blood glucose suggesting problems with homeostasis. *wfs1b* morpholino injected fish had a reduction in β-islet cells, which would suggest insulin production is the cause of this blood glucose reduction (O'Hare *et al.*, 2016). However, in diabetes mellitus we would expect an increase in fasted blood glucose which is not observed in wfs1 zebrafish.

The *wfs1* knockout models had a number of markers that shared similarities to WS in humans, such as infertility and features of anxiety. However, Optic Atrophy remains a significant issue for patients with WS as it currently has no available therapeutic management options Therefore in the following Chapter, this phenotype is discussed in detail in the zebrafish to determine whether the fish are a good model for all DIDMOAD characteristics.

4.9 Conclusions

The genetic knockout model of *wfs1a* and *wfs1b* was confirmed by Sanger sequencing. The models expression and tissue specificity was confirmed for the two genes. The models were compared to known functions in patients and other models with an increased response to heat shock and a number of phenotypic markers of WS. Fertility, anxiety and length were all affected in the zebrafish models, mirroring a number of phenotypes observed in patients. The *wfs1b* knockout act as a better representation of the phenotypes expressed in WS and had a more representative expression pattern.

Further work would be required to fully examine the anxiety by examining the shoaling, stress hormones or other markers of anxiety in the fish (Stewart *et al.*, 2012). Determining if the zebrafish have diabetes mellitus could be attempted with glucose tolerance test or histology of the liver to examine the pancreatic islet cells. p21 or cell cycle expression markers could be examined in greater detail to determine the difference in cell cycle regulation in the development of WS.

Chapter 5: Assessment of Retinal Structure and Function in wfs1 Mutant Zebrafish Models

5.1 Introduction

In human retinal cells, expression of wolfram is observed in retinal ganglion cells (RGCs), optic axons and the proximal optic nerve and also expressed in retinal pigment epithelial (RPE) when detected in culture (Schmidt-Kastner *et al.*, 2009). In the mouse retina wolframin was localised to amacrine, Müller cells, photoreceptors and horizontal cells (Kawano *et al.*, 2008), the authors were unable to conclude if the differences observed were due to tissue preparation or interspecies variation (Schmidt-Kastner *et al.*, 2009).

Optic atrophy (OA) is the second most common symptom in WS occurring in 82.14% of patients (de Heredia *et al.*, 2013). OA is the end point of any condition that leads to the death of retinal ganglion cells (RGCs) or the optic nerve, also referred to as optic neuropathy.

Patients with WS who develop OA presented with decreasing visual acuity and loss of colour vision, this progressed to a visual acuity of 6/60 in the majority of patients at varied rates of progression (Range 1-25 years median 8 years) (Barrett *et al.*, 1997). 58% of patients will develop OA as the second clinical symptom, which begins to develop in the early second decade. The probability of having developed OA before 26 years is 90% (de Heredia *et al.*, 2013). Alongside the reduced colour vision and visual acuity optic nerve atrophy, cataracts abnormal pupillary light reflexes, nystagmus, and visual fields defects have all been observed in WS patients (Hoekel *et al.*, 2014). Although some patients have been observed with diabetic retinopathy, the majority will not have these symptoms suggesting this is an independent mechanism from the diabetes (Barrett *et al.*, 1997).

RGC loss is seen in patients with WS with loss of myelination in the optic nerve (Ross-Cisneros *et al.*, 2013). The loss of myelination in WS is predominantly seen in the papillomacular bundle which is also seen in LHON (Ross-Cisneros *et al.*, 2013). The loss of these smaller axons is thought, in LHON, to be due to the large energetic demand in these axons, paired with a relatively low energetic potential (Pan *et al.*, 2012). As WS optic nerves follow a similar pattern it is hypothesised that energy production may be a key feature of OA in WS (Ross-Cisneros *et al.*, 2013).

One marker that appears to correlate with disease severity is retinal nerve fibre layer (RNFL) thickness, which demonstrates the importance the loss of RGCs has in the pathology of the disease (Hoekel *et al.*, 2014). Alongside this they also described patients with no ocular phenotypes and a thinning of RNFL suggesting a possible developmental condition worsening later in life. This compliments the theory of brain developmental problems in WS discussed in Chapter 6 (Hershey *et al.*, 2012; Hoekel *et al.*, 2014).

The *wfs1* knockout zebrafish will be assessed histologically and functionally to determine if they show signs of OA, a key hallmark of WS.

5.2 Embryo histology

At 5dpf zebrafish were fixed, processed, paraffin embedded and sectioned at 4µm. H&E stained sections were assessed for any abnormalities. As no significant changes could be seen in the *wfs1* knockouts and WS being a degenerative disease, aged zebrafish were also examined.

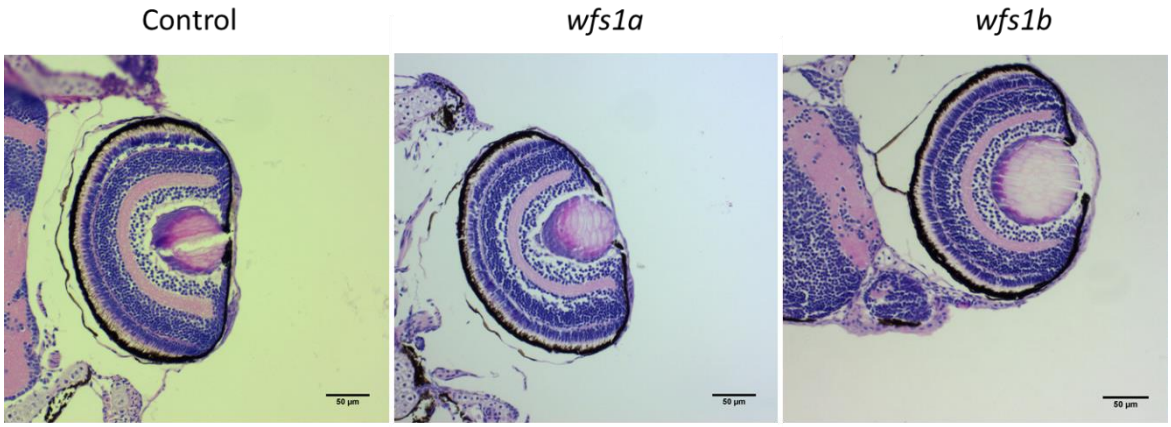

Figure 5.1 5dpf retinal sections. Control, *wfs1a* and *wfs1b* knockout larvae at 5 days were paraffin embedded and sectioned a 4µm. Sections were stained using H&E and imaged on Axio Imager Z1 fluorescence microscope (Zeiss). Scale bar 50µm.

5.3. Retinal Ganglionic Cell Count/Retinal Thickness

Wfs1 knockout zebrafish were aged to 4 and 12 months and the number of RGCs were assessed. The images seen in Figure 5.2A are representative images of 4 month zebrafish retinas. At 4 months of age both *wfs1a* and *wfs1b* knockouts had a significantly lower number of RGCs per 100µm ($p<0.005$ One way ANOVA with Bonferroni's Multiple Comparison Test). At 12 months of age the numbers of RGCs were also assessed. As the control values were not normally distributed Mann Whitney tests were performed between

controls and knockouts. There were significantly less RGCs in the knockouts (*wfs1a* p=0.0104 and *wfs1b* p<0.0001) as seen at 4 months. The RGC count in the *wfs1b* (18.99 RGCs) knockouts was also significantly lower than the *wfs1a* (21.67 RGCs, p=0.0036 unpaired t-test). As the RGC number was affected the effect of this on the optic nerve was assessed to determine if this was also impacted.

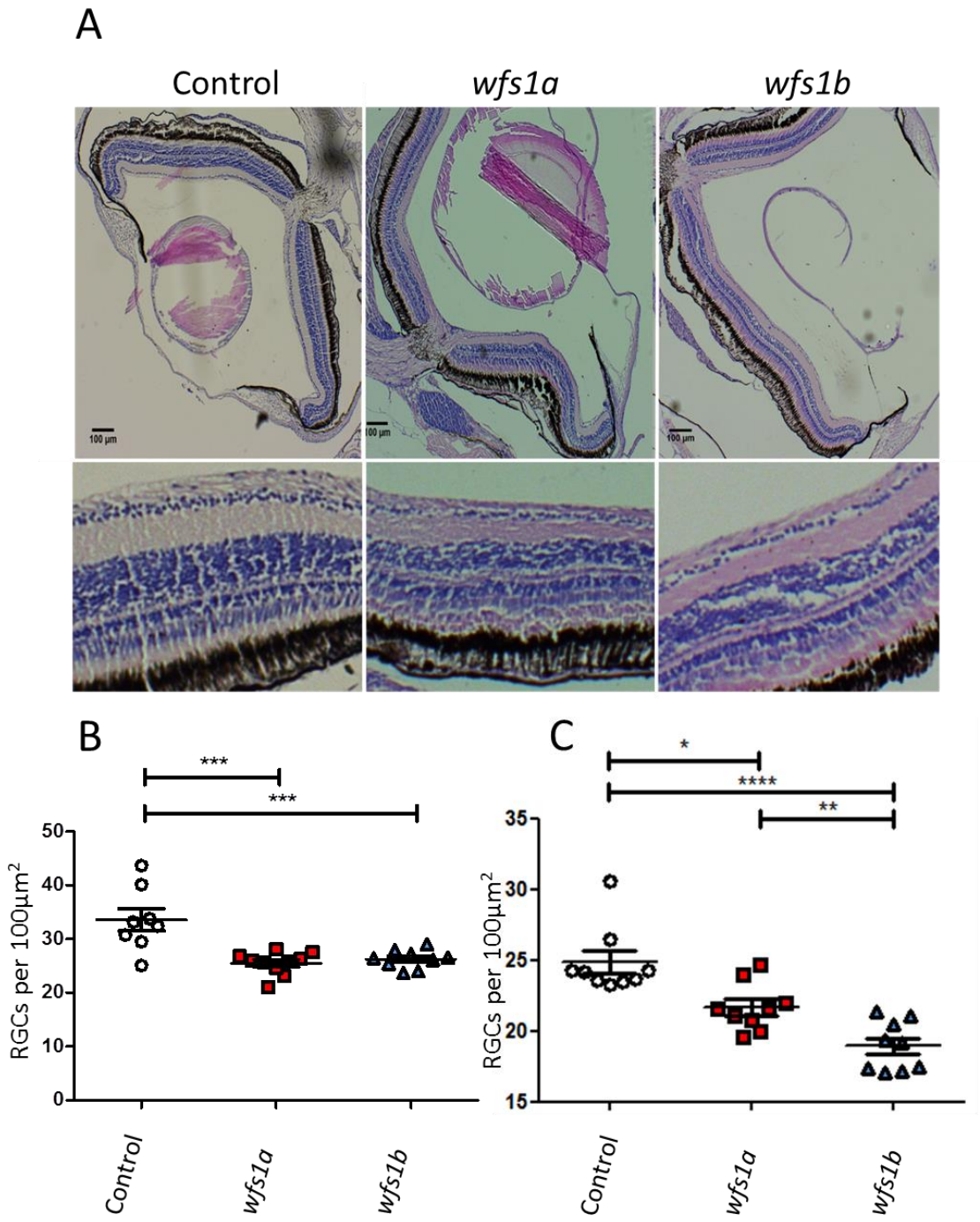

Figure 5.2 Adult Zebrafish Retinas and RGC counts. A: Representative sections of control and knockout retinas. Fixed and decalcified zebrafish heads were paraffin embedded and sectioned a 4µm. Sectioned were stained using H&E and imaged on Axio Imager Z1 fluorescence microscope (Zeiss). Scale bar 100µm. Six 100µm^2 areas along the retina were selected and the RGCs counted. B: RGC count per 100µm at 4 months of age control n=8 *wfs1a* n=10 *wfs1b* n=9. C: RGC count per 100µm at 12 months of age, n=9. Graphs plotted ± SEM, significance was calculated by One-way ANOVA with Bonferroni's multiple comparison tests. As control results were not normally distributed in Figure 6.3C Mann Whitney test were used vs control unpaired t-test *wfs1a/b* *p<0.05 **p<0.01, ***p<0.005 and ****p<0.001.

5.4 Optic Nerve Width

The optic nerve measurements were taken from sections of 4 month zebrafish retinas when the optic head was visible. No significant differences were seen (One-way ANOVA with Dunnett's Multiple Comparison Test) although the *wfs1a* and *wfs1b* knockouts had higher means (control 129.7µm, *wfs1a* 139.8µm and *wfs1b* 148.7µm). Due to the variability in data generated using this method, a different approach to measuring optic nerves was employed.

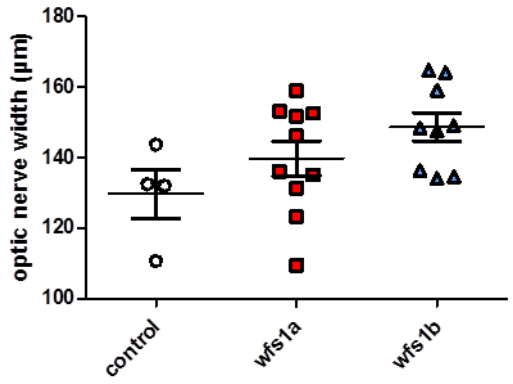

Figure 5.3 Optic Nerve Measurments at 4 months. Fixed and decalcified zebrafish heads were paraffin embedded and sectioned a 4µm. Sectioned were stained using H&E and imaged on Axio Imager Z1 fluorescence microscope (Zeiss). Retinal sections containing the optic head had the optic nerve width measured at the RPE layer (Figure 6.1). Graphs plotted ± SEM, significance was calculated by One-way ANOVA with One way ANOVA with Bonferroni's multiple comparison tests. Control n=4, *wfs1a* n=11 and *wfs1b* n=9.

5.4.1 Optical Coherence Tomography (OCT)

In order to get a more accurate representation of optic nerves in *wfs1* knockout zebrafish OCT was used (Figure 5.4). This was performed at 12 months and creates a cross section of live zebrafish retinas. The area in the middle with no layers represents the optic nerve; in *wfs1b* knockouts it was visibly smaller.

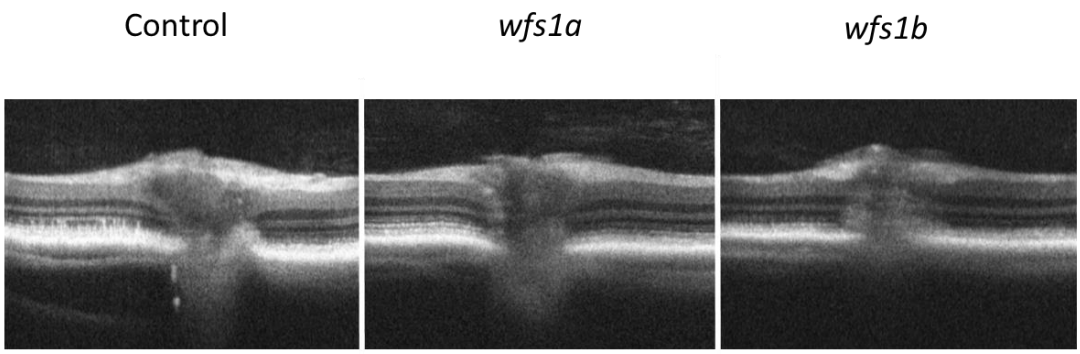

Figure 5.4 OCT representative images of 12 month zebrafish. OCT B-scan images showing Retinal cross sections of live 12 month zebrafish. Images taken on a Bioptigen Envisu R2200 SDOIS.

It was important to ensure the loss of RGCs and optic nerve had a functional effect on zebrafish vision.

5.5 Optokinetic Response (OKR)

To determine potential functional defects in the vision of knockout fish, the OKR was measured. This counts the number of zebrafish eye movements in response to a moving black and white grate. One eye movement can be seen in Figure 5.5 with a video in supplementary evidence 3.

Figure 5.5 Eye movement during OKR experiment.

Videos were recorded at 4 (Figure 6.6) and 12 (Figure 6.7) months and at a slower and faster speed. At 4 months there were significantly less eye movements in the *wfs1b* knockouts at both 8 ($p>0.05$) and 16rpm ($p>0.01$). The *wfs1a* knockouts at 8rpm had significantly less eye movements per minute but no change at 16rpm. This is not the expected outcome as the

quicker revolutions should be the first to demonstrate a difference, the data points are widely spread in the *wfs1a* knockouts compared to the control and *wfs1b* groups.

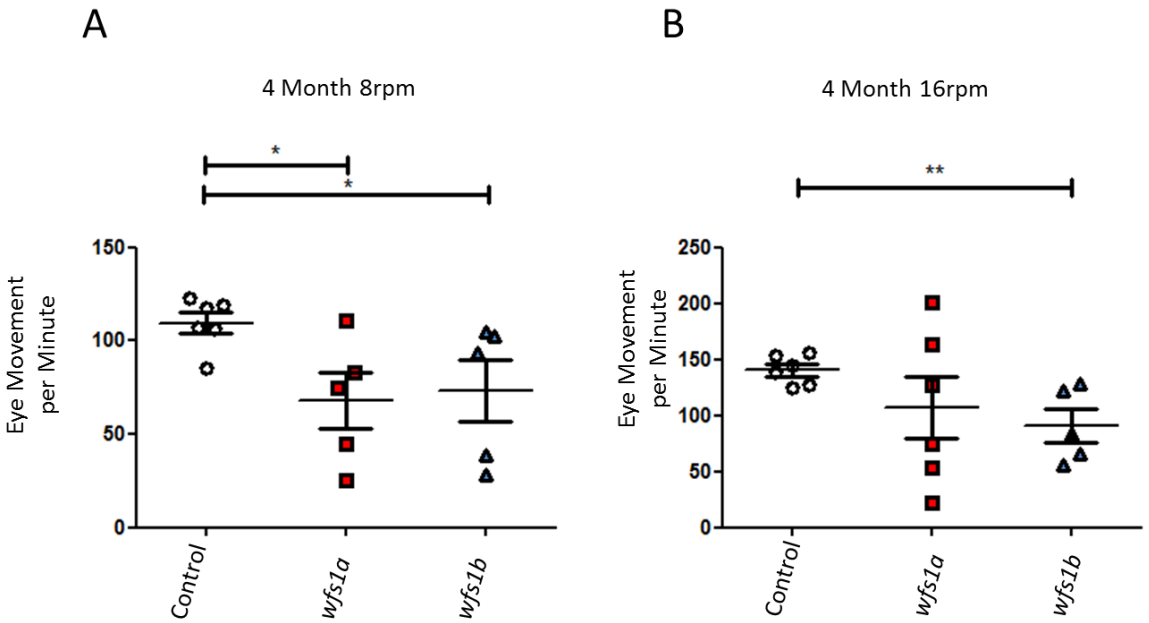

Figure 5.6 OKR Results of 4 Month Zebrafish. Videos were recorded of fish eye tracking and movements manually counted. Graphs plotted as mean ± SEM, significance was calculated One way ANOVA with Bonferroni's multiple comparison tests *p<0.05 and**p<0.01.

At 12 months the *wfs1a* zebrafish have no significant difference from the controls at 8 or 16rpm suggesting the 4 month results may have been an anomaly. However, the *wfs1b* knockout zebrafish have significantly less eye movements with a mean of 50 under both circumstances. One *wfs1b* zebrafish did not move at all suggesting it may be completely blind.

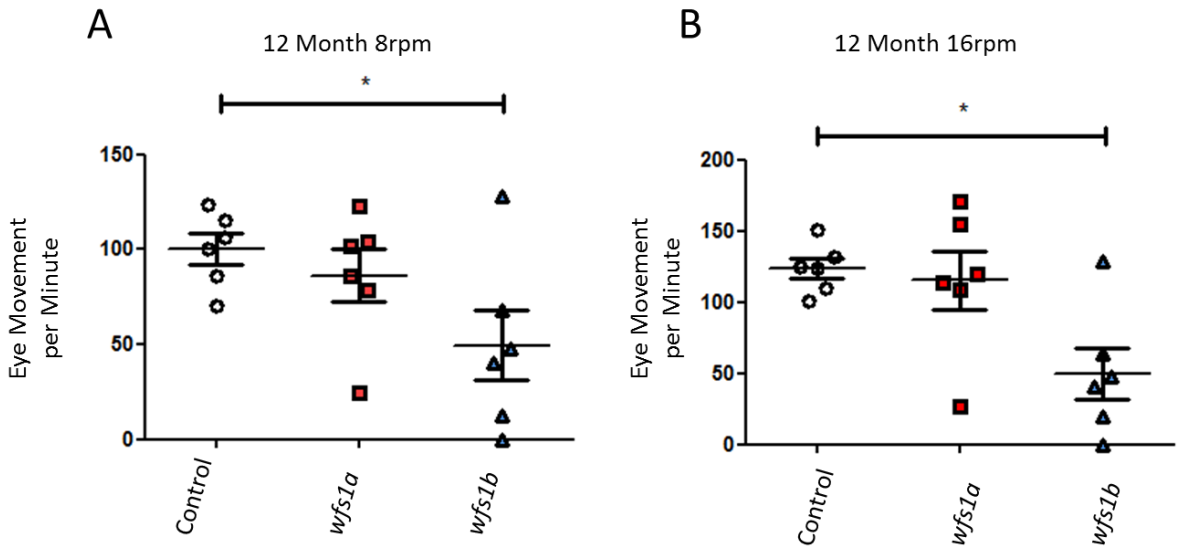

Figure 5.7 OKR Results of 12 Month Zebrafish. Videos were recorded of fish eye tracking and movements manually counted. Graphs plotted as mean ± SEM, significance was calculated One way ANOVA with Bonferroni's multiple comparison tests *p<0.05.

5.6 Electron Microscopy

The 12 month adult optic nerves were analysed for transmission electron microscopy (TEM) to look at myelination of the nerves and to look at mitochondrial structure and ER contacts (Newcastle University Electron Microscopy Research Services). When looking at the optic nerves under the electron microscope the fixation was not of an appropriate standard to look at in detail due to mitochondrial ultrastructure and ER contacts. This meant that no useful information could be taken from these experiments.

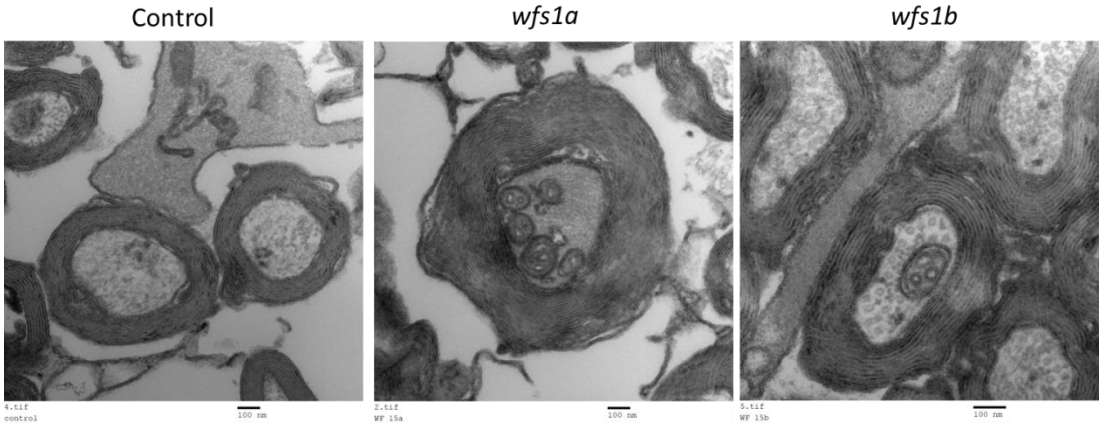

Figure 5.8 TEM images of 12 month zebrafish Optic Nerves. TEM imaging performed by Newcastle University Electron Microscopy Research Services. Optic nerves fixed in 3% glutaraldehyde. Scale bar 100nm.

5.7 Discussion

To determine the zebrafish models suitability as a model of WS, optic atrophy (OA) was assessed. As WS is multifaceted with severities and phenotypes varying with mutations, one of the more common phenotypes was chosen to look at in greater detail. 82.14% of patients develop OA within the disease course (de Heredia *et al.*, 2013). Although diabetes mellitus is more common with 98.21% of patients developing it (de Heredia *et al.*, 2013), with therapeutic screening in mind, OA cannot be managed in the same manner as diabetes so it was important the model matched this phenotypically. The zebrafish eye development, structure and function are comparable to the human eye making zebrafish an excellent model for OA (Richardson *et al.*, 2017).

Characterisation of optic atrophy in the *wfs1* zebrafish was carried out by: histological and functional assessments of the zebrafish retinas. As OA is a progressive disorder, a number of time points, embryonic, 4 months and 12 months, were analysed. At the embryonic stage histological sections were taken at 5dpf however, these were not quantified as orientation of larvae was not consistent.

In the adult fish loss of RGCs was observed in both *wfs1a* and *wfs1b* knockouts at both 4 and 12 months. At 4 months the RGC count was *wfs1a*-25.51 and *wfs1b*-26.27RGCs which was significantly lower than the controls 33.59RGCs. At 12 months however the *wfs1b* count had also dropped to be significantly lower than the *wfs1a* knockouts. This suggests a more severe retinal degeneration in the *wfs1b* knockout zebrafish at 12 months. As there was a loss of RGCs it was expected that a thinning of the optic nerve would be seen. When measuring the optic nerve width in retinal slices we looked to find the optic head and measure from there (Pei *et al.*, 2010). The measurements of the optic nerve were variable, mainly due to the orientation of the fish, which, if slightly different, would change the cutting angle of the retina; this could lead to varying sizes of the optic nerve at the optic head. As the zebrafish contains no macular this should not have affected the RGC counts. OCT was used to create cross sections of live zebrafish retinas (Toms *et al.*, 2017) Where the size of the optic nerve was visible. The size had visually decreased in the *wfs1b* knockouts at 12 months which would correlate with the loss of RGCs. Retinal nerve fibre layer (RNFL) thinning is a hallmark characteristic of OA in WS (Hoekel *et al.*, 2014) and the localisation of wolframin in human retinas is in the RGCs and optic nerve, and some expression seen in the

RPE (Schmidt-Kastner *et al.*, 2009). The zebrafish, especially *wfs1b*, models the thinning optic nerve and loss of RGCs, which is promising for a model of OA for WS.

To see if the histological changes were having any effect on the vision of the zebrafish, OKR experiments were performed. The OKR tests the zebrafish eye movements in response to a moving black and white grate (Cameron *et al.*, 2013). Eye movements for *wfs1b* knockouts were consistently, at both time points and speeds, significantly lower than the controls. The fact that at 12 months some of the *wfs1b* zebrafish made no eye movements suggests that some may even be completely blind at 12 months. The *wfs1a* knockout zebrafish only had a significantly lower number of eye movements at 4 months at 8rpm ($p>0.05$). It would be expected for the zebrafish to show a more severe phenotype at with the zebrafish, unable to distinguish between the separate bands of the grating. It would also be expected that since the *wfs1a* and *wfs1b* knockouts had similar reductions in RGCs they would have a similar loss in vision. The *wfs1a* results at 4 months had a much higher variation compared to the controls and *wfs1b* knockouts which highlights the possibility that some experimental error may have played a role in the *wfs1a* results. There could also be downstream complications as wolframin is expressed in the optic nerve (Schmidt-Kastner *et al.*, 2009) so complications in the neurons such as Ca^{2+} dysfunction, implicated in WS (Takei *et al.*, 2006), may play a role in signalling.

Expression may also play a role in the difference between the two knockout models. It was described in Chapter V that *wfs1a* expression is lower in the eyes compared to *wfs1b*. There may even be differences in expression between retinal cell types, as interspecies variation of expression in other retinal tissue, such as the Müller glial cells and neurons of the INL have been reported in the mouse that was not in the human retina (Kawano *et al.*, 2008; Schmidt-Kastner *et al.*, 2009). This could not be detected by PCR of the whole tissue. There is no antibody available for expression studies therefore it may be possible to perform in situ hybridisation to determine cell specific expression. It is also possible that the initial changes in RGC counts are caused by a neuronal developmental condition which progresses to a neurodegenerative phenotype, accounting for differences seen between the models. Neuronal development has been described as being affected in WS so may possibly explain differences in the early models (Hershey *et al.*, 2012; Cagalinec *et al.*, 2016). RNFL thickness has also been described as thinner even in patients with mild or no visual symptoms (Hoekel *et al.*, 2014). This can explain why we see 4 months *wfs1a* knockout zebrafish with a loss of

RGCs but no loss of visual acuity. The difference may come later which we see in *wfs1b* knockouts as they become more degenerative by 12 months.

Patients with OA tend to develop this within the first or second decade of life (de Heredia *et al.*, 2013). OA progress to a visual acuity of 6/60 or less in 35/45 patients (with a median time of 8 years) (Barrett *et al.*, 1997). Although the *wfs1b* zebrafish appear to lose a significant ability to distinguish a moving grate at 12 months, this is significantly longer in comparison for a zebrafish lifespan, in the wild zebrafish tend to live for 1 year and in captivity approximately 2 years. One explanation for this delay in onset may be the regenerative capacity of zebrafish RGCs (Sherpa *et al.*, 2008), this regeneration could be why we do not see a complete loss of vision in the *wfs1b* zebrafish. Another explanation for this could be the tissue differences between humans and zebrafish. It was hypothesised that the unmyelinated axons of the RGCs prior to the lamina cribrosa with the high energy demand and high mitochondria concentration may be playing a key role in OA in WS (Schmidt-Kastner *et al.*, 2009). As zebrafish RGC optic fibres are fully myelinated this might explain why we see a less obvious phenotype in the *wfs1* knockouts (Chhetri *et al.*, 2014a).

As myelination and mitochondrial dysfunction are thought to be affected in WS (Ross-Cisneros *et al.*, 2013; Cagalinec *et al.*, 2016; Lugar *et al.*, 2016) electron microscopy was performed on the 12 month zebrafish optic nerves to look at myelination and mitochondria ultrastructure and ER connections. This experiment did not work due to poor tissue preservation as the fixation was poor quality possibly due to the myelin providing a barrier to the fixative. This should be performed again but using a perfusion fixation to deliver the fixative to ensure higher quality fixation. Unfortunately due to time constraints this was not possible during this PhD.

Of the two zebrafish models the *wfs1b* knockout better resembled the OA phenotype seen in WS patients. The *wfs1b* knockout demonstrated a significant loss of RGCs and loss of visual function overtime. This again follows a recurring theme that *wfs1b* knockouts may slightly better model WS than *wfs1a*. The embryos also had slight changes in function which highlighted a possible developmental phenotype even if a change in structure was not obvious. Neuronal function and development alongside mitochondrial dysfunction are key elements that require further investigation from these results.

5.8 Conclusions

The *wfs1b* knockout model was a better representative model of OA in WS. A progressive loss of RGCs, thinning of the optic nerve and a functional loss of visual acuity was observed in this model by 12 months of age. The *wfs1a* knockout model developed a milder OA phenotype with a lower RGC loss and smaller changes in visual acuity.

Future work should examine the role of myelin and the mitochondrial function in the optic nerve. The mitochondrial connection to the endoplasmic reticulum could be examined using 3d-SEM with improved fixation of the zebrafish eyes. This would allow for a detailed picture of the optic nerve which myelination could also be measured. Expression profiles between the *wfs1a* and *wfs1b* knockouts would also be interesting to determine why *wfs1a* knockouts show a milder phenotype.

Chapter 6: Assessment of Early Neuronal Development in wfs1 Mutant Zebrafish Models

6.1 Introduction

WS is known to be a neurodegenerative disease (Grosse Aldenhovel *et al.*, 1991; Barrett *et al.*, 1995; Kinsley *et al.*, 1995), this tends to be the cause of death in patients due to brain-stem atrophy leading to central respiratory failure (Barrett *et al.*, 1995). A number of other neurological abnormalities have been described in patients with WS such as cerebellar ataxia and myoclonus (Barrett *et al.*, 1995) and alongside this patients are more likely to suffer from psychiatric disorders (Swift *et al.*, 1991).

The underlying mechanism of neurodegeneration in WS is not fully understood. A recent fly knockdown suggested wolframin may be having a protective role against stresses involved with aging in neurons (Sakakibara *et al.*, 2018). It has also been suggested that mitochondrial dysfunction may be important in neuronal degeneration. Whole transcriptome expression profiling of *WFS1* siRNAs HEK cells showed a number of changes in genes related to mitochondrial dysfunction (Koks *et al.*, 2013). Mitochondrial dysfunction and energy production is also thought to be disturbed in the optic nerve causing the degeneration of the smaller neurons in the optic nerve (Ross-Cisneros *et al.*, 2013). Mitochondrial dysfunction was also observed in cultured mouse neurons with trafficking and mitophagy changes which was hypothesised to be caused by changes in Ca^{2+} homeostasis (Cagalinec *et al.*, 2016). These neurons had a slight delay in growth suggesting wolframin may have a role in neuronal development.

Atrophy of the optic nerves, chiasm, cerebellum and brainstem were described in postmortum patients of WS (Barrett *et al.*, 1997). However, as another factor neuronal development has more recently been implicated in WS. The brain stem and cerebellum due to the nature of their development are thought to be more susceptible to changes in general neurodevelopment (Barkovich *et al.*, 2009). The brainstem and cerebellum volume were both observed as significantly smaller in WS patients, independent of disease progression (Hershey *et al.*, 2012). This alongside the reduced growth in isolated neurons suggests WS has both a developmental and a degenerative component to consider.

Although a number of changes in size can be observed in the zebrafish brain, the overall organization of major components of the zebrafish brain are comparable to human brains (Tropepe and Sive, 2003). Although the behaviours may not be as complex as rodent models there are a number of integrated neurological functions that affect behaviour (Lieschke and Currie, 2007). This allows for basic functional tests alongside histological to determine if altered neurogenesis or degradation are affecting animal behaviour.

Development of motor neurons in the zebrafish tail stems from three cell bodies in the spinal cord: Caudal, Middle and Rostral Primary motor neurons (CaP, MoP and RoP)(Myers *et al.*, 1986). These three bodies develop as described in Figure 6.1 to form functional motor neurons and neuromuscular junctions along the tail of the zebrafish. These neurons project from the spinal cord towards acetylcholine clusters (Panzer *et al.*, 2005).

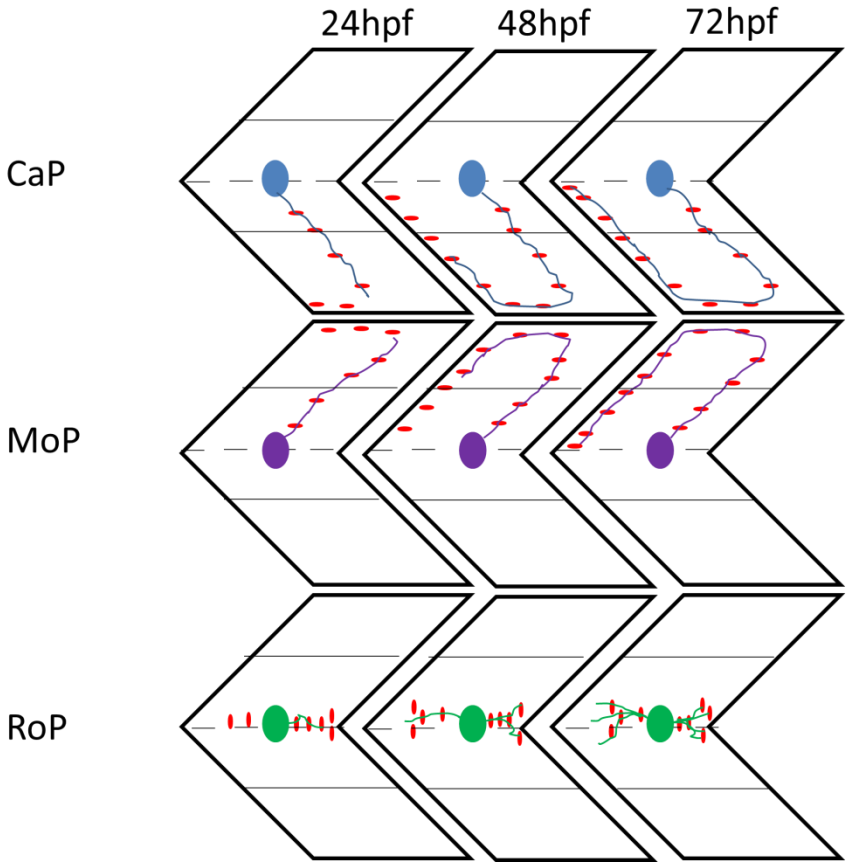

Figure 6.1 Caudal, Middle and Rostral Primary motor neurons development over the first 72 hours of zebrafish development. Neurons grow from neuronal body towards acetylcholine receptors (red circles) forming neuromuscular junctions.

Neurogenesis is suspected to be affected in patients with WS. Using a zebrafish model of WS we can monitor the development of the brain and motor neurons to determine if there is a developmental aspect to this neurodegenerative disease.

6.2 Neuronal Development Delay

24hpf zebrafish were immunostained using SV2 to visualise motor neurons and alpha bungarotoxin to visualise the acetylcholine receptors at the neuromuscular junctions. The motor neuron staining demonstrated differences in the *wfs1b* knockouts with a shortening of motor axons. This was quantified in Figure 6.2B, no difference was determined between control and *wfs1a* knockouts. Between the controls (79.86µm) and *wfs1b* (48.23µm) a significant difference was detected ($p<0.001$). A change was also observed between *wfs1a* and *wfs1b* knockouts ($p<0.01$).The alpha bungarotoxin staining although slightly fainter in the *wfs1b* knockouts clustered in the expected positions in all groups.

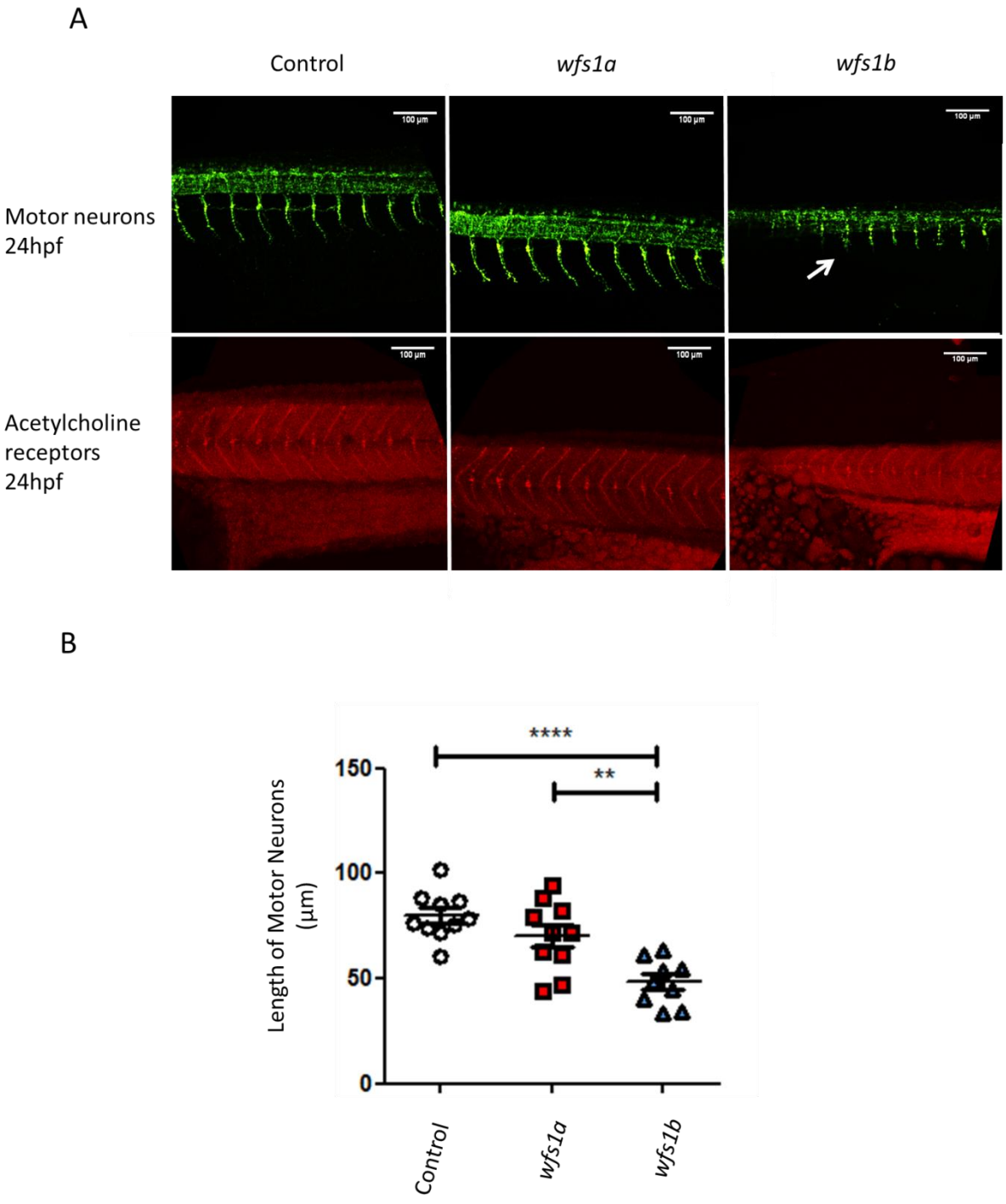

Figure 6.2 Motor neuron development at 24hpf. A: immunofluorescence of motor neurons and acetylcholine receptors. Motor neurons stained with SV2 in green, shorter axons are highlighted by white arrows; Acetylcholine receptors stained for alpha bungarotoxin in red. Max intensity projections imaged on Nikon confocal. B: Quantification of motor axon length at 24hpf. Data plotted mean ±SEM using Graphpad Prism n=9. Significance determined by One-Way ANOVA with Bonferroni multiple comparisons **p>0.01 ****p>0.0001.

To determine if this continued on through development motor neurons were stained again at 48hpf in Figure 6.3. At 48hpf the development of the motor neurons in *wfs1b* descended in the ventral direction to a similar position as the controls and *wfs1a* knockouts. When the length was quantified, no significant differences were measured. The next stage of development of the zebrafish motor neurons involves growth along the myoseptum this was imaged in Figure 6.4 to monitor any differences.

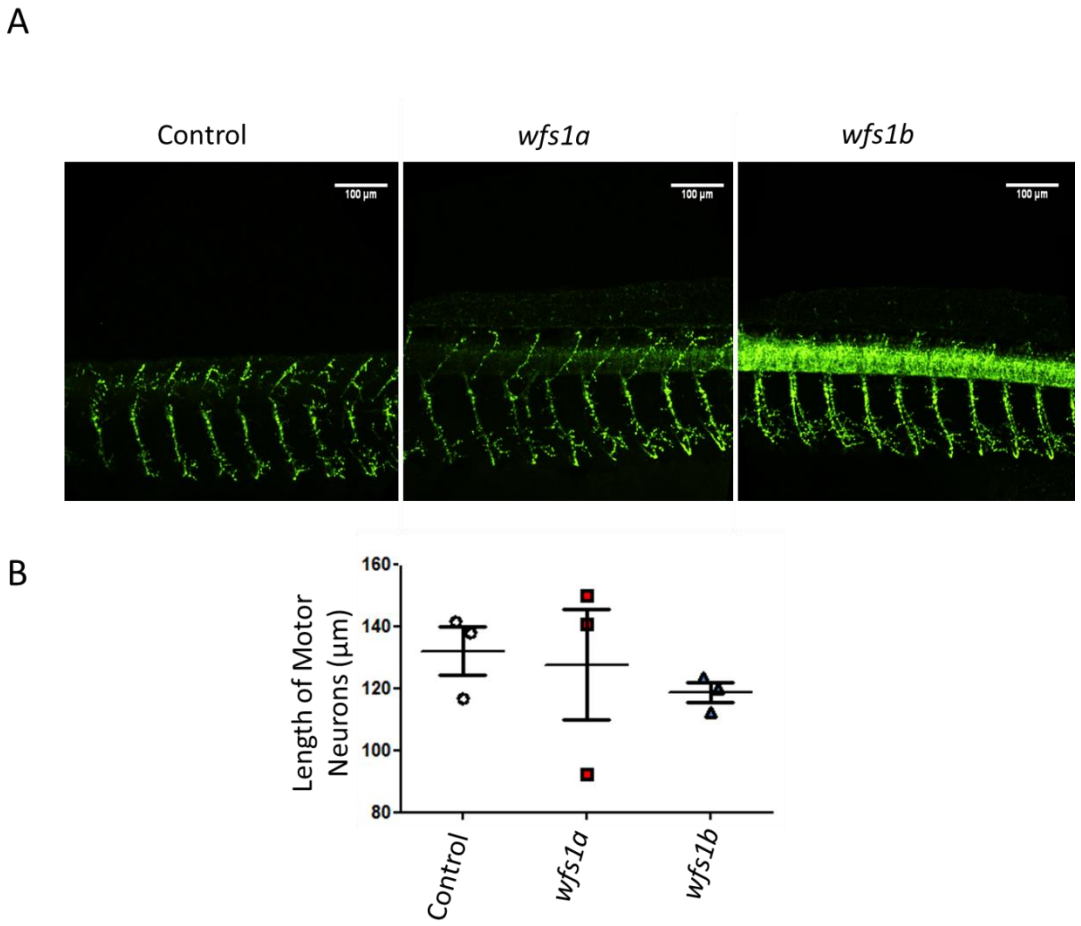

Figure 6.3 Lateral motor neuron development at 48hpf. A: immunofluorescence of motor neurons. Motor neurons stained with SV2 in green. B: Quantification of motor neuron length at 48hpf. Data plotted mean ±SEM using Graphpad Prism n=3. Significance determined by Kruskal-Wallis test with Dunns multiple comparisons due to unequal variances. Max intensity projections imaged on Nikon confocal.

The growth along the myoseptum is the next phase of growth as described in Figure 6.1. The axon growth along the myoseptum at 48hpf dobserved in Figure 6.4, appeared to be affected in both *wfs1a* and *wfs1b* knockouts. Although the majority of neurons have tracked into the correct positions there are gaps in the knockouts where there should be motor

neurons Figure 6.4 (marked by white arrows). Some staining can still be observed it may be a problem with axon branching in the development of the neurons being slightly delayed

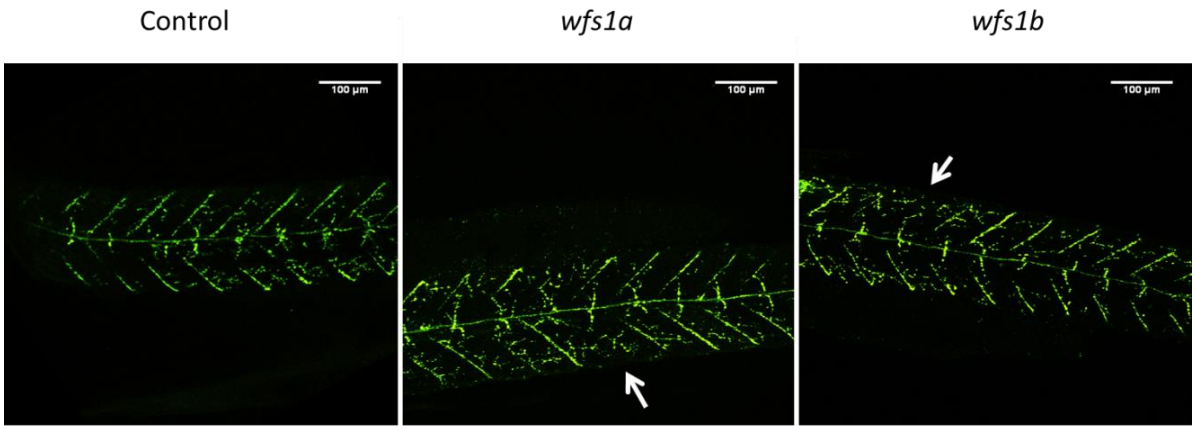

Figure 6.4 Motor neuron growth along the myoseptum at 48hpf. Immunofluorescence of motor neurons. Motor neurons stained with SV2 in green. White arrows indicate missing neurons. Max intensity projections imaged on Nikon confocal.

Acetylcholine receptors were also stained at 48hpf. Neurons grow towards acetylcholine receptors clusters. At the position of the missing neurons there is no obvious bungarotoxin staining as seen in the other myosepta.

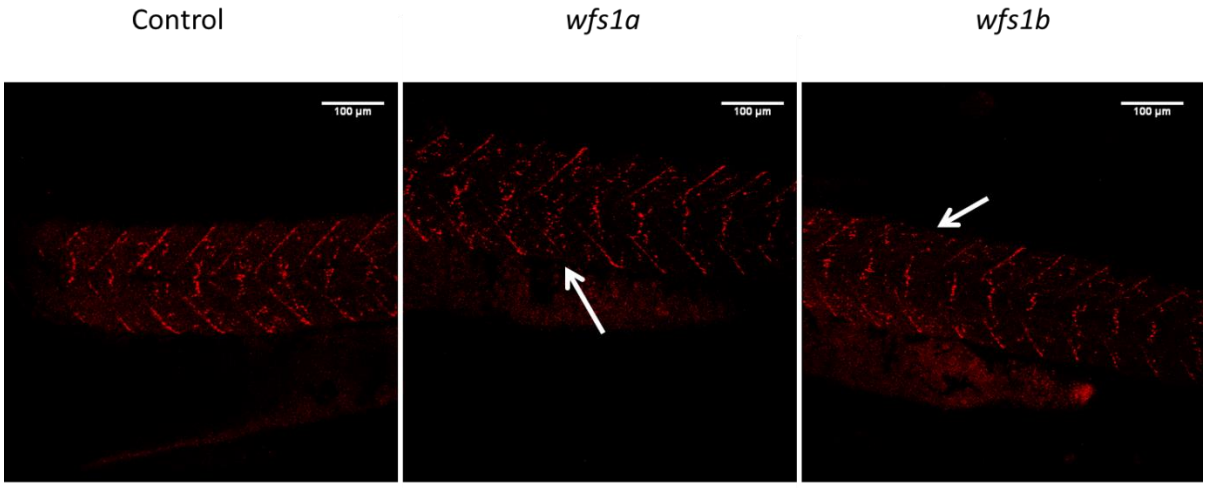

Figure 6.5 Acetylcholine receptors along the myoseptum at 48hpf. Immunofluorescence of acetylcholine receptors. acetylcholine receptors stained with alpha bungarotoxin in red. White arrows indicate missing neurons. Max intensity projections imaged on Nikon confocal.

Motor neuron development was observed at later timepoints to determine if this difference was corrected. 4dpf zebrafish were stained for motor neurons. At 4dpf the loss of axons along the myosepta had disappeared.

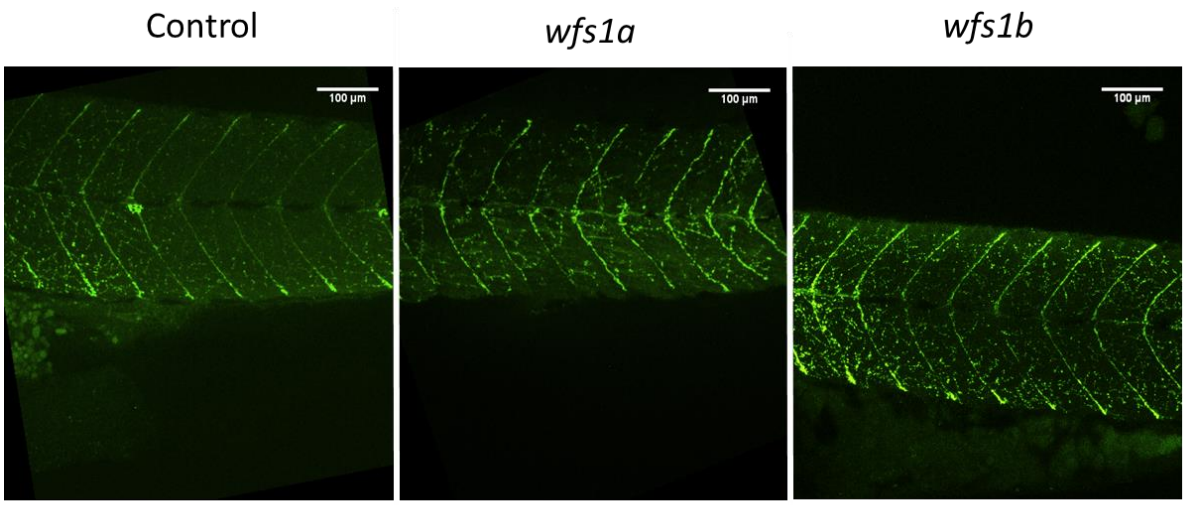

Figure 6.6 Motor neuron growth along the myoseptum at 4dpf. Motor neurons stained with SV2 in green. Max intensity projections imaged on Nikon confocal.

Although staining of motor neurons showed no changes at 4 days, an acetylcholinesterase (AChE) assay was performed to determine if an overall change in neuronal population could be determined. AChE is expressed in the CNS and has been observed in primary neurons of the zebrafish embryo (Bertrand *et al.*, 2001; Behra *et al.*, 2002). Measuring activity in homogenates of zebrafish embryos is an indirect way of measuring neural tissue. The knockout zebrafish both showed reductions in the amount of AChE activity at 3 and 5dpf ($p<0.01$ and $p<0.0001$ respectively). Only the *wfs1b* zebrafish had significantly reduced AChE activity at 4dpf.

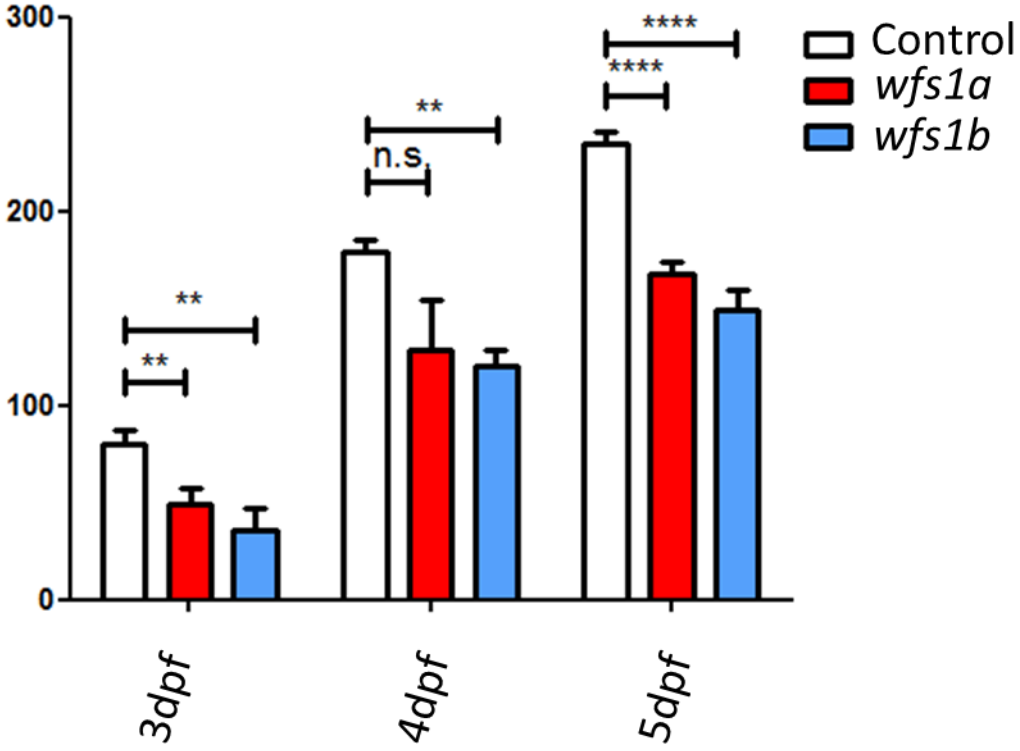

Figure 6.7 Acetylcholine esterase assay of developing zebrafish larvae 2-5dpf. Protein quantified using BCA assay and the acetylcholine esterase activity measured from 10µg of protein using a Varioskan LUX plate reader. Repeat data normalised to control of 1st plate. Data plotted mean ±SEM using Graphpad Prism, n=6. Significance determined by One-Way ANOVA with Bonferroni multiple comparisons **p>0.01 ****p>0.0001.

6.3 Zebrafish Brain Development and Degeneration

To look at the brain development, zebrafish were grown in 1-Phenyl-2-thiourea (PTU), to stop pigment formation. As the zebrafish heads are transparent the brain can be viewed. Part of the cerebellum can be easily measured, highlighted by the white arrow in Figure 6.8A. The area of the cerebellum was quantified by manually measuring on ImageJ. This showed a significant smaller area of cerebellum in *wfs1b* knockout zebrafish (p>0.05 against controls).

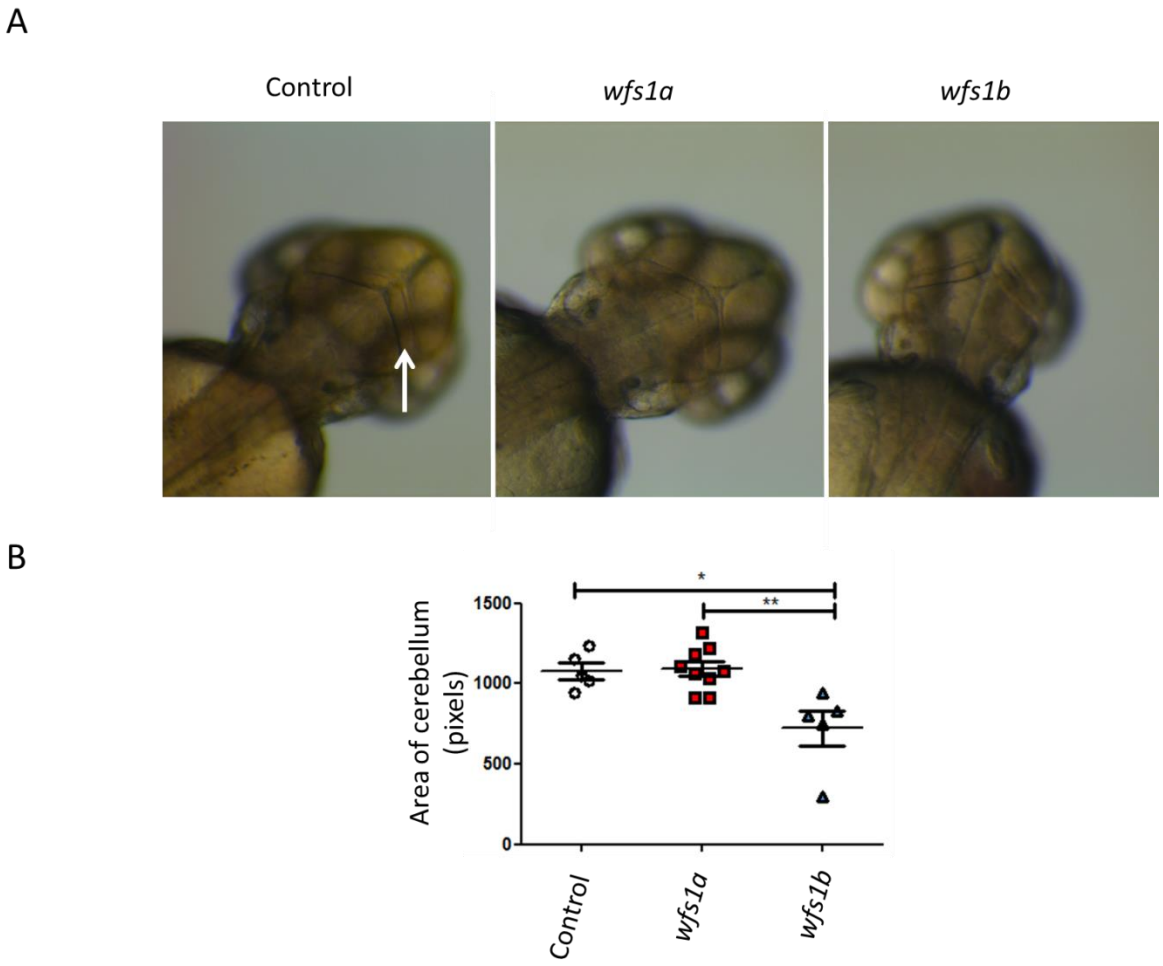

Figure 6.8 Brain development in wfs1 knockout zebrafish at 72hpf. A: Representative images of control and knockout brains viewed from overhead. Images from Leica MZ16F stereomicroscope with a Leica DFC420 C camera attachment. White arrow highlights the cerebellum in the control zebrafish. B: Quantification of zebrafish cerebellum area. Data plotted mean ±SEM using Graphpad Prism. Control n=5, wfs1a n=9 and wfs1b n=5. Significance determined by One-Way ANOVA with Bonferroni multiple comparisons *p>0.05 and **p>0.01.

The zebrafish brain also expresses AChE. Changes in brain AChE levels could provide an indirect measure of neurodegeneration in adult zebrafish as described in Figure 6.9. The two time points: 4 months and 12 months, showed a significant reduction of *wfs1a* and *wfs1b* AChE activity compared to controls ($p<0.001$ and $p<0.0001$). At 12 months wfs1a is no longer reduced in comparison to controls while *wfs1b* is significantly downregulated compared to controls ($p<0.0001$) and *wfs1a* ($p<0.001$).

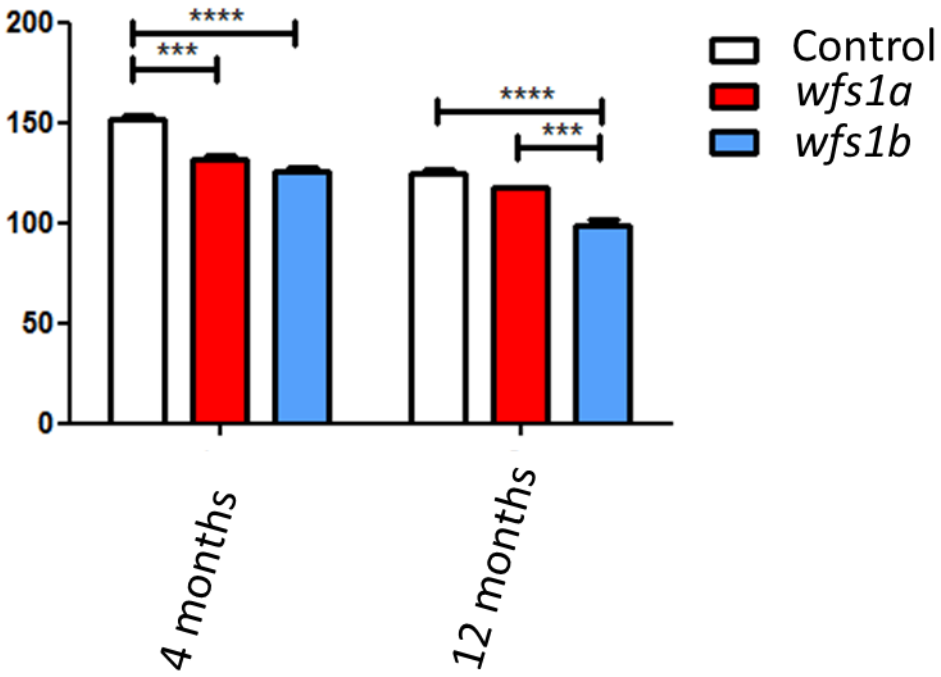

Figure 6.9 Acetylcholine esterase assay on brains of 4 and 12 month zebrafish. Protein quantified using BCA assay and the acetylcholine esterase activity measured from 10µg of protein using a Varioskan LUX plate reader. Data plotted mean ±SEM using Graphpad Prism n=3. Significance determined by One-Way ANOVA with Bonferroni multiple comparisons ***p>0.001 ****p>0.0001.

6.4 Functional Neuronal Impairment

To determine if the changes observed in neuronal development had a functional effect, two tests, spontaneous movement at 24hpf, and touch response at 48hpf, were carried out. The spontaneous movements of the *wfs1b* zebrafish were significantly higher compared to the controls and *wfs1a* knockouts ($p<0.01$). To determine if the *wfs1b* knockout embryos were moving due to delayed development, videos were recorded at 27hpf when the movement should stop. *wfs1b* knockouts continue to perform spontaneous movements when controls and *wfs1a*'s have ceased.

At 48hpf the touch response showed a significant decrease in the distance moved by the *wfs1b* zebrafish as compared to the controls ($p<0.01$), with the majority of *wfs1b* knockouts hardly moving at all.

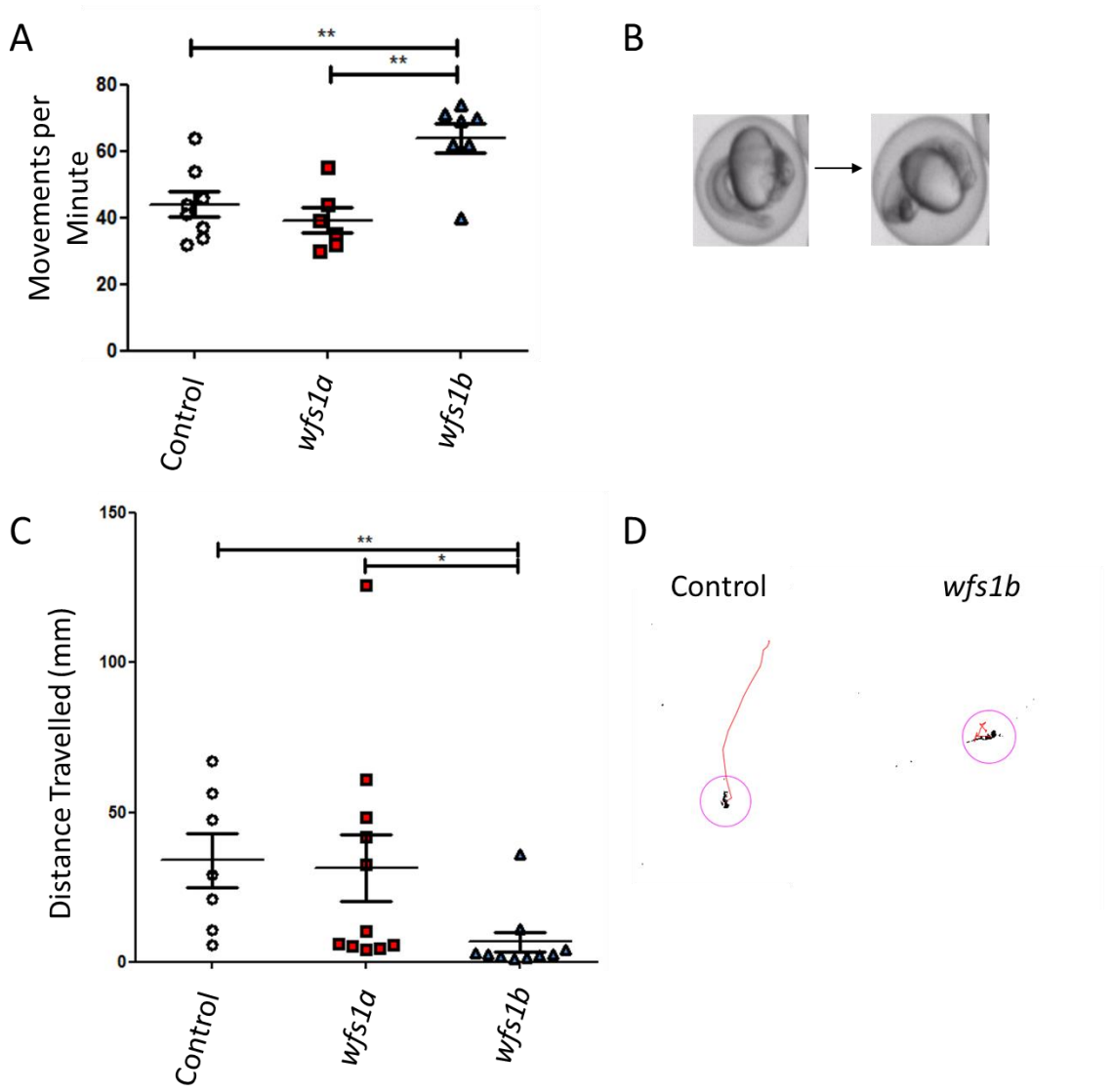

Figure 6.10 Functional assessment of neuronal development in developing zebrafish. A: Twitch response of zebrafish embryos at 24hpf, 15 embryos were recorded and the average movement per fish per minute calculated, control n=8 wfs1a n=6 wfs1b n=7. B: Image of a zebrafish moving within the chorion. C: Distance travelled following tactile stimulation: n=10. D: representative image of control vs *wfs1b* knockout zebrafish, red line represents distance travelled. Graphs plotted as mean ± SEM, significance was calculated by One way ANOVA with Bonferroni's multiple comparison tests *p<0.05 **p<0.01. Videos of twitch and touch response in supplementary evidence 5 and 6.

6.5 Muscle Structure

Muscle structure was observed to determine that differences in movement were neuronal and not caused by defects of muscle function. At 48hpf zebrafish were subjected to phalloidin staining for F-Actin, this shows the muscle fibres in the zebrafish tail. No differences in gross muscle fibre architecture could be distinguished between the controls and the knockouts.

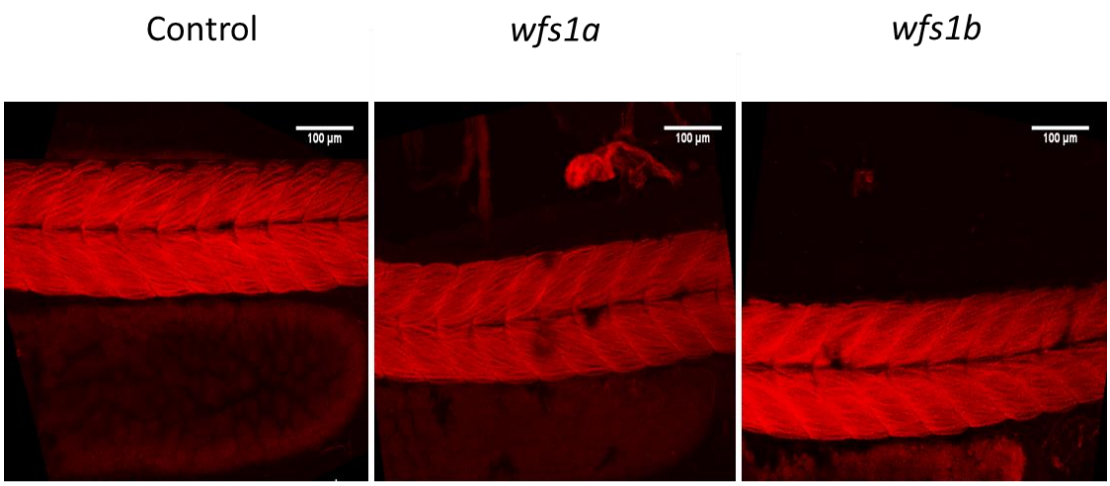

Figure 6.11 Muscle Fibre Immunostaining. F-actin stained using phalloidin to detect muscle fibres. Max intensity projections imaged on Nikon confocal.

6.6 Discussion

Neuronal development has become a new area of interest for the function of wolframin. The zebrafish offers a unique opportunity to model neuronal development in WS. As the zebrafish develop externally and are transparent it allowed for whole mount immunostaining of neuronal development and functional testing on the earliest time points of development. The *wfs1* knockouts particularly the *wfs1b* knockouts showed significant reductions in neuronal development.

At 24hpf there is a significant difference in length of the motor axons in *wfs1b* knockout zebrafish ($p>0.001$). The acetylcholine receptors develop in a similar pattern in all three conditions suggesting this is an axonal outgrowth defect rather than abnormal muscle development. The differences of length in the lateral growth of the motor neurons appear to be corrected at 48hpf. The dorsal growth along the myoseptum is affected in both *wfs1* knockouts, with motor neurons not growing along a number of myosepta. The expression patterns of the mutated genes may be accounting for a difference between the two models, as described in Figure 5.3. This showed *wfs1b* was expressed from the 1 cell stage while *wfs1a* expression increased later; the expression was also lower in neural tissue in adults. This explains the obvious differences at 24hpf and why only slight changes were observed at 48hpf.

To determine if these changes were carried into later developmental time points; at 4dpf missing axons could no longer be observed. This mirrors what was found in Wfs1 shRNA-transfected mouse neurons with a delay of growth at early stages which evened out in mature neurons (Cagalinec *et al.*, 2016). A very slight loss in the number of neurons was also observed in the knockout mouse neurons; this may be too subtle for detection with whole mount immunostaining. In order to determine if changes in neuronal development could be quantified, an acetylcholinesterase assay was performed. AChE breaks down acetylcholine and is expressed in the CNS cholinergic and noncholinergic fibers (Bertrand *et al.*, 2001; Behra *et al.*, 2002). This assay was used as its activity can be interpretted as an indirect measure of neuronal tissues. Differences were observed at and 3dpf, 4dpf ($p<0.01$) and 5dpf ($p<0.0001$) in *wfs1b* but only 3dpf and 5dpf in *wfs1a* knockouts. This is most likely due to the large SEM observed in *wfs1a* knockouts at 3dpf. The development was not progressing as fast in both *wfs1* knockouts. As the AChE assay took the whole zebrafish into account the

difference in AChE activity may be due to reduced brain development as this has been described patients with WS (Hershey *et al.*, 2012).

The *wfs1* embryos were grown in PTU which blocks pigment formation so they remain transparent for longer. Pictures of the brain could be taken in live zebrafish to determine if any gross morphological changes were occurring in knockout zebrafish. The zebrafish cerebellums were significantly smaller at 72hpf. This is in concurrence with the results found in patients that the cerebellum is reduced in volume, independent of disease progression (Hershey *et al.*, 2012). Cerebellum development is linked with general neurodevelopment disorders (Barkovich *et al.*, 2009).

The AChE activity was also measured in adult brains at 4 and 12 months. At 4 months reductions in AChE activity was reduced in both *wfs1a* and *wfs1b* knockouts. However, at 12 months the *wfs1a* knockouts showed no significant differences with controls while *wfs1b* knockouts were significantly lower than both. This could suggest a neurodevelopmental effect at the early time point and degeneration at the 12 month stage with a further reduction in AChE activity in *wfs1b* knockouts. Adults zebrafish brains undergo constant neurogenesis and neural regeneration (Schmidt *et al.*, 2013). This can explain why the brain AChE activity of *wfs1a* knockouts becomes similar to the controls overtime. The *wfs1b* knockouts never catch up which could either suggest problems in neurogenesis or neurodegeneration of the brain. To determine if degeneration is happening in the brain apoptotic markers could be monitored in zebrafish brains such as caspase 3.

To determine if the changes in zebrafish neuronal development had functional effects on the knockout zebrafish, behavioural tests were carried out. The spontaneous movement of zebrafish begins at 17hpf and gradually decreases in frequency until stopping at 27hpf (Saint-Amant and Drapeau, 1998; Menelaou *et al.*, 2008). As *wfs1b* knockout zebrafish were observed performing more movement at 24hpf it is likely the *wfs1b* knockouts are behind in development. Further evidence for this was provided when the zebrafish were recorded at 27hpf and *wfs1b* zebrafish were moving while controls and *wfs1a* fish had stopped spontaneously moving. At 48hpf the majority of *wfs1b* zebrafish moved very little, this was significantly lower than the controls and wfs1a knockouts ($p<0.01$ and $p<0.05$). In order to determine if this lack of movement was due to problems with muscle morphology, F-actin was stained for to look at muscle fibre structure. As no differences were detected in the

muscle fibre structure it shows a problem with neuronal signalling in response to the tactile stimulation.

Deficiencies in neuronal development have been detected in *wfs1* knockouts. This is observed in the immunostaining, the functional assays and the brain development. Although the when observing the immunostaining the deficiencies appear to be corrected by later developmental time points, the AChE assay determined that the deficiency in development continues past the 5 day point. This suggests that WS has a neuronal development condition that is compounded later in life by the neurodegeneration.

The *wfs1b* model appears to be more severely affected than *wfs1*a knockouts. Significant changes were observed in the early immunostaining and functional tests and brain development which suggested this knockout was affected more. This was not entirely surprising when looking at the localisation in Figure 5.3 where higher *wfs1b* expression was observed in the brain of the adult zebrafish. The AChE assay showed equal reductions in activity which was unexpected. As the AChE assay is an indirect measurement it may be possible that AChE itself has been affected by *wfs1* knockout or that other non-imaged neurons had a more severe phenotype in *wfs1a* knockout zebrafish.

As *WFS1*'s function in the neuron is not as well characterised as in pancreatic cells there are a number of theories of what *WFS1'*s function in neurons is. In cultured mouse and rat cells it is suggested that it plays a role in Ca^{2+} regulation and mitochondrial dynamics, while in the fly model these two things were not observed. However, the authors of the study hypothesise a neuroprotective role of wolframin against oxidative stress and ageing (Cagalinec *et al.*, 2016; Sakakibara *et al.*, 2018). As mitochondria play an important role in neurons and their history in the involvement of WS, mitochondrial function was looked at in more detail in the zebrafish model.

6.7 Conclusion

Early neuronal development in is impaired in the *wfs1* knockout models. Differences in motor neuron staining can be detected in the first 48 hours of development. Functional neuronal impairment is also detected in *wfs1b* knockout zebrafish, while no muscular changes could be observed by immunofluorescence. Changes in the AChE activity can be detected in 3-5dpf suggesting less neuronal tissue in larvae as they develop, which could also be observed in the knockout adult brains. This suggests a reduction in neuronal tissue

throughout the life of the zebrafish which may be comparable to patients with WS (Hershey *et al.*, 2012).

Future work could involve electrophysiological recording of muscles, nerves or in the brain to determine in detail if/where the nerve conduction fault occurs (Baraban, 2013). Mitochondrial co-localisation may also be useful in determining the involvement of energy production in the affected nerves, while Ca^{2+} homeostasis could also be studied in the nerve to determine if it is a factor in the changes in neurodevelopment.

Chapter 7: Mitochondrial Dysfunction in wfs1 Mutant Zebrafish Models

7.1 Introduction

WS historically was thought of as a mitochondrial disease, due to the phenotypes being similar to other ATP supply defect disorders such as LHON (Bu and Rotter, 1993). This was compounded by the discovery of a number of patients containing mtDNA deletions (Zeviani *et al.*, 1989; Rotig *et al.*, 1993). After the discovery of mutations in the *WFS1* gene describing an autosomal mutation and not mtDNA the role of mitochondria in WS became less clear (Inoue *et al.*, 1998; Strom *et al.*, 1998). Further evidence against mitochondrial involvement came with a study of 40 patients where no evidence supporting a role for mtDNA in WS was found and concluded that patients with mtDNA deletions were not typical of WS (Barrett *et al.*, 2000). In this study lack of changes in mitochondrial function in patient muscle biopsies were also described (Barrett *et al.*, 2000). Wolframin is also localised to the ER rather than mitochondria and the role in the ER stress response was suggested to be a key feature of WS (Takeda *et al.*, 2001; Yamaguchi *et al.*, 2004).

More recently the role of mitochondrial dysfunction in WS has been brought into question again. Silencing of *WFS1* in HEK cells upregulated pathways of mitochondrial damage (Koks *et al.*, 2013). Alongside this, dysfunctional mitochondrial trafficking was observed in developing cultured mouse neurons (Cagalinec *et al.*, 2016). More evidence for the role of mitochondrial dysfunction is seen in WS type 2. WS type 2 is caused by mutations in *CISD2* and has a similar phenotype to WS. Similar to *WFS1*, *CISD2* has roles in Ca^{2+} regulation, however no direct interactions between the two proteins has been discovered (Wiley *et al.*, 2013). *CISD2* has been shown to be directly involved in Ca^{2+} dynamics of the mitochondria (Wiley *et al.*, 2013; Rouzier *et al.*, 2017b). Knockout patient fibroblasts of *CISD2* had a number of other mitochondrial abnormalities including increased ER-mitochondria contact and a hyperfused mitochondrial network (Rouzier *et al.*, 2017b). A patient in 2012 was diagnosed with WS initially suspected to be mitochondrial disease due to biochemical data suggesting a complex I defect and multiple mtDNA deletions (Lieber *et al.*, 2012). The authors hypothesise that wolframin is affecting mitochondrial function and mtDNA maintenance.

The zebrafish mtDNA is comparable to humans, it contains all 44 genes that have this same gene order and is approximately 70% similar to the human mtDNA (Broughton *et al.*, 2001;

Steele *et al.*, 2014b). This makes zebrafish a useful model for the study of mitochondrial diseases. The external and rapid early development allows for a number of mitochondrial techniques to be performed that would be very difficult in more complex models. This includes assessing live *in vivo* mitochondrial dynamics, whole system OXHOPS measurements and neuronal development/degeneration (Stackley *et al.*, 2011; Steele *et al.*, 2014a; Dukes *et al.*, 2016). Zebrafish do have differences in the OXPHOS pathway, alternative pathways for complex III feeding have been suggested meaning to some extent zebrafish can bypass complex I and II (Pinho *et al.*, 2013). A Parkin knockout zebrafish with reduced complex I expression demonstrated no significant changes in swimming behaviour suggesting these alternative pathways may be able to alleviate some of the stress involved in complex I disorders (Flinn *et al.*, 2009).

The aim of this chapter was to observe the mitochondrial function of *wfs1* knockout zebrafish in order to better understand the mitochondrial role in the development of WS.

7.2 Mitochondrial Axonal Transport

As mitochondrial dynamics was affected in a culture model of WS, the effect of *wfs1* knockout on zebrafish dynamics was assessed in live embryos at 48hpf. To identify the correct neuron, GFP was expressed under the neuro-d promotor and the lateral line located. A mito-tagged RFP expressed under a neuro-d promotor was also expressed and mitochondria in the lateral line of the developing zebrafish were observed (Figure 7.1A). Analysis was performed using kymographs (Figure 7.1B) to track movement, velocity, distance and directional changes of mitochondria.

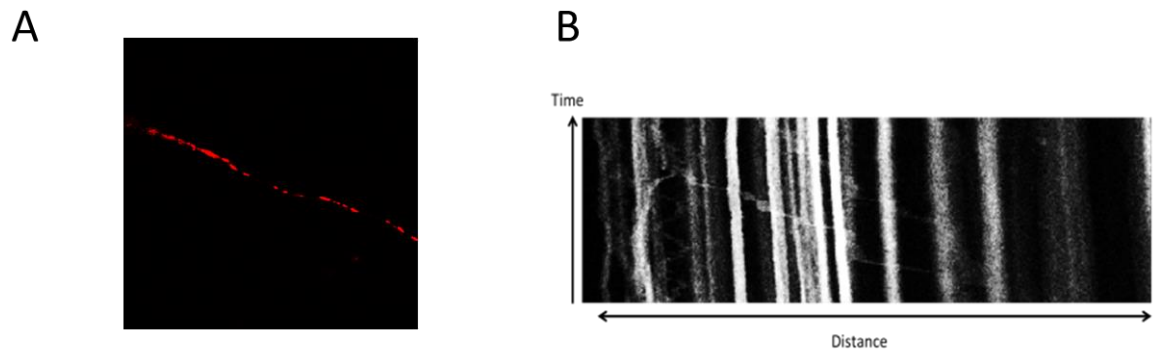

Figure 7.1 Mitochondrial Transport. A: A 60x confocal image of the mito-RFP in the zebrafish lateral line (video in supplementary evidence 7). B: A representative kymograph of movement in the lateral line. The white lines represent mitochondria and the movements can be measured and converted into velocity (distance/time).

The *wfs1* knockouts both had a reduction in the distance travelled by mitochondria. *Wfs1a* knockout mitochondria travelled 7.269µm less distance per movement ($p<0.01$) and *wfs1b* travelled 4.66µm less per movement ($p<0.001$). When the velocity of these mitochondrial movements was measured only the wfs1a knockouts were significantly different with a reduction of 0.2µm/s ($p<0.01$).

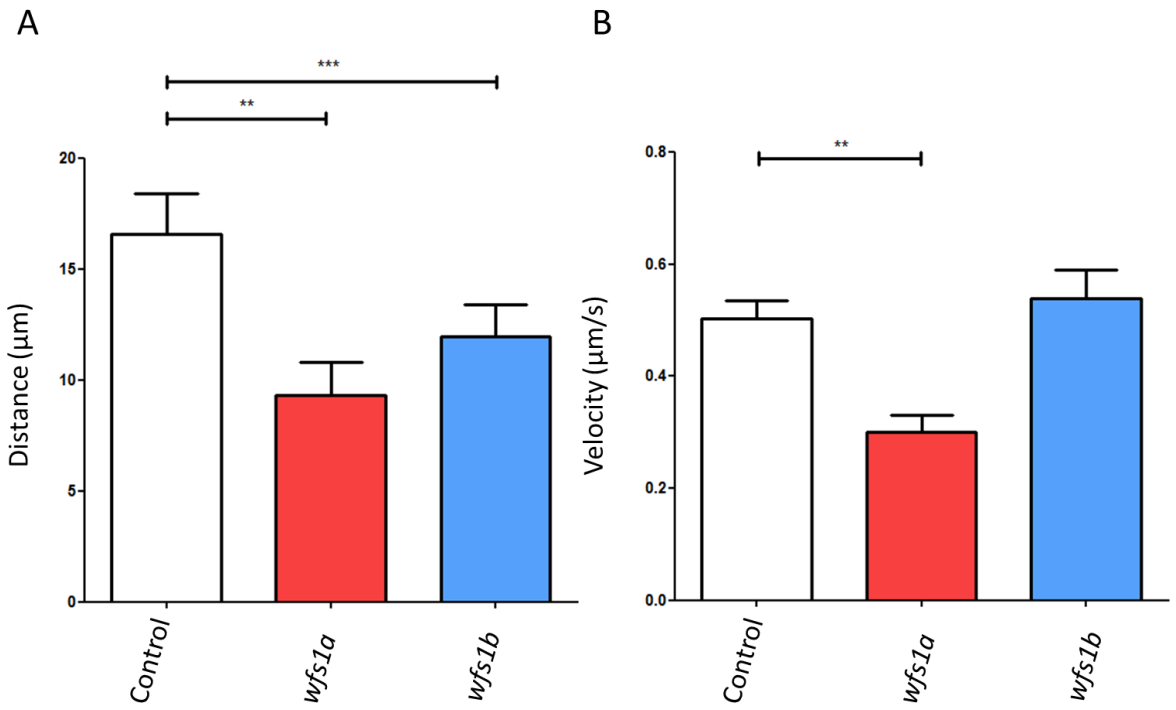

Figure 7.2 Quantification of Speed and Distance Travelled. A: Average distance travelled of moving mitochondria in the lateral line B: Average velocity of moving mitochondria in the lateral line. Control n=119 *wfs1a* n=73 *wfs1b* n=162. Statistics: Kruskal-Wallis test with Dunn's Multiple Comparison Test *p<0.05 **p<0.01, ***p<0.001 Graphs plotted mean +SEM.

The distance and velocity can also be separated into anterograde and retrograde movements. The only changes from the combined grouping were in the velocity where *wfs1b* knockouts move significantly slower than the control p<0.05. A result that was previously masked in Figure 7.2B.

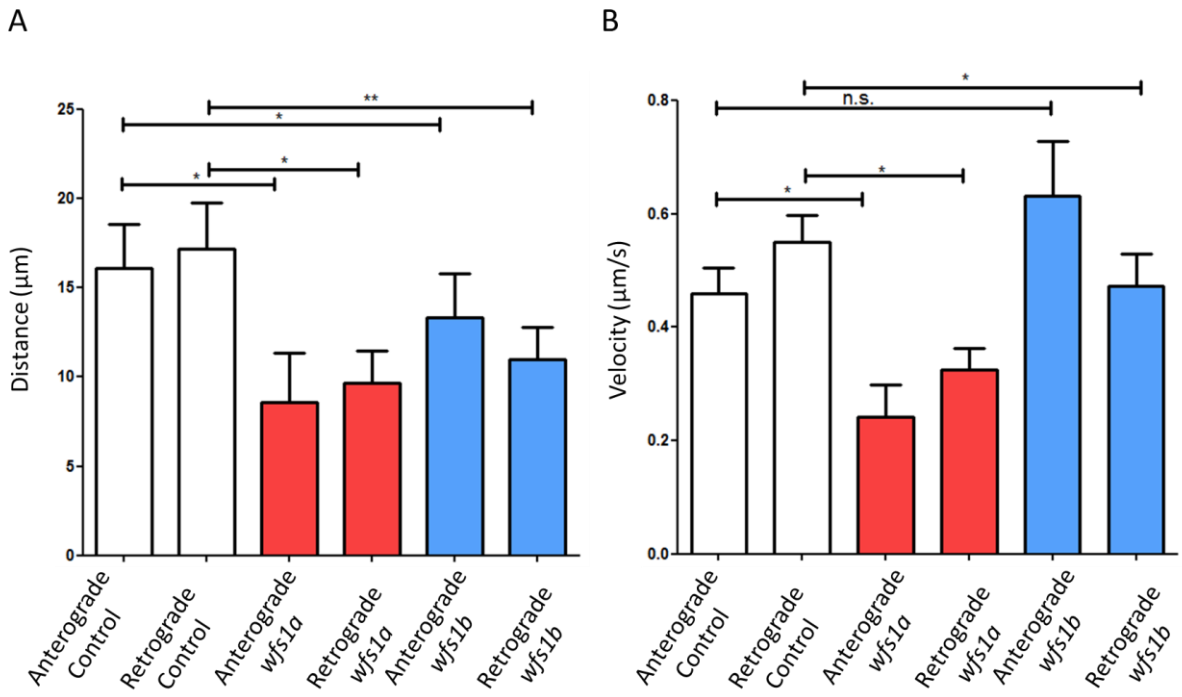

Figure 7.3 Quantification of Speed and Distance Travelled in Anterograde and Retrograde Directions. A: Average velocity of moving mitochondria in the lateral line B: Average distance travelled of moving mitochondria Anterograde Control n=63, Reterograde Control n= 56, Anterograde *wfs1a* n=22, Reterograde *wfs1a* n=51, Anterograde *wfs1b* n=67 and Reterograde *wfs1b* n=95. Statistics: Kruskal-Wallis test with Dunn's Multiple Comparison Test *p<0.05 and **p<0.01 Graphs plotted mean +SEM.

It also appeared the mitochondria were moving differently when the kymographs were analysed so to determine if this was the case the number of changes of movement of each mitochondria, and the percentage of time spent moving were measured. The *wfs1b* knockout zebrafish mitochondria had an increased number of changes in movement (p<0.05), such as moving to stationary or changes in anterograde or retrograde travel. The *wfs1b* knockouts also spent 60.85% of their time moving 20% more than controls (p<0.01).

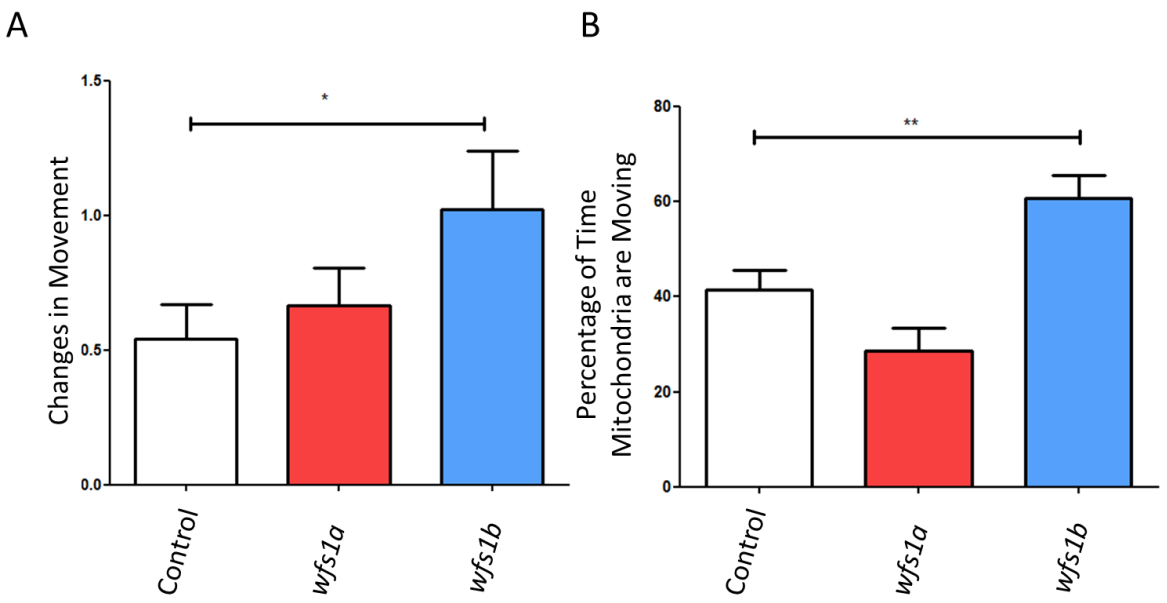

Figure 7.4 Changes in Phases of Mitochondrial Movement and Percentage of Time Moving. A: Number of changes in movement of mitochondria during 5 minute timelapse (anterograde←stationary→retrograde) Percentage of time mitochondria spend moving. Control n=129 *wfs1a* n=62 *wfs1b* n=85. Statistics: Kruskal-Wallis test with Dunn's Multiple Comparison Test *p<0.05 and **p<0.01 Graphs plotted +SEM.

7.3 Seahorse XF Mito Stress Test

In order to determine if zebrafish mitochondrial function was affected in knockout zebrafish a Seahorse XF Mito Stress Test was optimised and used on a Seahorse XFe96 on whole zebrafish larvae at 48hpf (Figure 7.5). The knockout *wfs1b* had severely affected mitochondrial respiratory function compared to controls. Oligomycin (blocks ATP production), FCCP (transports H^+ ions through inner membrane) and a combination of rotenone and antimycin A (blocks complex I+IV) were sequentially added to the zebrafish. These drugs allowed affect respiration in specific manners allowing the calculation of a number parameters: non-mitochondrial respiration, basal respiration, proton leak, max respiration, ATP production and spare respiratory capacity (Figure 7.5).

Basal Respiration was lower ($p<0.0001$) without a reduction in non-mitochondrial respiration, max respiration ($p<0.0001$), ATP production ($p<0.001$) and spare respiratory capacity ($p<0.001$) were all also significantly lower in *wfs1b* knockouts. The *wfs1a* knockouts had no significant differences from controls even though the majority had a lower mean OCR this fell within the range of standard error.

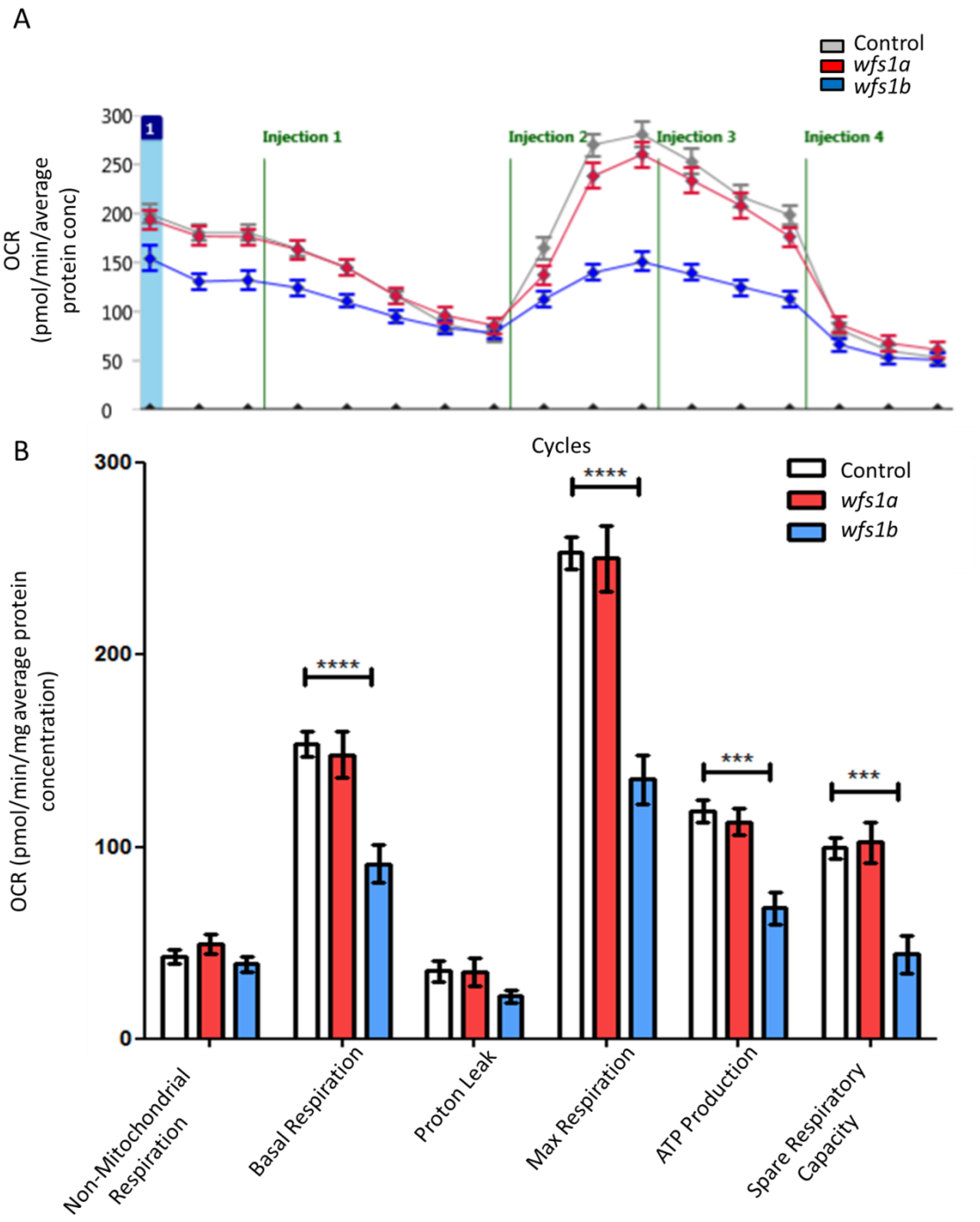

Figure 7.5 Seahorse XF Cell Mito Stress Test. A) Oxygen Consumption Rate vs Minutes, OCR was measured and plotted as mean ± SEM under the following conditions: basal conditions and following the sequential addition of oligomycin (injection 1), FCCP (injection 2/3) and rotenone with antimycin A (injection 4). B)The following parameters were calculated and plotted as mean ± SEM: Non-mitochondrial respiration, Basal respiration, Maximal respiration, Proton leak, ATP-prodiction and Spare respiratory capacity. Significance calculated using Two-way ANOVA with Bonferroni multiple comparisons. ***=p<0.001 ****=p<0.0001 ab n=60, *wfs1a* n=64 and *wfs1b* n=60.

7.4 mtDNA Levels

mtDNA was examined to determine if changes in mitochondrial function were due to mitochondrial biogenesis changes. The levels of mtDNA were measured using qPCR of *nd1* compared to the number of genomic copies of *ef1α*. If the ratio of *nd1* increases it suggests an increase in mtDNA. No significant differences were determined between the controls and *wfs1* knockouts, although *wfs1b* knockout means were slightly higher (0.475 ΔCT higher).

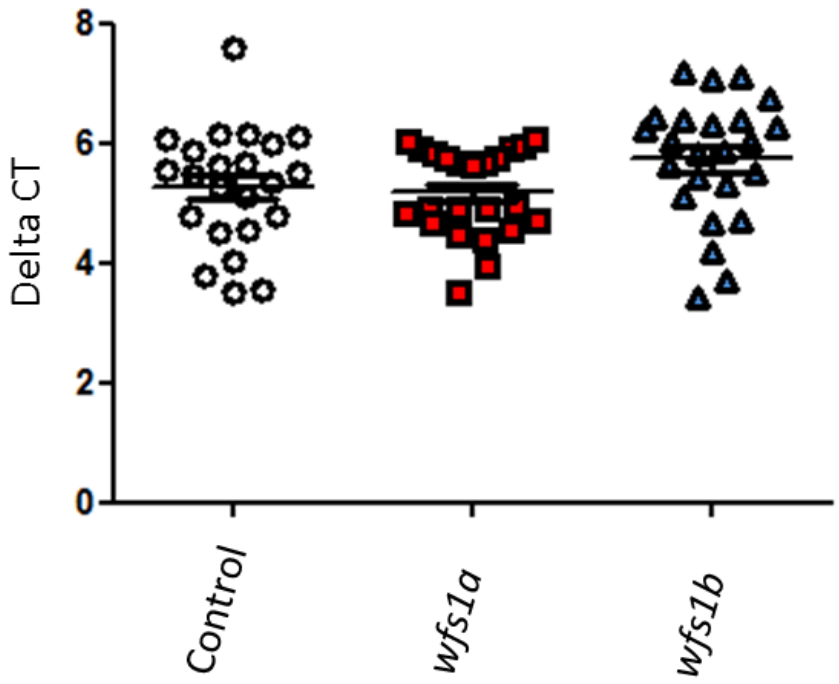

Figure 7.6 mtDNA Levels of 48hpf Zebrafish. ΔCT of *nd1* subtracted by ΔCT of *ef1α* of nuclear extracted DNA (Hot shot). Graphs plotted as mean ± SEM, significance was calculated by One way ANOVA with Bonferroni's multiple comparison tests no differences determined between groups, n=23

7.5 Mitochondrial Complexes

As no significant changes in mtDNA were observed, protein levels of the components of the OXPHOS system were examined. The OXPHOS complexes I-IV creates the proton gradient and V uses this to produce ATP. Complex I levels were examined to find the cause of respiratory changes.

At 48hpf complex I subunit NDUF9A levels was observed by Western blot. The *wfs1* knockouts had a reduced complex I amounts compared to controls with *wfs1b* being more

severely affected. Complex I densities were normalised to VDAC expression as a marker of mitochondrial loading.

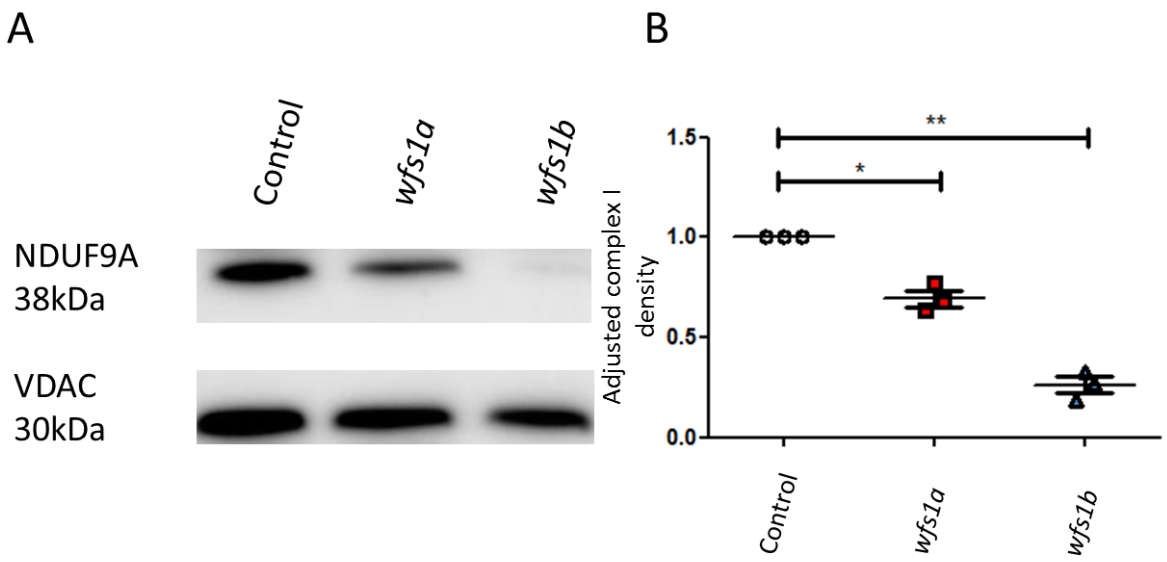

Figure 7.7 Complex I protein levels in 48hpf whole zebrafish lysates. A: NDUF9A and VDAC Western blots of control *wfs1a* and *wfs1b* knockout whole zebrafish lysates. B: Quantification of density normalised to VDAC as a mitochondrial loading control. Embryos at 48hpf taken for each genotype. Statistics: Paired t-test *p<0.05 and **p<0.01 Graphs plotted mean ± SEM

Heat shock show changes to BiP expression and zebrafish mortality in Chapter 5. To determine if heat shock was having any effect on mitochondrial proteins, zebrafish were heat shocked at 6hpf for one hour. The VDAC expression was very faint at 7hpf so a Coomassie staining was also performed to determine equal loading. The *wfs1a* knockout NDUF9A expression was higher than the control at 7hpf, while the *wfs1b* was lower which is consistent with the results at 48hpf. In heat shocked zebrafish there is a difference in NDUF9A expression in *wfs1a* knockouts.

No differences could be determined in ATP5A (complex V subunit) expression throughout.

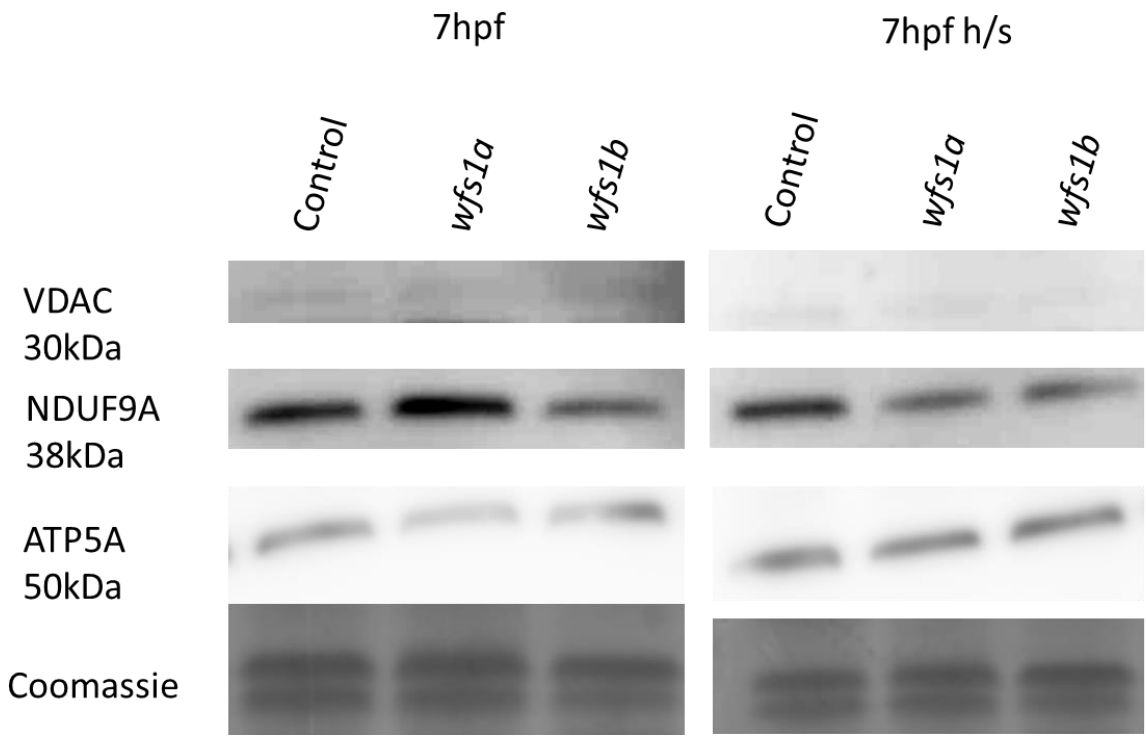

Figure 7.8 Complex I protein levels in 7hpf whole zebrafish lysates. VDAC, NDUF9A and ATP5A Western blots of control, *wfs1a* and *wfs1b* knockout and heat shocked equivalents, whole zebrafish lysates, Coomassie gel image to confirm equal loading. Embryos collected at 7hpf or after 1 hour of heat shock at 37^{o}C taken for each genotype.

In order to determine is tissue specificity may be a a factor in the complex I changes observed in Figure 7.6-7 adults zebrafish where disected and the brain eyes and muscle were used for protein analysis. Changes in the brain showed a higher protein level of NDUF9A in *wfs1a* knockouts and a reduction in *wfs1b* knockouts. The eye had reductions in NDUF9A in both knockouts with *wfs1b* being more severe. Muscle tissue had a large reduction in NDUF9A in *wfs1a* knockouts and a less severe reduction in *wfs1b*.

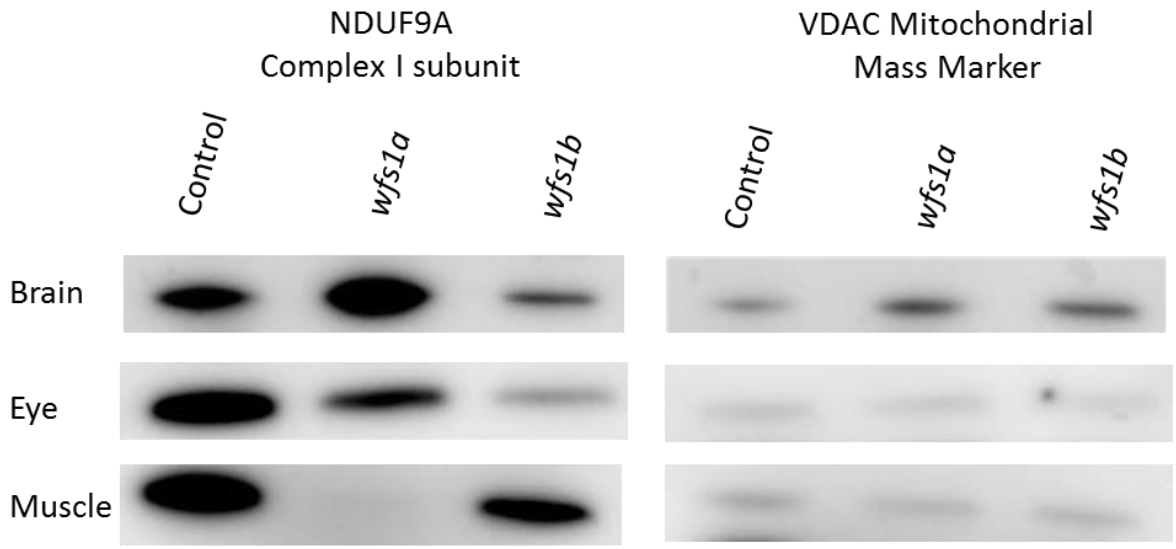

Figure 7.9 Complex I protein levels in adult tissue specific zebrafish lysates. NDUF9A and VDAC Western blots of control *wfs1a* and *wfs1b* knockout tissue zebrafish lysates from dissected brains, eyes and muscles.

The densities were quantified in imagej and normalised to VDAC for a mitochondrial loading control. When quantified, changes in the eye and the increase NDUF9A levels in the *wfs1a* knockout brain were not significant.

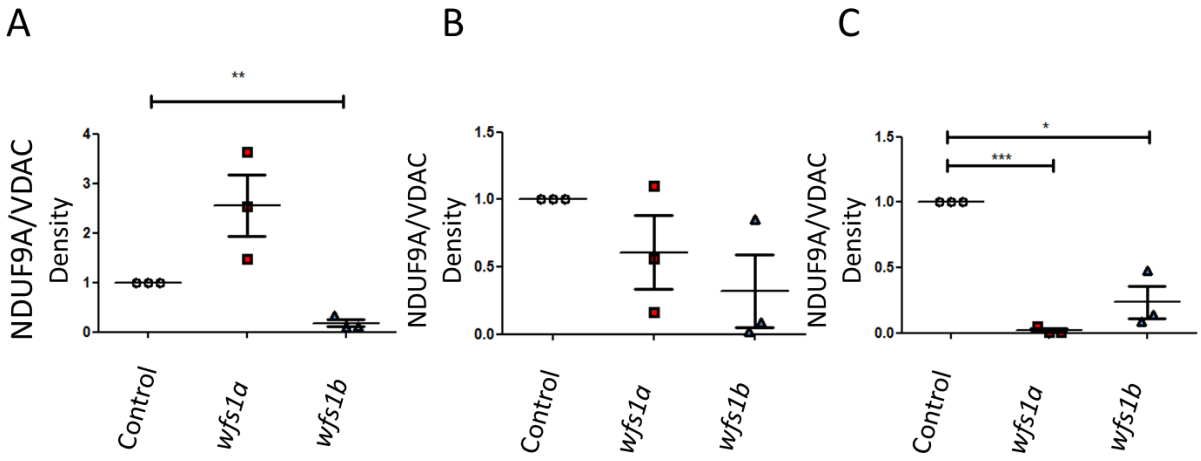

Figure 7.10 Quantification of density normalised to VDAC as a mitochondrial loading control. A: Brain Complex I/VDAC density. B: Eye Complex I/VDAC density. C: Muscle Complex I/VDAC density. Statistics: Paired t-test *p<0.05 and **p<0.01 Graphs plotted ± SEM

The other OXPHOS complexes were looked at to determine if this change was specific only to complex I, or if in general mitochondrial complexes were affected. In the brain and muscle it appeared this was only specific to complex 1. In *wfs1* knockouts NDUF9A was increased in

the brain and reduced in the muscle, while *wfs1b* was reduced in both. In the eye it appears VDAC expression may be effected causing a reduction in the other complexes in both *wfs1* knockouts.

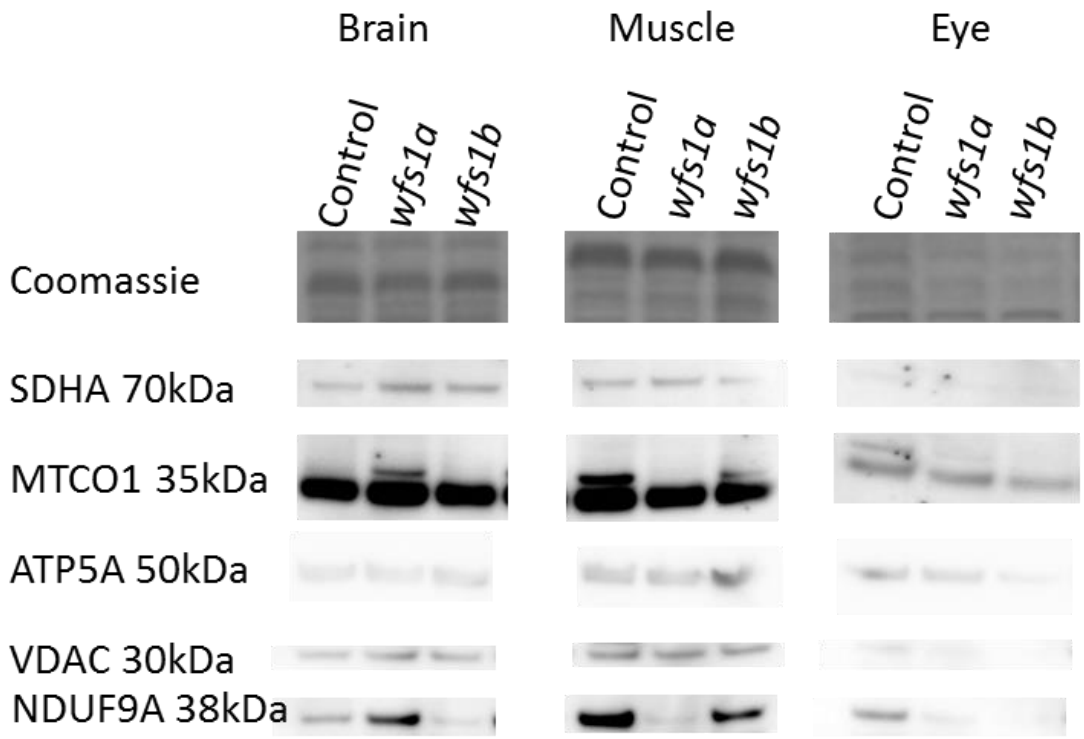

Figure 7.11 Western Blots of Adult Tissue Mitochondrial Complexes I, II, IV, V and VDAC. Coomassie for equal loading, SDHA (complex II), MTCO1 (complex IV), ATP5A (complex V) VDAC (mitochondrial loading control) and NDUF9A (complex I). Brain muscle and eye tissue dissected from adult zebrafish.

7.6 Native Page Gels

Native page gels were used to assess the integrity of the complex I structure. As observed from the previous blots less NDUF9A could be observed in the isolated mitochondria of *wfs1* knockouts. Mitochondria were isolated from zebrafish embryos by differential centrifugation and digitonin solubilisation.

The knockout *wfs1* isolated mitochondria had lower levels of NDUF9A detected in the higher molecular weight bands. This was observed at both 24 and 48hpf in the developing embryo.

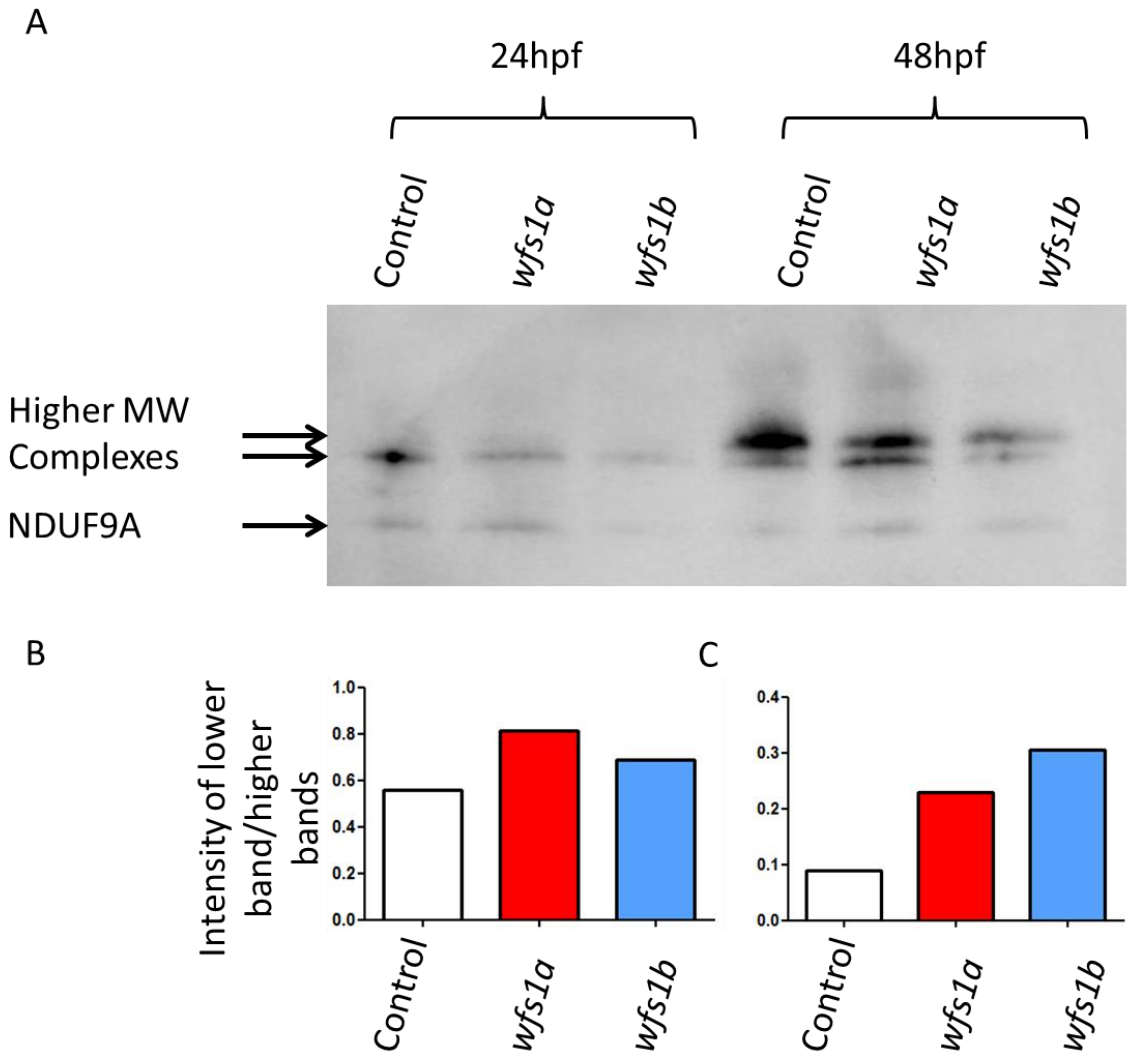

Figure 7.12 Blue Native PAGE Complex I Western Blots. A: BN-PAGE Western Blot of isolated mitochondria were isolated from zebrafish at 24hpf an 48hpf. Isolated mitochondria were run on a BN-PAGE. Complex I detected using NDUF9A antibody. B: Ratio of lower band/higher bands at 24hpf. C:Ratio of lower band/higher bands at 48hpf. Density determined on imagej for each band and ratios calculated n=1.

7.7 Mitochondrial Ca^{2+}

To determine if any changes in mitochondrial Ca^{2+} homeostasis could be observed, mitochondria were isolated from adult muscle tissue and Ca^{2+} uptake measured. Mitochondria Ca^{2+} uptake was measured in isolated mitochondria. 20µM $CaCl_2$ was added to 50µg of isolated mitochondria in an Oregon green dye which fluoresces when bound to Ca^{2+}. Oregon Green is cell impermeable so cannot enter the mitochondria therefore changes in this fluorescence originates from a loss of available Ca^{2+}. The results were plotted on the graph in Figure 7.14

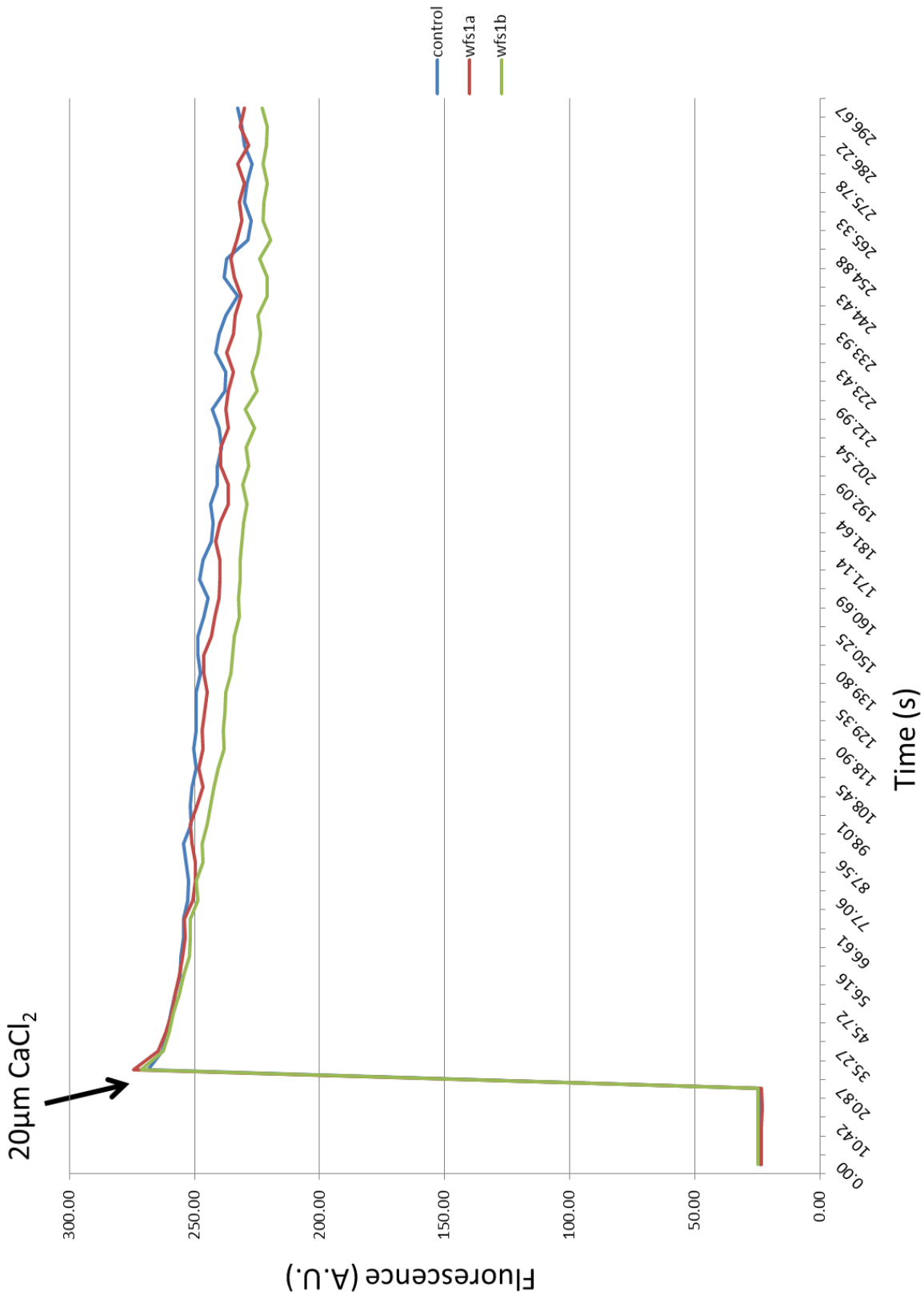

Figure 7.13 Isolated Mitochondria Ca^{2+} Uptake. 20µM $CaCl_2$ was added to 50µg isolated muscle tissue mitochondria and the reduction of flourescence over 5 minutes represents uptake of Ca^{2+}.

The difference in fluorescent units from $CaCl_2$ injection to the end of recording was plotted and the rate of change calculated and plotted. Although both *wfs1a* and *wfs1b* knockouts had increased levels of Ca^{2+} uptake these were both non-significant.

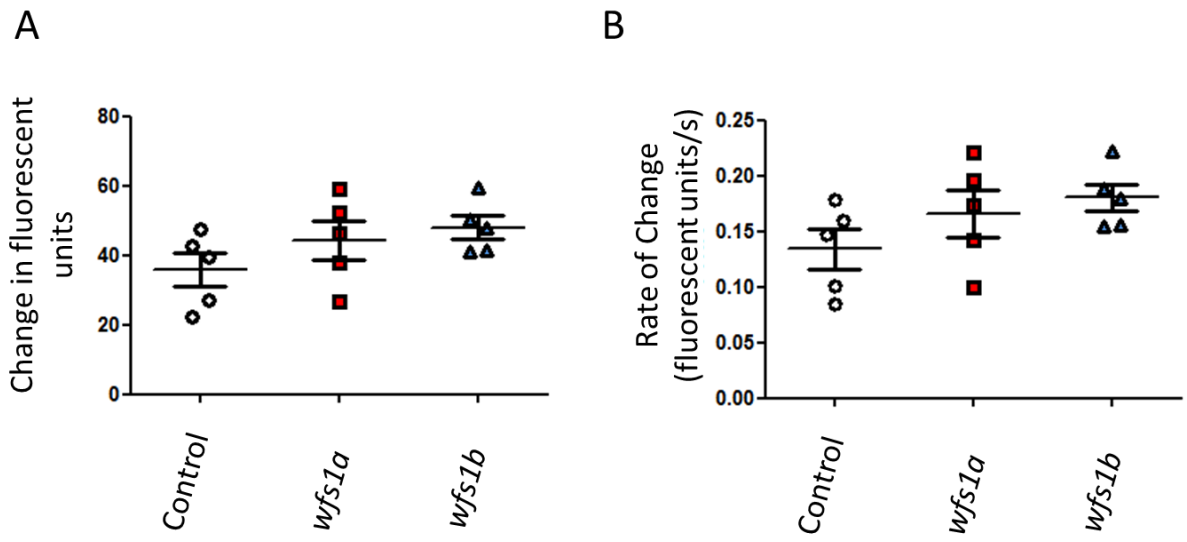

Figure 7.14 Quantification of Isolated Mitochondria Ca^{2+} Uptake. A: Differences in Flourescence of Oregon Green when 20µM $CaCl_2$ is added to the end of 5 minute period. B: Rate of change (Change over time). Graphs plotted mean ± SEM.

7.8 Discussion

The role of mitochondria in WS is not well understood. Using the zebrafish knockouts of *wfs1,* mitochondrial function was assessed to determine if it was involved in development of WS.

Mitochondrial trafficking was affected in *wfs1* knockouts. This is something that has been observed in cultured rat neurons before but not *in vivo* (Cagalinec *et al.*, 2016). The results confirmed mitochondrial dynamics were altered with distance of runs being lower in both knockouts and the cultured neurons described in Cagalinec *et al*.. Velocity was also decreased in culture which was observed in *wfs1a* knockouts. An increase in changes of direction was another change in culture which was replicated in the *wfs1b* knockouts. There is a difference between the zebrafish and the isolated cells, in the percentage of time the mitochondria spend moving. In culture ~40% mitochondria are motile for both control cells, control zebrafish and knockdown cells but, in *wfs1b* knockout zebrafish we see a significant increase in movement with *wfs1b* knockout mitochondria moving 20% more than controls. Changes in mitochondrial transport could be caused by changes in the cytosolic Ca^{2+} binding to the Miro/Milton complex.

Although slight changes in the difference between the results, the zebrafish and the shRNA silenced mouse neurons systems appear comparable (Cagalinec *et al.*, 2016). This was further demonstrated by the loss of ATP production which was downregulated in cultured neurons (by ATP assay) was also observed in the oxygen consumption measurement of the knockout zebrafish. However, by using the mitochondrial stress test we were also able to determine the *wfs1b* knockout zebrafish had significantly lower basal respiration without a change in the non-mitochondrial respiration. This suggests that the defect is in fact mitochondrial rather than glycolytic. A significant reduction in max respiration and spare respiratory capacity were also observed. Spare respiratory capacity changes are able to suggest if the fish are close to a bioenergetic limit (Brand and Nicholls, 2011). As spare respiratory capacity is lower in *wfs1b* knockout fish it is likely the variable high energy tissue such as neurons would be more severely affected (Brand and Nicholls, 2011). The smaller neurons in the optic nerve are the first to die off in WS. This is due to the large energetic demand in these axons paired with a relatively low energetic potential (Pan *et al.*, 2012; Ross-Cisneros *et al.*, 2013). A reduction in spare respiratory capacity would explain the predominant loss of these neurons during OA. This change in spare respiratory capacity

helps to explain the changes in early neuronal development. At early time points of neuronal development mitochondria operate very close to their max respiration with hardly any spare respiratory capacity (Agostini *et al.*, 2016). This could explain why neuronal development is delayed in the *wfs1b* model at early time points. In order to understand what was driving the respiratory changes in *wfs1b* knockouts the change in mtDNA was examined.

This was to determine if any changes in mitochondrial biogenesis could be found in *wfs1* knockouts. No significant differences were detected in *wfs1* knockout zebrafish; a very minor non-significant rise in copy number was detected in *wfs1b* knockouts. In LHON significantly higher numbers of mtDNA have been detected to act as a compensatory mechanism for changes in complex I (Giordano *et al.*, 2014). To determine if complex I changes could be observed, Western blots for the NDUF9A subunit of complex I levels were performed at 48hpf. When adjusted to account for VDAC expression complex I is downregulated in both *wfs1* knockouts and more severely in *wfs1b*. Finding a reduction in *wfs1a* knockouts was unexpected as it did not appear to affect the results from the oxygen consumption measurement, although the *wfs1a* results had a higher SEM than control zebrafish so a possible difference may be detected with higher n numbers. It is also possible that complex I is not the rate limiting step in this reaction meaning a slight reduction may not affect the max respiration.

As heat shocking the zebrafish showed changes in the death rate of *wfs1* knockout zebrafish the OXPHOS subunits were observed to determine if mitochondrial dysfunction had a role in this. After heat shocking *wfs1a* complex I levels appeared to fall although no changes were determined in controls and *wfs1b* knockouts. VDAC was also hard to detect so equal mitochondrial loading was not confirmed, even if the Coomassie staining determined equal protein loading. ATP5A for complex V had no changes between knockouts or heat shocked embryos. The UPR and mitochondrial function are closely linked with PERK playing an important role in mitochondrial function and ER-mitochondria interactions (Verfaillie *et al.*, 2012). ATF6 is also associated with changes in mitochondrial ultrastructure suggesting a possible link between the ER stress response and mitochondrial function (Wang *et al.*, 2018).

As the VDAC expression was difficult to detect it is hard to determine the overall effect heat shock had on the mitochondria. Electron Microscopy would be able to determine changes in ER-mitochondria contacts and ultrastructure changes. However, an interesting change was

complex I levels in *wfs1a* knockouts at 7hpf being higher than controls, when at 48hpf it was lower. It may be due to tissue specificity described in Chapter V that highlighted the muscular expression of *wfs1a*. The first post mitotic cells that will go on to develop axial somite-derived muscles can be defined at the 90%-epiboly stage (9hpf) (Kimmel *et al.*, 1995) which would explain why we do not observed this knockdown of NDUF9A at the earlier time point. This was further tested in isolated adult tissues.

Adult zebrafish were euthanized and their tissues dissected. Using lysates from the brain, the eyes and muscle NDUF9A and VDAC expression were observed. *wfs1b* knockouts had reductions in all three tissues, although not significant in the eye. *wfs1a* had a non-significant increase of expression in the brain, slightly non-significant reduced expression in the eyes and was almost undetectable in the muscles. This was unexpected as the largest differences between the disease models and controls have been in the *wfs1b* knockout models. The differences in expression may also explain why there are no significant changes in the oxygen consumption analysis, if one tissue type is masking a defect in another. A possible way to examine this would be to perform an oxygen consumption analysis on some dissociated cells of different tissue types or their isolated mitochondria. This upregulation of complex I may be a compensatory mechanism which would be interesting to determine if this is also the case in double knockout fish. Complex I reductions in the *wfs1b* explain why a reduced max respiration and spare respiratory capacity are observed in this knockout model. This, alongside changes in mitochondrial dynamics, would explain changes in neuronal development and degeneration seen in OA.

As quite severe reductions in complex I are described in *wfs1b* knockouts and certain tissues in *wfs1a* knockouts, it would be expected to see rather severe phenotypes. As mentioned previously a complex III feeding, suggests zebrafish can bypass complex I and II could be the reason especially in *wfs1a* why the phenotypes are more mild than expected (Pinho *et al.*, 2013). As with the embryos it was important to determine if other mitochondrial complexes were affected. There was less VDAC in the eyes of both knockouts so all changes in the eye could be linked to a reduction in the number of mitochondria rather than specific complexes. As we have observed in both *wfs1a* and *wfs1b* knockouts a reduction in RGCs may account for a reduction in mitochondria as a relatively high energy tissue, mitochondria are important in the optic nerve and RGCs. In the brain and muscle the only obvious changes were in complex I suggesting this change is specific.

To determine if this was having any effect on super complex formation Native gels were looked at in isolated mitochondria. Ratios of the lower weight NDUF9A bands were compared to the intensity of the higher weight bands. At 24hpf the changes were more subtle but at 48hpf the difference in higher molecular weight complexes was more striking with both *wfs1* knockouts. 48hpf had a lower ratio of higher weight complexes. This is an interesting observation as supercomplexes are important in energy production making electron transfer more efficient but also playing an important role in the stability of the complexes (Vempati *et al.*, 2009; Lapuente-Brun *et al.*, 2013; Maranzana *et al.*, 2013). However it is not certain if supercomplexes are not forming due to the reduction in complex I, or the lack of supercomplexes causing a reduction in complex I.

The composition of lipids in the IMM is important in the stability of these super complexes (Pfeiffer *et al.*, 2003). The mitochondrial connection at the ER is a vital for phospholipid production (Vance, 2015). If like in *CISD2* the connection at the MAM is not as tight (Rouzier *et al.*, 2017b), this process is likely effected. To determine if this is the case EM could demonstrate if connections between two organelles are effected. Lipidomics of isolated mitochondria or a phospholipid transfer assay would allow the determination of lipid concentrations (Kojima *et al.*, 2016). This could explain a reduction in supercomplex stability which could be responsible for the complex I reduction. It could also be possible that due to the subunits of complex I assembly factors having shorter half-lives (Kim *et al.*, 2012; Karunadharma *et al.*, 2015), are more susceptible to the possible effects of ER stress such as reduced transcription. RNAseq may be able to provide answers to this.

Mitochondrial Ca^{2+} uptake was observed in isolated mitochondria. There were no significant changes in *wfs1* knockouts. However, this is consistent with what has been reported in HEK293 *WFS1* knockdown cells were mitochondrial Ca^{2+} was essentially unaltered (Takei *et al.*, 2006). Cytosolic Ca^{2+} and ER flux have been reported to be altered in other cell types (Takei *et al.*, 2006; Cagalinec *et al.*, 2016). Cytosolic Ca^{2+} is being monitored by collaborators in live zebrafish and may provide answers to the role Ca^{2+} is playing in *wfs1* knockout zebrafish (Bakayan *et al.*, 2015).

Mitochondrial transport, respiration and complex I expression are all affected in *wfs1* knockout zebrafish. *wfs1b* knockouts again have a stronger phenotype apart from in the

muscle where the expression of *wfs1a* appears more important in the expression of complex I.

7.9 Conclusions

wfs1 knockout in the zebrafish has significant effects on the function and complex I expression. Changes in trafficking of mitochondria could be observed in both *wfs1* knockouts in the lateral line of the zebrafish. Mitochondrial respiration was reduced in *wfs1b* knockouts and reductions could be seen in complex I protein in the whole larvae, the brain and the muscle. Complex I protein concentration was also reduced in the whole larvae and the muscle in *wfs1a* knockouts. The formation of supercomplexes was reduced in both wfs1 knockouts while Ca^{2+} uptake and mtDNA levels remained unchanged.

Further experiments could involve in gel activity of the complexes in native gels or spectrophotometric assays of respiratory complex activity to further determine the effect of wfs1 knockout on respiratory function. Electron microscopy could help determine any morphological differences and also determine the role of the ER and mitochondrial connection in WS. Although no changes were determined in isolated mitochondrial Ca^{2+} uptake there may still be issues with ER Ca^{2+} leak through the IP_3R or problems with ER Ca^{2+} uptake through SERCA. To begin with cytosolic Ca^{2+} levels could be examined in live zebrafish using a red-emitting aequorin variant (Bakayan *et al.*, 2015). Cytosolic changes indicate any overall homeostasis dysfunctions that could be observed in greater detail.

Chapter 8: General Discussion

The aim of this project was to characterise zebrafish models of WS to further our understanding of the role of wolframin in WS. Specifically, the zebrafish model can provide insights into mitochondrial function regulation and neuronal development; something which is difficult to achieve in other animal models.

Both morpholino mediated knockdown and transgenic genomic knockouts were used to model WS. These models of *wfs1* knockdowns/kockouts acted as useful models of WS. A morpholino screen was utilised initially to determine the effectiveness of *wfs1a* and *wfs1b* knockouts. This demonstrated early on that *wfs1b* knockouts had a more significant effect on the zebrafish in the early development. However, significant problems with the morpholino model such as possible off target effects have made researchers wary of morpholino models (Kok *et al.*, 2015). Although a number of controls were carried out including p53 rescues and CRISPANT models a number of other controls needed for validation prior to publication including RNA rescue and multiple types of morpholino (Stainier *et al.*, 2017). With the purchase of mutant knockout zebrafish lines it was determined this would not be a worthwhile route to pursue to model WS.

In comparison to the knockout models a number of the morpholino phenotypes proved to be exaggerated such as the loss of eyes, tail abnormalities and obvious cranial shape changes. This could be explained by the upregulation of compensatory mechanisms seen in mutants, which are not affected by transcript altering morpholinos (Rossi *et al.*, 2015). The *wfs1a* splice blocking morpholinos only had a small increase in severity of phenotypes with the changes from normal zebrafish being non-significant. When expression of the *wfs1a* cDNA was observed at very early stages it was not expressed and the expression was much higher in the muscles when adult tissue transcripts were observed. This explains why a *wfs1a* morpholino was less effective as morpholinos are more effective in the first few days of development. The combination of the two morpholinos was lethal. A similar pattern was also seen in *wfs1* mutant crosses where one double knockout mutant was produced which was completely infertile. The *wfs1ab* knockout as a model was not pursued further due to breeding difficulties. The single knockout models were perused further.

The single knockouts were characterised in Chapter 5 and shared a number of characteristics with WS. Changes in the unfolded protein response were observed. This is a fundamental

pathway that has been shown to be affected in WS (Fonseca *et al.*, 2005). Unfortunately another important pathway, Ca^{2+} homeostasis, was not fully characterised. Although mitochondrial Ca^{2+} was examined, cytosolic Ca^{2+} which has been shown to be affected in a number of cell types has not yet been determined (Takei *et al.*, 2006; Zatyka *et al.*, 2015). Zebrafish from the study described here have been given to collaborators to determine if cytosolic Ca^{2+} is affected but the experiments had not been completed at the time of writing (Bakayan *et al.*, 2015).

The *wfs1* zebrafish did develop a number of phenotypes similar to humans. Zebrafish were smaller and patients have also been reported to be shorter (Lugar *et al.*, 2016). Problems were seen in the ears of the zebrafish with reductions in otolith size. Anxiety and fertility were also affected with zebrafish with them moving less in isolation and producing unfertilised embryos. These are all changes that can be linked with changes seen in WS patients (Urano, 2016). The two most common symptoms of WS in patients are diabetes mellitus and optic atrophy. Diabetes mellitus was studied in less detail in this project partially due to the large focus of other models on this particular facet and the previously published morpholino model also showed a loss of β-islet cells (O'Hare *et al.*, 2016). However, fasted blood glucose was significantly lower in *wfs1b* knockout zebrafish. Diabetes mellitus can also be managed by insulin treatment while optic atrophy has no treatment at all. OA was characterised in detail in the zebrafish knockouts in Chapter 4.

The zebrafish eyes early on in development did not show any obvious changes histologically. At 4 and 12 months changes were seen histologically in the quantification of RGCs showing reductions in both *wfs1a* and *wfs1b* knockouts. Alongside this functional data from OKR showed that *wfs1b* knockout fish had a reduction of visual acuity. OCT images were also taken of the optic nerve and *wfs1b* zebrafish at 12 months had a thinner optic nerve. This is comparable to the human condition suggesting we have an accurate model of OA in *wfs1b* knockouts. Unfortunately this comes around 4 to 12 months which removes one of the major benefits of zebrafish models which is the ability to use large numbers at early time points. However, this is a better fit in retinal degeneration than the mouse model and comparable in timescale of OA onset to the rat model (Bonnet Wersinger *et al.*, 2014; Plaas *et al.*, 2017).

The development of neurons in the *wfs1* knockout fish were also affected. Neuronal outgrowth was impeded in a similar to manner as to what has been previously observed in cultured mouse neurons (Cagalinec *et al.*, 2016). Functional tests also showed impaired neuronal signalling from the touch response experiments. The changes in neuronal growth and structure could be linked to the changes in ER stress, which may be reducing transcription. This could possibly be limiting growth. Another possibility is mitochondrial dysfunction causing a delay in growth. Developing neurons function close to the bioenergetics limit, while mature neurons have a larger spare respiratory capacity (Agostini *et al.*, 2016). In *wfs1b* knockouts the spare respiratory capacity is reduced and so is the size of the neurons observed at 24hpf. This reduction in energy availability may be delaying growth.

Reductions in acetylcholine esterase activity were observed in *wfs1a* knockouts at time points 3dpf and 5dpf this was also observed in *wfs1b* knockouts (3, 4 and 5dpf). This suggests that both knockouts either have less neuronal tissue or at least a reduction of AChE activity which has a vital role in regulating neuronal signalling. This was surprising as *wfs1a* knockout zebrafish showed no functional test differences from the controls. It could be possible that *wfs1a* zebrafish begin to show symptoms later in development due to the later onset of expression of *wfs1a* while *wfs1b* is expressed from the 1 cell stage. Functional tests like the touch response are much harder to carry out at later larvae time points as they begin moving independently at 4dpf. The AChE activity in the brains of *wfs1* knockouts were also altered. The results mirrored the data from the RGC counts where reductions were initially seen in *wfs1a* at 4 months with *wfs1b* knockouts becoming more severe at 12 months. It is possible we are observing an initial developmental deficit which is either corrected at later time points or degeneration in the adult *wfs1b* tissue or a combination of the two. Zebrafish neuronal tissue is capable of regenerating (Schmidt *et al.*, 2013). As neuronal generation is a high energy process this may play a key role in the differences in any regeneration/degeneration of the two zebrafish models (Agostini *et al.*, 2016).

Mitochondrial function was altered in both *wfs1* knockout models. In *wfs1a* knockouts transport, protein expression and supercomplex formation were all significantly altered while *wfs1b* knockouts also showed respiration deficiencies. The *wfs1a* knockout zebrafish muscles show quite large changes in complex I protein levels in adult tissue while the embryos and other tissues had less drastic reductions in NDUF9A compared to *wfs1b*

knockouts. Mitochondrial respiratory chain activities were shown to be within normal ranges in patient muscle biopsies (Barrett and Bundey, 1997). However, ATP production was reduced in isolated mouse neurons which may suggest tissue specificity to these mitochondrial dysfunctions (Cagalinec *et al.*, 2016). Future work on mitochondrial dysfunction should be performed on neurons derived from Induced pluripotent stem cells derived from patient cell lines to determine if an ATP reduction is also observed. Unpublished work from our group suggests in patient fibroblasts complex I activity is decreased when measured by Oxygraph (Dr David Moore, PhD Thesis 2016). These changes could be due to the changes in supercomplex formation observed in the zebrafish embryos, determining if this is true for *WFS1* patient fibroblasts would be an interesting observation.

The majority of results throughout this study shared a common theme: the *wfs1b* knockouts appear to have more severe phenotype than the *wfs1a* knockouts. This may be due to the expression of *wfs1a* which was shown to be expressed at a later time point and predominantly in the muscle. As muscle is not one of the main types of tissue affected in WS it is no surprise this model is a milder representation of WS. It would also be interesting to see proteins or transcripts that differ between the two models to determine why the *wfs1a* model is less severe. There may be compensatory mechanisms that are causing a protective effect. RNA-Seq or proteomics may provide large unbiased comparative studies to determine this while also providing comparisons to control tissue. For future experiments it would be beneficial to focus on the *wfs1b* knockout model only.

Knockout zebrafish could also be crossed to multiple fluorescent lines GAP43:GFP zebrafish have GFP in the RGCs (Diekmann *et al.*, 2015), *ptf1a*:eGFP;insa:mCherry have fluorescent pancreatic islet cells (O'Hare *et al.*, 2016) , fluorescent neurons could provide a live time lapse of development rather than fixed time points. The mitochondrial network could be assessed in more detail in transgenic lines (Kim *et al.*, 2008). A completely pigment free zebrafish line has also been developed which would allow for in detail Ca^{2+} imaging in the zebrafish retina (Antinucci and Hindges, 2016). Crossing to transgenic lines would require significant time ~8months to produce homozygotes and a further 3-4 months for those to begin breeding.

Electron microscopy should be an avenue that is explored further, 3d EM could have provided answers to important factors such as the ER and mitochondrial contacts that have

not been explored in this project (Wu *et al.*, 2017). This is an important factor in knockout *CISD2* fibroblasts which should be explored further in WS (Rouzier *et al.*, 2017b). The ER and mitochondrial connection is essential for ER flux, fission and lipid metabolism (Rowland and Voeltz, 2012). Unfortunately fixation of the optic nerves was not adequate for this in adult zebrafish, this can be attempted again in perfusion fixed adults, different tissue or possibly larvae.

Other possible future directions from this project include drug screening. The *wfs1b* model has a number of rapidly observable differences from controls at the larval stages. Mitochondrial respiration, neuronal development/function, size and response to heat shock could all be rapidly tested. This could be tested against various drug libraries due to the high number of zebrafish embryos. Promising candidates could be trialed for longer periods on adult zebrafish to determine the response to retinal degeneration. Dantrolene and sodium valproate could be tested due to their promising results in other models (Gharanei *et al.*, 2013; Lu *et al.*, 2014). Idebenone is another candidate that has shown promising results in LHON treatment (Carelli *et al.*, 2011). It is reported that Idebenone increases the ATP production in LHON fibroblasts, as maximum respiration of *wfs1b* zebrafish was reduced this could be a promising therapy (Yu-Wai-Man *et al.*, 2017).

In summary two models of WS have been characterised in this thesis. The model of *wfs1b* appears more severe than the *wfs1a* knockout. The *wfs1b* model more accurately models the important OA phenotype seen in WS. Overall the *wfs1b* model appears to be a better phenocopy of WS and testing of therapeutic compounds could be trialed on this line. Mitochondrial dysfunction was observed in this model including trafficking, complex I dysfunction and reductions in respiratory function. The insight gained into the function of mitochondria in WS can help further our understanding of the mechanisms of the disease in patients.

References

Abrahams, J.P., Leslie, A.G., Lutter, R. and Walker, J.E. (1994) 'Structure at 2.8 A resolution of F1-ATPase from bovine heart mitochondria', *Nature*, 370(6491), pp. 621-8.

Agostini, M., Romeo, F., Inoue, S., Niklison-Chirou, M.V., Elia, A.J., Dinsdale, D., Morone, N., Knight, R.A., Mak, T.W. and Melino, G. (2016) 'Metabolic reprogramming during neuronal differentiation', *Cell Death Differ*, 23(9), pp. 1502-14.

Amr, S., Heisey, C., Zhang, M., Xia, X.J., Shows, K.H., Ajlouni, K., Pandya, A., Satin, L.S., El-Shanti, H. and Shiang, R. (2007) 'A homozygous mutation in a novel zinc-finger protein, ERIS, is responsible for Wolfram syndrome 2', *Am J Hum Genet*, 81(4), pp. 673-83.

Andrews, R.M., Kubacka, I., Chinnery, P.F., Lightowlers, R.N., Turnbull, D.M. and Howell, N. (1999) 'Reanalysis and revision of the Cambridge reference sequence for human mitochondrial DNA', *Nat Genet*, 23(2), p. 147.

Antinucci, P. and Hindges, R. (2016) 'A crystal-clear zebrafish for in vivo imaging', *Sci Rep*, 6, p. 29490.

Applebury, M.L., Antoch, M.P., Baxter, L.C., Chun, L.L., Falk, J.D., Farhangfar, F., Kage, K., Krzystolik, M.G., Lyass, L.A. and Robbins, J.T. (2000) 'The murine cone photoreceptor: a single cone type expresses both S and M opsins with retinal spatial patterning', *Neuron*, 27(3), pp. 513-23.

Bagur, R. and Hajnoczky, G. (2017) 'Intracellular Ca(2+) Sensing: Its Role in Calcium Homeostasis and Signaling', *Mol Cell*, 66(6), pp. 780-788.

Bakayan, A., Domingo, B., Miyawaki, A. and Llopis, J. (2015) 'Imaging Ca(2+) activity in mammalian cells and zebrafish with a novel red-emitting aequorin variant', *Pflugers Arch*, 467(9), pp. 2031-42.

Ban, T., Ishihara, T., Kohno, H., Saita, S., Ichimura, A., Maenaka, K., Oka, T., Mihara, K. and Ishihara, N. (2017) 'Molecular basis of selective mitochondrial fusion by heterotypic action between OPA1 and cardiolipin', *Nat Cell Biol*, 19(7), pp. 856-863.

Baraban, S.C. (2013) 'Forebrain electrophysiological recording in larval zebrafish', *J Vis Exp*, (71).

Barkovich, A.J., Millen, K.J. and Dobyns, W.B. (2009) 'A developmental and genetic classification for midbrain-hindbrain malformations', *Brain*, 132(Pt 12), pp. 3199-230.

Barrett, T.G. and Bundey, S.E. (1997) 'Wolfram (DIDMOAD) syndrome', *J Med Genet*, 34(10), pp. 838-41.

Barrett, T.G., Bundey, S.E., Fielder, A.R. and Good, P.A. (1997) 'Optic atrophy in Wolfram (DIDMOAD) syndrome', *Eye (Lond)*, 11 (Pt 6), pp. 882-8.

Barrett, T.G., Bundey, S.E. and Macleod, A.F. (1995) 'Neurodegeneration and diabetes: UK nationwide study of Wolfram (DIDMOAD) syndrome', *Lancet*, 346(8988), pp. 1458-63.

Barrett, T.G., Scott-Brown, M., Seller, A., Bednarz, A., Poulton, K. and Poulton, J. (2000) 'The mitochondrial genome in Wolfram syndrome', *J Med Genet*, 37(6), pp. 463-6.

Barrientos, A., Volpini, V., Casademont, J., Genis, D., Manzanares, J.M., Ferrer, I., Corral, J., Cardellach, F., Urbano-Marquez, A., Estivill, X. and Nunes, V. (1996) 'A nuclear defect in the 4p16 region predisposes to multiple mitochondrial DNA deletions in families with Wolfram syndrome', *J Clin Invest*, 97(7), pp. 1570-6.

Behra, M., Cousin, X., Bertrand, C., Vonesch, J.L., Biellmann, D., Chatonnet, A. and Strahle, U. (2002) 'Acetylcholinesterase is required for neuronal and muscular development in the zebrafish embryo', *Nat Neurosci*, 5(2), pp. 111-8.

Berridge, M.J., Bootman, M.D. and Roderick, H.L. (2003) 'Calcium signalling: dynamics, homeostasis and remodelling', *Nat Rev Mol Cell Biol*, 4(7), pp. 517-29.

Berry, V., Gregory-Evans, C., Emmett, W., Waseem, N., Raby, J., Prescott, D., Moore, A.T. and Bhattacharya, S.S. (2013) 'Wolfram gene (WFS1) mutation causes autosomal dominant congenital nuclear cataract in humans', *Eur J Hum Genet*, 21(12), pp. 1356-60.
Bertolotti, A., Zhang, Y., Hendershot, L.M., Harding, H.P. and Ron, D. (2000) 'Dynamic interaction of BiP and ER stress transducers in the unfolded-protein response', *Nat Cell Biol*, 2(6), pp. 326-32.
Bertrand, C., Chatonnet, A., Takke, C., Yan, Y.L., Postlethwait, J., Toutant, J.P. and Cousin, X. (2001) 'Zebrafish acetylcholinesterase is encoded by a single gene localized on linkage group 7. Gene structure and polymorphism; molecular forms and expression pattern during development', *J Biol Chem*, 276(1), pp. 464-74.
Bestman, J.E., Stackley, K.D., Rahn, J.J., Williamson, T.J. and Chan, S.S. (2015) 'The cellular and molecular progression of mitochondrial dysfunction induced by 2,4-dinitrophenol in developing zebrafish embryos', *Differentiation*, 89(3-4), pp. 51-69.
Bezawork-Geleta, A., Rohlena, J., Dong, L., Pacak, K. and Neuzil, J. (2017) 'Mitochondrial Complex II: At the Crossroads', *Trends Biochem Sci*, 42(4), pp. 312-325.
Bill, B.R., Petzold, A.M., Clark, K.J., Schimmenti, L.A. and Ekker, S.C. (2009) 'A primer for morpholino use in zebrafish', *Zebrafish*, 6(1), pp. 69-77.
Bollimuntha, S., Pani, B. and Singh, B.B. (2017) 'Neurological and Motor Disorders: Neuronal Store-Operated Ca(2+) Signaling: An Overview and Its Function', *Adv Exp Med Biol*, 993, pp. 535-556.
Bonnet Wersinger, D., Benkafadar, N., Jagodzinska, J., Hamel, C., Tanizawa, Y., Lenaers, G. and Delettre, C. (2014) 'Impairment of visual function and retinal ER stress activation in Wfs1-deficient mice', *PLoS One*, 9(5), p. e97222.
Bradford, Y.M., Toro, S., Ramachandran, S., Ruzicka, L., Howe, D.G., Eagle, A., Kalita, P., Martin, R., Taylor Moxon, S.A., Schaper, K. and Westerfield, M. (2017) 'Zebrafish Models of Human Disease: Gaining Insight into Human Disease at ZFIN', *ILAR J*, 58(1), pp. 4-16.
Brand, M.D. and Nicholls, D.G. (2011) 'Assessing mitochondrial dysfunction in cells', *Biochem J*, 435(2), pp. 297-312.
Bravo, R., Parra, V., Gatica, D., Rodriguez, A.E., Torrealba, N., Paredes, F., Wang, Z.V., Zorzano, A., Hill, J.A., Jaimovich, E., Quest, A.F. and Lavandero, S. (2013) 'Endoplasmic reticulum and the unfolded protein response: dynamics and metabolic integration', *Int Rev Cell Mol Biol*, 301, pp. 215-90.
Broughton, R.E., Milam, J.E. and Roe, B.A. (2001) 'The complete sequence of the zebrafish (Danio rerio) mitochondrial genome and evolutionary patterns in vertebrate mitochondrial DNA', *Genome Res*, 11(11), pp. 1958-67.
Bu, X. and Rotter, J.I. (1993) 'Wolfram syndrome: a mitochondrial-mediated disorder?', *Lancet*, 342(8871), pp. 598-600.
Cagalinec, M., Liiv, M., Hodurova, Z., Hickey, M.A., Vaarmann, A., Mandel, M., Zeb, A., Choubey, V., Kuum, M., Safiulina, D., Vasar, E., Veksler, V. and Kaasik, A. (2016) 'Role of Mitochondrial Dynamics in Neuronal Development: Mechanism for Wolfram Syndrome', *PLoS Biol*, 14(7), p. e1002511.
Cameron, D.J., Rassamdana, F., Tam, P., Dang, K., Yanez, C., Ghaemmaghami, S. and Dehkordi, M.I. (2013) 'The optokinetic response as a quantitative measure of visual acuity in zebrafish', *J Vis Exp*, (80).
Carelli, V., La Morgia, C., Valentino, M.L., Rizzo, G., Carbonelli, M., De Negri, A.M., Sadun, F., Carta, A., Guerriero, S., Simonelli, F., Sadun, A.A., Aggarwal, D., Liguori, R., Avoni, P., Baruzzi, A., Zeviani, M., Montagna, P. and Barboni, P. (2011) 'Idebenone treatment in Leber's hereditary optic neuropathy', *Brain*, 134(Pt 9), p. e188.

Chakrabarti, R., Ji, W.K., Stan, R.V., de Juan Sanz, J., Ryan, T.A. and Higgs, H.N. (2018) 'INF2-mediated actin polymerization at the ER stimulates mitochondrial calcium uptake, inner membrane constriction, and division', *J Cell Biol*, 217(1), pp. 251-268.
Chen, H., Chomyn, A. and Chan, D.C. (2005) 'Disruption of fusion results in mitochondrial heterogeneity and dysfunction', *J Biol Chem*, 280(28), pp. 26185-92.
Chen, Y.F., Kao, C.H., Chen, Y.T., Wang, C.H., Wu, C.Y., Tsai, C.Y., Liu, F.C., Yang, C.W., Wei, Y.H., Hsu, M.T., Tsai, S.F. and Tsai, T.F. (2009) 'Cisd2 deficiency drives premature aging and causes mitochondria-mediated defects in mice', *Genes Dev*, 23(10), pp. 1183-94.
Chhetri, J., Jacobson, G. and Gueven, N. (2014a) 'Zebrafish--on the move towards ophthalmological research', *Eye (Lond)*, 28(4), pp. 367-80.
Chhetri, J., Jacobson, G. and Gueven, N. (2014b) 'Zebrafish—on the move towards ophthalmological research', *Eye*, 28(4), pp. 367-380.
Chinnery, P.F. and Hudson, G. (2013) 'Mitochondrial genetics', *Br Med Bull*, 106, pp. 135-59.
Chrispell, J.D., Rebrik, T.I. and Weiss, E.R. (2015) 'Electroretinogram analysis of the visual response in zebrafish larvae', *J Vis Exp*, (97).
Claessen, J.H., Kundrat, L. and Ploegh, H.L. (2012) 'Protein quality control in the ER: balancing the ubiquitin checkbook', *Trends Cell Biol*, 22(1), pp. 22-32.
Collins, T.J., Lipp, P., Berridge, M.J. and Bootman, M.D. (2001) 'Mitochondrial Ca(2+) uptake depends on the spatial and temporal profile of cytosolic Ca(2+) signals', *J Biol Chem*, 276(28), pp. 26411-20.
Conlan, A.R., Axelrod, H.L., Cohen, A.E., Abresch, E.C., Zuris, J., Yee, D., Nechushtai, R., Jennings, P.A. and Paddock, M.L. (2009) 'Crystal structure of Miner1: The redox-active 2Fe-2S protein causative in Wolfram Syndrome 2', *J Mol Biol*, 392(1), pp. 143-53.
Csordas, G., Renken, C., Varnai, P., Walter, L., Weaver, D., Buttle, K.F., Balla, T., Mannella, C.A. and Hajnoczky, G. (2006) 'Structural and functional features and significance of the physical linkage between ER and mitochondria', *J Cell Biol*, 174(7), pp. 915-21.
Cullinan, S.B., Zhang, D., Hannink, M., Arvisais, E., Kaufman, R.J. and Diehl, J.A. (2003) 'Nrf2 is a direct PERK substrate and effector of PERK-dependent cell survival', *Mol Cell Biol*, 23(20), pp. 7198-209.
Davies, K.M., Blum, T.B. and Kuhlbrandt, W. (2018) 'Conserved in situ arrangement of complex I and III2 in mitochondrial respiratory chain supercomplexes of mammals, yeast, and plants', *Proc Natl Acad Sci U S A*, 115(12), pp. 3024-3029.
De Falco, M., Manente, L., Lucariello, A., Baldi, G., Fiore, P., Laforgia, V., Baldi, A., Iannaccone, A. and De Luca, A. (2012) 'Localization and distribution of wolframin in human tissues', *Front Biosci (Elite Ed)*, 4, pp. 1986-98.
de Heredia, M.L., Cleries, R. and Nunes, V. (2013) 'Genotypic classification of patients with Wolfram syndrome: insights into the natural history of the disease and correlation with phenotype', *Genet Med*, 15(7), pp. 497-506.
Debattisti, V., Gerencser, A.A., Saotome, M., Das, S. and Hajnoczky, G. (2017) 'ROS Control Mitochondrial Motility through p38 and the Motor Adaptor Miro/Trak', *Cell Rep*, 21(6), pp. 1667-1680.
Diamond, J.S. (2017) 'Inhibitory Interneurons in the Retina: Types, Circuitry, and Function', *Annu Rev Vis Sci*, 3, pp. 1-24.
Diekmann, H., Kalbhen, P. and Fischer, D. (2015) 'Characterization of optic nerve regeneration using transgenic zebrafish', *Front Cell Neurosci*, 9, p. 118.
Doyon, Y., McCammon, J.M., Miller, J.C., Faraji, F., Ngo, C., Katibah, G.E., Amora, R., Hocking, T.D., Zhang, L., Rebar, E.J., Gregory, P.D., Urnov, F.D. and Amacher, S.L. (2008) 'Heritable targeted gene disruption in zebrafish using designed zinc-finger nucleases', *Nat Biotechnol*, 26(6), pp. 702-8.

Dukanovic, J. and Rapaport, D. (2011) 'Multiple pathways in the integration of proteins into the mitochondrial outer membrane', *Biochim Biophys Acta*, 1808(3), pp. 971-80.
Dukes, A.A., Bai, Q., Van Laar, V.S., Zhou, Y., Ilin, V., David, C.N., Agim, Z.S., Bonkowsky, J.L., Cannon, J.R., Watkins, S.C., Croix, C.M., Burton, E.A. and Berman, S.B. (2016) 'Live imaging of mitochondrial dynamics in CNS dopaminergic neurons in vivo demonstrates early reversal of mitochondrial transport following MPP(+) exposure', *Neurobiol Dis*, 95, pp. 238-49.
Eames, S.C., Philipson, L.H., Prince, V.E. and Kinkel, M.D. (2010) 'Blood sugar measurement in zebrafish reveals dynamics of glucose homeostasis', *Zebrafish*, 7(2), pp. 205-13.
Egan, R.J., Bergner, C.L., Hart, P.C., Cachat, J.M., Canavello, P.R., Elegante, M.F., Elkhayat, S.I., Bartels, B.K., Tien, A.K., Tien, D.H., Mohnot, S., Beeson, E., Glasgow, E., Amri, H., Zukowska, Z. and Kalueff, A.V. (2009) 'Understanding behavioral and physiological phenotypes of stress and anxiety in zebrafish', *Behav Brain Res*, 205(1), pp. 38-44.
Eisen, J.S. (1996) 'Zebrafish make a big splash', *Cell*, 87(6), pp. 969-77.
Eisen, J.S. and Smith, J.C. (2008) 'Controlling morpholino experiments: don't stop making antisense', *Development*, 135(10), pp. 1735-43.
El-Shanti, H., Lidral, A.C., Jarrah, N., Druhan, L. and Ajlouni, K. (2000) 'Homozygosity mapping identifies an additional locus for Wolfram syndrome on chromosome 4q', *Am J Hum Genet*, 66(4), pp. 1229-36.
English, A.R. and Voeltz, G.K. (2013) 'Endoplasmic reticulum structure and interconnections with other organelles', *Cold Spring Harb Perspect Biol*, 5(4), p. a013227.
Farmer, T., Naslavsky, N. and Caplan, S. (2018) 'Tying trafficking to fusion and fission at the mighty mitochondria', *Traffic*, 19(8), pp. 569-577.
Fawcett, T.W., Martindale, J.L., Guyton, K.Z., Hai, T. and Holbrook, N.J. (1999) 'Complexes containing activating transcription factor (ATF)/cAMP-responsive-element-binding protein (CREB) interact with the CCAAT/enhancer-binding protein (C/EBP)-ATF composite site to regulate Gadd153 expression during the stress response', *Biochem J*, 339 (Pt 1), pp. 135-41.
Fleisch, V.C. and Neuhauss, S.C. (2006) 'Visual behavior in zebrafish', *Zebrafish*, 3(2), pp. 191-201.
Flinn, L., Mortiboys, H., Volkmann, K., Koster, R.W., Ingham, P.W. and Bandmann, O. (2009) 'Complex I deficiency and dopaminergic neuronal cell loss in parkin-deficient zebrafish (Danio rerio)', *Brain*, 132(Pt 6), pp. 1613-23.
Fonseca, S.G., Fukuma, M., Lipson, K.L., Nguyen, L.X., Allen, J.R., Oka, Y. and Urano, F. (2005) 'WFS1 is a novel component of the unfolded protein response and maintains homeostasis of the endoplasmic reticulum in pancreatic beta-cells', *J Biol Chem*, 280(47), pp. 39609-15.
Fonseca, S.G., Ishigaki, S., Oslowski, C.M., Lu, S., Lipson, K.L., Ghosh, R., Hayashi, E., Ishihara, H., Oka, Y., Permutt, M.A. and Urano, F. (2010) 'Wolfram syndrome 1 gene negatively regulates ER stress signaling in rodent and human cells', *J Clin Invest*, 120(3), pp. 744-55.
Franke, W.W. and Kartenbeck, J. (1971) 'Outer mitochondrial membrane continuous with endoplasmic reticulum', *Protoplasma*, 73(1), pp. 35-41.
Fransson, S., Ruusala, A. and Aspenstrom, P. (2006) 'The atypical Rho GTPases Miro-1 and Miro-2 have essential roles in mitochondrial trafficking', *Biochem Biophys Res Commun*, 344(2), pp. 500-10.
Friedman, J.R., Lackner, L.L., West, M., DiBenedetto, J.R., Nunnari, J. and Voeltz, G.K. (2011) 'ER tubules mark sites of mitochondrial division', *Science*, 334(6054), pp. 358-62.
Fukuoka, H., Kanda, Y., Ohta, S. and Usami, S. (2007) 'Mutations in the WFS1 gene are a frequent cause of autosomal dominant nonsyndromic low-frequency hearing loss in Japanese', *J Hum Genet*, 52(6), pp. 510-5.

Gerhard, G.S., Kauffman, E.J., Wang, X., Stewart, R., Moore, J.L., Kasales, C.J., Demidenko, E. and Cheng, K.C. (2002) 'Life spans and senescent phenotypes in two strains of Zebrafish (Danio rerio)', *Exp Gerontol*, 37(8-9), pp. 1055-68.
Gharanei, S., Zatyka, M., Astuti, D., Fenton, J., Sik, A., Nagy, Z. and Barrett, T.G. (2013) 'Vacuolar-type H+-ATPase V1A subunit is a molecular partner of Wolfram syndrome 1 (WFS1) protein, which regulates its expression and stability', *Hum Mol Genet*, 22(2), pp. 203-17.
Giordano, C., Iommarini, L., Giordano, L., Maresca, A., Pisano, A., Valentino, M.L., Caporali, L., Liguori, R., Deceglie, S., Roberti, M., Fanelli, F., Fracasso, F., Ross-Cisneros, F.N., D'Adamo, P., Hudson, G., Pyle, A., Yu-Wai-Man, P., Chinnery, P.F., Zeviani, M., Salomao, S.R., Berezovsky, A., Belfort, R., Jr., Ventura, D.F., Moraes, M., Moraes Filho, M., Barboni, P., Sadun, F., De Negri, A., Sadun, A.A., Tancredi, A., Mancini, M., d'Amati, G., Loguercio Polosa, P., Cantatore, P. and Carelli, V. (2014) 'Efficient mitochondrial biogenesis drives incomplete penetrance in Leber's hereditary optic neuropathy', *Brain*, 137(Pt 2), pp. 335-53.
Gomes, L.C., Di Benedetto, G. and Scorrano, L. (2011) 'During autophagy mitochondria elongate, are spared from degradation and sustain cell viability', *Nat Cell Biol*, 13(5), pp. 589-98.
Grosse Aldenhovel, H.B., Gallenkamp, U. and Sulemana, C.A. (1991) 'Juvenile onset diabetes mellitus, central diabetes insipidus and optic atrophy (Wolfram syndrome)--neurological findings and prognostic implications', *Neuropediatrics*, 22(2), pp. 103-6.
Haghighi, A., Haghighi, A., Setoodeh, A., Saleh-Gohari, N., Astuti, D. and Barrett, T.G. (2013) 'Identification of homozygous WFS1 mutations (p.Asp211Asn, p.Gln486*) causing severe Wolfram syndrome and first report of male fertility', *Eur J Hum Genet*, 21(3), pp. 347-51.
Halperin, L., Jung, J. and Michalak, M. (2014) 'The many functions of the endoplasmic reticulum chaperones and folding enzymes', *IUBMB Life*, 66(5), pp. 318-26.
Harding, H.P., Zhang, Y., Bertolotti, A., Zeng, H. and Ron, D. (2000) 'Perk is essential for translational regulation and cell survival during the unfolded protein response', *Mol Cell*, 5(5), pp. 897-904.
Hartline, D.K. (2008) 'What is myelin?', *Neuron Glia Biol*, 4(2), pp. 153-63.
Hatanaka, M., Tanabe, K., Yanai, A., Ohta, Y., Kondo, M., Akiyama, M., Shinoda, K., Oka, Y. and Tanizawa, Y. (2011) 'Wolfram syndrome 1 gene (WFS1) product localizes to secretory granules and determines granule acidification in pancreatic beta-cells', *Hum Mol Genet*, 20(7), pp. 1274-84.
Head, B., Griparic, L., Amiri, M., Gandre-Babbe, S. and van der Bliek, A.M. (2009) 'Inducible proteolytic inactivation of OPA1 mediated by the OMA1 protease in mammalian cells', *J Cell Biol*, 187(7), pp. 959-66.
Hershey, T., Lugar, H.M., Shimony, J.S., Rutlin, J., Koller, J.M., Perantie, D.C., Paciorkowski, A.R., Eisenstein, S.A., Permutt, M.A. and Washington University Wolfram Study, G. (2012) 'Early brain vulnerability in Wolfram syndrome', *PLoS One*, 7(7), p. e40604.
Hetzer, M.W., Walther, T.C. and Mattaj, I.W. (2005) 'Pushing the envelope: structure, function, and dynamics of the nuclear periphery', *Annu Rev Cell Dev Biol*, 21, pp. 347-80.
Hilson, J.B., Merchant, S.N., Adams, J.C. and Joseph, J.T. (2009) 'Wolfram syndrome: a clinicopathologic correlation', *Acta Neuropathol*, 118(3), pp. 415-28.
Hirst, J. (2013) 'Mitochondrial complex I', *Annu Rev Biochem*, 82, pp. 551-75.
Hirst, J., King, M.S. and Pryde, K.R. (2008) 'The production of reactive oxygen species by complex I', *Biochem Soc Trans*, 36(Pt 5), pp. 976-80.
Hoekel, J., Chisholm, S.A., Al-Lozi, A., Hershey, T., Tychsen, L. and Washington University Wolfram Study, G. (2014) 'Ophthalmologic correlates of disease severity in children and adolescents with Wolfram syndrome', *J AAPOS*, 18(5), pp. 461-465 e1.

Hofmann, S., Philbrook, C., Gerbitz, K.D. and Bauer, M.F. (2003) 'Wolfram syndrome: structural and functional analyses of mutant and wild-type wolframin, the WFS1 gene product', *Hum Mol Genet*, 12(16), pp. 2003-12.
Hogewind, B.F., Pennings, R.J., Hol, F.A., Kunst, H.P., Hoefsloot, E.H., Cruysberg, J.R. and Cremers, C.W. (2010) 'Autosomal dominant optic neuropathy and sensorineual hearing loss associated with a novel mutation of WFS1', *Mol Vis*, 16, pp. 26-35.
Hoon, M., Okawa, H., Della Santina, L. and Wong, R.O. (2014) 'Functional architecture of the retina: development and disease', *Prog Retin Eye Res*, 42, pp. 44-84.
Howe, K., Clark, M.D., Torroja, C.F., Torrance, J., Berthelot, C., Muffato, M., Collins, J.E., Humphray, S., McLaren, K., Matthews, L., McLaren, S., Sealy, I., Caccamo, M., Churcher, C., Scott, C., Barrett, J.C., Koch, R., Rauch, G.J., White, S., Chow, W., Kilian, B., Quintais, L.T., Guerra-Assuncao, J.A., Zhou, Y., Gu, Y., Yen, J., Vogel, J.H., Eyre, T., Redmond, S., Banerjee, R., Chi, J., Fu, B., Langley, E., Maguire, S.F., Laird, G.K., Lloyd, D., Kenyon, E., Donaldson, S., Sehra, H., Almeida-King, J., Loveland, J., Trevanion, S., Jones, M., Quail, M., Willey, D., Hunt, A., Burton, J., Sims, S., McLay, K., Plumb, B., Davis, J., Clee, C., Oliver, K., Clark, R., Riddle, C., Elliot, D., Threadgold, G., Harden, G., Ware, D., Begum, S., Mortimore, B., Kerry, G., Heath, P., Phillimore, B., Tracey, A., Corby, N., Dunn, M., Johnson, C., Wood, J., Clark, S., Pelan, S., Griffiths, G., Smith, M., Glithero, R., Howden, P., Barker, N., Lloyd, C., Stevens, C., Harley, J., Holt, K., Panagiotidis, G., Lovell, J., Beasley, H., Henderson, C., Gordon, D., Auger, K., Wright, D., Collins, J., Raisen, C., Dyer, L., Leung, K., Robertson, L., Ambridge, K., Leongamornlert, D., McGuire, S., Gilderthorp, R., Griffiths, C., Manthravadi, D., Nichol, S., Barker, G., et al. (2013) 'The zebrafish reference genome sequence and its relationship to the human genome', *Nature*, 496(7446), pp. 498-503.
Hunte, C., Zickermann, V. and Brandt, U. (2010) 'Functional modules and structural basis of conformational coupling in mitochondrial complex I', *Science*, 329(5990), pp. 448-51.
Huynen, M.A., Duarte, I. and Szklarczyk, R. (2013) 'Loss, replacement and gain of proteins at the origin of the mitochondria', *Biochim Biophys Acta*, 1827(2), pp. 224-31.
Inoue, H., Tanizawa, Y., Wasson, J., Behn, P., Kalidas, K., Bernal-Mizrachi, E., Mueckler, M., Marshall, H., Donis-Keller, H., Crock, P., Rogers, D., Mikuni, M., Kumashiro, H., Higashi, K., Sobue, G., Oka, Y. and Permutt, M.A. (1998) 'A gene encoding a transmembrane protein is mutated in patients with diabetes mellitus and optic atrophy (Wolfram syndrome)', *Nat Genet*, 20(2), pp. 143-8.
Ishihara, H., Takeda, S., Tamura, A., Takahashi, R., Yamaguchi, S., Takei, D., Yamada, T., Inoue, H., Soga, H., Katagiri, H., Tanizawa, Y. and Oka, Y. (2004) 'Disruption of the WFS1 gene in mice causes progressive beta-cell loss and impaired stimulus-secretion coupling in insulin secretion', *Hum Mol Genet*, 13(11), pp. 1159-70.
Iwawaki, T., Hosoda, A., Okuda, T., Kamigori, Y., Nomura-Furuwatari, C., Kimata, Y., Tsuru, A. and Kohno, K. (2001) 'Translational control by the ER transmembrane kinase/ribonuclease IRE1 under ER stress', *Nat Cell Biol*, 3(2), pp. 158-64.
Jao, L.E., Wente, S.R. and Chen, W. (2013) 'Efficient multiplex biallelic zebrafish genome editing using a CRISPR nuclease system', *Proc Natl Acad Sci U S A*, 110(34), pp. 13904-9.
Jayashankar, V. and Rafelski, S.M. (2014) 'Integrating mitochondrial organization and dynamics with cellular architecture', *Curr Opin Cell Biol*, 26, pp. 34-40.
Jiang, D., Zhao, L. and Clapham, D.E. (2009) 'Genome-wide RNAi screen identifies Letm1 as a mitochondrial Ca2+/H+ antiporter', *Science*, 326(5949), pp. 144-7.
Kakiuchi, C., Ishiwata, M., Hayashi, A. and Kato, T. (2006) 'XBP1 induces WFS1 through an endoplasmic reticulum stress response element-like motif in SH-SY5Y cells', *J Neurochem*, 97(2), pp. 545-55.

Karasik, A., O'Hara, C., Srikanta, S., Swift, M., Soeldner, J.S., Kahn, C.R. and Herskowitz, R.D. (1989) 'Genetically programmed selective islet beta-cell loss in diabetic subjects with Wolfram's syndrome', *Diabetes Care*, 12(2), pp. 135-8.
Karnkowska, A., Vacek, V., Zubacova, Z., Treitli, S.C., Petrzelkova, R., Eme, L., Novak, L., Zarsky, V., Barlow, L.D., Herman, E.K., Soukal, P., Hroudova, M., Dolezal, P., Stairs, C.W., Roger, A.J., Elias, M., Dacks, J.B., Vlcek, C. and Hampl, V. (2016) 'A Eukaryote without a Mitochondrial Organelle', *Curr Biol*, 26(10), pp. 1274-84.
Karunadharma, P.P., Basisty, N., Chiao, Y.A., Dai, D.F., Drake, R., Levy, N., Koh, W.J., Emond, M.J., Kruse, S., Marcinek, D., Maccoss, M.J. and Rabinovitch, P.S. (2015) 'Respiratory chain protein turnover rates in mice are highly heterogeneous but strikingly conserved across tissues, ages, and treatments', *FASEB J*, 29(8), pp. 3582-92.
Kassahn, K.S., Dang, V.T., Wilkins, S.J., Perkins, A.C. and Ragan, M.A. (2009) 'Evolution of gene function and regulatory control after whole-genome duplication: comparative analyses in vertebrates', *Genome Res*, 19(8), pp. 1404-18.
Kaufman, R.J. (1999) 'Stress signaling from the lumen of the endoplasmic reticulum: coordination of gene transcriptional and translational controls', *Genes Dev*, 13(10), pp. 1211-33.
Kawano, J., Tanizawa, Y. and Shinoda, K. (2008) 'Wolfram syndrome 1 (Wfs1) gene expression in the normal mouse visual system', *J Comp Neurol*, 510(1), pp. 1-23.
Kettleborough, R.N., Busch-Nentwich, E.M., Harvey, S.A., Dooley, C.M., de Bruijn, E., van Eeden, F., Sealy, I., White, R.J., Herd, C., Nijman, I.J., Fenyes, F., Mehroke, S., Scahill, C., Gibbons, R., Wali, N., Carruthers, S., Hall, A., Yen, J., Cuppen, E. and Stemple, D.L. (2013) 'A systematic genome-wide analysis of zebrafish protein-coding gene function', *Nature*, 496(7446), pp. 494-7.
Kim, M.J., Kang, K.H., Kim, C.H. and Choi, S.Y. (2008) 'Real-time imaging of mitochondria in transgenic zebrafish expressing mitochondrially targeted GFP', *Biotechniques*, 45(3), pp. 331-4.
Kim, T.Y., Wang, D., Kim, A.K., Lau, E., Lin, A.J., Liem, D.A., Zhang, J., Zong, N.C., Lam, M.P. and Ping, P. (2012) 'Metabolic labeling reveals proteome dynamics of mouse mitochondria', *Mol Cell Proteomics*, 11(12), pp. 1586-94.
Kimmel, C.B., Ballard, W.W., Kimmel, S.R., Ullmann, B. and Schilling, T.F. (1995) 'Stages of embryonic development of the zebrafish', *Dev Dyn*, 203(3), pp. 253-310.
Kinsley, B.T., Swift, M., Dumont, R.H. and Swift, R.G. (1995) 'Morbidity and mortality in the Wolfram syndrome', *Diabetes Care*, 18(12), pp. 1566-70.
Kojima, R., Endo, T. and Tamura, Y. (2016) 'A phospholipid transfer function of ER-mitochondria encounter structure revealed in vitro', *Sci Rep*, 6, p. 30777.
Kok, F.O., Shin, M., Ni, C.W., Gupta, A., Grosse, A.S., van Impel, A., Kirchmaier, B.C., Peterson-Maduro, J., Kourkoulis, G., Male, I., DeSantis, D.F., Sheppard-Tindell, S., Ebarasi, L., Betsholtz, C., Schulte-Merker, S., Wolfe, S.A. and Lawson, N.D. (2015) 'Reverse genetic screening reveals poor correlation between morpholino-induced and mutant phenotypes in zebrafish', *Dev Cell*, 32(1), pp. 97-108.
Koks, S., Overall, R.W., Ivask, M., Soomets, U., Guha, M., Vasar, E., Fernandes, C. and Schalkwyk, L.C. (2013) 'Silencing of the WFS1 gene in HEK cells induces pathways related to neurodegeneration and mitochondrial damage', *Physiol Genomics*, 45(5), pp. 182-90.
Krebs, J., Agellon, L.B. and Michalak, M. (2015) 'Ca(2+) homeostasis and endoplasmic reticulum (ER) stress: An integrated view of calcium signaling', *Biochem Biophys Res Commun*, 460(1), pp. 114-21.
Lam, P.Y., Harvie, E.A. and Huttenlocher, A. (2013) 'Heat shock modulates neutrophil motility in zebrafish', *PLoS One*, 8(12), p. e84436.

Lane, N. and Martin, W. (2010) 'The energetics of genome complexity', *Nature*, 467(7318), pp. 929-34.
Lapuente-Brun, E., Moreno-Loshuertos, R., Acin-Perez, R., Latorre-Pellicer, A., Colas, C., Balsa, E., Perales-Clemente, E., Quiros, P.M., Calvo, E., Rodriguez-Hernandez, M.A., Navas, P., Cruz, R., Carracedo, A., Lopez-Otin, C., Perez-Martos, A., Fernandez-Silva, P., Fernandez-Vizarra, E. and Enriquez, J.A. (2013) 'Supercomplex assembly determines electron flux in the mitochondrial electron transport chain', *Science*, 340(6140), pp. 1567-70.
Larsson, N.G. (2010) 'Somatic mitochondrial DNA mutations in mammalian aging', *Annu Rev Biochem*, 79, pp. 683-706.
Lavrov, D.V. and Pett, W. (2016) 'Animal Mitochondrial DNA as We Do Not Know It: mt-Genome Organization and Evolution in Nonbilaterian Lineages', *Genome Biol Evol*, 8(9), pp. 2896-2913.
Lee, J.E., Westrate, L.M., Wu, H., Page, C. and Voeltz, G.K. (2016) 'Multiple dynamin family members collaborate to drive mitochondrial division', *Nature*, 540(7631), pp. 139-143.
Lemasters, J.J., Nieminen, A.L., Qian, T., Trost, L.C., Elmore, S.P., Nishimura, Y., Crowe, R.A., Cascio, W.E., Bradham, C.A., Brenner, D.A. and Herman, B. (1998) 'The mitochondrial permeability transition in cell death: a common mechanism in necrosis, apoptosis and autophagy', *Biochim Biophys Acta*, 1366(1-2), pp. 177-96.
Li, Y.N., Matsui, J.I. and Dowling, J.E. (2009) 'Specificity of the horizontal cell-photoreceptor connections in the zebrafish (Danio rerio) retina', *J Comp Neurol*, 516(5), pp. 442-53.
Lieber, D.S., Vafai, S.B., Horton, L.C., Slate, N.G., Liu, S., Borowsky, M.L., Calvo, S.E., Schmahmann, J.D. and Mootha, V.K. (2012) 'Atypical case of Wolfram syndrome revealed through targeted exome sequencing in a patient with suspected mitochondrial disease', *BMC Med Genet*, 13, p. 3.
Lieschke, G.J. and Currie, P.D. (2007) 'Animal models of human disease: zebrafish swim into view', *Nat Rev Genet*, 8(5), pp. 353-67.
Link, B.A. and Collery, R.F. (2015) 'Zebrafish Models of Retinal Disease', *Annu Rev Vis Sci*, 1, pp. 125-153.
Liu, J. and Lin, A. (2005) 'Role of JNK activation in apoptosis: a double-edged sword', *Cell Res*, 15(1), pp. 36-42.
Liu, Y., Fiskum, G. and Schubert, D. (2002) 'Generation of reactive oxygen species by the mitochondrial electron transport chain', *J Neurochem*, 80(5), pp. 780-7.
Lu, S., Kanekura, K., Hara, T., Mahadevan, J., Spears, L.D., Oslowski, C.M., Martinez, R., Yamazaki-Inoue, M., Toyoda, M., Neilson, A., Blanner, P., Brown, C.M., Semenkovich, C.F., Marshall, B.A., Hershey, T., Umezawa, A., Greer, P.A. and Urano, F. (2014) 'A calcium-dependent protease as a potential therapeutic target for Wolfram syndrome', *Proc Natl Acad Sci U S A*, 111(49), pp. E5292-301.
Lugar, H.M., Koller, J.M., Rutlin, J., Marshall, B.A., Kanekura, K., Urano, F., Bischoff, A.N., Shimony, J.S., Hershey, T. and Washington University Wolfram Syndrome Research Study, G. (2016) 'Neuroimaging evidence of deficient axon myelination in Wolfram syndrome', *Sci Rep*, 6, p. 21167.
Luo, S., Valencia, C.A., Zhang, J., Lee, N.C., Slone, J., Gui, B., Wang, X., Li, Z., Dell, S., Brown, J., Chen, S.M., Chien, Y.H., Hwu, W.L., Fan, P.C., Wong, L.J., Atwal, P.S. and Huang, T. (2018) 'Biparental Inheritance of Mitochondrial DNA in Humans', *Proc Natl Acad Sci U S A*, 115(51), pp. 13039-13044.
Luuk, H., Koks, S., Plaas, M., Hannibal, J., Rehfeld, J.F. and Vasar, E. (2008) 'Distribution of Wfs1 protein in the central nervous system of the mouse and its relation to clinical symptoms of the Wolfram syndrome', *J Comp Neurol*, 509(6), pp. 642-60.

Maranzana, E., Barbero, G., Falasca, A.I., Lenaz, G. and Genova, M.L. (2013) 'Mitochondrial respiratory supercomplex association limits production of reactive oxygen species from complex I', *Antioxid Redox Signal*, 19(13), pp. 1469-80.
Marra, M.H., Tobias, Z.J., Cohen, H.R., Glover, G. and Weissman, T.A. (2015) 'In Vivo Time-Lapse Imaging in the Zebrafish Lateral Line: A Flexible, Open-Ended Research Project for an Undergraduate Neurobiology Laboratory Course', *J Undergrad Neurosci Educ*, 13(3), pp. A215-24.
Matsunaga, K., Tanabe, K., Inoue, H., Okuya, S., Ohta, Y., Akiyama, M., Taguchi, A., Kora, Y., Okayama, N., Yamada, Y., Wada, Y., Amemiya, S., Sugihara, S., Nakao, Y., Oka, Y. and Tanizawa, Y. (2014) 'Wolfram syndrome in the Japanese population; molecular analysis of WFS1 gene and characterization of clinical features', *PLoS One*, 9(9), p. e106906.
Medlej, R., Wasson, J., Baz, P., Azar, S., Salti, I., Loiselet, J., Permutt, A. and Halaby, G. (2004) 'Diabetes mellitus and optic atrophy: a study of Wolfram syndrome in the Lebanese population', *J Clin Endocrinol Metab*, 89(4), pp. 1656-61.
Meeker, N.D., Hutchinson, S.A., Ho, L. and Trede, N.S. (2007) 'Method for isolation of PCR-ready genomic DNA from zebrafish tissues', *Biotechniques*, 43(5), pp. 610, 612, 614.
Meisinger, C., Sickmann, A. and Pfanner, N. (2008) 'The mitochondrial proteome: from inventory to function', *Cell*, 134(1), pp. 22-4.
Menelaou, E., Husbands, E.E., Pollet, R.G., Coutts, C.A., Ali, D.W. and Svoboda, K.R. (2008) 'Embryonic motor activity and implications for regulating motoneuron axonal pathfinding in zebrafish', *Eur J Neurosci*, 28(6), pp. 1080-96.
Meyer, A. and Schartl, M. (1999) 'Gene and genome duplications in vertebrates: the one-to-four (-to-eight in fish) rule and the evolution of novel gene functions', *Curr Opin Cell Biol*, 11(6), pp. 699-704.
Minauro-Sanmiguel, F., Wilkens, S. and Garcia, J.J. (2005) 'Structure of dimeric mitochondrial ATP synthase: novel F0 bridging features and the structural basis of mitochondrial cristae biogenesis', *Proc Natl Acad Sci U S A*, 102(35), pp. 12356-8.
Molina, A.J., Wikstrom, J.D., Stiles, L., Las, G., Mohamed, H., Elorza, A., Walzer, G., Twig, G., Katz, S., Corkey, B.E. and Shirihai, O.S. (2009) 'Mitochondrial networking protects beta-cells from nutrient-induced apoptosis', *Diabetes*, 58(10), pp. 2303-15.
Morcos, P.A., Vincent, A.C. and Moulton, J.D. (2015) 'Gene Editing Versus Morphants', *Zebrafish*, 12(5), p. 319.
Mustafi, D., Engel, A.H. and Palczewski, K. (2009) 'Structure of cone photoreceptors', *Prog Retin Eye Res*, 28(4), pp. 289-302.
Myers, P.Z., Eisen, J.S. and Westerfield, M. (1986) 'Development and axonal outgrowth of identified motoneurons in the zebrafish', *J Neurosci*, 6(8), pp. 2278-89.
Nasevicius, A. and Ekker, S.C. (2000) 'Effective targeted gene 'knockdown' in zebrafish', *Nat Genet*, 26(2), pp. 216-20.
Noji, H., Yasuda, R., Yoshida, M. and Kinosita, K., Jr. (1997) 'Direct observation of the rotation of F1-ATPase', *Nature*, 386(6622), pp. 299-302.
Noormets, K., Koks, S., Kavak, A., Arend, A., Aunapuu, M., Keldrimaa, A., Vasar, E. and Tillmann, V. (2009) 'Male mice with deleted Wolframin (Wfs1) gene have reduced fertility', *Reprod Biol Endocrinol*, 7, p. 82.
O'Connor, E., Phan, V., Cordts, I., Cairns, G., Hettwer, S., Cox, D., Lochmuller, H. and Roos, A. (2018) 'MYO9A deficiency in motor neurons is associated with reduced neuromuscular agrin secretion', *Hum Mol Genet*, 27(8), pp. 1434-1446.
O'Hare, E.A., Yerges-Armstrong, L.M., Perry, J.A., Shuldiner, A.R. and Zaghloul, N.A. (2016) 'Assignment of Functional Relevance to Genes at Type 2 Diabetes-Associated Loci Through Investigation of beta-Cell Mass Deficits', *Mol Endocrinol*, 30(4), pp. 429-45.

Odisho, T., Zhang, L. and Volchuk, A. (2015) 'ATF6beta regulates the Wfs1 gene and has a cell survival role in the ER stress response in pancreatic beta-cells', *Exp Cell Res*, 330(1), pp. 111-22.
Ogata, M., Hino, S., Saito, A., Morikawa, K., Kondo, S., Kanemoto, S., Murakami, T., Taniguchi, M., Tanii, I., Yoshinaga, K., Shiosaka, S., Hammarback, J.A., Urano, F. and Imaizumi, K. (2006) 'Autophagy is activated for cell survival after endoplasmic reticulum stress', *Mol Cell Biol*, 26(24), pp. 9220-31.
Osman, A.A., Saito, M., Makepeace, C., Permutt, M.A., Schlesinger, P. and Mueckler, M. (2003) 'Wolframin expression induces novel ion channel activity in endoplasmic reticulum membranes and increases intracellular calcium', *J Biol Chem*, 278(52), pp. 52755-62.
Ow, Y.P., Green, D.R., Hao, Z. and Mak, T.W. (2008) 'Cytochrome c: functions beyond respiration', *Nat Rev Mol Cell Biol*, 9(7), pp. 532-42.
Palty, R., Raveh, A., Kaminsky, I., Meller, R. and Reuveny, E. (2012) 'SARAF inactivates the store operated calcium entry machinery to prevent excess calcium refilling', *Cell*, 149(2), pp. 425-38.
Pan, B.X., Ross-Cisneros, F.N., Carelli, V., Rue, K.S., Salomao, S.R., Moraes-Filho, M.N., Moraes, M.N., Berezovsky, A., Belfort, R., Jr. and Sadun, A.A. (2012) 'Mathematically modeling the involvement of axons in Leber's hereditary optic neuropathy', *Invest Ophthalmol Vis Sci*, 53(12), pp. 7608-17.
Panzer, J.A., Gibbs, S.M., Dosch, R., Wagner, D., Mullins, M.C., Granato, M. and Balice-Gordon, R.J. (2005) 'Neuromuscular synaptogenesis in wild-type and mutant zebrafish', *Dev Biol*, 285(2), pp. 340-57.
Partridge, M., Vincent, A., Matthews, P., Puma, J., Stein, D. and Summerton, J. (1996) 'A simple method for delivering morpholino antisense oligos into the cytoplasm of cells', *Antisense Nucleic Acid Drug Dev*, 6(3), pp. 169-75.
Pathak, T. and Trebak, M. (2018) 'Mitochondrial Ca(2+) signaling', *Pharmacol Ther*.
Patton, E.E. and Zon, L.I. (2001) 'The art and design of genetic screens: zebrafish', *Nat Rev Genet*, 2(12), pp. 956-66.
Pei, W., Kratz, L.E., Bernardini, I., Sood, R., Yokogawa, T., Dorward, H., Ciccone, C., Kelley, R.I., Anikster, Y., Burgess, H.A., Huizing, M. and Feldman, B. (2010) 'A model of Costeff Syndrome reveals metabolic and protective functions of mitochondrial OPA3', *Development*, 137(15), pp. 2587-96.
Pekkurnaz, G., Trinidad, J.C., Wang, X., Kong, D. and Schwarz, T.L. (2014) 'Glucose regulates mitochondrial motility via Milton modification by O-GlcNAc transferase', *Cell*, 158(1), pp. 54-68.
Pelegri, F. (2003) 'Maternal factors in zebrafish development', *Dev Dyn*, 228(3), pp. 535-54.
Pfeiffer, K., Gohil, V., Stuart, R.A., Hunte, C., Brandt, U., Greenberg, M.L. and Schagger, H. (2003) 'Cardiolipin stabilizes respiratory chain supercomplexes', *J Biol Chem*, 278(52), pp. 52873-80.
Phillips, M.J. and Voeltz, G.K. (2016) 'Structure and function of ER membrane contact sites with other organelles', *Nat Rev Mol Cell Biol*, 17(2), pp. 69-82.
Pilz, D., Quarrell, O.W. and Jones, E.W. (1994) 'Mitochondrial mutation commonly associated with Leber's hereditary optic neuropathy observed in a patient with Wolfram syndrome (DIDMOAD)', *J Med Genet*, 31(4), pp. 328-30.
Pinho, B.R., Santos, M.M., Fonseca-Silva, A., Valentao, P., Andrade, P.B. and Oliveira, J.M. (2013) 'How mitochondrial dysfunction affects zebrafish development and cardiovascular function: an in vivo model for testing mitochondria-targeted drugs', *Br J Pharmacol*, 169(5), pp. 1072-90.

Plaas, M., Seppa, K., Reimets, R., Jagomae, T., Toots, M., Koppel, T., Vallisoo, T., Nigul, M., Heinla, I., Meier, R., Kaasik, A., Piirsoo, A., Hickey, M.A., Terasmaa, A. and Vasar, E. (2017) 'Wfs1- deficient rats develop primary symptoms of Wolfram syndrome: insulin-dependent diabetes, optic nerve atrophy and medullary degeneration', *Sci Rep*, 7(1), p. 10220.
Poston, C.N., Krishnan, S.C. and Bazemore-Walker, C.R. (2013) 'In-depth proteomic analysis of mammalian mitochondria-associated membranes (MAM)', *J Proteomics*, 79, pp. 219-30.
Prins, D., Groenendyk, J., Touret, N. and Michalak, M. (2011) 'Modulation of STIM1 and capacitative Ca2+ entry by the endoplasmic reticulum luminal oxidoreductase ERp57', *EMBO Rep*, 12(11), pp. 1182-8.
Prudent, J., Popgeorgiev, N., Bonneau, B., Thibaut, J., Gadet, R., Lopez, J., Gonzalo, P., Rimokh, R., Manon, S., Houart, C., Herbomel, P., Aouacheria, A. and Gillet, G. (2013) 'Bcl-wav and the mitochondrial calcium uniporter drive gastrula morphogenesis in zebrafish', *Nat Commun*, 4, p. 2330.
Puhka, M., Vihinen, H., Joensuu, M. and Jokitalo, E. (2007) 'Endoplasmic reticulum remains continuous and undergoes sheet-to-tubule transformation during cell division in mammalian cells', *J Cell Biol*, 179(5), pp. 895-909.
Rahn, J.J., Bestman, J.E., Stackley, K.D. and Chan, S.S. (2015) 'Zebrafish lacking functional DNA polymerase gamma survive to juvenile stage, despite rapid and sustained mitochondrial DNA depletion, altered energetics and growth', *Nucleic Acids Res*, 43(21), pp. 10338-52.
Rahn, J.J., Stackley, K.D. and Chan, S.S. (2013) 'Opa1 is required for proper mitochondrial metabolism in early development', *PLoS One*, 8(3), p. e59218.
Reinders, J., Zahedi, R.P., Pfanner, N., Meisinger, C. and Sickmann, A. (2006) 'Toward the complete yeast mitochondrial proteome: multidimensional separation techniques for mitochondrial proteomics', *J Proteome Res*, 5(7), pp. 1543-54.
Rendtorff, N.D., Lodahl, M., Boulahbel, H., Johansen, I.R., Pandya, A., Welch, K.O., Norris, V.W., Arnos, K.S., Bitner-Glindzicz, M., Emery, S.B., Mets, M.B., Fagerheim, T., Eriksson, K., Hansen, L., Bruhn, H., Moller, C., Lindholm, S., Ensgaard, S., Lesperance, M.M. and Tranebjaerg, L. (2011) 'Identification of p.A684V missense mutation in the WFS1 gene as a frequent cause of autosomal dominant optic atrophy and hearing impairment', *Am J Med Genet A*, 155A(6), pp. 1298-313.
Richardson, R., Tracey-White, D., Webster, A. and Moosajee, M. (2017) 'The zebrafish eye-a paradigm for investigating human ocular genetics', *Eye (Lond)*, 31(1), pp. 68-86.
Riggs, A.C., Bernal-Mizrachi, E., Ohsugi, M., Wasson, J., Fatrai, S., Welling, C., Murray, J., Schmidt, R.E., Herrera, P.L. and Permutt, M.A. (2005) 'Mice conditionally lacking the Wolfram gene in pancreatic islet beta cells exhibit diabetes as a result of enhanced endoplasmic reticulum stress and apoptosis', *Diabetologia*, 48(11), pp. 2313-21.
Robu, M.E., Larson, J.D., Nasevicius, A., Beiraghi, S., Brenner, C., Farber, S.A. and Ekker, S.C. (2007) 'p53 activation by knockdown technologies', *PLoS Genet*, 3(5), p. e78.
Roos, J., DiGregorio, P.J., Yeromin, A.V., Ohlsen, K., Lioudyno, M., Zhang, S., Safrina, O., Kozak, J.A., Wagner, S.L., Cahalan, M.D., Velicelebi, G. and Stauderman, K.A. (2005) 'STIM1, an essential and conserved component of store-operated Ca2+ channel function', *J Cell Biol*, 169(3), pp. 435-45.
Ross-Cisneros, F.N., Pan, B.X., Silva, R.A., Miller, N.R., Albini, T.A., Tranebjaerg, L., Rendtorff, N.D., Lodahl, M., Moraes-Filho, M.N., Moraes, M.N., Salomao, S.R., Berezovsky, A., Belfort, R., Jr., Carelli, V. and Sadun, A.A. (2013) 'Optic nerve histopathology in a case of Wolfram Syndrome: a mitochondrial pattern of axonal loss', *Mitochondrion*, 13(6), pp. 841-5.
Rossi, A., Kontarakis, Z., Gerri, C., Nolte, H., Holper, S., Kruger, M. and Stainier, D.Y. (2015) 'Genetic compensation induced by deleterious mutations but not gene knockdowns', *Nature*, 524(7564), pp. 230-3.

Rotig, A., Cormier, V., Chatelain, P., Francois, R., Saudubray, J.M., Rustin, P. and Munnich, A. (1993) 'Deletion of mitochondrial DNA in a case of early-onset diabetes mellitus, optic atrophy, and deafness (Wolfram syndrome, MIM 222300)', *J Clin Invest*, 91(3), pp. 1095-8.
Rouzier, C., Moore, D., Delorme, C., Lacas-Gervais, S., Ait-El-Mkadem, S., Fragaki, K., Burte, F., Serre, V., Bannwarth, S., Chaussenot, A., Catala, M., Yu-Wai-Man, P. and Paquis-Flucklinger, V. (2017a) 'A novel CISD2 mutation associated with a classical Wolfram syndrome phenotype alters Ca2+ homeostasis and ER-mitochondria interactions', *Hum Mol Genet*, 26(9), p. 1786.
Rouzier, C., Moore, D., Delorme, C., Lacas-Gervais, S., Ait-El-Mkadem, S., Fragaki, K., Burte, F., Serre, V., Bannwarth, S., Chaussenot, A., Catala, M., Yu-Wai-Man, P. and Paquis-Flucklinger, V. (2017b) 'A novel CISD2 mutation associated with a classical Wolfram syndrome phenotype alters Ca2+ homeostasis and ER-mitochondria interactions', *Hum Mol Genet*, 26(9), pp. 1599-1611.
Rowland, A.A. and Voeltz, G.K. (2012) 'Endoplasmic reticulum-mitochondria contacts: function of the junction', *Nat Rev Mol Cell Biol*, 13(10), pp. 607-25.
Ruggiano, A., Foresti, O. and Carvalho, P. (2014) 'Quality control: ER-associated degradation: protein quality control and beyond', *J Cell Biol*, 204(6), pp. 869-79.
Saint-Amant, L. and Drapeau, P. (1998) 'Time course of the development of motor behaviors in the zebrafish embryo', *J Neurobiol*, 37(4), pp. 622-32.
Sakakibara, Y., Sekiya, M., Fujisaki, N., Quan, X. and Iijima, K.M. (2018) 'Knockdown of wfs1, a fly homolog of Wolfram syndrome 1, in the nervous system increases susceptibility to age- and stress-induced neuronal dysfunction and degeneration in Drosophila', *PLoS Genet*, 14(1), p. e1007196.
Sam, W., Qin, H., Crawford, B., Yue, D. and Yu, S. (2001) 'Homozygosity for a 4-bp deletion in a patient with Wolfram syndrome suggesting possible phenotype and genotype correlation', *Clin Genet*, 59(2), pp. 136-8.
Samori, B., Lenaz, G., Battino, M., Marconi, G. and Domini, I. (1992) 'On coenzyme Q orientation in membranes: a linear dichroism study of ubiquinones in a model bilayer', *J Membr Biol*, 128(3), pp. 193-203.
Sampath, A.P. and Rieke, F. (2004) 'Selective transmission of single photon responses by saturation at the rod-to-rod bipolar synapse', *Neuron*, 41(3), pp. 431-43.
Sander, J.D., Cade, L., Khayter, C., Reyon, D., Peterson, R.T., Joung, J.K. and Yeh, J.R. (2011) 'Targeted gene disruption in somatic zebrafish cells using engineered TALENs', *Nat Biotechnol*, 29(8), pp. 697-8.
Sanes, J.R. and Masland, R.H. (2015) 'The types of retinal ganglion cells: current status and implications for neuronal classification', *Annu Rev Neurosci*, 38, pp. 221-46.
Schagger, H., Link, T.A., Engel, W.D. and von Jagow, G. (1986) 'Isolation of the eleven protein subunits of the bc1 complex from beef heart', *Methods Enzymol*, 126, pp. 224-37.
Schagger, H. and Pfeiffer, K. (2000) 'Supercomplexes in the respiratory chains of yeast and mammalian mitochondria', *EMBO J*, 19(8), pp. 1777-83.
Schindler, A.J. and Schekman, R. (2009) 'In vitro reconstitution of ER-stress induced ATF6 transport in COPII vesicles', *Proc Natl Acad Sci U S A*, 106(42), pp. 17775-80.
Schmidt-Kastner, R., Kreczmanski, P., Preising, M., Diederen, R., Schmitz, C., Reis, D., Blanks, J. and Dorey, C.K. (2009) 'Expression of the diabetes risk gene wolframin (WFS1) in the human retina', *Exp Eye Res*, 89(4), pp. 568-74.
Schmidt, O., Pfanner, N. and Meisinger, C. (2010) 'Mitochondrial protein import: from proteomics to functional mechanisms', *Nat Rev Mol Cell Biol*, 11(9), pp. 655-67.
Schmidt, R., Strahle, U. and Scholpp, S. (2013) 'Neurogenesis in zebrafish - from embryo to adult', *Neural Dev*, 8, p. 3.

Schmitt, S., Prokisch, H., Schlunck, T., Camp, D.G., 2nd, Ahting, U., Waizenegger, T., Scharfe, C., Meitinger, T., Imhof, A., Neupert, W., Oefner, P.J. and Rapaport, D. (2006) 'Proteome analysis of mitochondrial outer membrane from Neurospora crassa', *Proteomics*, 6(1), pp. 72-80.
Schuler, M.H., Lewandowska, A., Caprio, G.D., Skillern, W., Upadhyayula, S., Kirchhausen, T., Shaw, J.M. and Cunniff, B. (2017) 'Miro1-mediated mitochondrial positioning shapes intracellular energy gradients required for cell migration', *Mol Biol Cell*, 28(16), pp. 2159-2169.
Schwarz, D.S. and Blower, M.D. (2016) 'The endoplasmic reticulum: structure, function and response to cellular signaling', *Cell Mol Life Sci*, 73(1), pp. 79-94.
Sharma, V. and O'Halloran, D.M. (2014) 'Recent structural and functional insights into the family of sodium calcium exchangers', *Genesis*, 52(2), pp. 93-109.
Shen, J., Chen, X., Hendershot, L. and Prywes, R. (2002) 'ER stress regulation of ATF6 localization by dissociation of BiP/GRP78 binding and unmasking of Golgi localization signals', *Dev Cell*, 3(1), pp. 99-111.
Shen, J. and Prywes, R. (2004) 'Dependence of site-2 protease cleavage of ATF6 on prior site-1 protease digestion is determined by the size of the luminal domain of ATF6', *J Biol Chem*, 279(41), pp. 43046-51.
Sherpa, T., Fimbel, S.M., Mallory, D.E., Maaswinkel, H., Spritzer, S.D., Sand, J.A., Li, L., Hyde, D.R. and Stenkamp, D.L. (2008) 'Ganglion cell regeneration following whole-retina destruction in zebrafish', *Dev Neurobiol*, 68(2), pp. 166-81.
Sousa, J.S., D'Imprima, E. and Vonck, J. (2018) 'Mitochondrial Respiratory Chain Complexes', *Subcell Biochem*, 87, pp. 167-227.
Stackley, K.D., Beeson, C.C., Rahn, J.J. and Chan, S.S. (2011) 'Bioenergetic profiling of zebrafish embryonic development', *PLoS One*, 6(9), p. e25652.
Stainier, D.Y.R., Raz, E., Lawson, N.D., Ekker, S.C., Burdine, R.D., Eisen, J.S., Ingham, P.W., Schulte-Merker, S., Yelon, D., Weinstein, B.M., Mullins, M.C., Wilson, S.W., Ramakrishnan, L., Amacher, S.L., Neuhauss, S.C.F., Meng, A., Mochizuki, N., Panula, P. and Moens, C.B. (2017) 'Guidelines for morpholino use in zebrafish', *PLoS Genet*, 13(10), p. e1007000.
Steele, S.L., Prykhozhij, S.V. and Berman, J.N. (2014a) 'Zebrafish as a model system for mitochondrial biology and diseases', *Translational Research*, 163(2), pp. 79-98.
Steele, S.L., Prykhozhij, S.V. and Berman, J.N. (2014b) 'Zebrafish as a model system for mitochondrial biology and diseases', *Transl Res*, 163(2), pp. 79-98.
Stewart, A., Gaikwad, S., Kyzar, E., Green, J., Roth, A. and Kalueff, A.V. (2012) 'Modeling anxiety using adult zebrafish: a conceptual review', *Neuropharmacology*, 62(1), pp. 135-43.
Stowers, R.S., Megeath, L.J., Gorska-Andrzejak, J., Meinertzhagen, I.A. and Schwarz, T.L. (2002) 'Axonal transport of mitochondria to synapses depends on milton, a novel Drosophila protein', *Neuron*, 36(6), pp. 1063-77.
Streisinger, G., Walker, C., Dower, N., Knauber, D. and Singer, F. (1981) 'Production of clones of homozygous diploid zebra fish (Brachydanio rerio)', *Nature*, 291(5813), pp. 293-6.
Strom, T.M., Hortnagel, K., Hofmann, S., Gekeler, F., Scharfe, C., Rabl, W., Gerbitz, K.D. and Meitinger, T. (1998) 'Diabetes insipidus, diabetes mellitus, optic atrophy and deafness (DIDMOAD) caused by mutations in a novel gene (wolframin) coding for a predicted transmembrane protein', *Hum Mol Genet*, 7(13), pp. 2021-8.
Summerton, J. (1999) 'Morpholino antisense oligomers: the case for an RNase H-independent structural type', *Biochim Biophys Acta*, 1489(1), pp. 141-58.
Sun, F., Huo, X., Zhai, Y., Wang, A., Xu, J., Su, D., Bartlam, M. and Rao, Z. (2005) 'Crystal structure of mitochondrial respiratory membrane protein complex II', *Cell*, 121(7), pp. 1043-57.

Swift, R.G., Perkins, D.O., Chase, C.L., Sadler, D.B. and Swift, M. (1991) 'Psychiatric disorders in 36 families with Wolfram syndrome', *Am J Psychiatry*, 148(6), pp. 775-9.
Taanman, J.W. (1999) 'The mitochondrial genome: structure, transcription, translation and replication', *Biochim Biophys Acta*, 1410(2), pp. 103-23.
Takeda, K., Inoue, H., Tanizawa, Y., Matsuzaki, Y., Oba, J., Watanabe, Y., Shinoda, K. and Oka, Y. (2001) 'WFS1 (Wolfram syndrome 1) gene product: predominant subcellular localization to endoplasmic reticulum in cultured cells and neuronal expression in rat brain', *Hum Mol Genet*, 10(5), pp. 477-84.
Takei, D., Ishihara, H., Yamaguchi, S., Yamada, T., Tamura, A., Katagiri, H., Maruyama, Y. and Oka, Y. (2006) 'WFS1 protein modulates the free Ca(2+) concentration in the endoplasmic reticulum', *FEBS Lett*, 580(24), pp. 5635-40.
Teixido, E., Pique, E., Gomez-Catalan, J. and Llobet, J.M. (2013) 'Assessment of developmental delay in the zebrafish embryo teratogenicity assay', *Toxicol In Vitro*, 27(1), pp. 469-78.
Terasmaa, A., Soomets, U., Oflijan, J., Punapart, M., Hansen, M., Matto, V., Ehrlich, K., Must, A., Koks, S. and Vasar, E. (2011) 'Wfs1 mutation makes mice sensitive to insulin-like effect of acute valproic acid and resistant to streptozocin', *J Physiol Biochem*, 67(3), pp. 381-90.
The UniProt, C. (2017) 'UniProt: the universal protein knowledgebase', *Nucleic Acids Res*, 45(D1), pp. D158-D169.
Thisse, B., Thisse, C. (2004) 'Fast Release Clones: A High Throughput Expression Analysis', *ZFIN Direct Data Submission (http://zfin.org)*.
Thuerauf, D.J., Morrison, L. and Glembotski, C.C. (2004) 'Opposing roles for ATF6alpha and ATF6beta in endoplasmic reticulum stress response gene induction', *J Biol Chem*, 279(20), pp. 21078-84.
Tilokani, L., Nagashima, S., Paupe, V. and Prudent, J. (2018) 'Mitochondrial dynamics: overview of molecular mechanisms', *Essays Biochem*, 62(3), pp. 341-360.
Toms, M., Tracey-White, D., Muhundhakumar, D., Sprogyte, L., Dubis, A.M. and Moosajee, M. (2017) 'Spectral Domain Optical Coherence Tomography: An In Vivo Imaging Protocol for Assessing Retinal Morphology in Adult Zebrafish', *Zebrafish*, 14(2), pp. 118-125.
Tondera, D., Grandemange, S., Jourdain, A., Karbowski, M., Mattenberger, Y., Herzig, S., Da Cruz, S., Clerc, P., Raschke, I., Merkwirth, C., Ehses, S., Krause, F., Chan, D.C., Alexander, C., Bauer, C., Youle, R., Langer, T. and Martinou, J.C. (2009) 'SLP-2 is required for stress-induced mitochondrial hyperfusion', *EMBO J*, 28(11), pp. 1589-600.
Tropepe, V. and Sive, H.L. (2003) 'Can zebrafish be used as a model to study the neurodevelopmental causes of autism?', *Genes Brain Behav*, 2(5), pp. 268-81.
Uhlen, M., Oksvold, P., Fagerberg, L., Lundberg, E., Jonasson, K., Forsberg, M., Zwahlen, M., Kampf, C., Wester, K., Hober, S., Wernerus, H., Bjorling, L. and Ponten, F. (2010) 'Towards a knowledge-based Human Protein Atlas', *Nat Biotechnol*, 28(12), pp. 1248-50.
Urano, F. (2016) 'Wolfram Syndrome: Diagnosis, Management, and Treatment', *Curr Diab Rep*, 16(1), p. 6.
Vacaru, A.M., Di Narzo, A.F., Howarth, D.L., Tsedensodnom, O., Imrie, D., Cinaroglu, A., Amin, S., Hao, K. and Sadler, K.C. (2014) 'Molecularly defined unfolded protein response subclasses have distinct correlations with fatty liver disease in zebrafish', *Dis Model Mech*, 7(7), pp. 823-35.
Vance, J.E. (1990) 'Phospholipid synthesis in a membrane fraction associated with mitochondria', *J Biol Chem*, 265(13), pp. 7248-56.
Vance, J.E. (2015) 'Phospholipid synthesis and transport in mammalian cells', *Traffic*, 16(1), pp. 1-18.

Vempati, U.D., Han, X. and Moraes, C.T. (2009) 'Lack of cytochrome c in mouse fibroblasts disrupts assembly/stability of respiratory complexes I and IV', *J Biol Chem*, 284(7), pp. 4383-91.
Verfaillie, T., Rubio, N., Garg, A.D., Bultynck, G., Rizzuto, R., Decuypere, J.P., Piette, J., Linehan, C., Gupta, S., Samali, A. and Agostinis, P. (2012) 'PERK is required at the ER-mitochondrial contact sites to convey apoptosis after ROS-based ER stress', *Cell Death Differ*, 19(11), pp. 1880-91.
Vinothkumar, K.R., Zhu, J. and Hirst, J. (2014) 'Architecture of mammalian respiratory complex I', *Nature*, 515(7525), pp. 80-84.
Vora, A.J. and Lilleyman, J.S. (1993) 'Wolfram-Syndrome - Mitochondrial Disorder', *Lancet*, 342(8878), pp. 1059-1059.
Wang, S., Hu, B., Ding, Z., Dang, Y., Wu, J., Li, D., Liu, X., Xiao, B., Zhang, W., Ren, R., Lei, J., Hu, H., Chen, C., Chan, P., Li, D., Qu, J., Tang, F. and Liu, G.H. (2018) 'ATF6 safeguards organelle homeostasis and cellular aging in human mesenchymal stem cells', *Cell Discov*, 4, p. 2.
Wang, X. and Schwarz, T.L. (2009) 'The mechanism of Ca2+ -dependent regulation of kinesin-mediated mitochondrial motility', *Cell*, 136(1), pp. 163-74.
West, M., Zurek, N., Hoenger, A. and Voeltz, G.K. (2011) 'A 3D analysis of yeast ER structure reveals how ER domains are organized by membrane curvature', *J Cell Biol*, 193(2), pp. 333-46.
Westrate, L.M., Lee, J.E., Prinz, W.A. and Voeltz, G.K. (2015) 'Form follows function: the importance of endoplasmic reticulum shape', *Annu Rev Biochem*, 84, pp. 791-811.
Whitfield, T.T. (2002) 'Zebrafish as a model for hearing and deafness', *J Neurobiol*, 53(2), pp. 157-71.
Wiley, S.E., Andreyev, A.Y., Divakaruni, A.S., Karisch, R., Perkins, G., Wall, E.A., van der Geer, P., Chen, Y.F., Tsai, T.F., Simon, M.I., Neel, B.G., Dixon, J.E. and Murphy, A.N. (2013) 'Wolfram Syndrome protein, Miner1, regulates sulphydryl redox status, the unfolded protein response, and Ca2+ homeostasis', *EMBO Mol Med*, 5(6), pp. 904-18.
Wolfram DJ, W.H. (1938) 'Diabetes mellitus and simple optic atrophy among siblings: report of four cases', *Mayo Clinic Proceedings*, 13, pp. 715–718.
Wu, Y., Whiteus, C., Xu, C.S., Hayworth, K.J., Weinberg, R.J., Hess, H.F. and De Camilli, P. (2017) 'Contacts between the endoplasmic reticulum and other membranes in neurons', *Proc Natl Acad Sci U S A*, 114(24), pp. E4859-E4867.
Yamada, T., Ishihara, H., Tamura, A., Takahashi, R., Yamaguchi, S., Takei, D., Tokita, A., Satake, C., Tashiro, F., Katagiri, H., Aburatani, H., Miyazaki, J. and Oka, Y. (2006) 'WFS1-deficiency increases endoplasmic reticulum stress, impairs cell cycle progression and triggers the apoptotic pathway specifically in pancreatic beta-cells', *Hum Mol Genet*, 15(10), pp. 1600-9.
Yamaguchi, S., Ishihara, H., Tamura, A., Yamada, T., Takahashi, R., Takei, D., Katagiri, H. and Oka, Y. (2004) 'Endoplasmic reticulum stress and N-glycosylation modulate expression of WFS1 protein', *Biochem Biophys Res Commun*, 325(1), pp. 250-6.
Yu-Wai-Man, P., Soiferman, D., Moore, D.G., Burte, F. and Saada, A. (2017) 'Evaluating the therapeutic potential of idebenone and related quinone analogues in Leber hereditary optic neuropathy', *Mitochondrion*, 36, pp. 36-42.
Yu, D.Y., Cringle, S.J., Balaratnasingam, C., Morgan, W.H., Yu, P.K. and Su, E.N. (2013) 'Retinal ganglion cells: Energetics, compartmentation, axonal transport, cytoskeletons and vulnerability', *Prog Retin Eye Res*, 36, pp. 217-46.
Yu, S.B. and Pekkurnaz, G. (2018) 'Mechanisms Orchestrating Mitochondrial Dynamics for Energy Homeostasis', *J Mol Biol*.

Zahedi, R.P., Sickmann, A., Boehm, A.M., Winkler, C., Zufall, N., Schonfisch, B., Guiard, B., Pfanner, N. and Meisinger, C. (2006) 'Proteomic analysis of the yeast mitochondrial outer membrane reveals accumulation of a subclass of preproteins', *Mol Biol Cell*, 17(3), pp. 1436-50.
Zatyka, M., Da Silva Xavier, G., Bellomo, E.A., Leadbeater, W., Astuti, D., Smith, J., Michelangeli, F., Rutter, G.A. and Barrett, T.G. (2015) 'Sarco(endo)plasmic reticulum ATPase is a molecular partner of Wolfram syndrome 1 protein, which negatively regulates its expression', *Hum Mol Genet*, 24(3), pp. 814-27.
Zerbino, D.R., Achuthan, P., Akanni, W., Amode, M.R., Barrell, D., Bhai, J., Billis, K., Cummins, C., Gall, A., Giron, C.G., Gil, L., Gordon, L., Haggerty, L., Haskell, E., Hourlier, T., Izuogu, O.G., Janacek, S.H., Juettemann, T., To, J.K., Laird, M.R., Lavidas, I., Liu, Z., Loveland, J.E., Maurel, T., McLaren, W., Moore, B., Mudge, J., Murphy, D.N., Newman, V., Nuhn, M., Ogeh, D., Ong, C.K., Parker, A., Patricio, M., Riat, H.S., Schuilenburg, H., Sheppard, D., Sparrow, H., Taylor, K., Thormann, A., Vullo, A., Walts, B., Zadissa, A., Frankish, A., Hunt, S.E., Kostadima, M., Langridge, N., Martin, F.J., Muffato, M., Perry, E., Ruffier, M., Staines, D.M., Trevanion, S.J., Aken, B.L., Cunningham, F., Yates, A. and Flicek, P. (2018) 'Ensembl 2018', *Nucleic Acids Res*, 46(D1), pp. D754-D761.
Zeviani, M., Servidei, S., Gellera, C., Bertini, E., DiMauro, S. and DiDonato, S. (1989) 'An autosomal dominant disorder with multiple deletions of mitochondrial DNA starting at the D-loop region', *Nature*, 339(6222), pp. 309-11.
Zhu, J., Vinothkumar, K.R. and Hirst, J. (2016) 'Structure of mammalian respiratory complex I', *Nature*, 536(7616), pp. 354-358.
Zorov, D.B., Juhaszova, M. and Sollott, S.J. (2014) 'Mitochondrial reactive oxygen species (ROS) and ROS-induced ROS release', *Physiol Rev*, 94(3), pp. 909-50.

Appendix

Sumplimentary Evidence

https://drive.google.com/drive/folders/1HavMAZuPUFtJZFGFj642_OS9HHVjW4oR?usp=sharing

Conference Abstracts for Scientific Meetings

Euromit 2017, Cologne (Poster Presentation)

Neuronal Development and Mitochondrial Dysfunction Caused by wfs1 Mutations in a Zebrafish Model

George Cairns[1], Simon Ramsbottom[2], David Moore[1], Florence Burte[1], John Sayer[2], Patrick Yu-Wai-Man[134]

1 Wellcome Trust Centre for Mitochondrial Research Institute of Genetic Medicine, Newcastle University, Newcastle Upon Tyne, UK

2 Institute of Genetic Medicine, Newcastle University, Newcastle Upon Tyne, UK

3 NIHR Biomedical Research Centre at Moorfields Eye Hospital and UCL Institute of Ophthalmology, London, UK

4 Department of Clinical Neurosciences, School of Clinical Medicine, University of Cambridge, Cambridge, UK

Wolfram syndrome (WS) is a neurodegenerative disorder defined historically by the combination of diabetes insipidus, diabetes mellitus, optic atrophy and sensorineural deafness. It is now increasingly apparent that a significant proportion of patients (30-40%) will develop additional neurological impairment, in particular ataxia, epilepsy and dysfunction of the long corticospinal tract neurons. The majority of patients with WS harbour recessive mutations within the WFS1 gene (4p16.1), which encodes for the Wolframin protein. Wolframin is an endoplasmic reticulum (ER) transmembrane protein and the depletion in protein level contributes to the neuropathology of WS. Wolframin is implicated in a number of critical cellular pathways, including the ER stress response, calcium homeostasis, and mitochondrial biogenesis. Assays were designed and optimised to investigate neuronal development and mitochondrial dysfunction in zebrafish harbouring wfs1 mutations: spontaneous movement at 24 hours post fertilization (hpf) and touch response at 48hpf, which is an indicator of spinal cord and peripheral nervous system function. Immunostaining of the primary motor neurons were also performed to track their development in the tail. Mitochondrial axonal transport was quantified in vivo in wfs1 knockout zebrafish by tracking mitochondria along the lateral line at 48hpf with high-

resolution confocal microscopy. Abnormalities in spontaneous movement, touch response and primary motor neuron staining were all consistent with impaired neuronal development and maturation in our wfs1 Zebrafish models Depletion of the wolframin protein had a major impact on mitochondrial axonal transport with a significant impairment in trafficking. The wolframin protein plays an important role in neuronal development in early development and our data supports a role for mitochondrial dysfunction in the progressive neurodegenerative process seen in patients with WS.

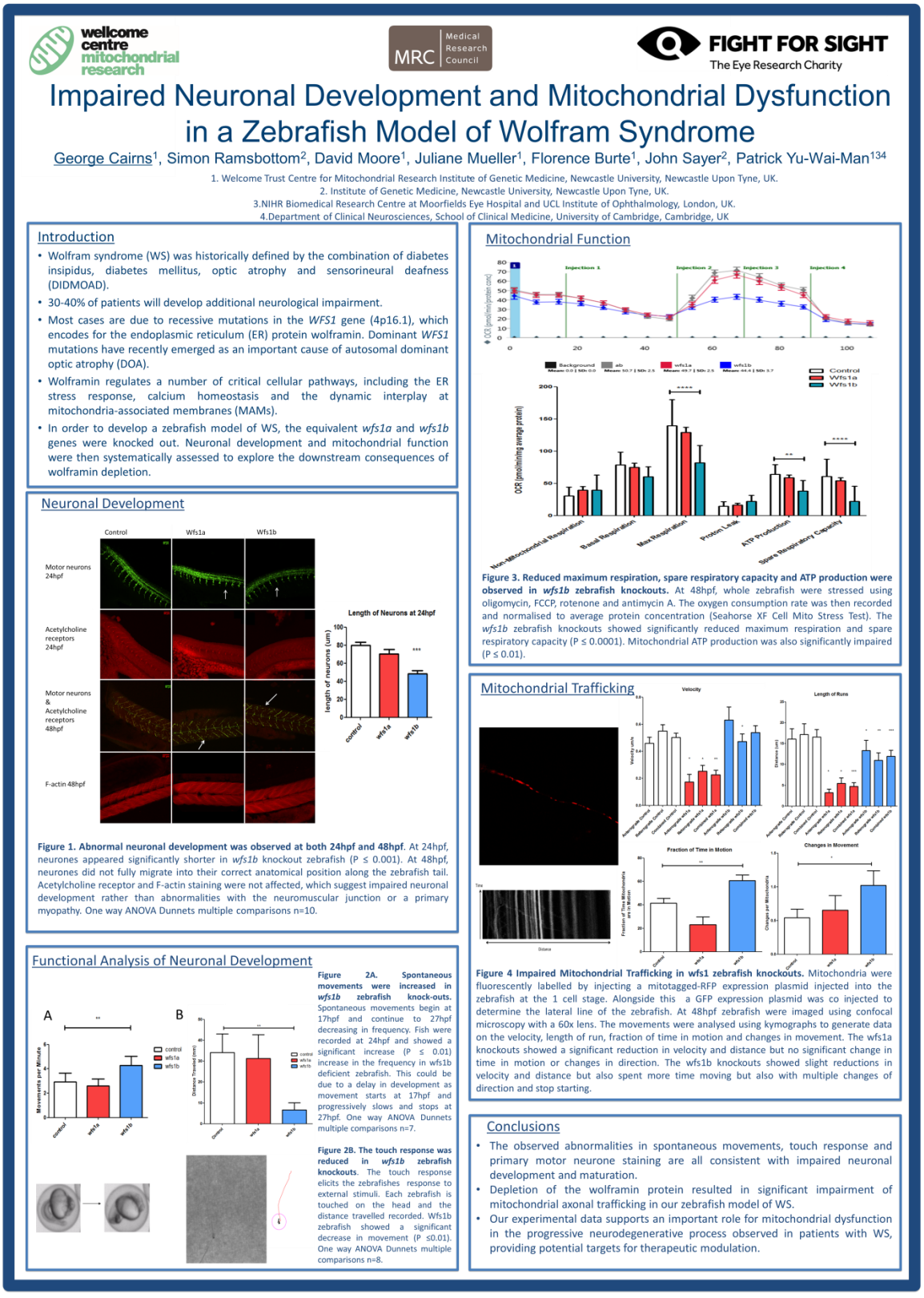

Early Career Mitoscientist Meeting 2017, Newcastle (Oral Presentation)

Mr George Cairns, Wellcome Centre for Mitochondrial Research, Newcastle University

Wolfram syndrome (WS) is a neurodegenerative disorder defined historically by the combination of diabetes insipidus, diabetes mellitus, optic atrophy and sensorineural

deafness. It is now increasingly apparent that a significant proportion of patients (30-40%) will develop additional neurological impairment, in particular ataxia, epilepsy and dysfunction of the long corticospinal tract neurons. The majority of patients with WS harbour recessive mutations within the WFS1 gene (4p16.1), which encodes for the Wolframin protein. Wolframin is an endoplasmic reticulum (ER) transmembrane protein and the depletion in protein level contributes to the neuropathology of WS. Wolframin is implicated in a number of critical cellular pathways, including the ER stress response, calcium homeostasis, and mitochondrial biogenesis. Assays were designed and optimised to investigate neuronal development and mitochondrial dysfunction in zebrafish harbouring wfs1 mutations: spontaneous movement at 24 hours post fertilization (hpf) and touch response at 48hpf. Immunostaining of the primary motor neurons were performed to track their development in the tail. Mitochondrial axonal transport and mitochondrial function was also tested using the: Seahorse XF Cell Mito Stress and axonal transport assay. Abnormalities in spontaneous movement, touch response and primary motor neuron staining were all consistent with impaired neuronal development and maturation in our wfs1 Zebrafish models Depletion of the wolframin protein had a major impact on mitochondrial function and the respiratory capacity of the mitochondria. Wolframin plays an important role in neuronal development in early development and our data supports a role for mitochondrial dysfunction in the progressive neurodegenerative process seen in patients with WS.

Fishmed 2018, Warsaw (Poster Presentation)

Neuronal Development and Mitochondrial Dysfunction caused by WFS1 Mutations in a Zebrafish model.

George Cairns1 , Florence Burte1 , John Sayer2 & Patrick Yu-Wai-Man3

1 Wellcome Trust Centre for Mitochondrial Research Institute of Genetic Medicine, Newcastle University, Newcastle Upon Tyne, UK

2 Institute of Genetic Medicine, Newcastle University, Newcastle Upon Tyne, UK

3 Department of Clinical Neurosciences, School of Clinical Medicine, University of Cambridge, Cambridge, UK

Wolfram syndrome (WS) is a neurodegenerative disorder defined historically by the combination of diabetes insipidus, diabetes mellitus, optic atrophy and sensorineural deafness. It is now increasingly apparent that a significant proportion of patients (30- 40%) will develop additional neurological impairment, in particular ataxia, epilepsy and dysfunction of the long corticospinal tract neurons. The majority of patients with WS harbour recessive mutations within the WFS1 gene (4p16.1), which encodes for the Wolframin protein. Wolframin is an endoplasmic reticulum (ER) transmembrane protein and the depletion in protein level contributes to the neuropathology of WS. Wolframin is implicated in a number of critical cellular pathways, including the ER stress response, calcium homeostasis, and mitochondrial biogenesis. Assays were designed and optimised to investigate neuronal development and mitochondrial dysfunction in zebrafish harbouring wfs1 mutations: spontaneous movement at 24 hours post fertilization (hpf) and touch response at 48hpf. Immunostaining of the primary motor neurons were performed to track their development in the tail. Mitochondrial axonal transport and mitochondrial function was also tested using the: Seahorse XF Cell Mito Stress and axonal transport assay. Abnormalities in spontaneous movement, touch response and primary motor neuron staining were all consistent with impaired neuronal development and maturation in our wfs1 Zebrafish models Depletion of the wolframin protein had a major impact on mitochondrial function and the respiratory capacity of the mitochondria. Wolframin plays an important role in neuronal development in early development and our data supports a role for mitochondrial dysfunction in the progressive neurodegenerative process seen in patients with WS.

Mitochondrial Medicine 2018, Cambridge (Poster Presentation/Lightning Talk)

Evidence of mitochondrial and visual dysfunction in a zebrafish wfs1 model of Wolfram syndrome

George Cairns[1], Florence Burte, Juliane Mueller[1], Angela Pyle[1], Maria Toms[5], Mariya Moosajee[5], John Sayer[2], Patrick Yu-Wai-Man[3,4,5]

1. Welcome Trust Centre for Mitochondrial Research, Newcastle University, Newcastle Upon Tyne, UK. 2. Institute of Genetic Medicine, Newcastle University, Newcastle Upon Tyne, UK. 3. Cambridge Centre for Brain Repair, Department of Clinical Neurosciences, University of Cambridge, Cambridge, UK. 4. MRC Mitochondrial Biology Unit, University of Cambridge,

Cambridge, UK. 5. NIHR Biomedical Research Centre at Moorfields Eye Hospital and UCL Institute of Ophthalmology, London, UK.

Wolfram syndrome (WS) is a neurodegenerative disorder defined historically by the combination of diabetes insipidus, diabetes mellitus, optic atrophy and sensorineural deafness. It is now increasingly apparent that a significant proportion of patients (30-40%) will develop additional neurological complications, in particular ataxia, epilepsy and degeneration of the long corticospinal tract neurones. The majority of patients with WS harbour recessive mutations within the WFS1 gene (4p16.1, OMIM 606201), which encodes for the Wolframin protein. Wolframin is an endoplasmic reticulum (ER) transmembrane protein and the depletion in protein level contributes to the neuropathology of WS. Wolframin is implicated in a number of critical cellular pathways, in particular the ER stress response and calcium homeostasis. Mitochondrial dysfunction is suspected to play a key role in the pathology of the disease. This link is highlighted by mutations in the CISD2 (4q24, OMIM 611507) gene, which also result in WS through a deleterious effect on mitochondrial calcium flux and disturbed ER-mitochondrial interactions. Changes in mitochondrial function were assessed in a wfs1 zebrafish model using a broad range of experimental methods in both larvae and adult fish. Mitochondrial axonal transport was quantified in vivo in wfs1 knockout zebrafish by tracking mitochondria along the lateral line at 48hpf with high-resolution confocal microscopy. Mitochondrial function was tested using a Seahorse XF Cell Mito Stress test. The mitochondrial respiratory chain complexes were assessed by SDS-PAGE and BN-PAGE. The functional consequences of wfs1 depletion in retinal ganglion cells were investigated with standardised visual function tests and our findings were corroborated with the histopathological findings in zebrafish retinas. We have characterised a wfs1 zebrafish model that faithfully recapitulates the clinical phenotype in patients with WS. Our results indicated that disturbed mitochondrial axonal transport and a reduction in mitochondrial complex I activity contribute to the loss of retinal ganglion cells and loss of visual function. Our disease model provides a versatile tool for further investigation the development and progression of WS and importantly, therapeutic drug screening.

Impaired Neuronal Development and Mitochondrial Dysfunction in a Zebrafish Model of Wolfram Syndrome

George Cairns[1,2], Florence Burte, Juliane Mueller[1], Maria Toms[5], Mariya Moosajee[5], Angela Pyle[1], John Sayer[2], Patrick Yu-Wai-Man[3,4,5]

1. Welcome Centre for Mitochondrial Research Institute of Genetic Medicine, Newcastle University, Newcastle Upon Tyne, UK.
2. Institute of Genetic Medicine, Newcastle University, Newcastle Upon Tyne, UK.
3. Cambridge Centre for Brain Repair, Department of Clinical Neurosciences, University of Cambridge, Cambridge, UK.
4. MRC Mitochondrial Biology Unit, University of Cambridge, Cambridge, UK.
5. NIHR Biomedical Research Centre at Moorfields Eye Hospital and UCL Institute of Ophthalmology, London, UK.

Introduction

- Wolfram syndrome (WS) is historically defined by the combination of diabetes insipidus, diabetes mellitus, optic atrophy and sensorineural deafness.
- Mutations in *WFS1* gene (4p16.1), which codes for wolframin, is the prevalent cause of WS.
- Implicated in a number of critical cellular pathways, including the ER stress response, calcium homeostasis, and insulin biogenesis.
- The equivalent genes were knocked out in a zebrafish model (wfs1a & wfs1b) to create a model of WS.
- Optic atrophy was assessed by histological analysis of retinal ganglion cells (RGCs) and through the optokinetic response in adult fish.
- To determine if mitochondrial function was impaired a number of parameters were tested using: western blots, copy number analysis, seahorse stress test and a mitochondrial tracking assay.

Optic Atrophy in wfs1 Knockout zebrafish

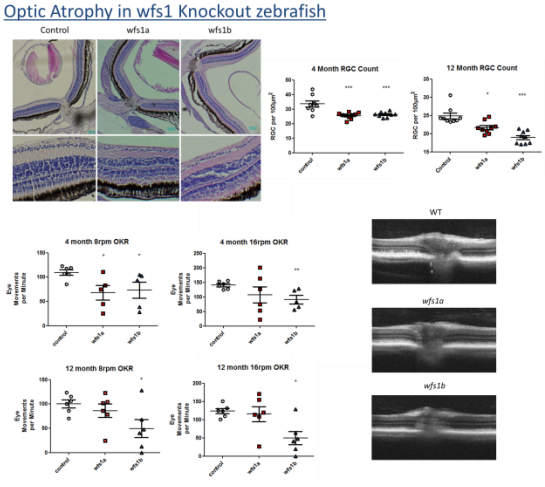

Figure 1 wfs1 knockout zebrafish have a reduced number of RGCs and visual impairment. At 4 months the zebrafish RGC count was significantly lower in both wfs1a and b fish. At 12 months however the wfs1b fish RGC counts are even lower which is reflected in the higher visual impairment seen in the OKR experiments of wfs1b knockout fish. Optical coherence tomography (OCT) also showed a thinning of the optic nerve in wfs1b knockouts at 12 months, suggesting the wfs1b model may be showing a more representative model of WS than the wfs1a knockout.

Mitochondrial Function

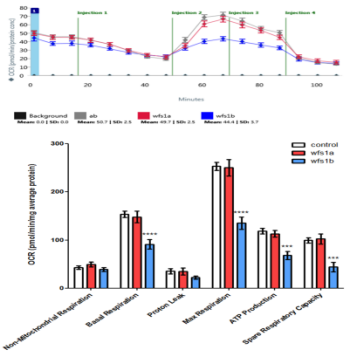

Figure 3 Seahorse XF Mito Stress Test wfs1b knockouts have a reduced Max respiration, ATP production and Spare respiratory capacity. At 48hpf whole zebrafish were stressed using oligomycin, FCCP, Rotenone and Antimycin A and the oxygen consumption rate recorded and normalised to average protein concentration. The wfs1b knockout showed significant reductions when Max respiration and Spare respiratory capacity were calculated $P \leq 0.0001$. While there was also a drop in ATP production $P \leq 0.01$.

Mitochondrial Trafficking

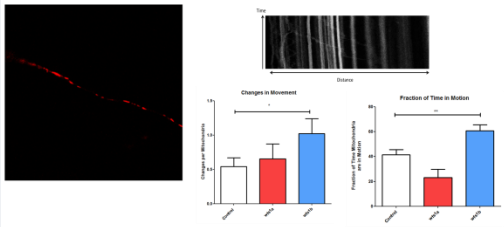

Figure 4 Impaired Mitochondrial Trafficking in wfs1 zebrafish knockouts. Mitochondria were fluorescently labelled by injecting a mitotagged-RFP expression plasmid injected into the zebrafish at the 1 cell stage. Alongside this a GFP expression plasmid was co injected to determine the lateral line of the zebrafish. At 48hpf zebrafish were imaged using confocal microscopy with a 60x lens. The movements were analysed using kymographs to generate data on the velocity, length of run, fraction of time in motion and changes in movement. The wfs1a knockouts showed a significant reduction in velocity and distance but no significant change in time in motion or changes in direction. The wfs1b knockouts showed slight reductions in velocity and distance, they also spent more time moving but also with multiple changes of direction and stop starting.

Mitochondrial Function

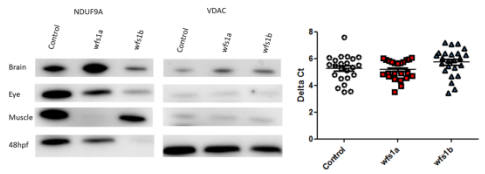

Figure 2 wfs1 knockdown zebrafish have reduced expression of NDUF9A and no significant copy number changes. Complex I subunit NDUF9A was immunoblotted for in both adult tissue and larval stages of zebrafish development and showed a knockdown in all cases in wfs1b and more tissue specificity in wfs1a. There were no significant differences in mitochondrial copy number suggesting no changes in mitochondrial biogenesis.

Conclusions

- Depletion of the wolframin protein had a major impact on visual function of the knockout zebrafish, in line with the progressive neurodegenerative process seen in patients with WS.
- The knockout of the wolframin protein plays an important role in mitochondrial dysfunction possibly through its relationship with complex I. Depletion of the wolframin protein had a major impact on mitochondrial axonal transport with a significant impairment in respiratory capacity.
- The wfs1b knockout model will be used in future as a drug screening model and to better develop the link between wfs1 and mitochondrial dysfunction.

Peer Reviewed Publications

O'Connor E, Phan V, Cordts I, **Cairns G**, Hettwer S, Cox D, et al. MYO9A deficiency in motor neurons is associated with reduced neuromuscular agrin secretion. Hum Mol Genet. 2018 Apr 15;27(8):1434-46. PubMed PMID: 29462312. Pubmed Central PMCID: 5991207

Alkanderi S, Molinari E, Elmaghloob Y, Stephen L A, Sammut V, Ramsbottom S A, Srivastava S, **Cairns G**, Edwards N, Rice S J, White K, Miles C G, Steel D, Ismail S, Sayer J A. ARL3 mutations cause Joubert syndrome by disrupting ciliary protein composition. 2018, Accepted AJHG The American Journal of Human Genetics.